

Lecture Notes in Civil Engineering

Yusuf A. Mehta · Iacopo Carnacina ·
D. Nagesh Kumar · K. Ramachandra Rao ·
Madhuri Kumari *Editors*

Advances in Water Resources and Transportation Engineering

Select Proceedings of TRACE 2020

 Springer

Lecture Notes in Civil Engineering

Volume 149

Series Editors

Marco di Prisco, Politecnico di Milano, Milano, Italy

Sheng-Hong Chen, School of Water Resources and Hydropower Engineering,
Wuhan University, Wuhan, China

Ioannis Vayas, Institute of Steel Structures, National Technical University of
Athens, Athens, Greece

Sanjay Kumar Shukla, School of Engineering, Edith Cowan University, Joondalup,
WA, Australia

Anuj Sharma, Iowa State University, Ames, IA, USA

Nagesh Kumar, Department of Civil Engineering, Indian Institute of Science
Bangalore, Bengaluru, Karnataka, India

Chien Ming Wang, School of Civil Engineering, The University of Queensland,
Brisbane, QLD, Australia

Lecture Notes in Civil Engineering (LNCE) publishes the latest developments in Civil Engineering - quickly, informally and in top quality. Though original research reported in proceedings and post-proceedings represents the core of LNCE, edited volumes of exceptionally high quality and interest may also be considered for publication. Volumes published in LNCE embrace all aspects and subfields of, as well as new challenges in, Civil Engineering. Topics in the series include:

- Construction and Structural Mechanics
- Building Materials
- Concrete, Steel and Timber Structures
- Geotechnical Engineering
- Earthquake Engineering
- Coastal Engineering
- Ocean and Offshore Engineering; Ships and Floating Structures
- Hydraulics, Hydrology and Water Resources Engineering
- Environmental Engineering and Sustainability
- Structural Health and Monitoring
- Surveying and Geographical Information Systems
- Indoor Environments
- Transportation and Traffic
- Risk Analysis
- Safety and Security

To submit a proposal or request further information, please contact the appropriate Springer Editor:

- Pierpaolo Riva at pierpaolo.riva@springer.com (Europe and Americas);
- Swati Meherishi at swati.meherishi@springer.com (Asia - except China, and Australia, New Zealand);
- Wayne Hu at wayne.hu@springer.com (China).

All books in the series now indexed by Scopus and EI Compendex database!

More information about this series at <http://www.springer.com/series/15087>

Yusuf A. Mehta · Iacopo Carnacina ·
D. Nagesh Kumar · K. Ramachandra Rao ·
Madhuri Kumari
Editors

Advances in Water Resources and Transportation Engineering

Select Proceedings of TRACE 2020

 Springer

Editors

Yusuf A. Mehta
Department of Civil and Environmental
Engineering
Henry M. Rowan College of Engineering
Rowan University
Glassboro, USA

D. Nagesh Kumar
Department of Civil Engineering
Indian Institute of Science Bangalore
Bengaluru, India

Madhuri Kumari
Department of Civil Engineering
Amity School of Engineering
and Technology
Amity University Uttar Pradesh
Noida, India

Iacopo Carnacina
Department of Civil Engineering
Liverpool John Moores University
Liverpool, UK

K. Ramachandra Rao
Department of Civil Engineering
Indian Institute of Technology Delhi
Delhi, India

ISSN 2366-2557

ISSN 2366-2565 (electronic)

Lecture Notes in Civil Engineering

ISBN 978-981-16-1302-9

ISBN 978-981-16-1303-6 (eBook)

<https://doi.org/10.1007/978-981-16-1303-6>

© The Editor(s) (if applicable) and The Author(s), under exclusive license to Springer Nature Singapore Pte Ltd. 2021

This work is subject to copyright. All rights are solely and exclusively licensed by the Publisher, whether the whole or part of the material is concerned, specifically the rights of translation, reprinting, reuse of illustrations, recitation, broadcasting, reproduction on microfilms or in any other physical way, and transmission or information storage and retrieval, electronic adaptation, computer software, or by similar or dissimilar methodology now known or hereafter developed.

The use of general descriptive names, registered names, trademarks, service marks, etc. in this publication does not imply, even in the absence of a specific statement, that such names are exempt from the relevant protective laws and regulations and therefore free for general use.

The publisher, the authors and the editors are safe to assume that the advice and information in this book are believed to be true and accurate at the date of publication. Neither the publisher nor the authors or the editors give a warranty, expressed or implied, with respect to the material contained herein or for any errors or omissions that may have been made. The publisher remains neutral with regard to jurisdictional claims in published maps and institutional affiliations.

This Springer imprint is published by the registered company Springer Nature Singapore Pte Ltd. The registered company address is: 152 Beach Road, #21-01/04 Gateway East, Singapore 189721, Singapore

Preface

Civil engineering primarily focuses on construction, operation, maintenance, and management of infrastructure including buildings and bridges; roads, railways, airports, ports, and harbors; dams and reservoirs; irrigation systems, river training, and flood mitigation works; water supplies and sewerage schemes. To keep the infrastructure future-ready, it is important that engineers work along with the UN Sustainable Development Goal (SDG) 11 which pertains to “Sustainable Cities and Communities” and SDG 9 which pertains to “Innovation and Infrastructure.”

With an aim to learn and share the latest findings, trends, and advances in civil engineering, the third international conference on “Trends and Recent Advances in Civil Engineering” (TRACE 2020) was hosted by the Department of Civil Engineering on August 20 and 21, 2020, at Amity University, Uttar Pradesh, Noida, India. The conference witnessed the participation and presentation of research papers from academia, industry expert, and researchers from R&D centers from India and abroad. The selected research papers were compiled and published in the form of conference proceedings.

This book titled *Advances in Water Resources and Transportation Engineering* is a compilation of the latest research works carried out by esteemed experts in water resources and transportation engineering. Each chapter corresponds to the latest technological application for solving challenges and problems encountered by water resources or transportation engineers. It aims to cover a broad spectrum of audience by covering interdisciplinary innovative research and applications in these areas. The objective of this compilation is to provide up-to-date information to those who are striving to contribute to this domain by utilizing the latest technology. The topics include technological intervention and solution for water security, sustainability in water resources and transportation infrastructure, crop protection, resilience to disaster like flood, hurricane, and drought, microplastics in river, and traffic congestion. The chapters present the latest areas of research like the application of remote sensing and software for solving real-time issues. We are hopeful

that it will prove to be of high value to graduate students, researchers, scientists, and practitioners working in water resources and transportation engineering domain.

Glassboro, USA
Liverpool, UK
Bengaluru, India
New Delhi, India
Noida, India

Yusuf A. Mehta
Iacopo Carnacina
D. Nagesh Kumar
K. Ramachandra Rao
Madhuri Kumari

Acknowledgements

From the conceptualization of conference TRACE 2020 to its outcome in form of the compiled books, the journey was exciting and fulfilling. As I write this session, it gives me a great sense of achievement not because “I” was working for it day and night but because I was part of the great “team” who wrote the success story of this conference.

Though we were challenged by COVID-19, we kept going because of the positive push and motivation of our honorable Founder, Dr. Ashok K. Chauhan, respected Chancellor, Dr. Atul Chauhan, and esteemed Vice Chancellor, Dr. Balvinder Shukla. I wish to thank them all for believing in us and guiding us for hosting the first ever online international conference in civil engineering domain. I am extremely thankful to our dynamic leadership team including Joint Heads of Institution and Head of the Department for providing valuable suggestions and support whenever it was required.

I am very thankful to the advisory committee and the organizing committee of TRACE 2020 who provided continuous support for the successful execution of the online version of the conference. I express my sincere appreciation to all our sponsors for their support: Academic Partners: Liverpool John Moores University, UK, Tribhuvan University, Nepal, Rowan University, USA; Industry Partner: Defense Infrastructure Planning and Management (DIPM) Council of India; Knowledge Partners: Institution of Civil Engineers (ICE), India; Indian Association of Structural Engineers (IAStructE); Women in Science and Engineering (WISE), India; Indian Geotechnical Society (IGS) and Indian Building Congress (IBC). I acknowledge the contribution of all the esteemed speakers from industry and academia for providing the insight on the latest trends and practices in civil engineering.

I wish to acknowledge and thank all the authors and co-authors of different chapters who cooperated with us at every stage of publication and helped us to sail through this mammoth task. Special thanks to all the national and international reviewers who helped us in selecting the best of the works as different chapters of the book.

I owe my sincere gratitude to my family members and faculty colleagues who helped me through the compilation of this book. Finally, I compliment the editing

team of Springer who provided all guidance and support to us in the compilation of the book and shaped up the book into a marketable product.

Dr. Madhuri Kumari
General Co-chair, Trace 2020, Professor,
Department of Civil Engineering, Dy. Director,
Placement and Industry Relations, Amity School
of Engineering and Technology
Amity University Uttar Pradesh
Noida, India

Contents

Nature-Oriented Paradigms for Urban Water Security: Perspective on Framework, Scale, and Sector	1
Negin Balaghi-Ficzkowski, Nidhi Nagabhatla, and Tariq A. Deen	
Sustainability in Transportation Infrastructure: Perspective of CREATEs, Rowan University	17
Deep Patel, Ahmed Saidi, Mohammad Jalayer, Daniel Offenbacher, and Yusuf A. Mehta	
Applications of Ground Penetrating Radar—A Comprehensive Case Study	31
P. Senthil, Alex Varughese, Hari Dev, and S. L. Gupta	
Risk Assessment of Pune Metro Underground Construction Using Risk Matrix and Expected Monetary Value	43
Shubhangi S. Wagh and Sandeep Potnis	
Linear Programming Model for the Design of Optimal Cropping Pattern for a Major Distributary Canal	57
S. B. Ganesh Kumar, B. R. Ramesh, and H. J. Surendra	
Analysis of Traffic Flow Characteristics Based on Area-Occupancy Concept on Urban Arterial Roads Under Heterogeneous Traffic Scenario—A Case Study of Tiruchirappalli City	69
Sandeep Singh, R. Vidya, Bishnu Kant Shukla, and S. Moses Santhakumar	
Sustainable Management of Stormwater to Prevent Urban Flooding Using SWMM	85
Anurag Swarnkar, Samir Bajpai, and Mani Kant Verma	
Decongesting Urban Roads: An Investigation into Causes and Challenges	95
Ekta Singh and Devendra Pratap Singh	

Assessing Contributions of Intensity-based Rainfall Classes to Annual Rainfall and Wet Days over Tehri Catchment, India	113
Sabyasachi Swain, Surendra Kumar Mishra, and Ashish Pandey	
Development of PCU Value of E-rickshaw on Urban Roads	123
Amir Ali Khan and Gyanendra Singh	
Performance Evaluation of Impact Stilling Basin Using ANSYS Fluent	139
Ishan Sharma, Ashish Mishra, and Rakesh Mehrotra	
Shoreline Change and Rate Analysis of Gulf of Khambhat Using Satellite Images	151
Keval Jodhani, Pulkit Bansal, and Priyadarshna Jain	
Investigating Resiliency of Infrastructure Against Hurricane Events: A Review	171
Uriel R. D. Clark, Jeong Eun Ahn, and Sarah K. Bauer	
Extraction of Surface Imperviousness from Land Use Land Cover Analysis for Part of Hyderabad City	179
Vinay Ashok Rangari, N. V. Umamahesh, and Ajey Kumar Patel	
Temporal Variation of Groundwater Levels by Time Series Analysis for NCT of Delhi, India	191
Riki Sarma and S. K. Singh	
Finite Element Modeling of Geogrid-Reinforced Unpaved Road	205
Rohan Deshmukh, S. Patel, and J. T. Shahu	
Hydrological Challenges in Riverfronts: A Case Study of Dravayawati Riverfront Project in Jaipur, Rajasthan	215
Kedar Sharma and Priyanka Gupta	
Analysis of Crop Protection Techniques Involving IoT	225
Prakriti Bhardwaj, Ranjan Verma, Parul Kalra, and Deepti Mehrotra	
Microplastic Detection and Analysis in River Yamuna, Delhi	233
Debarshi Ghosh and Madhuri Kumari	

About the Editors

Dr. Yusuf A. Mehta is professor in Department of Civil Engineering of Henry M. Rowan College of Engineering and has extensive experience in pavement systems and management. Dr. Mehta received his Ph.D. in Civil Engineering from The Pennsylvania State University in 1999 and and M.S. in Civil Engineering from The Oklahoma University in 1995. Dr. Mehta is a registered Professional Engineer in New Jersey. He has publications in refereed journals and international conferences. He has managed multiple projects of New Jersey Department of Transportation, Research and Innovative Technology Administration USDOT and New York State Department of Transportation. He received Aviation Research Award and New Jersey DOT Research Implementation Award in year 2012. He was recognized for his exemplary teaching by Mid-Atlantic American Society of Engineering Education in 2008. He received Louis J. Pignataro Memorial Transportation Engineering Education Award in 2013 for outstanding record of achievement in transportation engineering research, and undergraduate and graduate engineering education. He is Associate Editor of American Society of Civil Engineers Journal of Transportation Engineering. He is part of Editorial Board, Modern Traffic and Transportation Engineering Research (MTTER). He is member of American Society of Civil Engineers, Transportation Research Board, American Society for Engineering Education and Association of Asphalt Paving Technologist.

Dr. Iacopo Carnacina is Senior Lecturer in Civil Engineering at Liverpool John Moores University since year 2017. Prior to this he has been Lecturer and Researcher in River Engineering at UNESCO-IHE Institute for Water Education within the department of Water Science and Engineering. In 2006 he obtained his master degree in Hydraulic, Transportation and Territory Engineering from the University of Pisa, Italy. In 2010 he obtained his Ph.D. in Civil Engineering from the doctorate school of the University of Pisa “Leonardo da Vinci” Italy. Since 2007, he has also been a member of the professional body of Civil Engineers of the province of La Spezia, Italy. Previously, he was involved in the CARNOT/VITRE research project on sediment transportation of combined sewer networks using acoustic devices at the French Institute of science and technology for transport, development and networks

(IFSTTAR). After that, he worked for more than 5 years at AIR Worldwide, a catastrophe modeller firm, where he developed fluvial, pluvial and storm surge stochastic numerical models for the continental United States, Brazil, China, Central Europe, UK and Japan. There, he also worked as model manager and scientific lead for the new North Sea storm surge model in collaboration with Deltares, which resulted in development of new solutions using Delft3DFlexile Mesh. He is interested in local erosion in correspondence of hydraulic structures such as bridge, river training structures and dams, large scale numerical flood models and flood protection. He has also contributed to the study of sustainable river training structures, with focus on local erosion phenomena and morphology, design, energy dissipation and two phase flow development. His research focuses on the sustainable impact of hydraulic structures with focus micro-hydropower development in rural regions use of sustainable resource to optimize efficiency and minimize the environmental impact.

Prof. D. Nagesh Kumar is the Chairman, Centre for Earth Sciences, Indian Institute of Science, Bangalore. He has been working in the Department of Civil Engineering IISc since May 2002. Earlier he worked in IIT, Kharagpur (1994–2002) and NRSC, Hyderabad (1992–1994). He obtained Ph.D (Engg) from Indian Institute of Science, Bangalore, India in 1992. He visited Utah State University, USA in 1999 for 6 months on BOYSCAST fellowship. He worked as Visiting Professor in Ecole Nationale Supérieure des Mines, Saint-Etienne, France, in 2012. His research interests include Climate Hydrology, Water Resources Systems, Climate Change Impact on Water Resources, ANN, Evolutionary Algorithms, Fuzzy logic, MCDM and Remote Sensing & GIS applications in Water Resources Engineering. He has published more than 170 papers in leading international journals and conferences in his research fields. He has co-authored three text books viz., “Multicriterion Analysis in Engineering and Management” published by PHI, New Delhi and “Floods in a Changing Climate: Hydrologic Modeling” published by Cambridge University Press, U.K. and “Hydroclimatic Teleconnection: Indian Perspective” published by Scholars’ Press, Germany. He is Associate Editor for ASCE Journal of Hydrologic Engineering and ISH Journal of Hydraulic Engg. He received the best associate editor award for ASCE Journal of Hydrologic Engineering for the year 2014. He is in the Editorial Board of Open Hydrology Journal and Journal of Applied Computational Intelligence and Soft Computing. He has been reviewer for more than 65 international journals including Water Resources Research and Journal of Hydrology. He received IBM faculty award for the year 2012 for his outstanding research in the field of modeling hydrologic extremes using microwave remote sensing. He is a member, Working Group on Climate Change, International Association of Hydraulic Engineering and Research (IAHR), Spain. He is a Fellow of Institution of Engineers (India) and Indian Society for Hydraulics. He is a member of the AGU, IAHR, ASCE, IAHS (UK), IS-MCDM (USA) and Indian Society of Remote Sensing.

Dr. K. Ramachandra Rao is a professor in Department of Civil Engineering and Associate Faculty of Transportation Research and Injury Prevention Programme (TRIPP), Indian Institute of Technology, Delhi. He is a Transportation Engineering

specialist. After completing PhD in Transportation Engineering at IIT Kharagpur in 1998, he started his teaching career in School of Engineering - University of KwaZulu Natal, Durban, South Africa (formerly University of Durban-Westville). Subsequently, he worked in IIT Guwahati in Civil Engineering Department as Assistant Professor. Since 2003, he is working in IIT Delhi. Besides teaching and research, he is involved in various projects at national and international levels. He has published research papers in leading international journals and conferences in his research fields. The main focus area of his work during the past 5 years has been on development of traffic models in heterogeneous and safe environments. Besides, he is also working on improvements of Bus transport systems, road safety and low carbon mobility.

Dr. Madhuri Kumari received her PhD from The Energy Resource Institute (TERI) for her work on geostatistical modeling for prediction of rainfall in Indian Himalayas. She completed her M.Tech in Hydraulics and Water Resources Engineering from Institute of Technology, Banaras Hindu University and B.E in Civil Engineering from Andhra University and was awarded Gold Medal. She is working as Professor in Department of Civil Engineering, Amity School of Engineering and Technology, Amity University Uttar Pradesh, Noida, U.P. She has vast industry experience of 11 years and academic experience of around 11 years. Her research works in area of rainfall modelling have been published in reputed journals. Her research interest is in application of geographical information system in solving problems related to water resources engineering.

Nature-Oriented Paradigms for Urban Water Security: Perspective on Framework, Scale, and Sector



Negin Balaghi-Ficzkowski, Nidhi Nagabhatla, and Tariq A. Deen

Abstract Water security in urban areas is threatened by a multitude of direct and indirect drivers. On the one hand, the demand for water is increasing on a daily basis as the urban population and lifestyle needs increase; on the other hand, events such as floods, tropical cyclones, and other natural hazards result in disruption of water provisioning systems and processes. Additionally, climate change impacts such as heat waves and sea-level rise affect the sustainability of water supplies in urban areas. Conventionally, hard engineering structures and strategies have been implemented around the world to address water needs in urban areas and solutions that are often costly and intrusive to the natural environment. Nature-based solutions (NBS) in the past years emerged as a framework for exploring the potential of soft engineering solutions—as an alternative for managing urban planning, building climate resilience, and sustaining water needs of the urban communities. In this chapter, the following points are explained: (a) review of selected nature-oriented conceptual framings and practical options that apply to urban water systems, (b) illustration of existing NBS practices such as permeable pavements, green roofs, and bioretention ponds in urban landscape architecture planning, and (c) future of urban landscapes with comparative context of traditional versus nature-based water management practices. The conclusion draws attention to the UN Decade on Ecosystem Restoration (2021–2030) that is aiming to prevent, halt, and reverse the degradation of ecosystems globally. The aim is to present a synthesis that can steer integrated development planning while addressing basic water needs, climate resilience, and ecosystems protection in all settings and particularly in urban landscapes.

N. Balaghi-Ficzkowski (✉) · N. Nagabhatla · T. A. Deen
McMaster University, Hamilton, ON, Canada
e-mail: negin.balaghi@gmail.com

N. Balaghi-Ficzkowski
United Nations University Institute for Water, Environment, and Health, Hamilton, ON, Canada

N. Nagabhatla
The United Nations University Institute on Comparative Regional Integration Studies
(UNU-CRIS), Brugge, Belgium

Keywords Urban water security · Nature-based solutions (NBS) · Climate change · Natural hazards · Water resilience

1 Introduction

Driven by the prospect of social spaces and economic opportunities, more and more people have been moving into cities over the past century, resulting in urban population increase at a rate faster than ever before. In 1950, urban population accounted for 30% of the world's population; by 2014, this number increased to 54% [37]. As the urban population continues to grow, the urban landscapes become crowded, and the existing civil/municipal infrastructure deteriorates at a faster rate; social and public services are rendered insufficient, and the pressure for quick development rises. In the working group document to the Fifth Assessment Report of the Intergovernmental Panel on Climate Change, Revi et al. [26] illustrate how expanding urban centers is characterized by dense infrastructure which directly impacts inhabitants' vulnerability to weather disturbances and climate change impacts.

Data projections by the World Health Organization (WHO) indicate a continuous increase in urban population over the next few decades, projecting 2.5 billion people flow by 2050 [37]. This could be inferred as around 6.4 billion people living in cities in the next 30 years resulting in increased demand for food, energy, and water supply. The World Bank anticipates about 50% increase in urban water demands within the next 30 years [31]. Some trends are shown in Fig. 1.

According to a recent estimate, by 2030 (Sustainable Development Goals tenure) close to one billion additional people will live in cities in the Latin America and the Caribbean region which is currently considered the most urbanized developing region globally [35]. The already scarce freshwater supplies and the simultaneous impacts

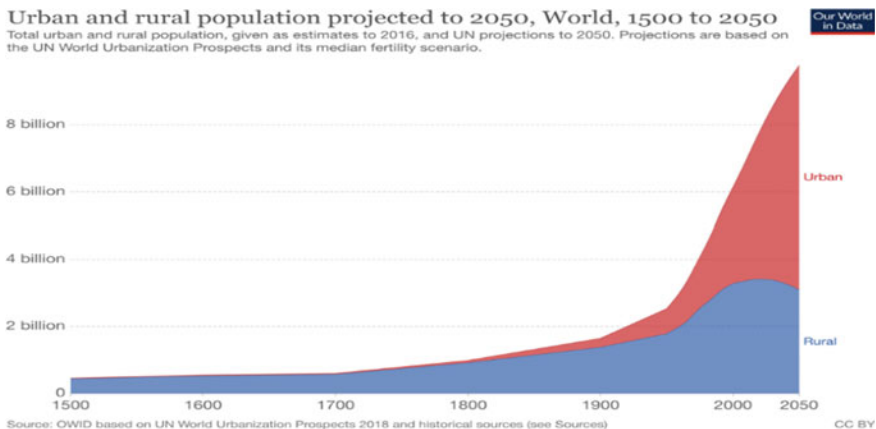


Fig. 1 Projected Urban Population by 2050 based on UN World Urbanization Prospects 2018 and others. *Source* ourworldindata.org [27]

of the water crisis, such as pollution and contamination, call for a paradigm shift to sustainable urban planning, more so in developing cities. This means infrastructure designs of cities must emphasize on community spaces, green zones, and water use–reuse–recycle systems. Moreover, climate change condition exacerbates water insecurity and adds additional need for developing (or adopting) efficient and effective water policies globally. The sustainability issue with the existing (mostly gray) infrastructure and the economic benefits of long-term planning require investigation of nature and resource-efficient solutions that offer multiple benefits to environmental and human health [39].

In this chapter, an overview of the nature-based solutions (NBS) framework is provided within the context of water security and with focus on urban landscapes. Furthermore, gaps and needs are analyzed by quoting examples of best practices worldwide to demonstrate integration of the nature-based solutions in urban planning. We discuss effective and appropriate implementation of NBS toward reducing exposure and vulnerability to urban water insecurity with respect to the Sustainable Development Goals (SDGs) and the New Urban Agenda which together present a foundation for climate and water resilient city planning.

2 Overview of Frameworks, Scale, and Sector: NBS and Water Security

A key reference to set the design of this chapter is the water security definition by UN-Water: “*the capacity of a population to safeguard sustainable access to adequate quantities of and acceptable quality water for sustaining livelihoods, human well-being, and socio-economic development, for ensuring protection against water-borne pollution and water-related disasters, and for preserving ecosystems in a climate of peace and political stability*” [36]. For the first time, this narrative presents water as an interlinked challenge within environmental, social, and political domains. Water security and climate resilience are inseparable, deeply and naturally interconnected [29]. The broad scope of water security framework of UN-Water [36] allows for developing the water security nexus, highlighting the interdependencies between achieving water, energy, and food security with the relational aspects of climate change adaptation (CCA), disaster risk reduction (DRR), and the objectives of human development, national security, and sustainable economic development (Fig. 2).

The integrated water resource management (IWRM) framework introduces three key aspects of *ecological sustainability*, *economic efficiency*, and *social equity* in water management and planning [9]. This framework bears flexibility in context of the larger water security nexus planning and implementation in all settings for urban, agricultural, industrial, and other economic sectors of computing water use; therefore, it has been adopted by many development agencies (including the World Banks and UNDP). IWRM as a water management framework complements the

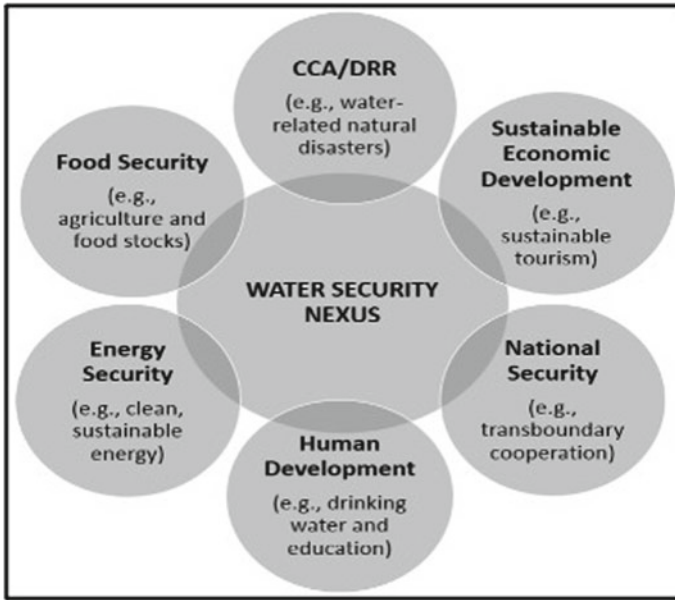


Fig. 2 Multiple challenges with relational aspects to the water security nexus (Figure by Tariq Deen)

water security perspective. As such, knowledge and experience between these two conceptual framings can be applied to urban water security agenda setting.

The water security challenges in the urban regions (city, township, or a municipality) are influenced by various drivers such as population density, lifestyle choices, and informal settlements. Climate change impacts on cities manifest in various ways, for instance, increasing heat island effect, dry conditions impacting water availability and recharge, sea-level rise (if that applies in geographical context), coastal or river flooding and erosion, storm surges and stormwater management, flooding, and health outcomes for these impacts noted as heat stress and respiratory disorders [26]. While all urban social groups are either directly or indirectly affected by climate change and environmental stresses, certain groups are more vulnerable; these include the elderly, children, pregnant women, the homeless, people living with disabilities, and people living with low levels of income [39]. Therefore, it is crucial to organize basic water provisioning needs and climate resilience programs for the benefit of all citizens [12].

The urban water security concept finds background in addressing water-related impacts of climate change that threatens cities. Post 2010, some cities have begun to implement strategies to protect their communities, infrastructure, and environmental resources from natural hazards and future impacts of climate change; for example, a public square built in Copenhagen that stores stormwater [20] or the “Sponge City” project constructed in Shenzhen that bears capacity to capture 60% of annual rainfall [5]. Shenzhen aims to minimize the impact of rapid urbanization on the

environment and water pollution to build a sustainable and healthy water circulation system in the future [5]. Nevertheless, implementing such projects often requires an understanding and awareness of ecosystem-based low-impact development (LID) solutions, justification of social and economic co-benefits, governance approach, engagement with multiple actors, and even new financing models [4].

Nature-based solutions (NBS) are initiatives that take advantage of the various mechanisms that nature provides at protecting communities from the destructive forces of natural hazards and other environmental changes. The International Union for Conservation of Nature (IUCN) explains NBS as “*actions to protect, sustainably manage and restore natural or modified ecosystem that address societal challenges effectively and adaptively, simultaneously providing human well-being and biodiversity benefits*” [6]. The framework has gained recognition due to the potential it carries to address the emerging challenges of water security and disaster risk management, climate change adaptation, environmental protection, water and human security, and projecting itself as a cost-effective measure compared to traditional hard engineering strategies (see various chapters in Multifunctional Wetlands [21]).

The 2018 UN World Water Development Report highlights the NBS framework as a solution to water crisis, stating that NBS can use or mimic natural processes to enhance water availability (e.g., soil moisture retention, groundwater recharge), improve water quality (e.g., natural and constructed wetlands, riparian buffer strips), and reduce risks associated with water-related disasters and climate change (e.g., floodplain restoration, green roofs). Two significant impacts of climate change on urban areas are reduced water availability (or water scarcity due to dry conditions or water pollution) and rise in unwanted water (flooding). Currently, the solutions to combat these challenges within the urban water management remain heavily dominated by traditional, human-built (‘gray’) infrastructure. The potential for NBS as a means to move beyond existing systems remains underutilized in addressing many of the water challenges, including in the urban settings [39]. The geographical location of an urban population provides some initial considerations for exploring applicable nature-based solutions for urban infrastructure developers. The potential solutions can address three main types of settings representing water security needs in an urban landscape: (a) land-locked urban areas, (b) coastal cities, and (c) watersheds, reservoirs, and other sources of water storage and protection. Some examples are listed in Annexure 1.

NBS systems could be implemented naturally through creation, protection, or restoration of only ecosystem elements. In a joint report, the World Bank Group and World Resources Institute (WRI) propose structural strategies aimed to advance the integration of green and gray infrastructure solutions to substitute, augment, or work in parallel with existing gray infrastructure in a cost-effective manner [4]. Strategizing the NBS approach in urban infrastructure planning aims to find a balance of the green and gray combination that maximizes the benefits and system efficiency of the solutions and minimizes the trade-offs between the costs and the environmental impacts.

A case study example illustrating NBS noted in the Mekong Delta in Vietnam reflects integration of green and gray infrastructure project, wherein mangrove ecosystems were rooted into the project design to restore the existing sea dikes. The rapid aquaculture expansion in late 1980s along the northern coast of Vietnam caused significant loss of mangrove forests that were acting as the area's natural defenses against coastal floods and erosion. To mitigate the impacts of the natural disasters and protect the ever-growing population, restoration of the mangrove forests was agreed as necessary and in 1994, Mangrove Plantation and Disaster Risk Reduction Project was launched to enhance the existing gray infrastructure by investing \$9 million in restoring 9000 hectares (ha) of mangroves area and as 100 km of dike lines by 2010. Noted was significant reduction of maintenance cost of dikes by \$80,000 and \$15 million saved as damage to private property and other public infrastructure also lowered considerably [14]. The coastal cities worldwide are hub of economic activity and therefore to maintain ecological and development balance remain pertinent to ensure sustainable development. It can be argued that often the cost of investment in NBS bears merit in medium to long terms planning, in comparison with short and quick gray infrastructure solutions [24]. In addition, strategies that can combine gray approach and NBS are also investigated by experts and agencies.

NBS is leveraging from existing concepts like the ecosystem-based adaptation (EBA) that propagates well-managed ecosystem as an adaptive tool to climate change and ecosystem-based disaster risk reduction (Eco-DRR) that considers well-managed ecosystem with an objective to reduce the effects of natural hazards that do not necessarily have to be linked to climate change [6]. These two approaches can be used in tandem with NBS to enhance ecological and social resilience, especially in the urban areas with high population density. For instance, mangrove ecosystems have traditionally functioned as a natural strategy for coastal protection because of its complex root structure and dense branch system. Global case studies illustrate how mangroves have helped maintain coastal soil structure and reduce wave energy during storm surges. If planned systematically, mangroves can significantly reduce exposure to coastal hazards like tsunamis and tropical cyclones [11].

Nature-based solutions are widely explored for coastal flooding. Most NBS (or hybrid-NBS) projects reported by the World Bank in 2017 are to combat ongoing river flooding challenges [4]. A good example is river reconnection in China [42]. The construction of dam and dike in the Yangtze River Basin in China from the 1950s to 1970s caused significant undesirable impacts on the existing river-lake wetlands systems. As a result, major flooding events were noted in 1990s that caused loss of life for thousands and direct economic losses in billions of dollars. In a partnership with World Wildlife Fund (WWF), the Chinese Government reconnected the Yangtze River with the disconnected lakes and rehabilitated the natural functions of the wetland system as an attempt to reverse the damages and mitigate the flooding risk. Noted was restoration of nearly 500 km² wetlands with floodwater retention capacity up to 300 cubic meter; amid other economic co-benefits of this project and was more than 17% increase in lake districts fisheries production [42].

NBS approach offers variety of co-benefits in tackling challenges related to urban water security and DRR. For example, for tropical regions coastal resilience

strategy, mangrove ecosystems can provide ecological co-benefits in terms of pollution control for aquatic and marine life. Kathiresan and Rajendra [18] show how Indian hamlets with mangroves were significantly less damaged after the 2004 Indian Ocean Tsunami, compared to those without a dense mangrove zone. Das and Vincent [7] observed that mangroves were able to buffer the 1999 super cyclone in Orissa, India. In other parts of the world, the European Union (EU) projects, focusing on efficient and effective design of NBS for restoration of degraded marine environments, demonstrate examples to scale and to support policy negotiations [13].

A common planning challenge for densely populated cities is spatial footage and a lack of available real estate to adopt or implement NBS [24]. Use of integration strategies in existing infrastructure is one of the common strategies in such situations. For instance, roof gardens (also known as living roofs, vegetated roofs, or eco-roofs) address space limitation in densely developed metropolitans. The roofs of buildings can host gardens comprising live vegetation, with innovative structures, built to application; however, the foundation of a layer of soil/growing material and a vapor seal to protect the building from water and vegetation roots are key design aspects, plus additional layers to transport water to a storage tank. These systems are adopted for stormwater management system in some instances, wherein collection of filtered water helps to reduce municipal water demand during dry periods. Around this foundation, construction of hybrid natural solutions plus hard engineering structures to relocate rainwater to storage tanks is an alternative. The stored water can be utilized for provisioning needs such as drinking water during conditions of water shortage. In addition, benefits such as regulation of temperature for the building are noted as the soil layers act as insulators [24]. So, the energy efficiency dimension applies, especially during summer months in buildings and establishments integrating NBS systems as measures for urban planning.

Ho Chi Minh City in Vietnam has a growing population of 8 million. Much of the city's natural landscape is converted to urban expansion and green spaces are limited to 0.25%. The natural drainage system is filled, encroached, or blocked by waste which results in flooding. Upstream development of the Saigon-Dong Nai River results in water shortages for the city during the dry season. The city is exploring options for sustainable urban planning, wherein houses are designed as "pots" with roof gardens to store stormwater and mitigate flooding impacts. A design includes placing a thick layer of soil on roofs to retain stormwater and planting banyan trees to make use of their aerial root system. The ground is made of permeable bricks to increase infiltration during rainfall events. This intervention was tested for the President Place that serves as office and commercial space. Leading to a successful experiment, the building received a Leadership in Energy and Environmental design (LEED) Gold certification in energy and water efficiency category. It used 50% less water than other non-LEED buildings quoted Asian Development Bank [2].

The final case study highlights the importance of policy implication in NBS implementation and developing integrated strategies for NBS deployment [30]. Peru has dealt with water crises related to El Niño for many years; a trend that has been intensified by the climate change effects during last decades. In 2016, the Peruvian lawmakers called the Sanitation Sector Reform Law aiming to remediate the

increasing water-related risks. This policy requires water utilities to earmark revenue from water tariffs for watershed conservation and climate change adaptation and to consider these strategies in the official budgeting and planning processes. The policy was implemented and for 4 years generated \$30 million for NBS via payments for ecosystem services and an additional \$86 million for climate change mitigation and disaster risk management [16].

3 Global Governance Tools for Sustainability and the Urban Water Security Context

Sustainable Development Goals (SDGs) are a set of 17 global goals that aim to end poverty, protect the planet, and ensure prosperity for all [41]. The SDGs are the successor to the Millennium Development Goals (2000–2015) and include 169 targets many of which are interlinked. With respect to urban water security, goals 6 (Clean Water and Sanitation), 11 (Sustainable Cities and Communities), 13 (Climate Action), and 15 (Life on Land) contain relative targets for addressing the issue. Some selected examples of SDG targets that apply to urban water security include SDG 6.6 calling for protection and restoration of water-related ecosystems, including mountains, forests, wetland, rivers, aquifers, and lakes; SDG 11.6 emphasizing reduction in the adverse per capita environmental impact of cities, including paying special attention to air quality and waste management. SDG 13.1 on strengthening resilience and adaptive capacity to climate-related hazards and natural disasters in all countries and SDG 15.1 ensuring the conservation, restoration, and sustainable use of terrestrial and inland fresh ecosystems and their services, in particular forests, wetlands, mountains, and drylands, in line with obligations under international agreements.

Water insecurity is an issue that is interconnected with other environmental and socioeconomic challenges, and SDGs provide a guiding framework for cities and communities to identify development priorities with a balanced approach (i.e., human and ecological development agendas addressed in tandem). For instance, SDG targets 6.6, SDG13, and SDG 15.1 all relate to the protection and restoration of aquatic ecosystems, noting that healthy ecosystems are better able to protect communities from climate change impacts and natural hazards and can better serve provisioning needs for people and populations such as drinking water. The concept of resilience is often associated with the defined frameworks, including NBS, steering the notion of creating systems that are better prepared to cope with and recover from natural disasters, environmental changes, and climate change, through the preserving and restoring of basic infrastructure and services. The SDG agenda can only be achieved when its implementation strategies are risk-informed, and water climate and disaster risks are tackled through integrated frameworks. Note that SDG 13.1 calls that countries must plan long-term development tools, rather than responding with short-term emergency measures.

Fig. 3 Seven goals of the Sendai framework figure. *Source* United Nations Office for Disaster Risk Reduction [38]



The Sendai Framework is the successor to the 2005–2015 Hyogo Framework for Action and was adopted at the Third UN World Conference on Disaster Risk Reduction in Sendai, Japan, in March 2015. This non-binding disaster risk reduction (DRR) agreement asserts that it is the responsibility of the state, local governments, the private sector, and other stakeholders to protect communities against natural hazards. The outcome of the framework states that the substantial reduction of disaster risk and losses in lives, livelihoods, and health in the economic, physical, social, cultural, and environmental assets of persons, businesses, communities, and countries covers a period from 2015 to 2030 [40]. The seven goals as summarized in Fig. 3 also link with SDGs to a fair extent.

Other international agreements, like the Paris Agreement, include high-level commitments to promote ecosystem-based solutions such as NBS. The New Urban Agenda [41] describes a vision, with principles and commitments, a call for action, and an implementation plan. It sets the pathway for Sustainable Cities and Human Settlements and is targeted toward the key stakeholders involved in urban governance and planning, including nation states, cities, UN agencies civil societies, and NGOs. The New Urban Agenda also highlights the human right principle and criteria in relation to drinking water and sanitation. Water is embedded within the vision, commitments, and call for action for this agenda offering incentives to design sustainable solutions for urban water management. The frameworks and principles provided assist urban leaders to develop and implement their vision for managing urban water needs and climate resilient cities. Commitments outlined in the New Urban Agenda is provided in Annexure 2. The goal to encourage collaborative action and vision is central to most global governance frameworks so that local governments, urban professionals, and individuals actively engage in addressing and finding solutions on urban water management challenges driven by paradigm shifts [15].

4 Key Discussion Points

NBS as a strategy is not to prevent weather disturbances, natural hazards, or environmental processes from occurring but rather to reduce the impact these disturbances have on infrastructure, human lives, and economic activity. Therefore, NBS can and will contribute to the SDG targets and the goals of the Sendai framework in the urban water security context and serve as a strategy to create a frame for policy changes at local government level while allowing focus on resilience in urban planning and infrastructure development.

While there is a growing appetite for investment globally to support nature-based initiatives, there are certain considerations and barriers to implementing NBS projects. NBS planning is often a long-term investment which requires commitments of states and communities through co-creation and consultative processes. In the current system, development priorities do not necessarily align with ecological benefits or inter-agency and regulatory approval processes, lack clarity, or are long and cost intensive. In addition, lack of awareness or shared knowledge about the success stories and best practices serve to limit scalability NBS options [17]. To overcome these underlined challenges, key considerations include careful evaluation, smart planning, minimization of trade-offs in infrastructure planning and participatory approach to project/program design. Some NBS projects are exceedingly context specific and needing customization, as such, technical expertise and systematic analysis on design, planning, and implementation are pertinent. For instance, drought management in urban environments can be challenging since droughts have wide-reaching spatial and temporal impacts including the effect on water availability. Hence, integrated design of a household/residential building to capture rainwater, store access water or recycle–reuse wastewater are options that can be implemented within the NBS framework. Some examples of such interventions are documented in the monograph, Multifunctional Wetlands-Pollution Abatement and Other Ecological Services from Natural and Constructed Wetlands [21].

Other important considerations in implementation of NBS are enabling conditions. Existing practices, programs, and policies need to be modified to allow unlocking NBS opportunities. During past few years, considerable effort toward establishing NBS frameworks is observed. For instance, in 2017 the World Bank outlined eight distinctive steps for planning and strategizing NBS implementation. Building on the work of the EKLIPSE project in the European Union, Raymond et al. [25] developed and proposed a seven-stage process for co-benefit assessment within policy and project implementation for NBS in urban areas. The importance of frequent engagement with stakeholders, continuous monitoring and evaluation post implementation, sharing best practices, and evaluating scaling potential are key dimensions that apply.

International Water Association (IWA) distributed 17 principles for water wise cities toward water sensitive urban infrastructure encouraging policy development at the local scale [15]. The initiative was reassuring for urban developers and decision-makers to share their experience with NBS and encourage mutual partnerships. Such

programs have informed systemic assessment of the values of NBS implementation, commenting that comprehensive evaluation of infrastructure financing and incentives for investing in nature-based infrastructure should be presented clearly to all level of stakeholders. Globally, the urban centers are exploring NBS as alternative based on existing best practices or customizing the framework to fit their settings; ecosystem restoration, wastewater management, water security planning, etc. Overall, NBS is a mixed result story indicating success, but also needs for refinement, possibility for integration with existing infrastructure options, and is an incessantly evolving phenomenon.

Another key aspect to NBS implementation especially for local stakeholders is incentivizing participation. Inclusion of NBS into the municipality codes and regulations is to help accelerate the regulatory and authorization processes, grants, and financial supports for research and related innovation, in particular establishment of financing models to facilitate and promote NBS investments. Green Climate Fund (GCF) is financing mechanisms created under the UN Framework Convention on Climate Change (UNFCCC)—though a handful of NBS projects are funded under this scheme, those focusing to reduce vulnerability and exposure to climate risks are paramount to generate multiple environmental benefits, among other criteria [10]; this could set a good reference for future investments.

5 Concluding Notes

Globally, the fast transition into a predominately urban habitation renders urban water security; a major challenge for many countries, particularly for the developing and emerging economies. The urban water management systems can directly impact the socioecological resilience, exposure, and vulnerability of the cities and inhabiting populations. The political stability, geographical location, regulatory norms, and governance techniques are some factors that have role in determining and steering the water secure futures for urban centers. Application of a water security framework to urban design and planning could provide planners, development managers, and decision-makers with an integrated guideline toward effective design solutions, recycle–reuse possibilities, and investment models and policies to address environmental and socioeconomic challenges related to the water sector. Furthermore, the framework can assist to achieve water-related SDGs. Adopting a NBS perspective toward urban water security could also mean tying together political, economic, and social processes toward tackling contemporary suite of challenges in the sustainability, climate change adaptation, and DRR context.

Innovative frameworks such as resilient urban architecture, NBS, and climate sensitive cities are gaining momentum as more urban spaces and communities realize that hard engineering solutions cannot be the only solution as often time those are expensive to construct and difficult to maintain. Comprehensive assessment of initiatives, projects, and programs as explained in this chapter illustrates that investing in NBS is gaining momentum, though NBS is not a “one-size-fit-all” framework. NBS

dimensions pertaining to socioecological and sociocultural settings are deterministic to the limitations and opportunities for this framework to be adopted and scaled for designing water secure cities and communities. The UN Decade on Ecosystem Restoration (2021–2030) with the vision of “*The healthier our ecosystems are, the healthier the planet - and its people*” aims to prevent, halt, and reverse the degradation of ecosystems which globally is expected to boost interest and investment in NBS as a prospective strategy for sustainable urban development [32].

Conflict of Interest The authors of this chapter have no conflict of interest to declare.

Annexure 1. Examples of Different Concepts Related to NBS (Data Source: Thupalli and Deen [33] and World Resource Institute forum on NBS (2018) and World Bank)

NBS category	Sub-category	Projects	Natural/ecological systems
Urban ecosystem restoration	<ul style="list-style-type: none"> • Ecological restoration • Ecological engineering • Forest landscape restoration 	This approach focuses on the recovery of degraded, damaged/destroyed ecosystem in urban environments. City of Santa Maria in California, USA (Community-Based Restoration Projects supported by NASA)	<ul style="list-style-type: none"> • Riverbeds and banks • Sandy beaches and dunes • Upland forests
Sector/resource-specific urban ecosystem-related approaches	<ul style="list-style-type: none"> • Ecosystem-based adaptation • Ecosystem-based mitigation • Climate adaptation services • Ecosystem-based disaster risk reduction 	Ecosystem-related approaches vary based on their objective (C.f. [3], Doswald and Osti [8]; Olivier et al. [22])	<ul style="list-style-type: none"> • Floodplains and bypasses or urban flood control • Forest restoration for carbon sequestration • Constructed wetlands • Inland wetlands
Urban infrastructure-related approaches	<ul style="list-style-type: none"> • Natural infrastructure • Green infrastructure 	Commonly notes in cities (C.f. Ozment et al. [23], Roth [28]) help restore and filter stormwater, avoid cost of stormwater runoff, capture and slow local precipitation, provide energy-saving option for the building	<ul style="list-style-type: none"> • Parks, open spaces, conservation areas • Green roofs • Permeable pavements

(continued)

(continued)

NBS category	Sub-category	Projects	Natural/ecological systems
Urban ecosystem-based management approaches at large scale and resource governance frameworks	<ul style="list-style-type: none"> • Integrated coastal zone management (ICZM) • Integration water resource management (IWRM) 	IWRM, and ICZM embeds the ecosystem-based management and ecosystem protection aspects of conservation and integrated management (c.f. Arkema et al. [1], Leslie and McLeod [19])	<ul style="list-style-type: none"> • Coastal wetlands • Mangrove forests • Reefs • Salt marches

Annexure 2. Commitments Outlined in the New Urban Agenda [34]

Commitment	Description
Providing basic services for all citizens	These services include access to safe and clean drinking water and sanitation
Promoting measures that support cleaner cities	Tackling air pollution in cities by increasing the use of renewable energy, providing greener public transport, and sustainably managing the natural resources
Strengthening resilience in cities to reduce the risk and the impact of disaster	Leaders have now committed to implement mitigation and adaptation measures to minimize the impacts of natural disasters. These measures include urban planning, quality infrastructure, and improving local responses for safety and environmental sustainability
Taking action to address climate change by reducing greenhouse gas emissions	Sustainable cities that reduce emissions from energy and build resilience can play a lead role. Leaders committed to involve with local governments and all actors of society to take climate change action and considering the Paris Agreement on climate change
Improving connectivity and support innovative and green initiatives	This includes establishing partnerships with businesses and civil society to find sustainable solutions to urban water challenges in case of flooding or any other risk disaster

(continued)

(continued)

Commitment	Description
Promoting safe, accessible, and green public space	Sustainable urban design plays a key role in ensuring the livability and prosperity of a city. The agenda calls for an increase in public spaces to facilitate human interaction by urban planning

References

1. Arkema KK, Abramson SC, Dewsbury BM (2006) Marine ecosystem-based management: from characterization to implementation. *Front Ecol Environ* 4(10):525–32
2. Asian Development Bank (ADB) (2016) Nature-based solutions for building resilience in towns and cities: case studies from the Greater Mekong Subregion. Mandaluyong City, Philippines
3. Baig SP, Rizvi A, Josella M, Palanca-Tan R (2016) Cost and benefits of ecosystem-based adaptation: the case of the Philippines. IUCN, Gland, Switzerland, viii, 32
4. Browder G, Ozment S, Rehberger Bescos I, Gartner T, Lange GM (2019) Integrating green and gray: creating next generation infrastructure. World Bank and World Resources Institute, Washington, DC
5. Chan FKS, Griffiths JA, Higgitt D, Xu S, Zhu F, Tang YT, Xu Y, Thorne CR (2018) “Sponge City” in China—a breakthrough of planning and flood risk management in the urban context. *Land Use Policy* 76:772–778. <https://doi.org/10.1016/j.landusepol.2018.03.005>
6. Cohen-Shacham E, Walters G, Janzen C, Maginnis S, eds. (2016) Nature-based solutions to address global societal challenges. International Union for Conservation of Nature (IUCN), Gland, Switzerland
7. Das S, Vincent JR (2009) Mangroves protected villages and reduced death toll during Indian super cyclone. *Proc Nat Acad Sci* 106(18):7357–7360
8. Doswald N, Osti M (2010) Ecosystem-based approaches to adaptation and mitigation—good practice examples and lessons learned in Europe. Technical Report. The Federal Agency for Nature Conservation (BfN)
9. Global Water Partnership (GWP) (2017) The need for an integrated approach. <https://www.gwp.org>
10. Green Climate Fund (GCF) (2018). <https://www.greenclimate.fund>
11. Guannel G, Arkema K, Ruggiero P, Verutes G (2016) The power of three: coral reefs, seagrasses and mangroves protect coastal regions and increase their resilience. *PLoS ONE* 11(7):e0158094
12. Hoekstra AY, Buurman J, van Ginkel KCH (2018) Urban water security: a review. *Environ Res Lett* 13(5):053002. <https://doi.org/10.1088/1748-9326/aaba52>
13. Horizon 2020 Expert Group for EUROPEAN COMMISSION (2015) Towards an EU research and innovation policy agenda for nature-based solutions and re-naturing cities. European Union. <https://doi.org/10.2777/765301>
14. IFRC (International Federation of Red Cross and Red Crescent Societies) (2018) Mangrove plantation in Viet Nam: measuring impact and cost benefit
15. IWA (International Water Association) (2016) The IWA principles for water wise cities. <https://iwa-network.org>
16. Jenkins M, Gammie G, Cassin J (2016) Peru approves new innovative environmental policies
17. Kabisch N, Stadler J, Korn H, Bonn A (2016) Nature-based Solutions to climate change mitigation and adaptation in urban areas
18. Kathiresan K, Rajendran N (2005) Coastal mangrove forests mitigated tsunami. *Estuarine Coast Shelf Sci* 65(3):601–606

19. Leslie HM, McLeod KL (2007) Confronting the challenges of implementing marine ecosystem-based management. *Front Ecol Environ* 5(10):540–548
20. Liu L, Fryd O, Zhang S (2019) Blue-green infrastructure for sustainable urban stormwater management—lessons from six municipality-led pilot projects in Beijing and Copenhagen. *Water* 11(10):2024. <https://doi.org/10.3390/w11102024>
21. Nagabhatla N, Metcalfe CD (2018) Multifunctional wetlands: pollution abatement and other ecological services from natural and constructed wetlands (environmental contamination remediation and management). Springer, Berlin. <https://doi.org/10.1007/978-3-319-67416-2>
22. Olivier J, Probst K, Renner I, Riha K (2013) Ecosystem-based adaptation (EbA). *Global Water Partnership*
23. Ozment S, DiFrancesco K, Gartner T (2015) The role of natural infrastructure in the water, energy and food nexus. *Nexus dialogue synthesis papers*. IUCN, Switzerland
24. Ozment, S, Ellison, G, Jongman, B (2019) Nature-based solutions for disaster risk management. The World Bank. Booklet No. 134847
25. Raymond CM, Frantzeskaki N, Kabisch N, Berry P, Breil M, Nita MR, Geneletti D, Calfapietra C (2017) A framework for assessing and implementing the co-benefits of nature-based solutions in urban areas. *Environ Sci Policy* 77:15–24. <https://doi.org/10.1016/j.envsci.2017.07.008>
26. Revi A, Satterthwaite DE, Aragón-Durand F, Corfee-Morlot J, Kiunsi RBR, Pelling M, Roberts DC, Solecki W (2014) Climate change 2014: impacts, adaptation, and vulnerability. Part A: global and sectoral aspects. Contribution of working group II to the fifth assessment report of the intergovernmental panel on climate change. In: Field CB, Barros VR, Dokken DJ, Mach KJ, Mastrandrea MD, Bilir TE, Chatterjee M, Ebi KL, Estrada YO, Genova RC, Girma B, Kissel ES, Levy AN, MacCracken S, Mastrandrea PR, White LL (eds), vol 2. Cambridge University Press, Cambridge, United Kingdom and New York, NY, USA, pp 535–612. ISBN: 9781107058163
27. Ritchie H (2018) Urbanization. *Our world in data*
28. Roth R (2013) Natural infrastructure: a climate-smart solution
29. Sandford R (2017) The human face of water insecurity. In: Devlaeminck D, Adeel Z, Sandford R (eds) *The human face of water security*. Springer, pp 1–24. <https://doi.org/10.1007/978-3-319-50161-1>
30. Sudmeier-Rieux K, Ash N, Murti R (2013) Environmental guidance note for disaster risk reduction. IUCN, Switzerland
31. The World Bank (2017). <https://www.worldbank.org>
32. The UN Decade on Ecosystem Restoration (2020) <https://www.decadeonrestoration.org>
33. Thupalli R, Deen TA (2017) An investment strategy for reducing disaster risks and coastal pollution using nature based solutions. In: Nagabhatla N, Metcalfe CD (eds) *Multifunctional wetlands: pollution abatement and other ecological services from natural and constructed wetlands*. Springer, pp 141–170. https://doi.org/10.1007/978-3-319-67416-2_5
34. UN-HABITAT (2017) New urban agenda. Report number: A/RES/71/256
35. UN-HABITAT (2014) The state of latin american and caribbean cities 2012: towards a new urban transition. Report number: HS/063/12E
36. UN-Water (2013). <https://www.unwater.org>
37. UNDESA (2014) World urbanization prospects: the 2014 revision, highlights. Report number: ST/ESA/SER.A/352
38. UNDRR (2015) Sendai framework for disaster risk reduction 2015–2030
39. UNESCO World Water Assessment Programme. <https://unesdoc.unesco.org>
40. UNISDR (2015) <https://www.preventionweb.net>
41. United Nations (2015) Transforming our world: the 2030 agenda for sustainable development. Report number: A/RES/70/1
42. Yu X, Jiang L (2009) Freshwater management and climate change adaptation: experiences from the central Yangtze in China. *Climate Dev*. <https://doi.org/10.3763/cdev.2009.0023>

Sustainability in Transportation Infrastructure: Perspective of CREATES, Rowan University



Deep Patel, Ahmed Saidi, Mohammad Jalayer, Daniel Offenbacher,
and Yusuf A. Mehta

Abstract This study presents an approach for improving sustainability in transportation infrastructure developed by the Center of Research and Education in Advanced Transportation Engineering Systems (CREATES) of Rowan University. This approach consists of two major research components: (a) transportation safety and management and (b) pavement construction materials and practices. First, the effectiveness of the Street-Smart New Jersey pedestrian safety campaign—a behavioral change awareness and a public education campaign were assessed so as to improve compliance with pedestrian and motorist laws. Video data were obtained in eight communities across the state of New Jersey in 2018–2019. The efficiency of the campaign was evaluated by comparing the rates of non-compliant pedestrian and driver behaviors before and after the campaign. The second research component focused on improving the performance of cold in-place recycling (CIR) mixtures using a balanced mix design (BMD) approach. Eight mixtures were prepared at different asphalt contents, compaction efforts, and curing processes. Laboratory testing was conducted to assess the resistance of CIR mixtures to pavement distresses (rutting and cracking) and to select optimum contents of asphalt binders at which the performance of these mixtures is optimal. Three mixtures were then selected to construct full-scale CIR sections using foamed asphalt in varied contents: 2, 3, and 4% by total mix weight, at a constant water content of 3%. All the sections were instrumented with asphalt strain gages, pressure cells, and thermocouples to evaluate the mechanistic responses of each section. A heavy vehicle simulator (HVS) was utilized to apply loading on the pavement sections using: (a) a truck tire with a 40 kN load and (b) an aircraft tire with a 100 kN load. Multiple field tests and visual inspections were carried out to determine: (1) rut accumulation using a surface profiler (2) the structural integrity using a heavy weight deflectometer before and after APT testing, and (3) cracking potential by assessing sensors' responses. Based on the outcomes of both research components, following the safety campaign can warrant

D. Patel · A. Saidi · M. Jalayer · D. Offenbacher · Y. A. Mehta (✉)

Department of Civil and Environmental Engineering, Center for Research and Education in
Advanced Transportation Engineering Systems (CREATES), Rowan University, Glassboro, NJ
08028, USA

e-mail: mehta@rowan.edu

considerable improvements in pedestrian and driver behaviors. In addition, the BMD approach can be used successfully to improve the resistance of CIR pavements to rutting and cracking.

Keywords Traffic safety and management · Cold in-place recycling · Balanced mix design approach · Laboratory performance · Accelerated pavement testing

1 Introduction

Sustainability is becoming a central component in the design and management of roadway infrastructure. In general, a sustainable transportation infrastructure ensures that all roadways meet societal needs and utilize resources effectively. More specifically, sustainable roadways consider the performance, environmental, social, and economic impacts in the decision-making process. The transportation industry offers an opportunity to improve sustainability from two perspectives: (i) traffic safety and management and (ii) construction materials and practices.

2 Traffic Safety and Management

Automobile crashes, including pedestrians, are a crucial roadway safety anxiety in New Jersey and across the USA. Although the rate of traffic fatalities has declined in the past twenty years, the percentage of pedestrian fatalities has risen as pedestrians continue to be extremely vulnerable roadway users. Within the year 2017, more than 85,000 pedestrian injuries and 5977 pedestrian fatalities were reported because of traffic crashes [1]. Almost a pedestrian was injured every eight minutes and killed every two hours in the course of a traffic collision, according to the National Highway Traffic Safety Administration (NHTSA). Looking at the percentage of pedestrian fatalities compared to the overall traffic fatalities, New Jersey ranks the second across the USA, with approximately 30% pedestrian fatalities [2]. Due to this high pedestrian fatality rate, Newark was assigned as the pedestrian safety-focused city and New Jersey as a pedestrian safety-focused state by the Federal Highway Administration (FHWA). In correspondence, the North Jersey Transportation Planning Authority (NJTPA) works together with private, community, and non-profit organizations in 2013 to pilot a Street-Smart NJ pedestrian safety program in five communities. Street-Smart NJ focused on educating the public, spreading safety awareness, and recording behavior change [3]. This study evaluates the effectiveness of a pedestrian safety campaign by comparing the rates of unsafe drivers and pedestrian behaviors before and after the pedestrian safety Street-Smart NJ campaign in several areas across New Jersey. The behaviors include drivers running red light signal or stop sign, drivers fail to stop for pedestrians when turning, drivers fail to stop before making a turn at a stop sign or red light, and pedestrian crossing against a signal

and unsafe crossing. Wherein, data from eight communities were measured and compared—Asbury Park, Woodbridge, Garfield, Newark, Morris Plains, Princeton, Rutherford, and Teaneck—in 2018–2019.

2.1 Method and Data

The site selection approach for the Street-Smart NJ campaign and the behavioral study was to find communities that could gain from an enhancement in pedestrian and driver behavior and may present quantifiable changes due to the campaign. Historical crash data, high crash locations, traffic and pedestrian volume, different population sizes of communities, wide range of geographical coverage of the region, and coordination with local communities were the factors considered for selecting the eight communities. An observational study was conducted to evaluate the campaigns' effectiveness in terms of changes in road users' behaviors. To do so, two types of data were collected: first, total counts of the non-compliant behavior incidents and (II) total counts of pedestrian and vehicles that were observed and have a chance to obey or disobey the traffic regulation.

The developed proxy measures provide an excellent opportunity to assess the non-compliant behavior and decide the applicable measure of exposure in each study area in the Street-Smart NJ campaign.

Proxy 1: Unsafe Crossing and Crossing against the Signal: A pedestrian begins crossing the street while the signal indicates “Don’t Walk” or crosses more than half of the street outside of the crosswalk. The measure of exposure is the overall number of pedestrians crossing the street [3–5].

Proxy 2: Turning Vehicle Fails to Stop for Pedestrian: A vehicle making a left or right turn at an unsigned intersection approach or at a green signal fails to stop for a pedestrian crossing parallel to the crosswalk. The measure of exposure is the overall number of right or left turning vehicles when pedestrians are approaching or crossing using a crosswalk so that turning vehicles have an opportunity to stop for pedestrians properly [3–5].

Proxy 3: Failure to Stop before Right Turn at Stop Sign or Red Signal: At an unsignalized intersections, a right turn vehicle fails to make a complete stop for pedestrians before making a right turn at a stop sign. The measure of exposure is the overall number of right-turning vehicles that approach the stop sign. For a signalized intersection, a right-turning vehicle fails to make a complete stop and stay stopped for pedestrians before making a right turn on red. The measure of exposure is the overall number of right-turning vehicles that approach the stop bar on a red signal because all cars should stop before proceeding, whether a pedestrian is present or not [3–5].

Proxy 4: Vehicles Running Stop Sign or Red Light Signal: At a vehicle unsignalized intersections, this proxy is a vehicle passing the intersection fails to make a

complete stop at the stop sign. For a signalized intersection, it is the sum of vehicles that enter the intersection and passed an intersection when the traffic signal is red. The measure of both unsignalized and signalized exposure is the total number of vehicles that enter the intersection [3–5].

2.2 Statistical Analysis

Assuming everyone who walks or drives through the intersection decides to disobey or obey traffic rules with some likelihood independent of other pedestrians and driver behavior. Based on the hypothesis, each pedestrian or driver who has a chance to be engaged in non-compliant behavior, i.e., unsafe behavior, will choose to disobey or obey traffic rules, following a Bernoulli (binary) process. To examine if a difference in the rate of non-compliant behavior is significant, the statistical evaluations verify whether or not it is possible to reject the null hypothesis that the behavior did not change. The essential formula to calculate the significance is as follows:

$$Z = \frac{\hat{\rho}_2 - \hat{\rho}_1}{\sqrt{\hat{\rho}(1 - \hat{\rho})\left(\frac{1}{n_1} + \frac{1}{n_2}\right)}} \quad (1)$$

$$\hat{\rho} = \frac{X_1 - X_2}{n_1 - n_2} \quad (2)$$

$$\hat{\rho}_1 = \frac{X_1}{n_1} \quad (3)$$

$$\hat{\rho}_2 = \frac{X_2}{n_2} \quad (4)$$

where n_1 is a count of pedestrian or vehicles observed in pre-campaign data; n_2 is a count of pedestrian or vehicles observed in post-campaign data; X_1 is the count of non-compliant incidents observed in pre-campaign data; X_2 is the count of non-compliant incidents observed in post-campaign data; $\hat{\rho}_1$ is a likelihood that a driver or pedestrian did not obey with the regulations in pre-campaign data; $\hat{\rho}_2$ is a probability that a driver or pedestrian did not obey with the rules in post-campaign data; and $\hat{\rho}$ is a extracted sample ratio or a combined average of likelihoods. The measured change in the rate of non-compliance is the difference of probability ($\hat{\rho}_2 - \hat{\rho}_1$). A negative value shows a reduction in the rate of pedestrian and drivers participating in unsafe behaviors, demonstrating enhancement in traffic safety. This study considered a significant level of 95% [3–5].

2.3 Results and Discussion

This study demonstrates an overall decrease in dangerous behaviors following the campaigns, and many of these reductions were statistically significant (Table 1).

In this study, Garfield's three-leg intersection was a signalized intersection, and a stop sign controlled the three-leg intersection in Woodbridge and Rutherford. The four-leg intersections at Teaneck, Asbury park, Princeton, and Newark are the signalized intersection. Lastly, the one five-leg interaction at Morris Plains is also a signalized intersection. Regarding the statistical significance, signalized intersection showed a significant reduction in non-compliant behavior for all four proxies. Table 2 represents the aggregated results for the signalized and unsignalized intersection for each proxy.

After the campaign, a significant decrease in non-compliant events among drivers and pedestrians was seen. However, the improvement in driver behavior was twice compared to pedestrian behavior. In terms of the overall evaluation, the impact of weather or temperature change could have played a vital role in these outcomes. For instance, an increase in unsafe pedestrian behavior could be seen due to cold weather because pedestrians try to rush in cold weather. On the other hand, drivers in adverse weather conditions incline to be driving more carefully that increase driver's safety compliance. Table 3 shows the difference in the rate of non-compliance behavior for drivers and pedestrians.

Inclusive, the observational study demonstrated noteworthy positive outcomes for the Street-Smart NJ intervention. The combined results from all measured communities exhibited a noteworthy decrease in non-compliant activities among pedestrians and drivers. In terms of the road user, 41% and 21% drop in non-compliant behavior of drivers and pedestrian, respectively. 60.3% decrease in drivers failing to stop before turning right on red or at a stop sign, 45.2% decrease in drivers running a red light or stop sign, 40% decrease in turning vehicle failing to stop for a pedestrian, and 21% decrease in pedestrians crossing against the signal or outside the crosswalk were evaluated. There were statistically significant enhancements for proxies 2, 3, and 4 at three-leg intersections and for all four proxies at four-leg intersections in terms of the intersection geometry. Also, there was significant decreases in proxy 3, 4 observed at five-leg intersections.

3 Sustainable Pavement Construction Materials and Practices

Sustainable construction materials and practices have been researched and discussed in an effort to reduce economic costs and natural resource usage. Generally, research has identified several technologies and methods to achieve more sustainable construction practices (Fig. 1), including the use of greater amounts of recycled materials, reduce energy usage through warm-mix asphalt (WMA) as standard practice, create

Table 1 Difference in the rates of non-compliant behaviors from the pre- to post-campaign [4, 5]

Grouping	Measure	Pre-campaign			Post-campaign			Change			Significance test
		Sample n_1	Non-compliant	Rate \hat{p}_2 (%)	Sample n_2	Non-compliant	Rate \hat{p}_2 (%)	%	$\hat{p}_2 - \hat{p}_1$	P-value	
3-leg intersections	Proxy 1	608	157	26	707	160	23	-12.4	-	0.089	Insignificant
	Proxy 2	279	100	36	298	60	20	-43.8	-	0.000	Significant
	Proxy 3	402	310	77	493	131	27	-65.5	-	0.000	Significant
	Proxy 4	3724	281	8	3996	216	5	-28.0	-	0.000	Significant
4-leg intersections	Proxy 1	4455	1277	29	3141	702	22	-22.0	-	0.000	Significant
	Proxy 2	1356	532	39	1208	284	24	-40.1	-	0.000	Significant
	Proxy 3	430	115	27	422	53	13	-53.0	-	0.000	Significant
	Proxy 4	17,415	248	1	16,679	115	1	-51.6	-	0.000	Significant
5-leg intersections	Proxy 1	134	50	37	111	31	28	-25.2	-	0.060	Insignificant
	Proxy 2	27	10	37	42	15	36	-3.6	-	0.456	Insignificant
	Proxy 3	58	29	50	18	5	28	-44.4	-	0.049	Significant

(continued)

Table 1 (continued)

Grouping	Measure	Pre-campaign			Post-campaign			Change			Significance test
		Sample n_1	Non-compliant	Rate \hat{p}_2 (%)	Sample n_2	Non-complaint	Rate \hat{p}_2 (%)	%	$\hat{p}_2 - \hat{p}_1$	P-value	
All Intersections	Proxy 4	7030	303	4	5577	94	2	-60.9	-	0.000	Significant
	Proxy 1	5197	1484	29	3959	893	23	-21.0	-	0.000	Significant
	Proxy 2	1662	642	39	1548	359	23	-40.0	-	0.000	Significant
	Proxy 3	890	454	51	933	189	20	-60.3	-	0.000	Significant
	Proxy 4	28,169	832	3	26,252	425	2	-45.2	-	0.000	Significant

Note Proxy 1: Unsafe Crossing and crossing against the signal, Proxy 2: turning vehicle fails to stop for pedestrian, Proxy 3: failure to stop before right turn at stop sign or red signal, and Proxy 4: vehicles running stop sign or red light signal

Table 2 Difference in rate of non-compliant behaviors based on intersection traffic control [4, 5]

Traffic control	Proxy 1 (%)	Significant Test	Proxy 2 (%)	Significant Test	Proxy 3 (%)	Significant test	Proxy 4	Significance test
Signalized	- 21.5	Significant	- 37.8	Significant	- 55.0	Significant	- 59.7	Significant
Unsignalized	- 8.4	Insignificant	- 50.7	Significant	- 22.1	Significant	- 16.5	Significant

Table 3 Difference in rates of non-compliant behaviors from the pre- to post-campaign at all intersections [4, 5]

Road users	Change of non-compliant behavior (%)	Significance test
Driver	- 41	Significant
Pedestrian	- 21	Significant

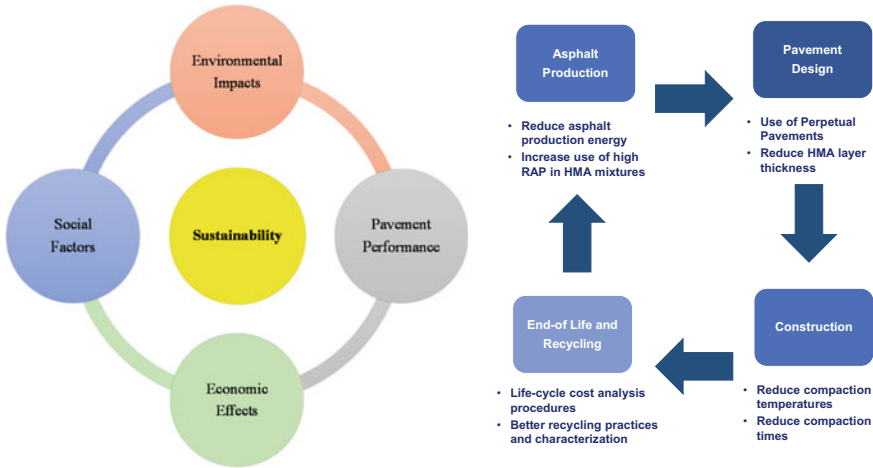


Fig. 1 Key factors of pavement sustainability and selected approaches to improve the sustainability of asphalt pavement materials and practices

longer-lasting pavements through the concepts of perpetual pavements, optimize construction design and techniques, and more frequent use of pavement preservation rehabilitation. In many cases, these topics, among others, have proven efficient performance and greater sustainability but have not been widely adopted due to remaining gaps in research. This chapter highlights a research approach taken at Rowan University’s Center for Research and Education in Advanced Transportation Engineering Systems (CREATEs) that explored several aspects of an emerging sustainable pavement rehabilitation technique.

In an effort to improve the sustainability of pavement rehabilitation and management, an extensive research study on cold in-place recycling (CIR) was conducted at Rowan University CREATEs. CIR is a rehabilitation technique of deteriorated asphalt pavements using reclaimed asphalt pavement (RAP), recycling agent (e.g., foamed asphalt), and/or chemical additives (e.g., Portland cement) at ambient temperatures [6]. In the past, this construction practice has been successfully used for rehabilitating low, medium, and high-volume roadways. CIR technology can effectively treat different types of pavement distresses such as ruts, cracks, and potholes [7–9]. Although extensive research had been conducted on CIR, limitations regarding mix design, performance considerations, and economic impacts were unfounded. Therefore, additional research was needed to further research CIR mixes, design methods,

performance, and economic benefits. Rowan University CREATEs instituted a comprehensive research approach that was structured in four stages:

- *Stage 1:* Develop a novel mix design procedure for CIR that can be widely implemented.
- *Stage 2:* Assess the accuracy of the novel mix design procedure using laboratory testing under various conditions.
- *Stage 3:* Verify the novel mix design procedure and laboratory results using full-scale accelerated pavement testing.
- *Stage 4:* Determine the economic, energy, and environmental benefits of using CIR based on the developed mix design and performance.

3.1 CIR Laboratory Research Studies (Stage 1 and Stage 2)

The initial goal of the CIR research study was to develop a novel mixture design procedure for CIR mixtures. For this, CIR mixtures considering different forms of CIR pavements: two asphalt binders (emulsion and foamed asphalt) and compacted at two compaction efforts (30 and 70 gyrations) using a superpave gyratory compactor (SGC). All the CIR mixtures were produced at constant contents of water and cement of 3% and 1% by total weight, respectively, similar to those used in literature. The curing process consisted of placing the compacted CIR specimens in an oven at two temperatures (10 and 60 °C) for 72 h. A novel CIR mixture design procedure was developed following a performance-balanced mixture design (BMD) approach. Asphalt pavement analyzer (APA) and dynamic complex modulus ($|E^*|$) tests were used to assess the rutting performance of CIR mixtures, while indirect tensile strength (ITS) and semi-circular bend (SCB) tests were used to evaluate the cracking resistance of these mixtures. From this study, the developed BMD procedure was used successfully for selecting optimum contents of emulsified and foamed asphalt for CIR mixtures. The final optimum recycling agent contents varied between 2.6 and 3.2% by total mix weight [10].

To further explore the influence of CIR components (recycling agent type, compaction effort, and curing process) on the rutting and cracking performance, a secondary laboratory research study was conducted on different CIR mixtures prepared using the developed BMD approach (Phase 1). Laboratory performance tests were conducted, including rutting performance tests—APA and dynamic $|E^*|$ test—and cracking performance tests—ITS and SCB tests. Statistical analysis was performed on the CIR performance measures using ANOVA to identify the impact of different CIR properties on each performance measure. Results showed that higher compaction level or/and higher curing temperature led to increased rutting resistance in both emulsion and foamed asphalt CIR mixtures. Finally, it was also found that CIR mixtures prepared with emulsion presented cracking resistance than the ones prepared with foamed asphalt [11].

3.2 CIR Accelerated Pavement Testing (APT) Research Study (Stage 3)

Based on the results of laboratory performance analyses of CIR mixtures (Stages 1 and 2), full-scale field testing of CIR mixtures using the novel BMD was warranted. Thus, three full-scale CIR test sections were designed and constructed at the Rowan University Accelerated Pavement Testing Facility (RUAPTF). All three sections were constructed using CIR mixes prepared with a foamed asphalt binder (PG 64-22). Different foamed asphalt contents were used for each of the CIR mixes used to construct the full-scale sections: 2, 3, and 4% (by total weight) to assess the accuracy of the BMD process. No cement was added into the CIR mixes to isolate the effect of CIR asphalt content on performance. Pavement sensors such as asphalt strain gages, pressure cells, and thermocouples were embedded within each section to evaluate the traffic responses. A heavy vehicle simulator (HVS) was used to simulate traffic loading on each full-scale pavement section. Conventional single-axle truck traffic (40 kN) was applied to each section. The traffic loading was then accelerated through the application of higher loading (100 kN). As accelerated loading was applied, a number of field tests and visual inspections were performed to determine: (1) permanent deformation using a surface profiler (2) heavy weight deflectometer before and after APT, and (3) visual cracking inspection. The results showed that the CIR section with 3% binder content presented the highest cracking resistance under repeated truck and aircraft loading verifying the previous laboratory findings [12].

3.3 CIR Economic and Environmental Research Study (Stage 4)

After evaluating the performance benefits of CIR from both laboratory and field testing, there was a need to determine the economic and environmental benefits of using CIR to facilitate greater interest and broader implementation. Therefore, the focus of the final research study was to compute and compare the construction costs, energy usage, and environmental benefits of using CIR as a pavement rehabilitation technique. For this effort, the costs of using emulsified CIR (CIR-E) and foamed asphalt CIR (CIR-F) mixes were compared to conventional two-inch HMA mill and overlays. Construction costs, energy consumption, and environmental (greenhouse gas) emissions were compared for each pavement rehabilitation technique. An equivalent pavement structure was used for the pavement rehabilitation comparisons based on the AASHTO 1993 design method. Results of the study showed reduced initial construction costs of using CIR compared to conventional HMA mill and overlay. Energy savings of up to 63% were also found when using CIR mixtures compared with the HMA mill and overlay. Overall, when considering all costs, cost savings of approximately \$34,000–\$39,000 per lane mile were observed when using CIR with

HMA overlays and total cost savings between 41 and 47% over traditional HMA mill and overlays [13].

4 Conclusion

This study provides a description of two research approaches for improving sustainability in transportation infrastructure based on the perspective of CREATES, Rowan University. The first research approach presents an observational evaluation of the Street-Smart NJ pedestrian safety intervention. In order to examine the effectiveness, the campaign, before and after campaign data collection were conducted in the selected communities. Based on the statistical analysis results, pedestrian intervention showed extensive success in major areas, however not entirely so. To be particular, urban intersections with heavy traffic flow (e.g., Newark) exhibited more coherent enhancements in safety performance as an outcome of education and enforcement compared to suburban locations (e.g., Garfield) with lower traffic volumes. Also, the changes to the three-vehicle behavior proxies improved across almost all sites when the observations are considered collectively. The data confirmed that the Street-Smart NJ program methodology demonstrated success in reducing risky behaviors among drivers and pedestrians. This study is constrained by the fact that changes in observed behaviors were evaluated, and the eventual effect on safety depends on the extent to which these behaviors are correlated with pedestrian safety and crash risk. The findings of this research sustain that programs associated with education and enforcements activities such as Street-Smart NJ pedestrian safety campaign can be useful in supporting engineering safety advancements. Such achievement calls attentions toward the importance of implementing high-level systemic solutions in combination with fine-tuned engineering solutions at such communities.

The second research approach taken to assess the sustainable construction material was innovative in that it started with small laboratory tests and expanded—(i) identified a novel approach to sustainable materials, (ii) verified the novel approach with small-scale laboratory testing, (iii) verified it with full-scale field performance, and (iv) quantified and presented the benefits of using more sustainable material. The final stage (Stage 4) was imperative to this approach because it provided realistic information regarding the physical cost savings and environmental impact of using the more sustainable material. Although this research process cannot be followed in all cases, the tiered approach taken in this study provided an economical and efficient way of researching sustainable construction materials and practices.

References

1. Governors Highway Safety Association (GHSA) (2019) Pedestrian traffic fatalities by state. Available online <https://www.ghsa.org>
2. National Highway Traffic Safety Administration (NHTSA) (2018) State of New Jersey highway safety plan. Available online https://www.nhtsa.gov/sites/nhtsa.dot.gov/files/documents/new_jersey_fy2018_hsp.pdf
3. North Jersey Transportation Planning Authority (NJTPA) (2019) Street smart New Jersey observational pedestrian safety study: final report. Street smart. Available online https://bestreetsmartnj.org/wp-content/uploads/2019/08/NJTPA-Observational-Final-Report_08122019.pdf
4. Jalayer M, Patel D, Szary P, Hamas K (2020, Aug) An observational analysis of pedestrian safety campaign: a case study in New Jersey. In: International conference on transportation and development 2020. American Society of Civil Engineers, Reston, VA, pp 182–193
5. Patel D (2020) Evaluating the effectiveness of the pedestrian safety intervention program: behavioral and observational approach
6. American Association of State Highway and Transportation Officials (AASHTO) (1998) Report on cold recycling of asphalt pavements. AASHTO-AGC-ARTBA joint committee task force 38 report. American Association of State Highway and Transportation Officials
7. Forsberg A, Lukanen E, Thomas T (2001) Blue earth county CSAH20—an engineered cold in-place recycling project. Transportation Research Board, Washington, D.C.
8. Fiser J, Varaus M (2014) Cold recycling of pavements in the Czech Republic. Czech Republic, Department of Roads
9. Mondarres A, Rahimzadeh M, Zarrabi M (2014) Field investigation of pavement rehabilitation utilizing cold in-place recycling. *Resour Conserv Recycl* 83:112–120
10. Saidi A, Ali A, Lein W, Mehta Y (2019) A balanced mix design method for selecting the optimum binder content of cold in-place recycling asphalt mixtures. *Transp Res Rec* 2673(3):526–539
11. Saidi A (2019) Laboratory evaluation of cold in-place recycling asphalt mixtures using a balanced mix design
12. Saidi A, Ali A, Mehta Y, Cox BC, Lein W (2020) Full-scale evaluation of balanced cold in-place recycling (CIR) asphalt mixtures using a heavy vehicle simulator. In: Accelerated pavement testing to transport infrastructure innovation. Springer, Cham, pp 339–347
13. Offenbacher D, Saidi A, Ali A, Mehta Y, Decarlo C, Lein W Forthcoming “economic and environmental cost analysis of cold in-place recycling”. *J Mater Civ Eng*. [https://doi.org/10.1061/\(ASCE\)MT.1943-5533.0003610](https://doi.org/10.1061/(ASCE)MT.1943-5533.0003610)

Applications of Ground Penetrating Radar—A Comprehensive Case Study



P. Senthil, Alex Varughese, Hari Dev, and S. L. Gupta

Abstract Ground penetrating radar (GPR) is used to obtain subsurface information based on the properties contrast in the medium. GPR is generally employed for detecting underground utilities and can be used for applications such as subsurface stratigraphy, archaeology, forensics and detecting reinforcements. In this paper, comprehensive case study on GPR covering applications of four cases in utility detection for trenchless drilling and excavation; two cases in depth of rock for estimating constructing materials and foundations; and two cases in dam health monitoring are discussed. Penetration depth and resolution depend on frequency of EM waves generated by antenna. The use of different frequency antenna for each application is emphasised. Methodology adopted for GPR scanning upstream vertical face of dam and downstream face of dam was given. GPR was effectively employed to locate utility, estimate depth of overburden, and thickness of masonry and its homogeneity in the old ageing dams.

Keywords GPR applications · Dam health monitoring · Utility survey · Antenna frequency · Depth to bed rock

1 Introduction

Ground penetrating radar (GPR) survey is non-invasive geophysical techniques for locating the buried objects. It is also extensively used in geological application (delineation of bed rock profile), dam health monitoring (i.e. to investigate the continuity of medium), civil engineering (roads, bridges and reinforcement scan), archaeology and forensics applications. GPR survey produces two-dimensional section of subsurface without any drilling or trenching. Large area can be covered in short time with

P. Senthil (✉) · A. Varughese · H. Dev · S. L. Gupta
Central Soil and Materials Research Station, New Delhi 11016, India
e-mail: senthilcsmrs@gmail.com

use of GPR survey. It can be used for the following three major civil engineering applications.

- (a) Underground utility survey
- (b) Delineation of bed rock profile
- (c) Dam health monitoring / diagnostics investigation.

2 GPR—Principles

GPR is a technique based on the principles of RAdio Detection And Ranging (RADAR) to measure the location and size of targets buried in visually opaque material [1]. GPR injects electromagnetic waves (EM), typically in the range of 25–2500 MHz into the medium, from transmitting antenna. When EM wave encounters the interface of other medium having contrast in electrical properties, part of wave gets reflected back to the receiver antenna and remaining is transmitted into deeper medium. The radar system will measure the time elapsed between transmission and arrival of waves. In reality, the GPR (antenna) is moved along a profile and time elapsed is recorded with short intervals. Unit of measurement for travel time in GPR is “nanoseconds”. Continuous record of signals produces two-dimensional subsurface section along a profile. Subsurface velocity of EM wave is to be estimated and given as input for determining the depth of objects having contrast in electrical properties.

The penetration depth and resolution of GPR depend on the electrical properties of medium and antenna frequency used. The penetration depth of EM waves in ice medium is maximum; i.e. few hundred metres, whereas in clayey soil, the penetration depth is limited to few centimetres only.

$$\text{Interface depth} = \text{two-way travel time} \times \text{velocity} / 2 \quad (1)$$

Generally, the range of two-way travel time setting required varies from 10 to 500 ns. Relative permittivity of the subsurface material (soil, rock, concrete or any other) governs the velocity of electromagnetic wave. Relative permittivity (E_{rm}) is the ratio of the permittivity of the material (E_m) divided by the permittivity of air (E_o), or

$$E_{rm} = E_m / E_o \quad (2)$$

Relative permittivity for air and water is 1 and 81, respectively. EM velocity in material is determined from the following equation:

$$\text{Velocity through medium} = \text{EM wave velocity in air} / \sqrt{E_{rm}} \quad (3)$$

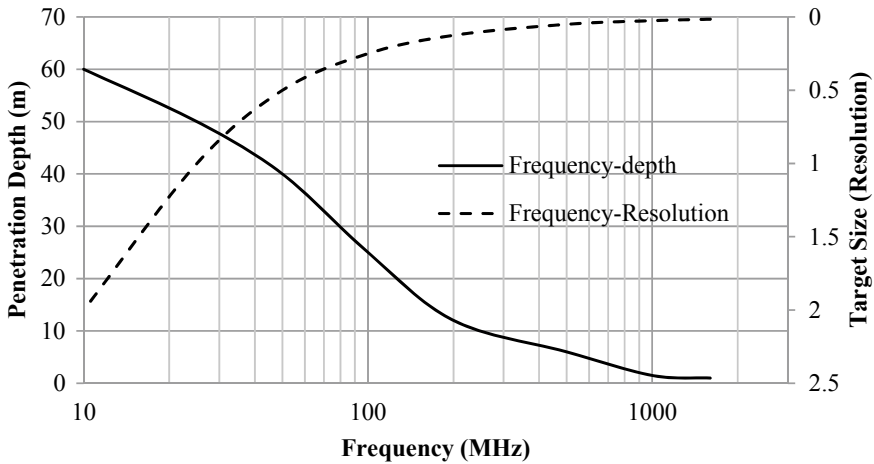


Fig. 1 Frequency-resolution-penetration depth chart (penetration depth is also affected by the medium where GPR survey is employed)

EM wave velocity in air and water is 0.305 m/ns and 0.034 m/ns, respectively. The values of relative permittivity and EM wave velocity for selected materials can be found in Davis and Annan [2].

Lower-frequency (≤ 100 MHz) antenna gives higher penetration depth but lower resolution and higher frequency antenna (≥ 500 MHz) give lower penetration depth but high resolution. The typical frequency-depth-resolution plot is shown in Fig. 1.

3 Underground Utility Survey

Following are the typical examples where GPR was employed for detection of underground utilities including water supply line, sewer, cavity, cable and tunnels. GPR survey will facilitate in taking preventive action so that these utilities may not cause hindrance during construction. In general, antenna frequency used for the utility detection purpose was 300 MHz.

3.1 Four Crossings at New Delhi

Mahanagar Telephone Nigam Ltd. (MTNL) proposed to lay communication cables across important crossings in New Delhi using trenchless technology in 1998. It was essential to locate underground utilities at that location in order to lay cables at convenient depth. Due to heavy traffic during day time, the filed work was carried out

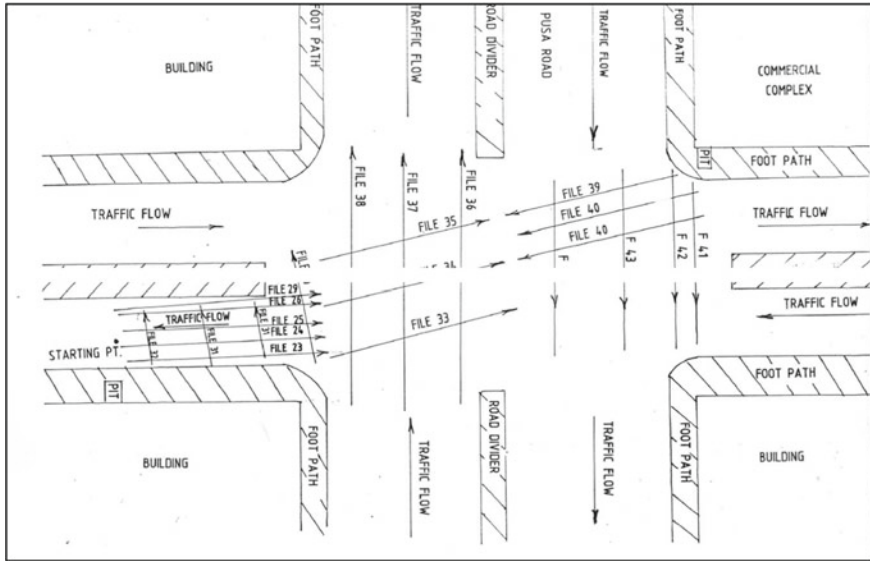


Fig. 2 GPR survey map of four crossing at Pusa Road, Delhi

during night time [3]. A 300 MHz antenna was employed for scanning of underground utilities at following locations:

- (a) **Puchkuian road:** Overall 20 profile lines were surveyed including 9 lines across the road and remaining along the road.
- (b) **Pusa road:** Overall 20 profile lines were surveyed including 9 lines across the road. The profile map is shown in Fig. 2.
- (c) **DB Road:** Total 15 profile lines were surveyed.
- (d) **Park street:** Total 12 GPR lines were surveyed including 4 lines across the road.

Based on GPR survey, 2 m depth of clear zone was identified for carrying out cabling work.

3.2 Punjabi Bagh Crossing

Public Works Department, Delhi, took up construction work of flyover at Punjabi Bagh crossing, New Delhi. GPR survey was conducted using 300 MHz antenna to find out utilities upto 3.5 m below ground level at crossing before excavation [4].

Based on GPR survey, the presence of pipes at a depth between 0.5 and 1.5 m was detected and mapped for taking precautionary measures during excavation.

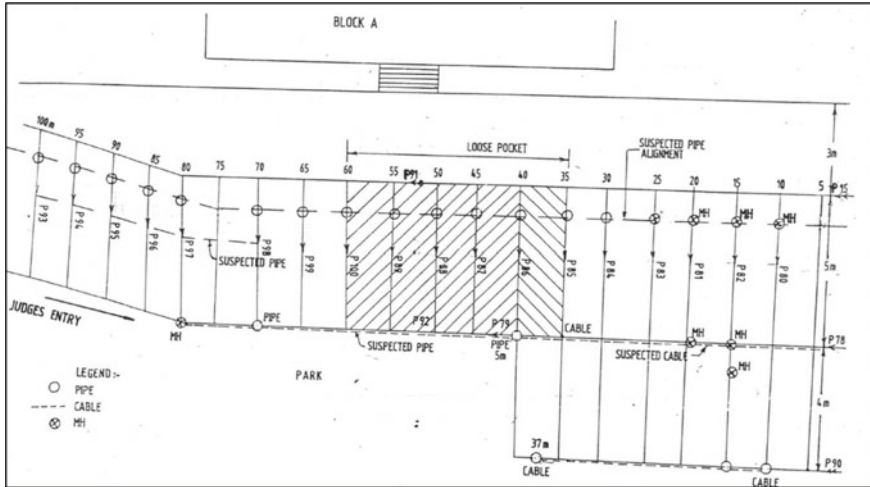


Fig. 3 GPR survey map of underground parking at Delhi High Court

3.3 Underground Parking at Delhi High Court

GPR survey was conducted at the construction site of basement parking for additional court building at Delhi High Court, New Delhi. GPR was towed manually in grid pattern of 10×5 m with target depth of 5 m. Twenty-four profile lines covering 328 m total length were surveyed. A loose pocket from 35 to 60 m (P85–P100) as shown in Fig. 3 was detected at 4.5 m depth from ground level. A pipe passing along road at a depth of 1.6 m was also detected [5].

3.4 Construction Site of Boys Hostel “D”, IIT Delhi

GPR survey was carried out at boys Hostel “D” site near existing Satpura hostel in the premises of IIT, Delhi. The land was fairly even, and the number of manholes was existed in the survey area. Monostatic 300 MHz antenna was used for underground utility survey [6].

GPR was towed manually at 5 m interval in both the directions forming 5×5 m grid. Total of 25 profile lines covering 850 m length of survey were carried out at the site. On perusal of GPR records, sewer line passing parallel to the boundary wall of DG shed and water reservoir were detected at 4 m depth. Also, an electrical cable passing at 0.6 m below was detected, and the same was visible at point of excavation.

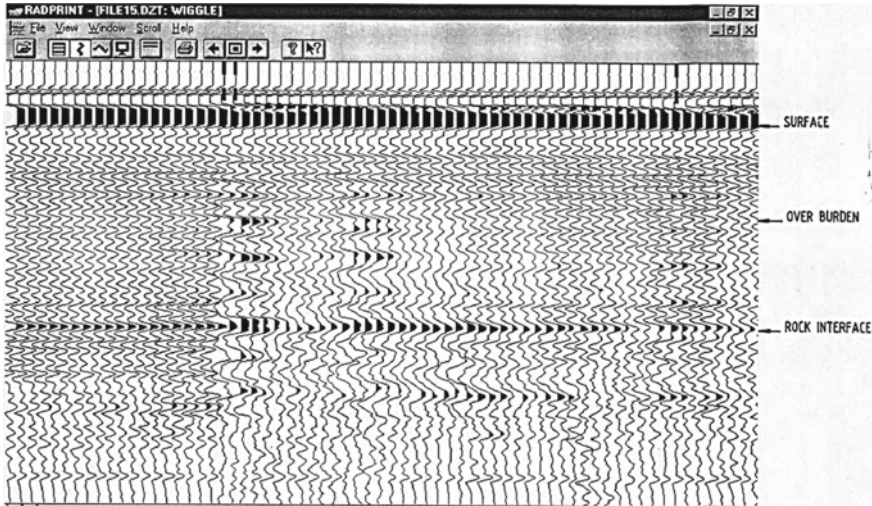


Fig. 4 GPR wiggle trace showing bedrock in Asena quarry area survey

4 Delineation of Bed Rock

4.1 Tehri Project, Uttrakhand

Tehri Dam is the highest dam in India, i.e. 260.5 m high earth and rock fill dam built across Bhagirathi River, a tributary of Ganga River. It has created submergence of 42 km² with storage capacity of 3450 MCM. The water stored is being served for irrigation, water supply and hydro power generation.

GPR survey was conducted using 80 MHz antenna in Asena quarry for the assessing the overburden thickness [7, 8]. This quarry was proposed to obtain rip-rap material. GPR survey was conducted for five profiles at different locations for a total length 130 m. The quarry area was 22,000 m² (200 m × 110 m) between EL 950.0 and 1100.0 m. The depth of overburden in the estimated was 18 m, and in some portion, it ranged from 12 to 18 m. GPR wiggle trace for one profile is shown in Fig. 4.

The quantity of rip-rap material was estimated based on the GPR survey at Asena quarry site.

4.2 Ganvi Hydroelectric Project, Himachal Pradesh

Ganvi Hydroelectric Project generates 22.5 MW by utilising 7.25 m³/s discharge of River Ganvi, a tributary of River Sutluj. GPR was used during construction of this project to estimate the depth to bed rock at anchor blocks in the penstock alignment.

The diameter and length of the penstock are 1.4 m and 600 m, respectively. GPR survey along with seismic refraction survey was carried out for determining bed rock profile.

GPR survey carried out on sloping terrain and bed rock profile along penstock alignment was mapped for locating foundation of anchor blocks [9].

5 Dam Health Monitoring/Diagnostics Investigation

GPR survey also employed to identify cracks, cavities and damages in the dam body. The survey can predict the stratigraphy of the dam body material based on properties contrast. Case studies of GPR surveys in diagnostic investigations of old dams are presented below. Apart from GPR, geophysical methods like seismic refraction survey, resistivity imaging and tomography techniques can be employed for dam diagnostics investigations [10].

5.1 Mulla Periyar (Baby Dam)

The Periyar Reservoir Project was designed and executed by Col. John Pennycuik to divert west flowing River Periyar to the east to extend irrigation in the Vaigai basin. The main dam is solid masonry gravity dam 56.64 m height and 366 m length. Adjacent to main dam, in order to plug the saddle, a baby dam of 16 m height, 75 m length also constructed with rubble masonry.

GPR survey was carried out on the dam body to locate the presence of voids/cavities, if any, in the structures using 80 MHz (on dam top), 300 MHz (downstream face) and 500 MHz (upstream face) frequency antennas [11].

Top of dam: 80 and 300 MHz antenna were utilised for conducting GPR survey on dam top with 2 m interval along dam axis. The depth of observation was 18 m.

Upstream face of dam: A total of 24 survey lines using 500 MHz antenna were conducted on downstream face at regular intervals. The GPR profiles lines are shown in Fig. 5.

Downstream face of dam: Antenna with 500 MHz frequency was tied with the coir rope and pulled from bottom to top, ensuring proper contact with upstream face of dam. The observations were made at 5 m interval initially. Further, dam was scanned using 500 MHz antenna at 2 m interval. Total of 24 survey lines using 500 MHz antenna conducted on downstream face at regular intervals.

The GPR survey indicated absence of any cavity on the dam body. Further, integrity and homogeneity of dam were ascertained. The thickness of masonry on upstream face varied from 1.25 m (top) to 1.75 m (bottom); whereas on downstream face, it varied from 1.75 to 1.5 m in slope portion and 1.25–1.0 m in vertical portion.

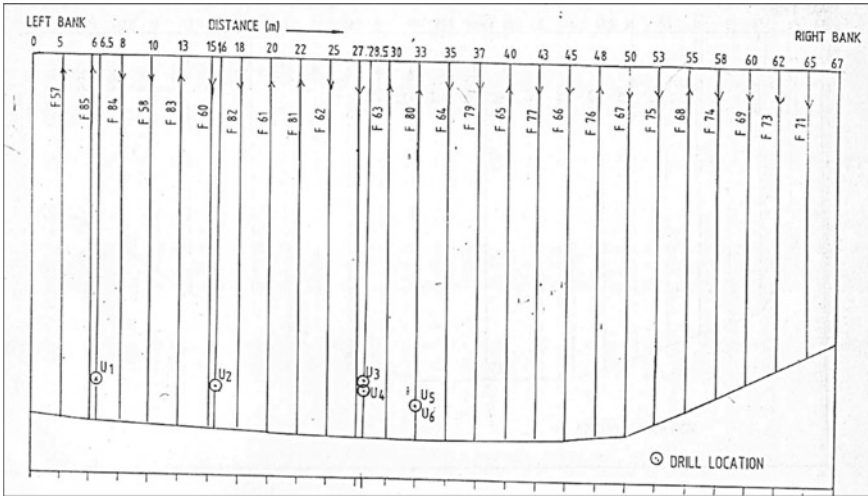


Fig. 5 GPR profile lines in upstream face of Baby dam (Mulla Periyar), Tamil Nadu

5.2 Lower Jhelum H.E. Project

The Lower Jhelum Project components includes dam, water conductor system of 8750 m length and power house housing three turbine of 35 MW each. The dam is built across River Jhelum in Baramullah District of J&K is located on the Jhelum River at Gantamulla in Baramullah District of Jammu and Kashmir. Power generation at this project was stopped due to sudden collapse of trash rack. It was suspected that collapsed piers might have damaged the upstream face of dam.

GPR survey was conducted on upstream face of dam using 500 MHz antenna with penetration depth of 2 m [12]. The antenna was tied with coir rope and was pulled from bottom to top ensuring the proper contact with upstream face of dam. A total of 20 profile lines were scanned at spacing of 1.5/2.0 m interval. The photograph of GPR scanning on upstream face of dam is shown in Fig. 6. Based on the GPR survey, the presence of cavity or damaged portion was ruled out on the upstream face of dam.

5.3 Matatila Dam Project

Matatila Dam is earthen dam with stone masonry having 6.3 km length built across the River Betwa. The project serves as multipurpose for water supply, irrigation and hydro power. The spillway section of length and height is 490 m and 45.7 m, respectively. The project installed capacity is 3×10.2 MW.



Fig. 6 Photograph of GPR scan on upstream face of Lower Jhelum Dam

The GPR survey was carried out to demarcate leakage points in dam body around a water supply intake pipe of 35 cm diameter [13]. Total of 42 profile lines using 80 MHz frequency antenna were conducted across and along the dam axis. The GPR profile along with intake pipe alignment is shown in Fig. 7. No anomaly indicating leakage through dam body was detected.

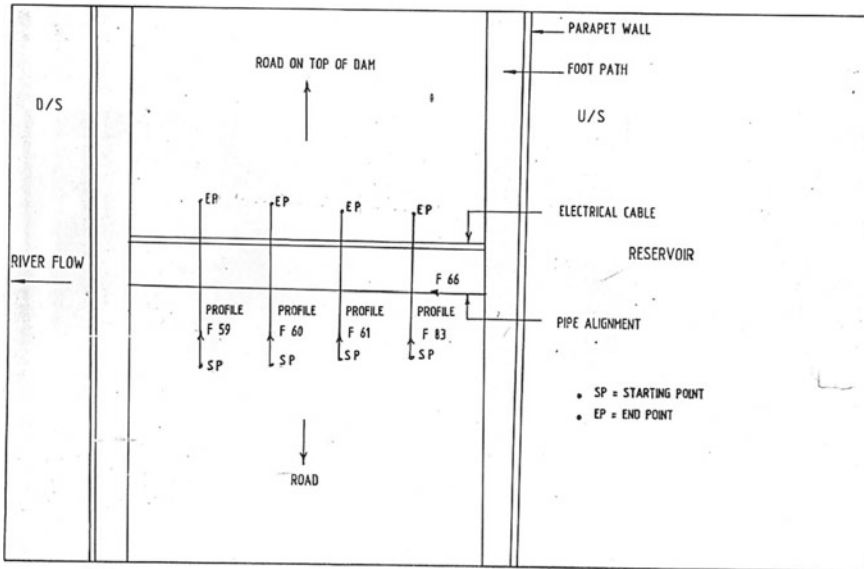


Fig. 7 GPR profile lines in Matatila Dam, Jhansi, Uttar Pradesh

6 Summary

Based upon the case histories of GPR applications in underground utility scan, delineation of bed rock profile and diagnostics investigations of old dams, the following are inferred;

- GPR survey can be used for detection of any buried utility for laying cable using trenchless technology and planning excavation for construction of new buildings. Mostly 300 MHz frequency antenna was used, and depth of investigation was less than 5 m.
- GPR can be employed for delineation of bed rock profile for locating foundation and also for estimating the quantity of construction materials. Generally, 80 MHz frequency antenna was used and depth of investigation was about 25 m.
- GPR was also successfully employed for finding the integrity and homogeneity of dam. The GPR investigations assisted in judging the thickness of masonry on upstream and downstream faces of old dams. The integrity of upstream faces of dam was scanned using 500/300 MHz frequency antenna with penetration depth of 3 m. Interior body of dam was scanned through 80 MHz frequency antenna, and the depth of investigation is about 20 m.

Overall GPR methods proved to be a successful tool in number of applications, and its use can be extended to all its civil engineering applications.

Acknowledgements Author wants to thank Director, CSMRS for granting permission to publish this paper. The case studies presented in this paper are compilation of work done by CSMRS, and their contribution is highly acknowledged.

References

1. Daniels D, Utsi EC (2015). GPR case histories and known physical principles. In: Proceedings of 7th international workshop on ground penetrating radar IWAGPR
2. Davis JL, Annan AP (1992) Ground penetrating radar for high resolution mapping of soil and rock stratigraphy. *Geophys Prospect* 37:195–207
3. CSMRS (1998) EG-I/98/1. Report on ground penetrating radar at four crossings. New Delhi
4. CSMRS (2000) EG-I/2000/5. Report on ground penetrating radar survey at Punjabi Bagh crossing
5. CSMRS (2004) 3/EG/CSMRS/E/08/2004. Report on ground penetrating radar survey of construction site of underground parking at Delhi High court
6. CSMRS (2006) 3/EG/CSMRS/E/12/2006. Report on GPR survey at construction site of boys hostel “D” near existing Satpura hostel at Indian Institute of Technology, Delhi, New Delhi
7. CSMRS (2004) 5/EG/CSMRS/E/09/2004. Report on ground penetrating radar survey of Asena Quarry Site Tehri HEP (Uttaranchal)
8. Khanna R, Gupta SL (2012) Role of ground penetrating radar for site investigations and site characterization—case studies. In: Proceedings of Indian geotechnical conference, Paper A-106
9. Varughese A, Khanna R (2017) Geophysical investigations using ground penetrating radar (GPR) for hydroelectric projects. *Water Energy Int* 60
10. Rana S (2017) Integrated geophysical approach for dam health checks and dam condition monitoring. *J Geophys* XXXVIII(1):63–67
11. CSMRS (2000) EG-I/2000/4. Field and laboratory investigations carried out on the baby dam of Mulla Periyar, Tamil Nadu
12. CSMRS (2002) EG/2002/3. Report on geophysical investigations using ground penetrating radar at lower Jhelum HEP in Jammu and Kashmir
13. CSMRS (2003) CSMRS/EG/2003/1. Report on ground penetrating radar survey and under-water scanning of upstream face using ROV at Matatila Dam Project-Jhansi (UP)

Risk Assessment of Pune Metro Underground Construction Using Risk Matrix and Expected Monetary Value



Shubhangi S. Wagh and Sandeep Potnis

Abstract Many complexities can be observed in the construction of tunnels for Pune metro (the second-largest city in the state of Maharashtra, India). It inherently involves many risky activities like excavation and lining, transportation of material, scaling and mucking, ventilation, cutter head intervention of tunnel boring machine (TBM) in compressed as well as in open mode, handling of tunnel machinery, working in narrow space, overloading of the crane, temporary segment dismantling, etc. Although tunneling for metro rail is risky, the risk involved is more in the longer tunnels. To save valuable resources and winning the trust of the client, risk assessment for each activity during tunnel construction is crucial. The expository literature review indicates that very few studies are available on risk assessment of each activity of tunnel construction in India using TBM. This study presents a case study on risk assessment of underground construction for the Pune metro. The work provides an insight into risk which occurs during the construction and describes general consideration for the uncertainties during execution. The paper provides the qualification and quantification for the risks in metro tunnel using risk matrix and expected monetary value (EMV) analysis. The risk matrix is the most effective tool for risk assessment and qualitative risk analysis. And EMV is succeeded using recommendations accessible in the literature of domain of risk management. Though it is a straightforward method, it is a productive application for the quantification to accomplish the goals of the metro tunnel project in terms of controlling the time delay and cost overrun as well. After the qualification of the risk process, quantitative assessment can be done for the further elected majors to choose the suitable reaction schemes. To manage the risk-associated cases efficiently. TBM data has been taken into account for risk assessment.

S. S. Wagh

Research Scholar, Dr. Vishwanath Karad MIT World Peace University, Pune, MAHARASHTRA 411038, India

S. Potnis (✉)

Professor and Head, Tunnel Engineering Program, Dr. Vishwanath Karad MIT World Peace University, Pune, MAHARASHTRA 411038, India

e-mail: sandeep.potnis@mitwpu.edu.in

Keywords Metro tunnel · Tunnel boring machine (TBM) · Risk matrix · Expected monetary value (EMV) · Time delay · Cost overrun

1 Introduction

Pune metro rail project contract underground construction (UGC)-1 comprised the construction of twin-bored tunnels, ramp, and cut and cover tunnels, cross passages, and two underground stations. The total length of TBM tunneling for Pune metro underground construction is approximately 4.73 km including both tunnels. As the compacted basalt is present in the soil strata of the Pune city, the earth pressure balance (EPB) type of tunnel boring machine having diameter of 6.61 M is used for the construction of underground metro twin tunnel. According to the International Association of Engineering Insurers (IAEI), a financial loss of higher than 50 million euros was experienced in the worlds' 18 biggest tunneling projects from 1994 to 2005 because of underground construction misfortunes (Bluckert et al. 2006). Due to limited prior knowledge of geotechnical ambiguity, there is a provocation of sustainable safety throughout the complete tunneling project with no delays or no cost overrun. The risks are frequently attached to some type of recommendation. Tunneling works to manipulate risk for all parties which are not directly involved in the project. Because of the intrinsic unpredictability of ground (Subsoil) and the presence of appreciable groundwater, there may be remarkable cost overhead and time overrun risks along with some environmental risks. Along with these due to spectacular underpass collapses and other catastrophes recently, there is a probability of huge no. of misfortunes at the time of tunneling work. Project risk is the unresolved matter or circumstances that if it occurs, have a positive or negative impact on project goals. The successive indicators of the construction management systems are including finalizing the project with cost features and time features, within the decided cost and time and also within the required quality, safety, and environmental criteria. Accurate estimation and schedule must be categorizing in contemplation of intersecting the overall cost and time boundaries of the project. There are many circumstances where there could be a hindrance in activities, whether they are within a limit to the critical path or not, which results in delay in the overall project period. These time overruns will accordingly have an adverse effect on the quality, cost, and also on the safety of the project.

2 Literature Review

Risk is the maneuver of measurement of likelihood, intensity, and manifestation to all hazards for an activity. There are always the chances of failure in the execution of planned activities in infrastructure projects. So, the project risks affect the chances of occurrences of unknowing of the technical, scheduler, and budgetary outcomes.

One researcher named Williams and Dorofee [1] had worked on growing methods by which risk management can be put into the practice. The observed risks should be divided into different categories, to facilitate the decision making about risk response strategies. Several researchers like, Johnson and Rood, and Ashley [2, 3], have classified risks on the basis of various parameters. According to Roetzheim [4], the probability of recognized risks can have a value with a range between 0 and 1 which indicates 0 or 100% chance of happening. However, on the other hand, the priority connected with every risk origin from some work package/ activity is always equal to 1. Repetition of events and weight is always proportional to the cumulative likelihood factor (CLF). A number of variations of risk management approach have been proposed by different authors and researchers. According to Jamal and Kaith [5], risk management can be divided into four activities: risk identification, risk Analysis and evaluation, response management, and system administration. Royer [6] has pointed out that “unmanaged or unmitigated risks are one of the primary causes of project failure”; hence, risk management is the crucial step of project management. Hillson [7] has shown that for clear understanding and management of the risks, the risk management is an activity aimed at identification and assessment of the risks.

Lack of effective risk management can lead to delay of projects, budget over run, and missing the critical performance targets. Soren [8] also pointed out that there can be any combinations of these troubles. He has given guidelines for tunneling risk management at pre-construction, construction, and operation phase of the tunnel project. The most important step in the process of risk management is the identification of risk. All the potential hazards, which may adversely affect the project goals, are shortlisted in this step. According to Ahmad, Berman, and Sataporn [9], various methods such as brainstorming, checklist, cause-effect diagram, tree diagram, hazard and operability study, fault tree, decision tree, failure mode and effect analysis, Delphi technique and interviews can be implemented for identification of major risks. Akin-toye [10] has concluded that, in case of large construction projects such as bridges and tunnels, risk management remains prominent feature of the project management to minimize the uncertainties and surprises.

Sharma [11] worked on general and specific requirements for safety during the construction of road tunnels by giving remedial measures for the risks and identified the gaps for the improvement in current field practice in India. Also, Marekar et al. [12] worked on the method of risk measurement of project risk, based on the risk matrix method. Hanna [13] worked on the effective implementation of accepted matrix beliefs to reduce the limitations of risk matrix and improve performance by risk analysis within the educated company. In spite of the restriction, the study identifies the risk matrix to be an applicable tool for qualitative risk assessment. According to Haytham [14], the risks are to identify the risks and developed strategies to reduce or avoid negative risks and on the other hand to catch opportunities. He focuses on the qualitative assessment of TBM tunneling project.

Limao et al. [15] work on a multilayer data combination frame which is suggested for the safety risk approach with both hard as well as soft data considerable. The result specifies that the progress procedure is effective for integrating many source instructions to accomplish a more precise outcome for the safety risk approach. As

Roopdarshan [16] said that the expected monetary value is a straightforward but constructive risk measurement quantitatively and will help to support the business objectives of the RMC crop in terms of RMC production and supply. Therefore, in the literature, it can be concluded that (i) a risk is a component which cannot be eliminated, and suitable risks mitigation measures are to be suggested which would enable to reduce identified project risks. (ii) EMV is the most widely used method, as this technique does not require any costly resources, only the experts' opinion. (iii) This technique gives the average outcome of all uncertain events. (iv) A proper risk mitigation plan is developing for the identified risks, and it ensures better and smooth achievement of project goals within specified time, cost, and quality parameter.

Objectives of this work are decided as follows:

1. To find and study the parameters that affect cost overruns and planning as a whole.
2. To increase the no. of distribution charts of occurrence, cost–effect, and time effect (risk matrix).
3. To quantify the impact of risk on the cost and time of the project using expected monetary value (EMV) tool.

3 Research Methodology

The risk assessment is a systematic process which consist of identifying, analyzing, and responding to the risks. The main purpose of the assessment incorporates maximizing of probability and of good events with reducing the probability of unfavorable events to the project. In the assessment process, there are mainly time and cost, both are the most important parameters to categorize the risk. As per the procedure, the first step is a literature review, and on site observations were used to identify the risk factors, and then discussion with an industry expert regarding the risk factors is identified and categorizing those identified risks based on technical, contractual, political, and environmental and precautionary. The risk assessment is the second stage in which there is a focus mainly on risk scenario, which is considered. Under this process, the risk matrix is used for qualitative risk assessment by giving a rating to every risk scenario by using a 5-point Likert scale and prioritizing the risk as per risk rating. The next stage is to perform a quantitative risk assessment by using the expected monetary value under which critical risk factors are decided. While the last and important stage is formulating the risk response strategy from this, estimated duration and cost with risk response plans are formulated for the consideration of ongoing tunnel construction projects. The format of this paper considers risk as a future event with a negative event in time and cost for organization executing metro tunneling project and for which feasible results can be forecasted on the basis of probability. Approach for this work consists of three levels

1. Risk identification, classification, and categorization
2. Risk qualification and prioritization

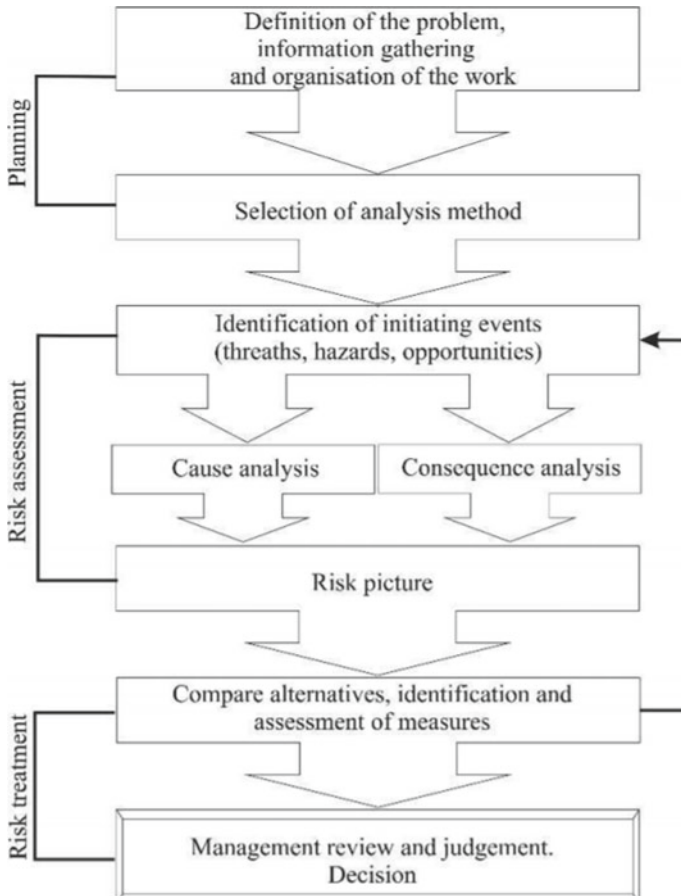


Fig. 1 Main step of risk analysis process

3. Risk quantification (Fig. 1).

3.1 Risk Matrix

A risk matrix is a table with categories of the probability of occurrence or frequency on an axis and the amount of impact on a second axis. Risk matrices are used mostly in risk management. Within the matriculation risk, there is a combination of probability, and the results are often met with a limited number of species considering different colors. These colors are usually green, yellow, and red representing low, medium, and large hazards, respectively. This can be obtained from the risk score given by the merger of probability and consequences. According to Davidson and his partner, risk matriculation can be used to measure risk levels. The possibilities for the emergence

Table 1 Scale of likelihood and consequences

Value scale	Assessment of likelihood (<i>P</i>)	Assessment of impact (<i>C</i>)
1	Very unlikely	First aid/very minor
2	Unlikely	Medical treatment/low effect
3	Possible	Lost time/rest injury/medium
4	Likely	Fatality/high effect
5	Very likely	Multiple fatality/extreme high effect

Source Marekar et al. [12]

Table 2 Impact matrix

Rank	Schedule	Cost	Safety
Very high	> 1 Month	> \$1000,000	Multiple fatality
High	> 1 week	< \$1000,000	Single fatality
Moderate	> 1 day	< \$100,000	Lost time/rest injury/medium
Low	< = 1 day	< \$10,000	Medical treatment/low effect
Very low	< 8 h	< \$1000	First aid/very minor

Source Marekar et al. [12]

and other approaches are also explored in different categories and identified in the risk matrix. The scale of likelihood, consequences, and impact of these risks on the project was mentioned in Tables 1 and 2, etc. The result is in the way of measuring points from one to five as shown in Table 3. The number of occurrences and the risk factors are changed from a scale of one to five to zero to one using the following formula (Figs. 2, 3, 4 and Tables 4, 5).

$$\text{Required score} = (\text{Responded score} * 0.2) \tag{1}$$

Source: Marekar et al. [12].

3.2 Risk Prioritization

Risk prioritization is done to prioritize risk so that risks posed to stimulate project objectives are selected for distribution. Because of this, it is possible for the results

Table 3 Questioner responses

S. No.	Identified risks	Response on scale 1-5		
		P	C/S	R
1	Movement of trailer truck	4	5	H
2	Hit or crushed by moving trailer	4	5	H
3	Failure of crane while lifting loads	4	5	H
4	Improper set up /stabilization	4	5	H
5	Slings breakage/ failure	3	3	M
6	Over loading of crane	3	3	M
7	Collision of lifting equipment's / load	4	5	H
8	Falling of load	4	5	H
9	Lack of oxygen/improper lighting	2	2	L
10	Inadequate ventilation	2	2	L
11	Fire explosion and flying particles	3	5	M
12	Electrocution	4	4	H
13	Breakage of lifting pin	4	2	M
14	Water leakage from segment	1	1	L
15	Derailing of locomotive during in and out of the tunnel	4	4	H
16	Fall or tilting of segment	4	4	H
17	Cutter head intervention of both open and compressed mode	4	4	H
18	High underground water pressure	3	3	M
19	Improper grouting at the time of segment erection	3	3	M
20	Building settlement due to TBM vibration	3	4	M
21	Falling of load	4	5	H
22	Ring erection – crushing/ fractured/drop segment	4	5	H
23	Unsafe handling of chemical	4	3	M
24	Control of construction waste	4	5	H

to be set for individual risks based on the matrix used (probability–consequences matrix) (Fig. 5).

3.3 Expected Monetary Value

At this stage of the proposed approach, risks that could cause significant costs and overtime will be determined to get an idea of the overall risk of the project in terms of operating time and costs on site. The proposed format for this purpose is proposed, which will be used to collect data related to the probability and consequences of the “significant” as well as the high risk of exposure to time and cost. The likelihood of the identified risks can have a value ranging from 0 to 1, which indicates a 0–100% chance of occurrence (Figs. 6, 7 and Table 6).

A standard equation for EMV is shown below.

$$EMV = \text{Consequences of an single risk} \times \text{Probability of this consequences} \quad (2)$$

Source: Roopdarshan et al. [16].

SEVERITY/ IMPACT CRITERIA		PROBABILITY FOR POTENTIAL INCIDENT SEVERITY/ IMPACT				
Personnel	Operations	(1) Very Unlikely	(2) Unlikely	(3) Possible but unusual	(4) Likely not surprising	(5) Very Likely no doubt
(1) First Aid	Slight (<\$1,000) 8 hours	1	2	3	4	5
(2) Medical Treatment	Minor (<\$10,000) <= 1 day	2	4	6	8	10
(3) Lost Time/ Rest. Injury	Medium (<\$100,000) > 1 day	3	6	9	12	15
(4) Single Fatality	Major (<\$1,000,000) > 1 week	4	8	12	16	20
(5) Multiple Fatality	Extensive (>\$1,000,000) > 1 month	5	10	15	20	25
1 – 6	Low Risk	Personnel with competency and skills to perform the job have the authority to proceed after verbally discussing the job requirements with anyone performing the work with them. May be acceptable; however, review task to see if risk can be reduced further.				
7 – 15	Medium Risk	Job shall only proceed with appropriate authorization after consultation with HS&E personnel and assessment team. Where possible, the job shall be redefined to take account of the hazards involved or the risk shall be reduced further prior starting the job (TRA Section 4, RISK IDENTIFICATION, ASSESSMENT AND CONTROL).				
16 – 25	High Risk	The job must not proceed until it has been redefined or further control measures put in place to reduce risk. The controls shall be re-assessed for adequacy prior to starting the job.				

Fig. 2 Risk matrix use for qualitative risk assessment



Fig. 3 Strategies for negative risks. Source Mohamed et al. [17]

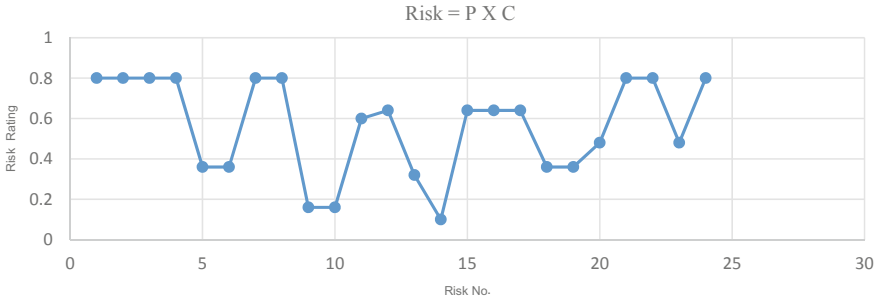


Fig. 4 Risk rating given by industrial experts

Table 4 Calculation of risk impact and occurrences

S. No.	P		C		Risk = $P \times C$
	Responded score	Score (P)	Responded score	Score (C)	
1	4	0.8	5	1.0	0.8
2	4	0.8	5	1.0	0.8
3	4	0.8	5	1.0	0.8
4	4	0.8	5	1.0	0.8
5	3	0.6	3	0.6	0.36
6	3	0.6	3	0.6	0.36
7	4	0.8	5	1.0	0.8
8	4	0.8	5	1.0	0.8
9	2	0.4	2	0.4	0.16
10	2	0.4	2	0.4	0.16
11	3	0.6	5	1.0	0.6
12	4	0.8	4	0.8	0.64
13	4	0.8	2	0.4	0.32
14	1	0.1	1	0.1	0.1
15	4	0.8	4	0.8	0.64
16	4	0.8	4	0.8	0.64
17	4	0.8	4	0.8	0.64
18	3	0.6	3	0.6	0.36
19	3	0.6	3	0.6	0.36
20	3	0.6	4	0.8	0.48
21	4	0.8	5	1.0	0.8
22	4	0.8	5	1.0	0.8
23	4	0.8	3	0.6	0.48
24	4	0.8	5	1.0	0.8

Fig. 5 Risk prioritization

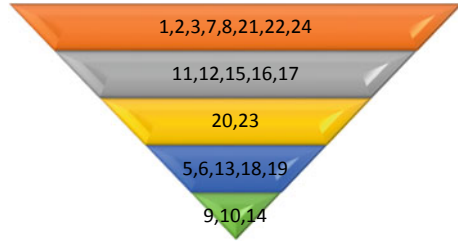


Fig. 6 Expected monetary value (time) h

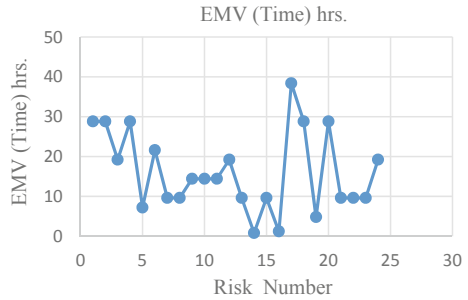
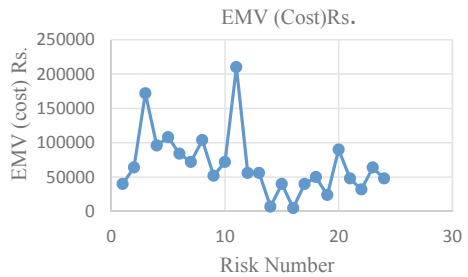


Fig. 7 Expected monetary value (cost) INR



EMV value is for threat expressed as negative values and for opportunity as positive value.

4 Results and Discussion

Risk analysis/evaluation was performed by using the risk matrix and EMV based on the identified risk scenarios. Table 3 presents the identified risk responses on a scale of 1–5 (Likert scale) given by industrial experts. In the category of tunnel construction-related works, the risk events, such as building condition survey, cutter head intervention, falling or tilting of the segment, ring erection, high underground water pressure, and improper grouting, were the main causes of time delay and cost

Table 5 Risk prioritization

Priority	Risk no.
First	1, 2, 3, 7, 8, 21, 22, 24
Second	11, 12, 15, 16, 17
Third	20, 23
Fourth	5, 6, 13, 18, 19
Fifth	9, 10, 14

overrun. Risk prioritization is to be done using risk rating given by industrial experts as shown in Fig. 4. As per risk prioritization movement of the trailer truck, hit or crushed by moving trailer, failure of the crane while lifting loads, ring erection, and control of construction waste were the critical risk scenarios. Due to these risks, time may increase up to 134.4 h. and cost may increase up to INR. 580,000; hence, it is necessary to mitigate first prioritize risks initially. Similarly, mitigate all prioritize risks sequentially, so that cost and time of the project may not increase. Table 5 summarizes all the categories of a tunnel construction project. As shown in the table, it is found that the total risk amount of INR. 1,634,000/- and time delayed for these risks is 386 h of the total project duration.

5 Conclusion

Based on the above results, it can be concluded that risk can be measured using the risk model and the priority model. This will be with caution in order to monitor and reduce the risk in infrastructure project. All projects should be managed to catch their objectives. The scope of risk management is not be restricted to planning stage only, but it should go through execution phase. Tunnels constructions are complex and risky projects which involve management of several risks. In this paper, it is shown that risks at the stage of the execution of project are the prime cause of project delay, cost overrun, and safety hazard. These risks can be controlled by implementing risk remedies. This paper presents the risk qualification and quantification perspective for TBM metro tunneling. The information is collected from tunneling site observations and consultation with a team of engineers working on the TBM project in Pune in India. The answer to the question of each TBM tunneling activity was developed as a result of this study. Consistent measurement, probability, and outcomes were also collected in the same risk assessment groups that had a significant impact on the goal of the project. The risk assessment concept proposed in this paper, using EMV, is a more accurate and productive tool for measuring risk in terms of time and cost. This approach can be used satisfactorily for decision making at the initial point of each TBM tunneling project. It facilitates the identification of high-risk areas that need to be managed and monitored to achieve project objectives in terms of cost and time. This idea can be made acceptable by including a computer decision support system, as long as the relevant information is available. It is shown that if the risks

Table 6 Expected monetary value

Risk No.	Threat (T)/opportunity (O)	Probability (<i>L</i>)	Impact on time (h)	EMV (time) h	Impact on cost	EMV (cost) Rs.
1	T	0.8	36	28.8	50,000	40,000
2	T	0.8	36	28.8	80,000	64,000
3	T	0.8	24	19.2	215,000	172,000
4	T	0.8	36	28.8	120,000	96,000
5	T	0.6	12	7.2	180,000	108,000
6	T	0.6	36	21.6	140,000	84,000
7	T	0.8	12	9.6	90,000	72,000
8	T	0.8	12	9.6	130,000	104,000
9	T	0.4	36	14.4	130,000	52,000
10	T	0.4	36	14.4	180,000	72,000
11	T	0.6	24	14.4	350,000	210,000
12	T	0.8	24	19.2	70,000	56,000
13	T	0.8	12	9.6	70,000	56,000
14	T	0.1	8	0.8	70,000	7000
15	T	0.8	12	9.6	50,000	40,000
16	T	0.1	12	1.2	50,000	5000
17	T	0.8	48	38.4	80,000	40,000
18	T	0.6	48	28.8	150,000	50,000
19	T	0.6	8	4.8	40,000	24,000
20	T	0.6	48	28.8	150,000	90,000
21	T	0.8	12	9.6	60,000	48,000
22	T	0.8	12	9.6	40,000	32,000
23	T	0.8	12	9.6	80,000	64,000
24	T	0.8	24	19.2	60,000	48,000

are identified and controlled using this approach. It leads to reduction in excessive costs and completion period of the project.

References

1. Williams RC, Walker AJ, Dorofee AJ Putting risk management into practice. IEEE Softw 3:75–81
2. Johnson J, Rood OE (1977) Elements of fair and profit equitable profit determination for construction contract negotiations: Draft Report CERL
3. Ashley DB (1981) Construction project risks: mitigation and management. In: Proceedings of PMI/internet joint symposium. Project Management Institute, Drexel Hill, PA, pp 331–340

4. Roetzheim W (1988) Structured computer project management. Prentice Hall, New Jersey
5. Jamal F, Bahar AL, Kaith CC (1990) Systematic risk management approach for construction projects. *J Constr Eng Manage* 116(3):533–545
6. Royer PS (2000) Risk management: the undiscovered dimension of project management. *PM Netw* 14:36770, 31–40
7. Hillson D (2000) Extending the risk process to managing opportunities. *Int J Project Manage* 20:235–240
8. Soren DE, Per T, Jorgen K, Trine HV (2004) Guideline for tunneling risk management: International Tunneling Association, working group No. 2. *Tunnel Undergr Space Technol* 19:217–237. [10.1016/j.tust.2004.01.001](https://doi.org/10.1016/j.tust.2004.01.001)
9. Ahmed A, Berman K, Sataporn A (2007) A review of techniques for risk management in project-benchmarking. *Int J* 14(1):22–36
10. Akintoye A (2008) Project risk management practice—the case of a South african utility company. *Int J Project Manage* 26:149–163
11. Sharma AK (2019) Safety management of road tunnel during construction—a case study. *Int J Eng Trends Technol (IJETT)* 67(5)
12. Marekar MS, Patil R, Tank C (2014) Risk assessment for infrastructure projects case study—Pune metro rail project. *Int J Eng Manage Res* 4(5). ISSN No. 2250-0758
13. Hanna L (2016) The risk matrix as tool for risk analysis
14. Haytham B (2016) The major risk in TBM bored tunnels projects: research gate 307862462. <https://doi.org/10.13140/RG.2.2.34092.67203>
15. Limao Z, Xianguo W, Hongping Z, Simaan M (2017) AbouRizk: perceiving safety risk of buildings adjacent to tunneling excavation: an information fusion approach. *Autom Constr* 73:88–101. <https://doi.org/10.1016/j.autcon.2016.09.003>
16. Roopdarshan W, Vinay T, Sajal K (2010) Risk quantification using EMV analysis—a strategic case of ready mix concrete plants. *Int J Comput Sci (IJCSI)* 7(5): 399–408
17. Mohemad SB, Omar AM, Ahemad MA (2015) Identification and assessment of risk factors affecting construction projects. *HBRC J* 2017(13):202–216

Linear Programming Model for the Design of Optimal Cropping Pattern for a Major Distributary Canal



S. B. Ganesh Kumar, B. R. Ramesh, and H. J. Surendra

Abstract There is a need to augment the irrigation operation policy, change of cropping pattern to improve the efficiency of canal system and to increase the overall productivity in the command area. This paper reports an optimal cropping pattern in a detailed way for the design of a major distributary of Harihar branch canal with primary objective of maximizing the crop production under available water resources. Considering the affinity of the farmers towards the wet crops, optimum cropping pattern is designed. Command area was divided into head middle and tail areas in each distributary and cropping pattern and was suggested according to the water availability during different rotation period, area available for cultivation, farmer priority based on soil health card report, soil fertility and land suitability based on multicriteria analysis to increase the productivity. Considering the rotation policy followed in the canal and water deficit between 100 and 50%, a linear programming model (LP model) is developed. Linear programming model is used to maximize the yield of the command area. Constraints are crop variety, fertilizer availability, farmer's preference and area availability. Conclusions are drawn about the extent of notified crops that could be grown and the corresponding economic benefits.

Keywords Linear programming · Command area · Optimization · Optimal crop pattern: surplus–deficit analysis

S. B. Ganesh Kumar
Department of Civil Engineering, EWCE, Bangalore, Karnataka, India

B. R. Ramesh
Department of Civil Engineering, NMIT, Bangalore, Karnataka, India
e-mail: ramesh.br@nmit.ac.in

H. J. Surendra (✉)
Department of Civil Engineering, ATRIA IT, Bangalore, Karnataka, India
e-mail: surendra@atria.edu

1 Introduction

Major contribution towards Indian economy is the agriculture. After Independence, there is uplift in production due to improvement in irrigation facilities through different irrigation projects. Cropping pattern optimization along with land and water constraint is to improvise the crop production with the available resources. Singh et al. [5] predicted cropping pattern for maximum benefit using linear programming modelling with land and water availability constraints and recommended the conjunctive use of water. Raul et al. [4] used linear programming method to maximize the yield. Panda et al. [3] developed optimization model for cropping pattern prediction in the canal command area along with the equitable water allocation for the head, middle and tail portion with the multi-objective paradigm of minimization of surplus water zone wise and the maximization of the cultivation area and net returns. Bojang et al. [2] used popular tool for solving the LP optimization, to maximize the yield command area. Srinivasareddy et al. [6] assessed the drought vulnerability through climatic index. Aymen et al. [1] done the land suitability evaluation. Xue et al. [7] worked on aerobic rice for optimizing yield, water requirement and water productivity.

This paper describes linear programming mathematical model methodology to suggest an optimal cropping pattern with an objective of yield maximization. This model considers the available cultivable area, water and other constraints for a selected distributary of Harihar Branch canal of Bhadra command area in Karnataka state, India.

2 Materials and Methods

2.1 Study Area

Bhadra command region lies between $14^{\circ} 21' - 14^{\circ} 30'$ N latitude and $75^{\circ} 47' - 75^{\circ} 57'$ E longitude and falls under the Land of Agroclimatic zone-4 of Karnataka (India). Canal irrigation system consists of both left and right bank canal. Right bank canal runs 103 km with an area of 75,311 ha. Davangere branch canal takes off at 103 km among the four bank canal. Canal runs for a distance of 99 km with a command area of 45,278 ha. It has discharging capacity of 33.4 cumecs with 27 distributaries. Branch canal of Harihar takes off at 65 km from the branch canal of Davanagere. It runs for a distance of 22 km with 18 distributaries having total length of 80.40 km with a discharging capacity of 10.307 cumecs in a command area of 14,996 ha. The present study is under the 10th distributary of the middle portion of the Harihar branch canal.

The soil characteristics of right bank canal comprise 8.5% black soil and 93.5% red soil, whereas in left bank canal 7% black soil and 93% red soil. The command area receives 58% southwest monsoon and 22% north east monsoon and 20% of

rainfall during summer. The average rainfall of Davangere station is 657 mm and of Harihar station is 637 mm.

2.2 Deficit–surplus Analysis Based on the Operation Policy

In Bhadra command area, irrigation department decides the number of days the main canal has to supply water, after ascertaining water available in the Bhadra dam in the beginning of the kharif and rabi season. The water is led to the canals coming under main canal are run in rotation (generally 10 days ON and 10 days OFF). The crops to be grown in the command area will be notified by the department after knowing the days of canal to be run during particular season.

The water requirement of the crops notified during the study period is computed using the Penman Montaitth method considering the various meteorological data for 2001–2014. The main canal under this system is working for 110 days with 12 rotations. The distributary under the present study is working under operation during 1, 3, 5, 7, 9 of each 10 days and 11th rotation for 5 days. The water to be supplied for the crops shall match for successive two rotations as one of the rotations will be OFF. Hence, the requirement for the notified crops is given in Table 1.

The water supplied in the distributary during the above rotation must match the water requirement of the crop. However, it is observed that there was deficit supply in all rotation (Table 2). Hence, there is a need for the development of the model for cropping pattern.

In order to properly distribute the water till tail end, 10th distributary (which is taken for present study) is divided in head reach, middle reach and a tail reach. There are 36 outlets in the distributary. Based on outlets configuration and the area served by each outlets, the canal is trifurcated in to head, middle and tail reaches. Head reach whose total discharge is in this reach is about 0.680 cumecs for total command area of 1010 ha. Middle reach whose total discharge is in this reach is about 0.420

Table 1 Crop water requirement for different rotations based on the operation policy

Water required in rotation No.	Paddy	Sugarcane	Plantation	Semidry
<i>Depth of water requirement in m</i>				
1	0.280	0.228	0.169	0.142
3	0.314	0.254	0.188	0.221
5	0.347	0.286	0.212	0.251
7	0.318	0.283	0.205	0.246
9	0.303	0.251	0.194	0.159
11	0.142	0.080	0.085	0.049
Total	1.705	1.381	1.053	1.069

Table 2 Surplus–deficit supply in the distributaries for notified crops during the rotation operation

Rotation operation	Irrigation water requirement in ha-m					IWR as per operation policy	Surplus–deficit
	Paddy	Sugarcane	Plantation	Maize	Total		
<i>Depth water requirement in ha-m</i>							
Rotation-1	8.101	13.00	2.68	77.13	100.91	230.410	– 77.91
Rotation-2	9.290	14.43	2.98	102.81	129.50	OFF	
Rotation-3	9.290	14.43	2.98	130.35	157.05	335.072	– 182.58
Rotation-4	10.180	16.07	3.31	148.46	178.03	OFF	
Rotation-5	10.774	17.17	3.53	158.49	189.97	379.943	– 227.45
Rotation-6	10.774	17.17	3.53	158.49	189.97	OFF	
Rotation-7	10.174	17.06	3.45	156.54	187.23	371.711	– 219.21
Rotation-8	9.575	16.94	3.37	154.59	184.48	OFF	
Rotation-9	9.575	16.94	3.37	113.30	143.19	256.270	– 103.77
Rotation-10	9.207	13.25	3.10	87.51	113.08	OFF	
Rotation-11	4.420	4.78	1.42	30.86	41.48	82.961	– 6.71
Rotation-12	4.420	4.78	1.42	30.86	41.48	OFF	

Even rotation signifies OFF, Odd rotations signifies ON and signifies the Flow condition in the distributary as per the operational policy

cumecs to total command area of 697 ha. Tail reach whose total discharge is in this reach is about 0.659 cumecs to total command area of 1008 Ha.

2.3 Linear Model for Cropping Pattern Optimization

Proper cropping pattern should be designed to bridge the gap of deficit in water supply so that the distributary functions at optimal conditions.

The main objective is to maximize the yield or production in the command area with the available resources in the crop duration. It is represented by mathematical equation:

Functional objective:

$$\text{Max } Y = \sum_{i=1}^I \sum_{j=1}^J \sum_{k=1}^K Y_i A_{ijk} \tag{1}$$

where,

Y Production per hectare of crop area of i th crop.

A_i Area of the i th crop.

- I* Number of crops grown in season [1 = Paddy, 2 = Sugarcane, 3 = Plantation (Areca nut), 4 = Maize, 5 = Aerobic rice, 6 and 7 is Baby corn (double crop)].
- J* Reach of the irrigation crop (1 = Head reach, 2 = Middle reach, 3 = Tail reach).
- K* Irrigation crop water requirement for required for different rotation (1, 2, 3, 4, 5, 6 rotation numbers).
- A_{ijk} Area of *i*th crop under *j*th reach for *k*th rotation in (ha).

2.4 Constraints of Water Availability

The total water availability for command area (*A*) in the respective distributary is fixed, and it is divided into three reaches: *J* = head (*H*), middle (*M*) and tail (*T*), and the mathematical representation of area constraint is given in equation

$$\sum_{i=1}^I \sum_{j=1}^J \sum_{k=1}^K A_{ijk} IWR_{ik} \leq \sum_{j=1}^J \sum_{k=1}^K WAR_{jk} \tag{2}$$

where

- IWR_{ik} is the depth of irrigation water requirement for *i*th crop in the *k*th rotation in m.
- WAR_{jk} is the volume of water available at the distributary head for rotation at different reach in ha-m.

2.5 Constraints for Area Availability

The total area under various crops during any period of irrigation shall be less than or equal to the total notified cropping pattern from the department (*A*) in the distributary. The command area is fixed and is divided into three reaches, *j* is head (*H*), middle (*M*) and tail (*T*) reach, and therefore the mathematical representation of area constraint is given in equation

$$\sum_{i=1}^I \sum_{j=1}^J A_{ij} \leq A \tag{3}$$

where

- A* Total notified command area from the department of the all the crop in the command area in ha.

2.6 Crop Priority by Farmer as Per Soil Health Card Report Constraints

Farmers prefer to grow certain crops in their land by applying extra fertilizer required for his preferred crop. The farmer consults in regard to extra fertilizer application for his preferred crop from the agricultural department. The total area under each preferred crop shall be less than the notified crop area (generally farmers prefer either wet crop or plantation crop). The constrain can be written as

$$\sum_{i=1}^I APF_i \leq \sum_{i=1}^I A_i \quad (4)$$

where

APF_i Area of i th crop preferred by the farmer.

2.7 Crop Area Constraints in Respect Natural Soil

The command area is suited for certain crop which are suggested for particular crop by agricultural department for its natural fertility using nominal fertilizer dosage to be used.

The soil fertility and land suitability based on multicriteria analysis are studied by Aymen et al. [1], using GIS (5) by considering this constrain can be written as

$$\sum_{i=1}^I ASF_i \leq \sum_{i=1}^I A_i \quad (5)$$

where,

ASF_i Area of i th crop suggested on the basis of soil fertility with optimal dosage of the fertilizer.

2.8 Crop Area Constraints

The command area is already having certain plantation crops. In deciding cropping pattern, we can alter the area under plantation. Therefore, in this model water required for plantation crop during the rotation period cannot be altered. In the command area, there are two sugar factories, hence to a maximum of 60% area is suggested for sugarcane. The constraint for sugarcane for head and middle reach is fixed to maximum of 25% of notified sugarcane crop area. As the farmers prefer to grow

wet crop and plantation at the head, dry crop like maize is not preferred at the head. However, maximum area up to 75% of the notified dry crop area is suggested for the middle and tail reach. Aerobic rice is better choice for the tail end command area farmers who prefer to grow wet crop in place of sugarcane or dry crop is studied by Subramanian et al. and Xue et al., as it yields more and profitable crop with less water requirement (6 and 7). In the present study, minimum of 10% of notified dry crop to 100% is suggested. If any extra water is available in any rotation, baby corn (short duration) crop can be used as a double crop within the season is suggested in the constraint as below

$$\sum_{i=1}^I A_{ij} \leq \sum_{i=1}^I A_i * CF_i \tag{6}$$

where

CF_i Crop percentage factor for *i*th crop.

2.9 Fertilizer Constraints

The fertilizer availability for the command area is fixed, as government allocates fertilizer and the seeds to each district in the state this constraint must be used in cropping pattern decision. The fertilizer constraint is written as below

$$\sum_{i=1}^I \sum_{j=1}^J A_{ij} FR_{ij} \leq TFA \tag{7}$$

where

TFA Total fertilizer availability in the command area.

FR_{ij} Fertilizer requirement for *i*th crop in the *k*th reach of the distributary.

3 Results and Discussion

Tenth distributary deficit-surplus analysis in Harihar branch canal suggests that operation is sub-optimal in the distributary. It is identified from the crop water requirement studies that the water supplied to the distributaries during the rotation period cannot cater to the demand of the notified crop in the season. Also, the water availability in the reservoir will not be always 100%, it varies temporally. Hence, in present study water availability to the distributary is varied between 100 and 50% for the same rotation period to understand how much of notified cropping could be achieved and the consequent economic benefit.

Table 3 Predicted cropping pattern through LP model in the tenth distributary of Harihar branch canal of Bhadra command area

WA-total	Paddy	Sugarcane	Plantation	Maize	Aerobic rice	Babycorn-1	Babycorn-2	Total
<i>Area in hectares</i>								
100	0.00	72.13	34.00	0.00	359.41	122.32	199.39	787.25
95	0.00	72.13	34.00	0.00	336.74	115.50	188.67	747.04
90	0.00	72.13	34.00	0.00	314.19	108.67	177.87	706.85
85	0.00	72.13	34.00	0.00	291.58	101.85	167.12	666.68
80	0.00	72.13	34.00	0.00	268.92	95.05	156.39	626.48
75	0.00	72.13	34.00	0.00	246.33	88.21	145.60	586.26
70	0.00	72.13	34.00	0.00	223.72	81.40	134.85	546.09
65	0.00	72.13	34.00	0.00	201.06	74.59	124.11	505.89
60	0.00	72.13	34.00	0.00	178.40	67.78	113.37	465.69
55	0.00	72.13	34.00	0.00	155.79	60.97	102.63	425.52
50	0.00	72.13	34.00	0.00	133.38	53.89	90.93	384.32

The optimal cropping areas for different types of crops under lp modelling for varied percentage of water availability in each reach [head, middle and tail reach] are done separately, and the total crops suggested for the command area are presented in Table 3 and there on the yield that can be achieved is presented in Table 4.

The predicted percentage of cropping pattern at the different reaches for varied percentage of water from 100 to 50% is presented in Fig. 1, it can be seen as a maximum of 53.23% of notified area when water availability is 100–25.99% of notified area, and when water availability is 50%, it can only be achieved.

The predicted economic benefit with reference to notified cropping pattern for carried percentage of water availability from 100 to 50% is presented in Fig. 2. The percentage economic benefit that can be achieved is carried from 82 to 48.5%.

4 Conclusion

Water availability in the distributary is surplus at the beginning and end rotations in the distributary for about 40 days, which can be utilized effectively to grow green leafy vegetables. This will provide additional profit to the farmers. In conclusion, linear programming can be used as a versatile tool for fixing the cropping pattern for a command area for varied water distribution and cropping pattern.

Table 4 Predicted yield from the cropping area with help of linear programming model in the distributary

WA-total	Paddy	Sugarcane	Plantation	Maize	Aerobic Rice	Babycorn-1	Babycorn-2	Total
100	0.00	5120.95	425.00	0.00	19,767.57	2324.14	3788.41	31,426.07
95	0.00	5120.95	425.00	0.00	18,520.70	2194.58	3584.65	29,845.88
90	0.00	5120.95	425.00	0.00	17,280.50	2064.64	3379.49	28,270.58
85	0.00	5120.95	425.00	0.00	16,036.72	1935.23	3175.33	26,693.22
80	0.00	5120.95	425.00	0.00	14,790.66	1805.87	2971.32	25,113.80
75	0.00	5120.95	425.00	0.00	13,548.17	1676.00	2766.31	23,536.42
70	0.00	5120.95	425.00	0.00	12,304.39	1546.58	2562.15	21,959.07
65	0.00	5120.95	425.00	0.00	11,058.33	1417.23	2358.14	20,379.64
60	0.00	5120.95	425.00	0.00	9812.27	1287.88	2154.12	18,800.21
55	0.00	5120.95	425.00	0.00	8568.48	1158.47	1949.96	17,222.86
50	0.00	5120.95	425.00	0.00	7335.89	1023.82	1727.74	15,633.39

Yield in Quintal and for Sugarcane in Tonne

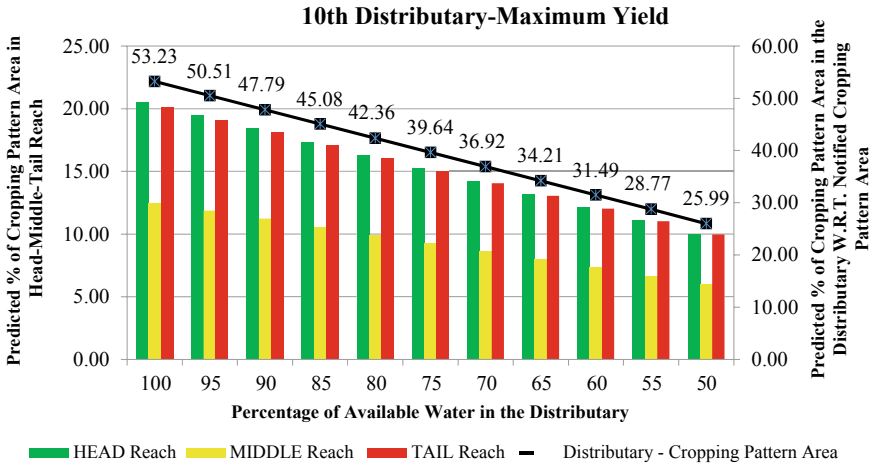


Fig. 1 Predicted cropping pattern area covered in the distributary by linear programming

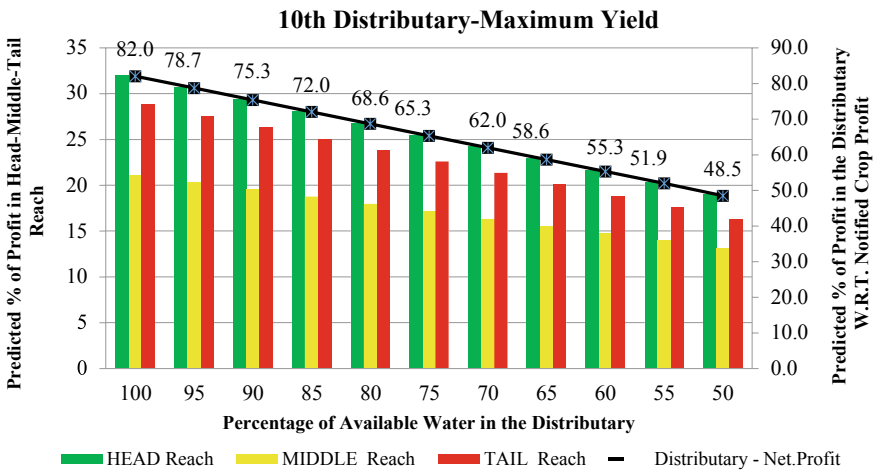


Fig. 2 Predicted net returns from the cropping pattern area covered in the distributary by linear programming



References

1. Aymen ALT, Al-husban Y, Farhan I (2020) Land suitability evaluation for agricultural use using GIS and remote sensing techniques: the case study of Ma'an Governorate, Jordan. Egypt J Remote Sens Space Sci. <https://doi.org/10.1016/j.ejrs.2020.01.001>
2. Bojang PO, Yu P, Yang T, Kuo CM (2016) Optimal cropping patterns for profit maximization using a linear programming model: a case study in Njawara Village, The Gambia. In: 12th international conference on hydro science and engineering. hydro science and engineering for environmental resilience, Nov 6–10, Tainan, Taiwan

3. Panda RK, Panigrahy N, Mohanty S, Brahmanand PS, Kumar A, Raju PV, Rao VV (2018) Optimal cropping pattern design for a major distributary of Hirakud canal command in India. *Sustain Water Resour Manage* 4:1051–1062
4. Raul SK, Panda SN, Inamdar PM (2011) Sectoral conjunctive use planning for optimal cropping under hydrological uncertainty. *J Irrig Drain Eng* 138(2):145–155
5. Singh A (2017) Optimal allocation of water and land resources for maximizing the farm income and minimizing the irrigation-induced environmental problems. *Stoch Env Res Risk Assess* 31(5):1147–1154
6. Srinivasareddy GS, Shivakumarnaiklall HS, Keerthy NG, Garag PRASAD, Jothi EP, Challa O (2019) Drought vulnerability assessment in Karnataka: through composite climatic index. *MAUSAM* 70(1):159–170
7. Xue CY, Yang XG, Bouman BAM, Deng W, Zhang Q, Yan W, Zhang T, Rouzi A, Wang H (2008) Optimizing yield, water requirements, and water productivity of aerobic rice for the North China Plain. *Irrig Sci* 26(6):459–474

Analysis of Traffic Flow Characteristics Based on Area-Occupancy Concept on Urban Arterial Roads Under Heterogeneous Traffic Scenario—A Case Study of Tiruchirappalli City



Sandeep Singh , R. Vidya, Bishnu Kant Shukla ,
and S. Moses Santhakumar

Abstract In developing nations such as India, the urban arterial roads carry various vehicles that follow weak lane discipline. During peak hours of traffic, the degree of heterogeneity is so high that it leads to improper utilization of the roadway facility, thereby affecting the functional and operational characteristics of the traffic stream. This paper proposes to analyse the traffic flow characteristics of the urban arterial road stretches with heterogeneous traffic conditions in Tiruchirappalli city, India, using the macroscopic fundamental diagrams (MFDs). The three essential traffic variables include speed–flow–area-occupancy on one side and speed–flow–density on the other side. This paper gives a systematic general idea to analyse the heterogeneous traffic considering the area-occupancy as a concentration performance measure instead of the conventionally followed density concept. The MFDs are established using the speed–flow–area-occupancy and speed–flow–density, and a comparison was made between them for bidirectional traffic. The study shows that the traffic stream characteristics analysed using the speed–flow–area-occupancy method give reliable and consistent results with the highest values of goodness-of-fit parameter coefficient of determination (R^2) when compared to the speed–flow–density method. As a result, using area-occupancy as a performance measure, one can quantify changes in traffic characteristics in terms of vehicular interactions. The study results may be useful to researchers, traffic engineers, and practitioners for developing macroscopic capacity models for urban arterial roads under heterogeneous traffic conditions.

S. Singh · S. Moses Santhakumar
Department of Civil Engineering, National Institute of Technology Tiruchirappalli,
Tiruchirappalli, India
e-mail: moses@nitt.edu

R. Vidya
School of Civil Engineering, SASTRA University, Tanjore, India
e-mail: vidya@civil.sastra.ac.in

B. K. Shukla (✉)
Department of Civil Engineering, JSS Academy of Technical Education, Noida, India
e-mail: bishnukantshukla@gmail.com

Keyword Traffic characteristics · Heterogeneous traffic · Dynamic passenger car unit · Macroscopic fundamental diagrams (MFDs) · Area-occupancy

1 Introduction

Traffic management has primarily become a major issue in developing nations such as India, where vehicle movement is abreast on the roadway. This traffic behaviour is attributed to roadway geometric features, vehicles' dynamic parameters, and driver behaviour. Besides, road traffic in India is exceptionally heterogeneous when compared to traffic across the globe. The traffic in India constitutes numerous categories of vehicles plying on the same roadway with weak lane discipline. Due to these adverse characteristics of the traffic, the traditionally used speed–flow–density models might not be accurate under heterogeneous traffic conditions. Speed–density models assume a linear relationship between them, which may not be accurately replicating the real-field conditions.

The characteristics of traffic under such scenarios are vital and need immediate attention, which is to be analysed because there are limited studies pertaining to addressing such issues. This necessitates the need to investigate the traffic characteristics of the urban arterial corridors. Mallikarjuna and Rao [1], and Arasan and Dhivya [2] introduced the concept of area-occupancy to overcome this difficulty by analysing by speed–flow–area-occupancy models. Area-occupancy was found to be consistent for determining the space utilized by a vehicle on a roadway, and it gave accurate values under the different proportions of traffic and conditions of the roadway [3]. The concept of density is valid only under lane-based traffic, wherein the individual vehicle speeds and physical dimensions do not vary significantly. Also, density is usually considered as a measure of concentration over space, while occupancy is considered as a measure of concentration over time.

In the light of the above scientific consensus regarding vehicle occupancy, area-occupancy is used instead of density for traffic characteristics analysis. Hence, the study investigates and analyses the appropriateness of using area-occupancy as an alternative measure for traffic density to analyse the traffic flow characteristics on an urban arterial road stretch carrying heterogeneous traffic.

2 Literature Review

Many research works were carried out in the past in different countries focusing on understanding the traffic characteristics for analysing the macroscopic fundamental diagrams (MFDs), but the assumption of vehicle heterogeneity was not deeply explored. Early research works mainly focused on homogeneous traffic. The traffic density, which is indicated as the total number of vehicles present over a unit length of roadway, is generally used as a measure of performance of a roadway. This concept

can be validated only under such traffic conditions where homogeneity and lane discipline prevails. However, in India, where heterogeneous traffic conditions prevail with weak lane discipline, a major difference in dimensions and speeds of various vehicle categories plying on the same roadway lane is observed [4]. Therefore, Chandra and Verma [5] recommended that for heterogeneous traffic conditions, the measure of density should be used, taking into account the horizontal projected area of the vehicle for traffic analysis.

Mallikarjuna and Rao [1] have initially carried out a study on the area-occupancy of vehicles, considering the area of the projection of vehicle ($\text{length} \times \text{breadth}$). Arasan and Dhivya [2] compared the area-occupancy concept with the traffic speed and flow for homogeneous traffic using simulation techniques. Mishra et al. [3] developed an area-occupancy–speed–flow relationship model using simulation techniques. Kumar et al. [4] developed a homogeneous equivalent based on area-occupancy under varying non-lane-based heterogeneous traffic. The authors validated the concept of area-occupancy-based PCU estimation at different traffic compositions and flow levels of heterogeneous traffic. In another study, Arasan and Dhivya [6] came up with a new area-occupancy concept to determine traffic concentration under heterogeneous conditions. The authors suggest that the area-occupancy-based approach is useful in clearly explaining the concentration of the roadway segment.

Geroliminis and Sun [7] conducted field experiments to investigate the scatter of macroscopic fundamental diagrams (MFDs) using flow and occupancy under congested conditions. Mallikarjuna and Rao [8] have attempted to comprehensively study the area-occupancy concept to model the traffic under heterogeneous conditions. They considered the important microscopic characteristics of individual vehicles like longitudinal gaps, lateral gaps, and lateral positions to formulate the cellular automata (CA)-based traffic flow models. The authors found that the area-occupancy is useful in describing the lateral gap maintaining the behaviour of vehicles, and it is useful in modelling the cellular automata (CA) structure depending on varying traffic conditions. However, recently Kumar et al. [9] proposed a new concept for PCU estimation based on the matrix method using area-occupancy. They have used area-occupancy as a traffic performance measure under non-lane-based heterogeneous traffic conditions.

As it is evident from the literature mentioned above, several studies have been done by researchers in the past. However, still, an exploratory-based study is not critically analysed using speed, flow, and area-occupancy. This disparity among traffic variables instigates the need for this research work. The present research aims to add to this literature through providing insights in comparing area-occupancy and density parameters.

3 Research Framework

Traffic data was collected using videotaping techniques on a bidirectional urban arterial road stretch in Tiruchirappalli city, India. A study methodology is proposed to

investigate the appropriateness of speed, flow, and area-occupancy against the speed, flow, and density parameters using the macroscopic fundamental diagrams (MFDs). The premise of using the area-occupancy instead of density as a measuring unit for traffic concentration is that because it determines the operational performance of the urban arterial roads. Since the representation of the concentration of traffic as density might not be appropriate for heterogeneous traffic, as well as practically, measuring the field density under such traffic conditions is a tedious work, the area-occupancy concept was used. Later, flow–area-occupancy and speed–area-occupancy plots were compared with the flow–density and speed–density plots, respectively, to analyse the accuracy of the concept of area-occupancy. The coefficient of determination (R^2) was used as the measure of effectiveness to do so.

4 Study Area

The Tiruchirappalli (Trichy) city is one of the major urban areas in Tamil Nadu, India, with a population of around 1.63 million, with an area of 167.23 km² was chosen as the study area. The location suitable for the study was identified as one of the most congested road stretches (Near Gandhi market). A bidirectional roadway section was selected for this study, as depicted in Fig. 1.

The Gandhi market area is one of the Trichy city’s largest perishable goods market complex. The market has two blocks for vegetable shops and one each for fruit and flower shops. It also has a food grain market spread over 52 acres. The wholesale vegetable market is provided with the provision of godowns, parking space for trucks,

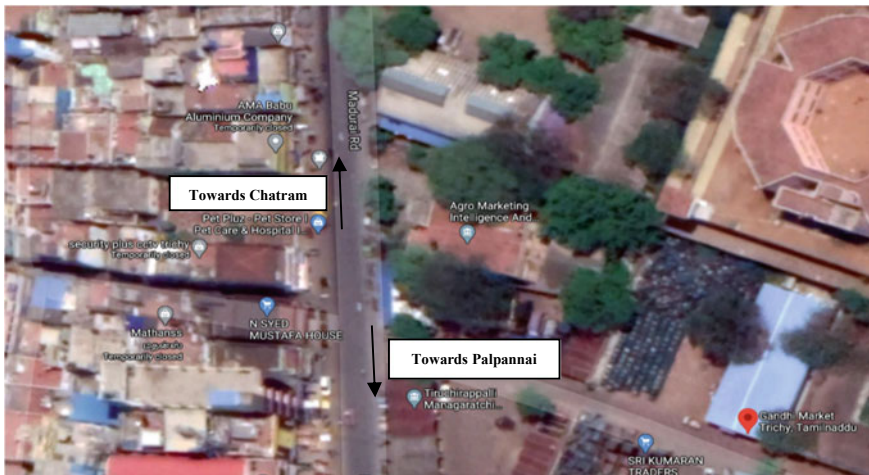


Fig. 1 Snapshot from Google earth showing the study sites

public toilets, cement concrete roads, solar streetlights, a fire-fighting system, and a water supply. The traffic in this area is congested during the peak hours of day.

5 Data Collection and Extraction

The mid-block section of an urban arterial road stretch in Tiruchirappalli city, India, was selected as the study site, which is an undivided two-lane, a two-way roadway with about 1.2 m unpaved shoulder in each side with side drain and central line marking. For analysing the fundamental traffic flow relationships for a particular road stretch, among three basic traffic variables, speed, flow, and area-occupancy, a 27 m longitudinal section of the road stretch was selected in both the directions of the traffic. Traffic data was captured using a high mast-mounted video camera on the side of the road in a manner such that the whole trap area demarcated on the ground was clearly visible enough to enable decoding of the traffic volumes and speeds of different vehicle types. The traffic data was collected during the morning peak hours (8:00 am–11:00 am). The complete traffic data collection was conducted under normal weather conditions with minimum and maximum temperature of the day being 30.1 °C and 36.7 °C, respectively. Field data collected at the study sections was then taken back to the laboratories and replayed on screens, and the extracted information regarding classified traffic volume counts for every 15-min time interval from the entire survey duration was carried out. The recorded videos were replayed in the laboratory for extracting the volume count, speed, and area-occupancy. The field data collection was extracted using Full Motion Video 6.0 (FMV6). Mpeg format video files were played on a computer screen after copying recordings from each camera. The FMV6 player can segregate the video into frames, which can then be noted down by stopping playback and navigating forward and backward to get frame reading when the vehicle crosses the reference point.

The road traffic in the study section was found to be majorly occupied by private vehicles like cars (CAR) and two wheelers (TW) and public transport vehicles like corporation buses (BUS). Other types of vehicles like auto-rickshaws (AR), trucks (TR), cycle-rickshaw (CR), and cycles (CY) are also found to be plying on the urban arterial road. A wide variation in the physical nature of the vehicles is observed even within the vehicle class. However, for better understanding and analysis, this intra-class classification among the vehicles was simplified, and the ideal physical vehicular dimensions were adopted as described in the Indo-Highway Capacity Manual (Indo-HCM: 2017) [13], which are shown in Table 1.

The roadway characteristics of the study sections were such that it had plain and level terrain. There was no horizontal curvature or vertical gradient involved, no pavement defects on the road surface, no direct access points, no side friction in terms of public transport stops, bus bays, and truck lay-byes coupled with the absence of significant pedestrian activity or slow-moving vehicles such as bicycles, rickshaws, and animal carts, no work zone activity at or near the section, and no incidents or

Table 1 Vehicle dimensions at selected study sites

Class of vehicle	Length (m)	Width (m)	Area (m ²)
CAR	3.72	1.44	5.36
TW	1.87	0.64	1.20
AR	3.20	1.40	4.48
TR	7.50	2.35	17.63
BUS	10.10	2.43	24.54
CR	2.66	1.16	3.09
CY	1.90	0.45	0.86

Note: *CAR* cars, *TW* two wheelers, *AR* auto-rickshaws, *TR* trucks, *BUS* buses, *CR* cycle rickshaws, and *CY* cycles

crashes at the time of observation at or near the section. These conditions prevailing in the study section, thus, ensured an uninterrupted traffic flow.

Volume count extraction was conducted along with the traffic composition extraction of the arterial road stretches, and these are presented graphically in Figs. 2 and 3, respectively.

The traffic flow was found to vary between 1000 and 1200 vehicles per hour for the Chatram direction, whereas for the Palpannai direction, it varied between 700 and 1000 vehicles per hour. The traffic flow has reached the peak traffic condition between 9:15 am and 9:45 am for the Chatram direction. The traffic towards the Chatram direction was observed to be more than that in the Palpannai direction.

Figure 3a, b shows that maximum vehicular mode share is with the two wheelers, which contribute about 69% towards Chatram direction and 67% towards Palpannai direction. The dominance of two wheelers characterizes both the traffic directions. Unexpectedly, cars had a lower mode share with 6% and 4% towards Chatram direction and Palpannai direction, respectively. However, non-motorized vehicles

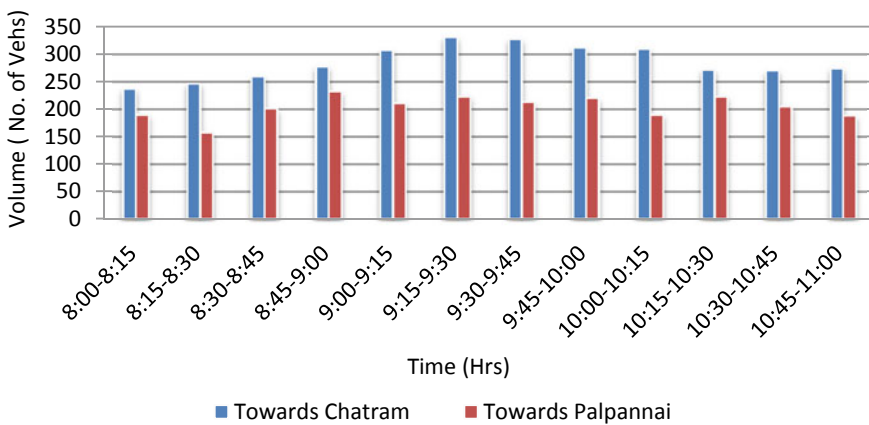


Fig. 2 Variation of traffic volume at selected study sites

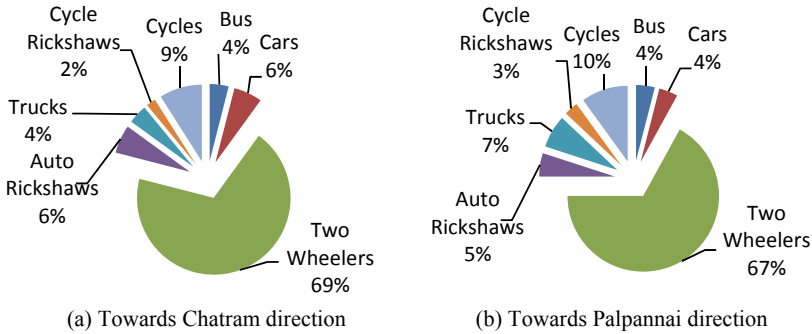


Fig. 3 Vehicular composition at selected study sections

(NMVs), which include the cycles rickshaws and cycles, carried 11% and 13% of the mode share towards Chatram direction and Palpannai direction, respectively. Trucks and buses had a nearly equal percentage of share, ranging between 4 and 7% in both traffic directions.

6 Data Analysis

The increase in the growth rate of the different types of vehicles has increased the degree of heterogeneity in Indian traffic. This impact has resulted in mixed traffic behaviour and abreast vehicle movement in the same road space. Under such conditions, the concept of density can no longer be used to produce accurate and reliable resultant values. Hence, it is considered alarming and imperative to study the traffic characteristics using the speed, flow, and area-occupancy parameters.

6.1 Statistical Analysis of Speed Characteristics

Under mixed traffic conditions, the speed differential among the different vehicle types is large [10]. In order to plot the speed–flow curve, a 15-min interval of traffic data was evaluated to reflect the change in speed and flow accurately. Speed and flow were evaluated separately for both traffic directions. The spread ratio (SR) was calculated using Eq. (1).

$$SR_i = \frac{V_{85} - V_{50}}{V_{50} - V_{15}} \tag{1}$$

Table 2 indicates that the SR values for different categories of vehicles, which indicate the unusual distribution of the speeds among the vehicles. This primary

Table 2 Descriptive statistics on vehicle speeds

Class of vehicle	Study section direction	Mean	SD	Maximum	V_{15}	V_{50}	V_{85}	SR
CAR	Chatram	42	8.74	55	15	44	50	0.39
	Palpannai	45	6.38	58	21	46	52	0.52
TW	Chatram	46	9.87	56	22	49	52	0.48
	Palpannai	44	7.44	60	20	48	56	0.49
AR	Chatram	36	6.04	48	16	39	44	0.46
	Palpannai	39	5.11	51	17	40	45	0.48
TR	Chatram	40	11.55	47	21	42	44	0.52
	Palpannai	42	9.81	52	18	45	49	0.44
BUS	Chatram	39	12.66	48	19	42	45	0.48
	Palpannai	41	10.79	49	22	44	46	0.52
CR	Chatram	12	8.69	19	8	14	16	0.65
	Palpannai	13	8.11	25	9	15	21	0.84
CY	Chatram	15	7.99	22	7	17	19	0.46
	Palpannai	16	7.28	21	9	18	19	0.53

Note: *CAR* cars, *TW* two wheelers, *AR* auto-rickshaws, *TR* trucks, *BUS* buses, *CR* cycle rickshaws, *CY* cycles, *SD* standard deviation, V_{15} 15th percentile, V_{50} 50th percentile, V_{85} 85th percentile, and *SR* speed ratio

reason for these speed variations may be due to the complex physical and operational vehicle characteristics and driving behaviour conditions.

6.2 Estimation of Dynamic Passenger Car Unit Using the Speed–Area Ratio Method

PCU estimation is vital in assessing the performance of traffic facilities. The Indian Roads Congress (IRC) suggests a static set of PCU values for various classes of vehicles in IRC:106 (1990) [11] for urban roads in India based on limited empirical studies. However, Chandra and Sikdar [12] developed a mathematical Eq. (2) for estimating the DPCU factors. Recently, the Indo-Highway Capacity Manual (Indo-HCM: 2017) [13] suggested the DPCU factors, considering the dynamic nature of the traffic. The mechanical and operational characteristics of a standard car are considered to be standard, and hence CAR is taken as a reference vehicle for converting mixed traffic into the equivalent homogeneous traffic. In this study, DPCU is used as a conversion factor.

$$DPCU_i = \frac{V_c/V_i}{A_c/A_i} \quad (2)$$

Table 3 DPCU values of different classes of the vehicle

Class of vehicle	Speed (kmph) (towards Chatram)	Speed (kmph) (towards Palpannai)	Area (m ²)	Average DPCU	Std. Dev. of DPCU	Average DPCU	Std. Dev. of DPCU)
				(towards Chatram)		(towards Palpannai)	
CAR	42	45	5.36	1.00	0.11	1.00	0.08
TW	46	44	1.20	0.20	0.01	0.23	0.03
AR	36	39	4.48	0.98	0.14	0.96	0.18
TR	40	42	17.63	3.45	0.89	3.52	0.77
BUS	39	41	24.54	4.93	0.70	5.03	0.62
CR	12	13	3.09	2.02	0.05	2.00	0.04
CY	15	16	0.86	0.45	0.06	0.45	0.05

Note: *CAR* cars, *TW* two wheelers, *AR* auto-rickshaws, *TR* trucks, *BUS* buses, *CR* cycle rickshaws, *CY* cycles, and *DPCU* dynamic passenger car unit

where

$DPCU_i$ Dynamic passenger car unit of *i*th vehicle.

V_c Average speed of the car (kmph).

V_i Average speed of the *i*th vehicle (kmph).

A_c Projected area of the car (m²).

A_i Projected area of the *i*th vehicle (m²).

The DPCU factors estimated using the speed–area ratio method for both directions of traffic are shown in Table 3.

6.3 Relationship Between Traffic Flow Parameters and Area-Occupancy

Most of the studies have conceptualized the fundamental macroscopic relationships between traffic flow and density without exploring the impact of vehicular heterogeneity. Mallikarjuna and Rao [1] developed area-occupancy concept to represent the traffic density of a roadway in India. In this paper, this area-occupancy concept is used instead of density for the traffic characteristics analysis. Area-occupancy is defined as the proportion of time the vehicle area occupies the observation zone area for the total observation time [14]. The detection zone considered in this study is 27 m × 3.5 m, where 27 m is the trap length, and 3.5 m is the one-lane width of the roadway. The area-occupancy is expressed, as shown in Eq. (3).

$$\text{Area-occupancy} = \frac{\sum_i a_i * \sum_i (t_i)_{AO}}{A * T} \tag{3}$$

where

- a_i Area of detection zone occupied by i th vehicle (m^2).
- A Area of the road stretch (m^2).
- T Total observation time (s).
- $(t_i)AO$ Time during which the detection zone is occupied by i th vehicle (s) for area-occupancy (AO).

Singh et al. [15] defined the Indian traffic as quasi lane disciplined, where some vehicles follow lane discipline and some do not follow lane discipline. Under such traffic conditions, Mishra et al. [3] developed the simulation models based on the relationships between area-occupancy–speed–flow and proved that the concept of area-occupancy as appropriate and alternative for the measurement of density for heterogeneous traffic. Besides, Kumar et al. [4] reported the same on the basis that the area-occupancy takes into consideration the effect of both static and dynamic characteristics of vehicles over the section.

6.3.1 Speed–Flow Plots

Speed is a fundamental measure of traffic performance [16]. In order to plot the speed–flow curve, a 15-min interval traffic is evaluated to reflect the change in speed and volume accurately. Speed and volume were evaluated separately for both the traffic directions. Thus, the computed flow in the aggregated 15-min time interval is converted from vehicles per hour to DPCU per hour using the respective estimated DPCU values of the vehicle class. The speed–flow plots for the traffic towards Chatram and Palpannai are shown in Figs. 4 and 5, respectively.

Regression analysis was carried out between the traffic variables (speed and flow). The R^2 values obtained are 0.8241 and 0.7192 for the traffic towards the Chatram direction and towards the Palpannai direction, respectively. Figures 4 and 5 shows

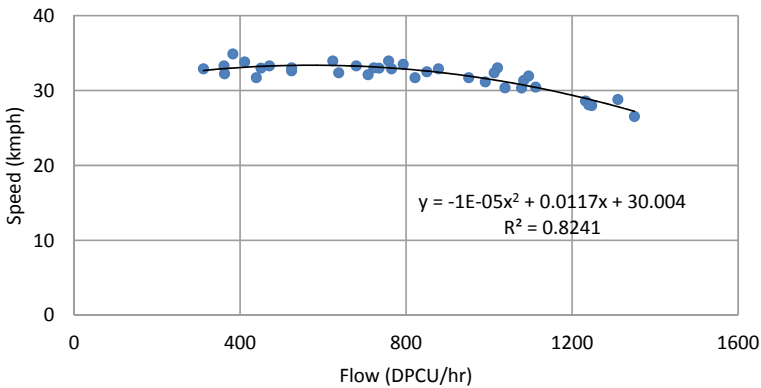


Fig. 4 Speed–flow plot for the traffic towards Chatram direction

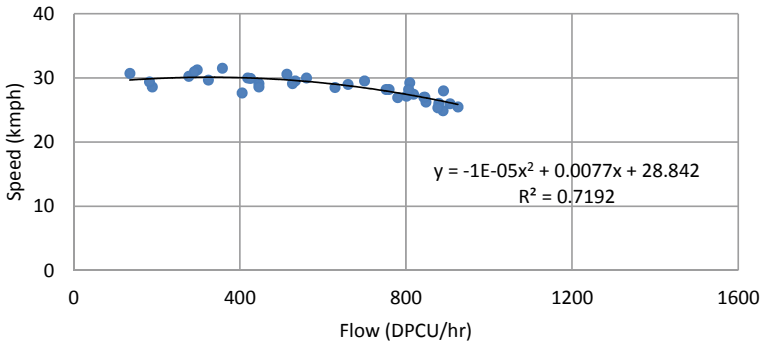


Fig. 5 Speed–flow plot for the traffic towards Palpannai direction

that traffic speed decreases gradually with the increase in traffic flow. The main reason for this was envisaged to be due to the increase in the area-occupancy of the vehicles. When flow increases, traffic on the roadway also increases, thus influencing the free movement of vehicles leading to speed reduction. This is consistent with the results from other studies [3, 17].

6.3.2 Flow–Area-Occupancy Versus Flow–Density Plots

The flows versus area-occupancy and flows versus density plots for traffic towards Chatram are illustrated in Fig. 6a, b, respectively.

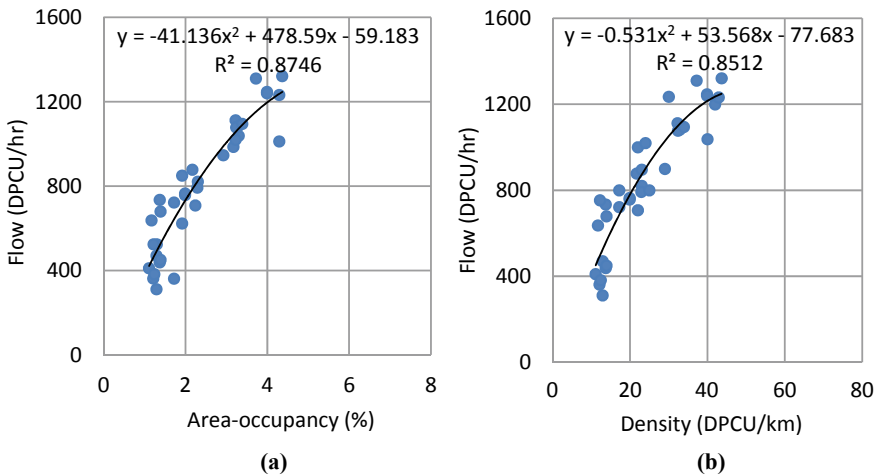


Fig. 6 Flow–area-occupancy versus flow–density plots for the traffic towards Chatram

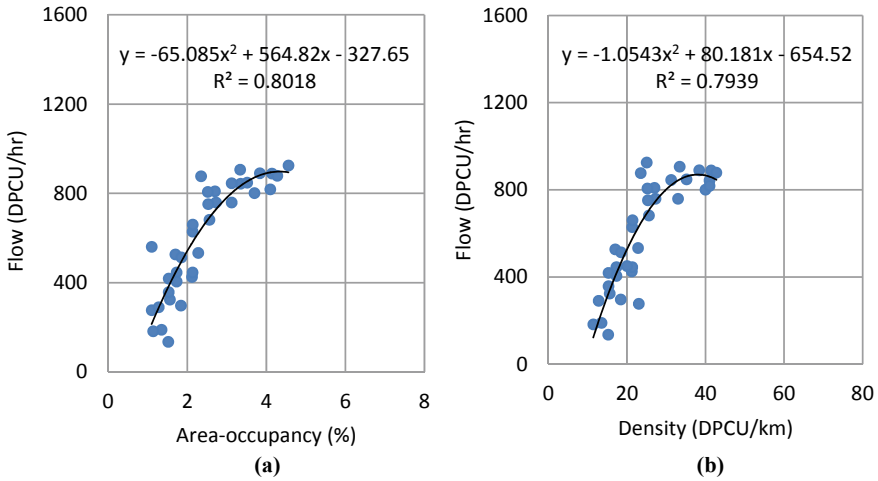


Fig. 7 Flow–Area-occupancy versus flow–density plots for the traffic towards Palpannai

The flows versus area-occupancy and flows versus density plots for traffic towards Palpannai are illustrated in Fig. 7a, b, respectively.

The polynomial equation of the second degree is used to establish the relationships between the flow–area-occupancy and flow–density plots. Regression analysis was carried out to examine the relationship between the flow–area-occupancy and flow–density plots.

The R^2 values of 0.8746 and 0.8512 for flow–area-occupancy and flow–density, respectively, towards Chatram, were achieved, whereas the R^2 values of 0.8018 and 0.7939 for flow–area-occupancy and flow–density, respectively, towards Palpannai were achieved. The R^2 values for flow–area-occupancy plots were found to be higher when compared to the flow–density plots for both directions of traffic.

It can be observed from Figs. 6 and 7 and the respective equations of the regression line that with an increase in the traffic flow, the area-occupancy, and density of traffic increases. The lower vehicle flow levels imply a significant extension to higher area-occupancy levels under the less congested traffic regime. This low-flow regime allows the traffic stream to achieve stable area-occupancy, eventually averting the traffic breakdown. Thus, this avoids the capacity to drop and keep a considerable buildup of the vehicles so that the traffic facility can accommodate higher occupancy of vehicles at low-speed levels.

6.3.3 Speed–Area-Occupancy Versus Speed–Density Plots

The speed versus area-occupancy and speed versus density plots for traffic towards Chatram are illustrated in Fig. 8a, b, respectively.

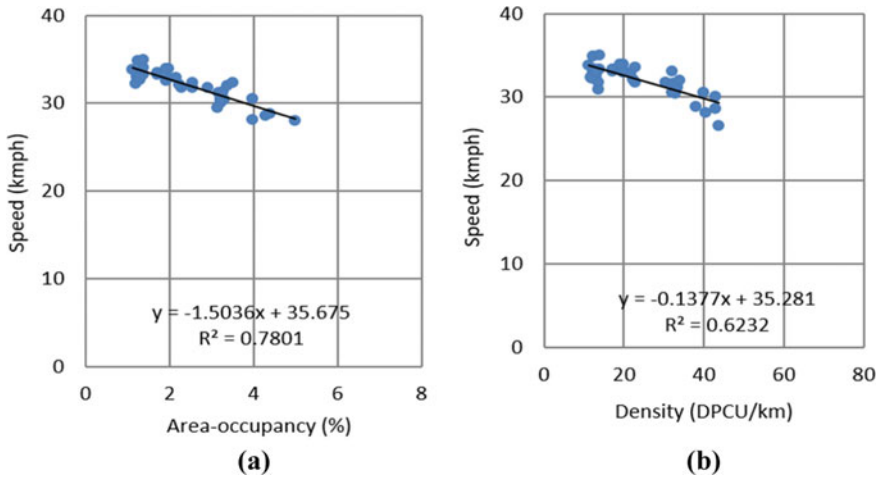


Fig. 8 Speed–area-occupancy versus speed–density plots for the traffic towards Chatram

The speed versus area-occupancy and speed versus density plots for traffic towards Palpannai are illustrated in Fig. 9a, b, respectively.

The polynomial equation of the second degree shows R^2 values for speed–area-occupancy and speed–density curves as 0.7801 and 0.6232, respectively, for the traffic towards Chatram direction. While the R^2 values for speed–area-occupancy and speed–density curves were found to be 0.8118 and 0.6746, respectively, for the traffic towards the Palpannai direction. The R^2 values for speed–area-occupancy plots were found to be higher when compared to the speed–density plots for both directions of traffic.

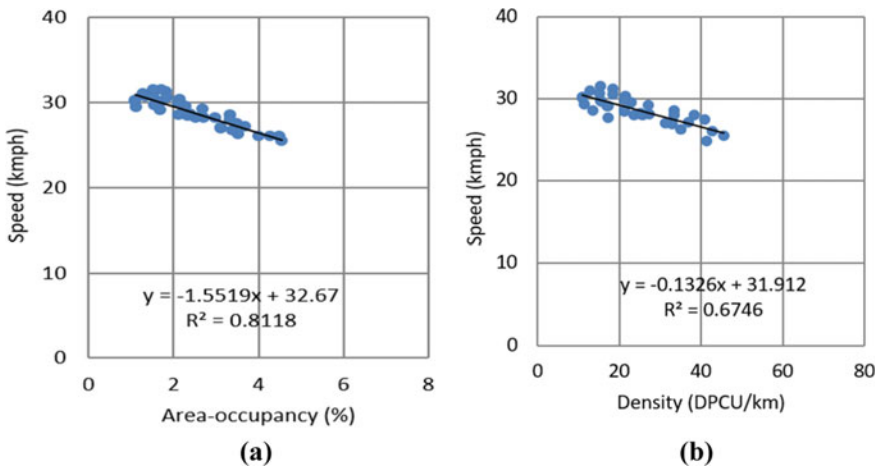


Fig. 9 Speed–area-occupancy versus speed–density plots for the traffic towards Palpannai

Equations of the regression line shown in Figs. 8 and 9 show that the vehicle speed decreases with an increase in area-occupancy and density of traffic. In other words, a large number of vehicles can travel at low speeds with smaller headway and spacing, maintaining a stable and high movement of vehicles. This traffic regime allows the traffic stream to achieve stable area-occupancy or density, preventing traffic breakdown. However, higher percentage of TWs affect the traffic flow due to their filtering, swerving or weaving, and tailgating behaviour through the traffic [18].

7 Results

A quick examination of speed–flow–area-occupancy and speed–flow–density plots shows the sufficient conditions for the existence of macroscopic fundamental diagrams (MFDs) for heterogeneous traffic. The regression fit analysis was performed to examine the goodness-of-fit of the linear model. The rational R^2 values of the combined plot was found to be indicating a decent fit. The flow–area-occupancy and speed–area-occupancy plots, which resulted in higher R^2 values, were found to be more congruent and dependable compared to flow–density and speed–flow plots, respectively, for both the directions of traffic. Also, the traffic characteristics of both the urban arterial stretches were found to be dissimilar. It was clear that because of the complexity in vehicle characteristics and traffic composition, the boundary conditions of MFDs differed significantly. However, the functional plots obtained for flow–area-occupancy and speed–area-occupancy were found to be representing the real-field conditions, indicating that area-occupancy as a measure of concentration is consistent and valid.

8 Concluding Remarks

The primary objective of the paper was to carry out the traffic flow characteristics analysis on the three fundamental parameters: speed, flow, and area-occupancy considering heterogeneous traffic conditions. The area-occupancy concept was investigated for its appropriateness in the MFDs instead of conventional MFDs. The model has a logical explanation for the effect of independent variables on capacity. This study has shown that the measurement of area-occupancy in the field is more straightforward as compared to traffic density.

Speed patterns of vehicles were identified, and the descriptive statistical analysis was carried out to have a basic understanding of the speed characteristics. Speed–flow–density plots were established for traffic data that revealed a linear relationship between the two flow parameters. A regression model was developed to verify the linear model using the R^2 values. Jam density and free flow speeds were estimated through the plots. In addition, speed–flow, flow–area-occupancy, and speed–area-occupancy were developed for the observed values, and a quadratic relationship

between these parameters was verified through regression fit analysis. Since the capacity depends on the roadway, traffic, and driver behaviour conditions, the estimated values could reflect the conditions for roads, traffic, and drivers of the roadway under study.

Thus, for an uninterrupted heterogeneous traffic flow moving on the two-lane road section selected for the survey, parameter distributions and fundamental relationships among the key variables were examined and ascertained through this exploratory study. The area-occupancy approach may help understand traffic characteristics for the development of better traffic models and the evaluation of urban roads. Also, it may improve the traffic stream models for a more comprehensive analysis of traffic studies. As a whole, the area-occupancy approach can be used as the beginning point to understand the dynamic behaviour involved in the overall traffic system under heterogeneous traffic conditions.

9 Limitations and Future Scope

The study is carried out in selected locations of Tiruchirappalli city, India. A similar analysis can be done in many other urban arterials and sub-arterials with a varying number of lanes. It is recommended to extend this research using comprehensive field data obtained from various regions across India.

References

1. Mallikarjuna C, Rao KR (2006) Area occupancy characteristics of heterogeneous traffic. *Transportmetrica* 2(3):223–236. <https://doi.org/10.1080/18128600608685661>
2. Arasan VT, Dhivya G (2008) Measuring heterogeneous traffic density. *Int J Civil Env Str Const Arch Eng* 2(10):236–240
3. Mishra R, Kumar P, Arkatkar SS, Sarkar AK, Joshi GJ (2017) Novel area occupancy-based method for passenger car unit estimation on multilane urban roads under heterogeneous traffic scenario. *Trans Res Rec J Trans Res Board* 2615:82–94. <https://doi.org/10.3141/2615-10>
4. Kumar P, Raju N, Mishra A, Arkatkar SS, Joshi GJ (2018) Validating area occupancy-based passenger car units and homogeneous equivalent concept under mixed traffic conditions in India. *J Transp Eng Part A Syst* 144(10):04018064
5. Chandra S, Verma VS (1995) Capacity of urban roads using area density concept. *J REAAA* 5:14–20
6. Arasan VT, Dhivya G (2010) Methodology for determination of concentration of heterogeneous traffic. *J Trans Sys Eng Info Tech* 10(4):50–61
7. Geroliminis G, Sun J (2011) Properties of a well-defined macroscopic fundamental diagram for urban traffic. *Transp Res Part B* 45:605–617
8. Mallikarjuna C, Rao KR (2011) Heterogeneous traffic flow modelling: a complete methodology. *Transportmetrica* 7(5):321–345. <https://doi.org/10.1080/18128601003706078>
9. Kumar P, Arkatkar SS, Joshi GJ (2018) New approach for estimating passenger car units on multilane urban roads with heterogeneous traffic conditions. *J Transp Eng Part A Syst* 144(3). <https://doi.org/10.1061/JTEPBS.0000117>

10. Dhamaniya A, Chandra A (2017) Influence of operating speed on capacity of urban arterial midblock sections. *Int J Civ Eng* 15:1053–1062. <https://doi.org/10.1007/s40999-017-0206-7>
11. Indian Roads Congress: 106 (1990) Guidelines for capacity of urban roads in plain areas. Indian Roads Congress, New Delhi, India
12. Chandra S, Sikdar PK (2000) Factors affecting PCU in mixed traffic situations on urban roads. *Road Trans Res* 9(3):40–50
13. Indian Highway Capacity Manual (Indo-HCM): (2017) Central Road Research Institute, New Delhi, India
14. Asaithambi G, Kanagaraj V, Srinivasan KK, Sivanandan R (2018) Study of traffic flow characteristics using different vehicle following models under mixed traffic conditions. *Transp Lett* 10(2):92–103. <https://doi.org/10.1080/19427867.2016.1190887>
15. Singh S, Panda RK, Saw DK, Selvaraj MS (2020) Effect of heavy transport vehicles on speed-flow characteristics of mixed traffic on multi lane divided intercity highways. In: Proc. 13th Asia Pacific Transportation Development Conference (ASCE), Shanghai, China, 176–185. <https://doi.org/10.1061/9780784482902.021>
16. Singh S, Shukla BK, Santhakumar SM (2020) Infra-red sensor-based technology for collecting speed and headway data on highways under mixed traffic conditions. In: Proc. 2020 7th International Conference on Signal Processing and Integrated Networks (IEEE), Noida, India, 607–611. <https://doi.org/10.1109/SPIN48934.2020.9070829>
17. Singh S, Kumar A, Niyas M, Santhakumar SM (2020) Multivariate analysis of freeways speed and time headway under mixed traffic streams. In: Proc. 2020 International Conference on COMMunication Systems & NETWORKS (IEEE), Bengaluru, India, 116–121. <https://doi.org/10.1109/COMSNETS48256.2020.9027497>
18. Singh S, Barhmaiah B, Kodavanji A, Santhakumar SM (2020) Analysis of two-wheeler characteristics at signalised intersection under mixed traffic conditions: A case study of Tiruchirappalli city. In: Proc. 13th Asia Pacific Transportation Development Conference (ASCE), Shanghai, China, 35–43. <https://doi.org/10.1061/9780784482902.005>

Sustainable Management of Stormwater to Prevent Urban Flooding Using SWMM



Anurag Swarnkar, Samir Bajpai, and Mani Kant Verma

Abstract Stormwater is an essential component of the urban water cycle, and its improved management is beneficial in managing water requirements of cities and improving urban life in environmental, economic, and social aspects. Increasing industrial and anthropogenic activities have significantly raised the necessity of discharging the runoff safely. In most of the cities, the existing stormwater drains are in the dilapidated stage, resulting in clogged drains, which causes frequent urban flooding. This paper elucidates the present status of management of the stormwater drainage system in Raipur City, capital of Chhattisgarh State, India. The estimation of the stormwater runoff and identification of the urban flooding hotspots are the principal objectives of this work. To develop an integrated approach for examining the effects of urban growth on surface runoff at the local level, the stormwater management model (SWMM) is employed. From the results, the drainage network of the city is found to be incapable of accommodating the inflow runoff, which results in the nodes getting flooded frequently. Therefore, the improper drainage system is the root cause of urban flooding at most of the hotspots. It is also found that the stormwater obtained from the rooftops is comparatively less contaminated as compared to the roadside drains and thus can be diverted and stored for further uses. This study will certainly help to develop effective stormwater management strategies, especially over the Raipur City.

Keywords Stormwater · Runoff · SWMM · Raipur City · Drainage

A. Swarnkar (✉)

Centre for Transportation Systems, Indian Institute of Technology Roorkee, Roorkee 247667, India

e-mail: anuragswarnkar91@gmail.com

A. Swarnkar · S. Bajpai · M. K. Verma

Department of Civil Engineering, National Institute of Technology Raipur, Raipur 492010, India

1 Introduction

The world has witnessed rapid urbanization over the last few decades. One of the many complex problems resulting from increased urbanization is related to the management of stormwater, producing significant problems such as regular flooding, erosion, sedimentation, drainage problems [1–4]. The point and non-point source release of various pollutants is also adversely affecting the stormwater quality. Improper management of stormwater may lead to economic losses [5]. Stormwater management is the process of managing the quantity and quality of stormwater by using both structural or engineered control devices and systems. Stormwater runoff occurs when the rain falls over the land surface, such as roads, parking lots, rooftops, and other impervious surfaces that prevent water from soaking into the ground to the landscape. This increases the quantity of stormwater runoff generated during the monsoon season. Estimation of such runoff reaching the storm sewers, therefore, is dependent on the intensity, duration of precipitation, characteristics of the tributary area, and the time required for such flow to reach the sewer [6–10]. The intense rainfall events occur frequently over the urban regions, especially due to climate change, which further deteriorates the problems [11–18]. In this regard, proper stormwater management is pivotal.

Sustainable stormwater management practices tend to reduce the volume and remove the pollutants from runoff generated on their development sites lowering the impact of stormwater runoff [19–21]. Therefore, it is essential to develop a low-impact development for managing stormwater along the roadways, parking lots and on the nalas and river banks.

Stormwater modeling has a major role in preventing issues such as flash floods and urban water-quality problems. However, in-detail modeling of large urban areas is time-consuming. However, modeling of large urban is time-consuming as detailed input data is required for model calibration. Stormwater models with low spatial resolution may be cherished if the results provided by the model are satisfactory.

Despite the defects in the input data, the process adopted in this study for catchment delineation and subdivision is relatively fast and accurate. Developing a low-resolution sub-catchment for Storm Water Management Model (SWMM) is a complex task. However, SWMM provides acceptable results for such cases too [22]. Thus, SWMM is applied in this study.

2 Study Area and Data Used

Raipur is the capital of Chhattisgarh State, India, and expands from 21.20° to 21.32° latitude and 81.58° to 81.68° longitude [22, 23]. The surface runoff from the drainage system in Raipur City embraces of a hierarchical system of natural and man-made drains, water bodies that ultimately discharge into River Kharun flowing through the west side of the city [20]. The current stormwater collection network seems to be

unplanned as well as inadequate, with coverage of a mere 6.48% of total area with a total length of drainage network being 63.58 km, resulting in frequent overflows. The low carrying capacity and poor conditions of the stormwater drain in some areas have resulted in constant inundation of the majority of areas in the city, especially the low-lying areas. Due to the lack of the data availability, it was difficult to carry out the modeling for the whole Raipur City. Since Raipur City is categorized into different wards, a small drainage area of a particular ward was taken for detailed analysis. The selected area is the V.V. Vihar colony (ward no. 27, zone no. 2), presented in Fig. 1.

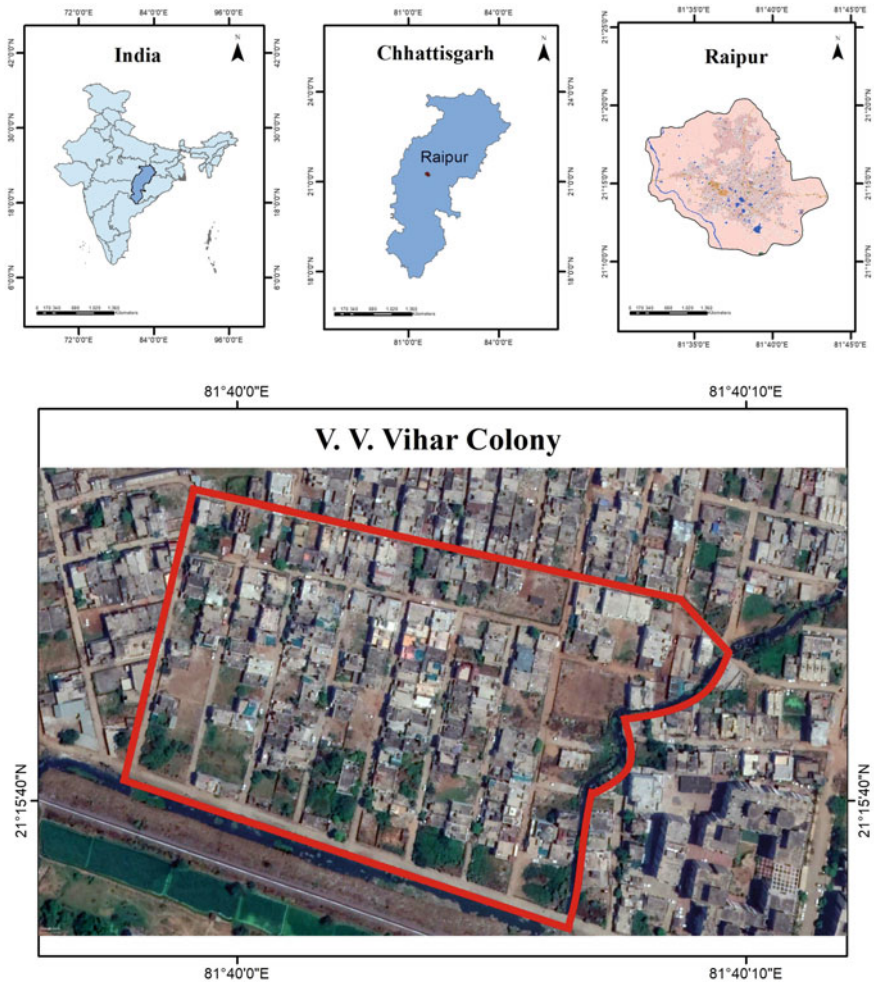


Fig. 1 Location of V.V. Vihar colony from ward no. 27, zone no. 2, Raipur District, Chhattisgarh

3 Methodology

As the study deals with the urban stormwater management, it is necessary to find the boundary of Raipur urban City. This was done in ArcGIS 10.1, wherein a map downloaded from the Bhuvan website was imported. Thereafter, the map was georeferenced, taking four points within the map, coordinates of which were already known. For georeferencing, it is necessary to take at least three points within the map; the coordinates of the fourth point is then taken automatically. This georeferenced map was exported and was used as the base map for drawing the boundary of the Raipur City. A high-resolution map was also downloaded from Google Map Downloader. Although the map downloaded was a picture without any properties, it helped explore various locations of the city. A DEM is taken as the input file for plotting the contours and the slope map. The contour map and slope map helps us to define the direction of the flow, identification of the low lying areas, etc. Both the maps were prepared in ArcGIS 10.1. The slope of the study area was calculated by the percent rise method using the Arc-Hydro tools. The highest slope of the Raipur City calculated using ArcGIS 10.1 was 113.27%, whereas, for the flat surface, it was 0%. To prepare the contour, we have to process the DEM using the tool 'focal statistics' so that all the tiles in the DEM are converted into circles from the square.

The data obtained from Municipal Corporation Raipur was imported in ArcGIS 10.1. The spatial reference of the data obtained was different from that used to adopt while working in ArcGIS. The spatial reference given to all the data is WGS_1984. The data was exported in Google Earth by creating KML file using the tool conversion tool 'layer to kml.' All the data were visualized in Google Earth to get the real scenario of the study area, such as the number of buildings, roadways, drainage networks, and open space. After importing all the datasets, attributes were prepared and calculated as per the new spatial reference. To calculate the attributes, the spatial reference of the map layer has to be set as WGS_1984 UTM Zone 44 N. The spatial reference for the map layer is WGS_1984 UTM Zone 44 N, whereas the data which are included in that map layer has WGS_1984 as their spatial reference. Low lying areas were identified and located using all the prepared datasets. The dark tiles in the DEM show the location having low elevation. The DEM was overlapped with the high-resolution city map, adjusting the transparency of the DEM layer; the low lying areas were marked. Out of the marked location, V.V. Vihar Colony was selected for the analysis.

Many other low lying locations were also obtained from other sources such as news reports, local government reports, and survey other than the analysis done in ArcGIS 10.1. Some of the low lying areas were V.V. Vihar Colony, Jalvihar colony, forest colony, RDA colony, Anupam Nagar, Indravati colony, Khadan Nagar, Mahavir Nagar, Krishna Nagar, Choubey Colony, Panchsheel Nagar. A customer survey was also done in some of the above areas to get information about the current scenario. It was found that some of the areas have recovered from poor drainage systems resulting in a lack of floods. The people residing in respective areas told that after

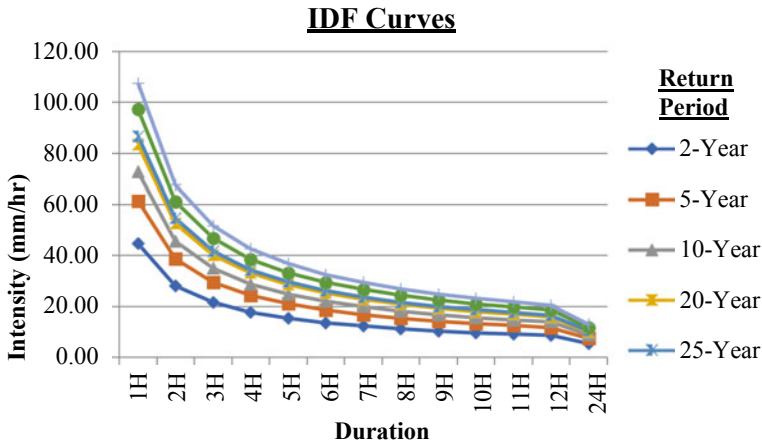


Fig. 2 IDF curves over the study area

retrofitting of drains, the stagnation time of the stormwater has reduced compared to earlier situations.

SWMM 5.1 is used to manage the drainage system of the study area. Since the data prepared in ArcGIS 10.1 cannot be exported/imported in SWMM 5.1, we have to use the image file of the study area as the backdrop image and draw all the objects by tracing the backdrop image. To run the model in SWMM, it is necessary to feed the rainfall time series data in an hourly format. Computation of hourly data from daily data was done using the Indian Meteorological Department IMD 1/3rd rule [24]. IDF curves were generated to determine the intensity of the rainfall event at various time durations for different return periods (Fig. 2). Before preparing the curve, goodness of fit test was done for the available rainfall data. This test was carried out for Gumbel's distribution, Poisson's distribution, and normal distribution. It was found out that the rainfall data follows Gumbel's extreme Value Type-1 distribution. The model was also simulated for the forecasted rainfall for 10 years from 2015 to 2025. Based on the model and improved conduit dimensions, there was no flooding identified in the study area. It was observed that no nodes were flooded with the proposed dimensions. The nodes (denoted by J) and conduits (denoted by C) are presented in Fig. 3.

4 Results and Discussion

For the system just evaluated, the report indicates satisfactory simulation results, with negligible mass balance continuity errors for both runoff and routing (-0.28% and -0.032), respectively, if all data were entered correctly. Also, of the 24.035 inches of rain (in terms of total volume, division by area gives rainfall depth) that fell



Fig. 3 Nodes and conduits depicted for the study area

on the study area, 1.75 in. infiltrated into the ground, and essentially the remainder became runoff.

It was found that the nodes J25, J27, J29 are flooded for 0.92, 1.03, 1.13 h, respectively. In SWMM, flooding will occur when the water surface at a node exceeds the maximum allocated depth. Similarly, the conduits C23, C25, C27 are surcharged for 0.90, 1.02, 1.12 h. The conduits were at full capacity and therefore appeared to be slightly undersized. The water elevation profile and time series plot of these conduits are shown in Fig. 4.

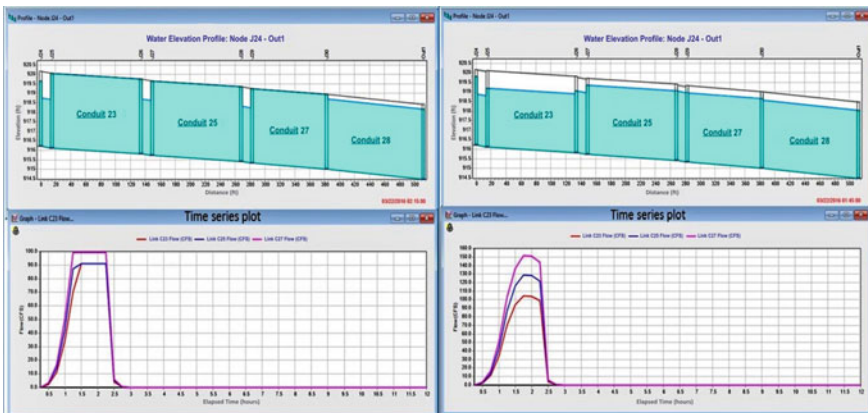


Fig. 4 Water elevation profile and time series plot of conduits C23, C25, and C27 for existing and proposed dimensions

The excess rainfall can be stored at a suitable location so that it may prevent flooding, provide groundwater recharge, and, when treated, can also act as a source to fulfill the domestic needs. Based on the contours of the area, two suitable sites are marked within the study area for the storage of stormwater (Fig. 5). The combined area of the reservoir was computed as 2012 m². The average depth of the reservoir is kept as 3 m, resulting in a joint capacity of 3036 m³. The first pond may act as a settling tank or an oxidation pond, providing treatment to the incoming stormwater. The surplus water from the first pond will be fed to the second pond, and in this sequence, other suitable location or existing pond may be selected for storing the surplus stormwater.



Fig. 5 Location of the reservoirs within the study area

5 Conclusion

The rainfall and catchment characteristics have a strong influence on urban stormwater. Accurate assessments of stormwater will result in the effective design of urban stormwater management systems. Lack of availability finding the relevant available and derived hydrological data such as water flow in natural and man-made drains can be obtained by the designers/engineers by calibrating the model processes. The present work may be extended to provide sustainable stormwater management for the entire city. The network of stormwater drains of adequate capacity will provide effective drainage and prevent flooding of the area. The stormwater, which was creating a nuisance, can be converted into a valuable source. The storage of stormwater in small and big ponds will recuperate the existing ponds in the city as well as create new ponds. This will provide potential groundwater recharge and additional water sources.

References

1. Gupta K (2007) Urban flood resilience planning and management and lessons for the future: a case study of Mumbai, India. *Urban Water J* 4(3):183–194
2. Young KD, Dymond RL, Kibler DF (2011) Development of an improved approach for selecting stormwater best management practices. *J Water Resour Plann Manage* 137(3):268–275
3. Swain S, Dayal D, Pandey A, Mishra SK (2019) Trend analysis of precipitation and temperature for Bilaspur District, Chhattisgarh, India. In: World environmental and water resources congress 2019: groundwater, sustainability, Hydro-climate/climate change, and environmental engineering. American Society of Civil Engineers, Reston, VA, pp 193–204
4. Sörensen J, Persson A, Sternudd C, Aspegren H, Nilsson J, Nordström J, Jönsson K, Mottaghi M, Becker P, Pilesjö P, Larsson R, Berndtsson R, Mobini S (2016) Re-thinking urban flood management—time for a regime shift. *Water* 8(8):332
5. Barbosa AE, Fernandes JN, David LM (2012) Key issues for sustainable urban stormwater management. *Water Res* 46(20):6787–6798
6. Swain S, Verma MK, Verma MK (2018) Streamflow estimation using SWAT model over Seonath river basin, Chhattisgarh, India. In: Singh V, Yadav S, Yadava R (eds) Hydrologic modeling. Water science technology library, vol 81, pp 659–665
7. Davis AP, Shokouhian M, Sharma H, Minami C (2001) Laboratory study of biological retention for urban stormwater management. *Water Environ Res* 73(1):5–14
8. Swain S, Nandi S, Patel P (2018) Development of an ARIMA model for monthly rainfall forecasting over Khordha district, Odisha, India. In: Sa P, Bakshi S, Hatzilygeroudis I, Sahoo M (eds) Recent findings in intelligent computing techniques. Advances international system computing, vol 708, pp 325–331
9. Brown RR (2005) Impediments to integrated urban stormwater management: the need for institutional reform. *Environ Manage* 36(3):455–468
10. Swain S, Patel P, Nandi S (2017) A multiple linear regression model for precipitation forecasting over Cuttack district, Odisha, India. In: 2017 2nd international conference for convergence in technology (I2CT). IEEE, pp 355–357
11. Dayal D, Swain S, Gautam AK, Palmate SS, Pandey A, Mishra SK (2019) Development of ARIMA model for monthly rainfall forecasting over an Indian river Basin. In: World environmental and water resources congress 2019: watershed management, irrigation and drainage,

- and water resources planning and management. American Society of Civil Engineers, Reston, VA, pp 264–271
12. Abebe AJ, Price RK (2005) Decision support system for urban flood management. *J Hydroinform* 7(1):3–15
 13. Swain S (2017) Hydrological modeling through soil and water assessment Toolin a climate change perspective a brief review. In: 2017 2nd international conference for convergence in technology (I2CT). IEEE, pp 358–361
 14. Swain S, Patel P, Nandi S (2017). Application of SPI, EDI and PNPI using MSWEP precipitation data over Marathwada, India. In: 2017 IEEE international geoscience and remote sensing symposium (IGARSS). IEEE, pp 5505–5507
 15. Swain S, Mishra SK, Pandey A (2020) Assessment of meteorological droughts over Hoshangabad district, India. *IOP Conf Ser Earth Environ Sci* 491(1):012012
 16. Swain S, Sharma I, Mishra SK, Pandey A, Amrit K, Nikam V (2020) A framework for managing irrigation water requirements under climatic uncertainties over Beed district, Maharashtra, India. In: World environmental and water resources congress 2020: water resources planning and management and irrigation and drainage. American Society of Civil Engineers, Reston, VA, pp 1–8
 17. Radmehr A, Araghinejad S (2014) Developing strategies for urban flood management of Tehran city using SMCDM and ANN. *J Comput Civ Eng* 28(6):05014006
 18. Swain S, Mishra SK, Pandey A, Dayal D (2021) Identification of meteorological extreme years over central division of Odisha using an index-based approach. In: Pandey A, Mishra S, Kansal M, Singh R, Singh VP (eds) *Hydrological extremes*. Water science technology library, vol 97. Springer Cham, pp 161–174
 19. Hammer TR (1972) Stream channel enlargement due to urbanization. *Water Resour Res* 8(6):1530–1540
 20. Aadhar S, Swain S, Rath DR (2019) Application and performance assessment of SWAT hydrological model over Kharun river basin, Chhattisgarh, India. In: World environmental and water resources congress 2019: watershed management, irrigation and drainage, and water resources planning and management. American Society of Civil Engineers, Reston, VA, pp 272–280
 21. Zevenbergen C, Veerbeek W, Gersonius B, Van Herk S (2008) Challenges in urban flood management: travelling across spatial and temporal scales. *J Flood Risk Manage* 1(2):81–88
 22. Khan AA, Ahmad M (2014) Integration of stormwater drains with lakes: expectations and reality—a case of Raipur, India. *Hydrol Current Res* 5(2):1
 23. Swain S, Verma M, Verma MK (2015) Statistical trend analysis of monthly rainfall for Raipur district, Chhattisgarh. *Int J Adv Eng Res Stud IV(II):87–89*
 24. Palaka R, Prajwala G, Navyasri KVS, Anish IS (2016) Development of intensity duration frequency curves for Narsapur mandal, Telangana state, India. *Int J Res Eng Technol* 5(6):109–113

Decongesting Urban Roads: An Investigation into Causes and Challenges



Ekta Singh  and Devendra Pratap Singh 

Abstract It is well established that urban transport plays an important role in making cities livable and sustainable. Further, fast growth in urbanization and industrialization demands the use of more vehicles which leads to an imbalance between infrastructure availability and mobility demand. Historically, planners and decision-makers have proposed and practiced divergent approaches and policies for dealing with congestion. However, it is realized that traditionally it has been easier to advocate the novel approaches in the planning of new cities and also in cities that follow stricter regulations and are less dense. Nonetheless, it is experienced that much of the urbanization is happening in the existing cities, and in most of the developing countries the existing cities are characterized by narrow roads that are incapable of accommodating the growing traffic and have inadequate provision for parking, loading, and unloading facilities. This is further aggravated by the changing land use of the existing and mainly the old city areas. Eventually, this results in delays, deteriorating health of the city inhabitants, and fatalities due to road accidents. This harrowing experience severely undoes the benefits arising from the agglomeration effect of the urban economy. The situation is worse in metropolitan cities like Delhi, Mumbai, Lima, Bogota, and many capital cities across the developing world. In developing countries, multimodal traffic further worsens the situation. Many cities have implemented diverse strategies like introducing bus rapid transit systems, metro rail lines, constructing ring roads, and flyovers, but, still have failed to combat the growing menace of traffic congestion. New Delhi the capital city of India despite having one of the highest density of roads in the world and having a state-of-the-art metro transport network has failed to tackle daily congestion problems. With this background, the present paper attempts to identify the major issues and challenges on a typical arterial road that leads to congestion. The paper is based on a case study approach and attempts to identify and address the congestion issues on a 2.1 km stretch of Guru Ravidas Marg in New Delhi. There are multitudes of indicators and measurements

E. Singh (✉)
CityDialogue, Noida, India
e-mail: consultantektasingh@gmail.com

D. P. Singh
ASAP, Amity University Uttar Pradesh, Noida, India

available to analyze congestion levels. The authors adopted the common techniques of the **traffic volume** and **level of service** to establish the congestion level. Apart from this, the authors analyzed various other physical attributes like **land use, street characteristics, and parking trends** to comprehend the issues and challenges.

Keywords Urban roads · Congestion · India · Traffic volume · Level of service · Land use

1 Introduction

Fast growth in urbanization and industrialization demands an efficient urban transport system for effective and easy movement of people and freight. This transport or means of mobility within the growing cities play an important role in making cities livable and sustainable. In the absence of adequate and effective facilities and systems for mobility, the city tends to become unproductive. One of the major ills of ineffective transport planning in urban areas is traffic congestion. It is well established that urban transport plays an important role in making cities livable and sustainable. In the absence of adequate facilities for the mobility of people and movement of logistics, the city gives a depressive look. Further, fast growth in urbanization and industrialization demands the use of more vehicles which leads to an imbalance between infrastructure availability and mobility demand. Historically, planners and decision-makers have proposed and practiced divergent approaches and policies for dealing with congestion. However, it is realized that traditionally it has been easier to advocate the novel approaches in the planning of new cities and also in cities that follow stricter regulations.

Nonetheless, it is experienced that much of the urbanization is happening in the existing cities, and in most of the developing countries the existing cities are characterized by narrow roads that are incapable of accommodating the growing traffic and have inadequate provision for parking and loading and boarding facilities [8]. This is further aggravated by the changing land use of the existing and mainly the old city areas. Eventually, this results in delays, wastage of precious hours, deteriorating health of the city inhabitants, and fatalities due to road accidents. This harrowing experience severely undoes the benefits arising from the agglomeration effect of the urban economy. The situation is worse in metropolitan cities like Delhi, Mumbai, Lima, Bogota, and many capital cities across the world. In developing countries, multimodal traffic further worsens the situation. Many cities have implemented diverse strategies like introducing bus rapid transit systems, metro rail lines, constructing ring roads, and flyovers [3], but, still have failed to combat the growing menace of traffic congestion.

New Delhi the capital city of India despite having one of the highest density of roads in the world and having a state-of-the-art metro transport network has failed to tackle daily congestion problems [7]. With this background, the present paper attempts to identify the major issues and challenges on a typical arterial road that

leads to congestion. The paper is based on a case study approach and attempts to identify and address the congestion issues on a 2.1 km stretch of Guru Ravidas Marg in New Delhi. Before conducting any case study, it is impertinent to understand from existing studies what have been the common causes of congestion in similar scenarios and how to measure congestion. In the following section, a brief review of existing literature is conducted.

2 Literature Review

Several studies have been conducted in the past that analyze the various aspects mainly vehicular traffic pattern, road capacity, and design, changing land-use pattern, and changing demand pattern of road movement to gather its impact on traffic congestion. The causes of traffic congestion are categorized in terms of micro-level factors and macro-level factors [9]. Micro-level factors are one arising from the immediate context that is too many vehicles moving at the same time or under the capacity of roads. On other hand, macro-factors are the result of broader contexts like rapid increase in urbanization, car ownership status, changing land patterns, and increasing buying capacity of the urban population.

A study highlighted that traffic congestion on urban roads is mainly attributed to the growing difference in the demand and supply capacity of the road due to the increasing motor vehicle population [5]. This increase in motor vehicle population is primarily attributed to increasing population and urbanization rate, mostly in countries transiting from developing to developed, mainly China and India the two major growing economies of the world [1]. The vehicle population in China has been increasing at more than 30% and at around 10% in India [12].

Nonetheless, some studies advocate that a mere increase in vehicular population is not the main contributor to rising congestion levels in urban cities [1]. According to Alam and Ahmed, slower traffic and mismanagement between the demand for and supply of transport services have been also causing traffic congestion in the cities of Ghana in Bangladesh and Varanasi in India. A study also revealed that traffic congestion is one of the major side effects of urban land redevelopment projects in a few cases due to inappropriate land-use allocations and mismanagement of transport facilities [15]. Several researches are also conducted to understand the travel behavior pattern with respect to land-use mixture and development density and to analyze the causes of congestion [6]. It can be summarized based on the above review that traffic congestion in urban areas is not attributed to any one major reason but is very subjective with respect to context and also is a result of different urban traits and concerns which are mainly physical redevelopment, urban population growth, inappropriate road, and street designs and rapidly changing mobility behavior. Hence to resolve the congestion-related problems at the micro-level, it is pertinent to first measure the level of congestion and then investigate the causes. In the following section, a brief discussion of the methodology adopted by the authors to measure the congestion level is discussed.

3 Methodology

In this study, the authors attempt to capture the challenge of congestion in the communities across an arterial road in the New Delhi area. The tools utilized to identify the level of congestion rely on the two most common and well-established techniques of measuring traffic volume and level of service [13]. Further, a detailed analysis of the changing land-use pattern, street characteristics, and parking trend is conducted. The challenges and issues are captured both through comprehensive visual and traffic surveys and qualitative interviews of the different actors. The three wards of Govindpuri, Kalkaji, and East of Kailash ward are surveyed for this purpose. The traffic-related surveys are conducted at four different times of the day, across three different days. Days were identified after a pilot reconnaissance and traffic survey conducted over a fortnight, to understand the peak traffic days and time, as several studies have highlighted the relevance of peak traffic days and time in arriving at the root cause of congestion in any locality [11].

4 Discussion

4.1 Introduction to Study Area

According to ITDP, Delhi is considered to be the most congested city in India, followed by Bengaluru, Mumbai, Hyderabad, Kolkata, Chennai, and Ahmedabad. According to RITES, in Delhi, around 1,400 vehicles are added annually to the roads, which results in more vehicles on road every day, and hence, Delhi faces a traffic congestion problem. As stated earlier, Delhi has one of the highest densities of road network in the world, and road density (km of road per 100 km² of land area) of Delhi is 2240 for the year 2016, a figure calculated from the data available on Delhi Traffic Police Web site [4]. Despite this, it fails to manage the congestion issues on the majority of its urban roads. A significant cause of this is the sharp increase in the vehicular population of Delhi over the period 2001–2011 and also a significant increase in the population of Delhi that has grown by 1.59% signifying a rapid increase in the workforce that require substantial mobility means (Fig. 1). Registered motor vehicles grew by 10.28% which leads to an imbalance between infrastructure availability and mobility demand (Table 1).

This rapid increase in vehicular population results in a low roadway level of service (LOS) on urban roads that means the number of vehicles or traffic volume, like trucks, buses, private cars, etc., exceeds the existing road capacity [14]. According to the statistics of the National Capital Region Planning Board, Ministry of Urban Development, GoI, there is an inadequate supply of urban roads in comparison with the increase in the vehicular population over the last decade. The road network of Delhi increased from 28508 km in 2001 to 29030 km in 2011 that is around 2% of the increase while the vehicular population grew by almost 10%. Apart from the

Fig. 1 Population growth rate versus vehicular growth rate (in percent) Delhi (2000–2011). *Source* Ministry of Road Transport and Highways, GoI Delhi

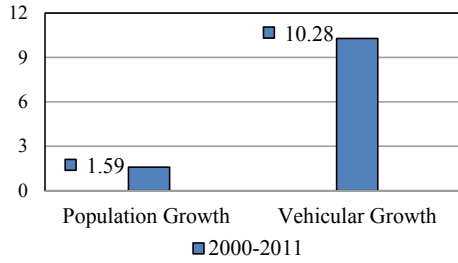


Table 1 Population versus number of registered vehicles (Delhi-2016)

Attribute	Quantity
Population	200,000
Total registered vehicle	9,634,976
Road length (in kms)	33,260

Source Delhi Traffic Police

increase in the number of vehicles, the roads of Delhi are characterized by mixed traffic with no discrete segregation of lanes and road section. The traffic type includes private vehicles, two wheelers, four wheelers, public vehicles, buses, and trucks, auto-rickshaws, including both manually driven cart and animal carts and pedestrians. All this leads to heavy traffic congestion, decreased vehicular speed, and other ill effects like air pollution. This scenario is typical of the major arterial roads of Delhi. For this study, Guru Ravidas Marg was selected. From here onward, the road is addressed as Ravidas Marg. The description of the Ravidas Marg is provided in the next section.

Guru Ravidas Marg: Site Description

Ravidas Marg is located in South Delhi in Zone F (Fig. 2) and falls under three wards, i.e., Kalkaji ward (196), Govindpuri Ward (195), and East of Kailash ward (190).

Fig. 2 Location map zone 1, New Delhi. *Source* Author’s illustration





Fig. 3 2.1 km stretch of the Guru Ravidas Marg. *Source* Author's illustration

Table 2 Guru Ravidas Marg basic statistics

Attribute	Description
Length of stretch	2.1 km
Right of way	28–36.3 m
Total area	203 ha
Population	1.12 Lakhs
Population density	9800 Person per km ²

Source Data from Delhi Development Authority

The stretch connects two important arterial roads—Outer Ring Road in the north and Mehrauli-Badarpur Road in the south (Fig. 3). It connects the area with the rest part of the city and serves as a prime linkage to access residential colonies, schools, colleges, and industries. It also connects to major landmarks in the area includes Lotus Temple, Nehru Place, Deshbandhu College, Govindpuri Metro, and Okhla industrial area. The population of the area under consideration is 1.12 lakh and the population density is 9800 persons per km² (Table 2). The area is a prominent residential neighborhood in South Delhi, but over time it has grown as major retail and wholesale destination. It is flanked by residential colonies authorized and unauthorized, markets, schools, and industrial area (Okhla), mostly with access from this road.

The length of the Ravidas Marg is 2.1 km, and Right of Way¹ (R.O.W) varies from 28 m in North to 36.3 m in South. The study stretch lies in two different wards, i.e., Govindpuri Ward (195) and Kalkaji Ward (196). The total area under Govindpuri Ward (195) is 78 ha, whereas the total area under Kalkaji Ward (196) is

¹R.O.W is a type of easement granted or reserved over the land for transportation purposes, and this can be for a highway, public footpath, rail transport, canal, as well as electrical transmission lines, oil, and gas pipelines.

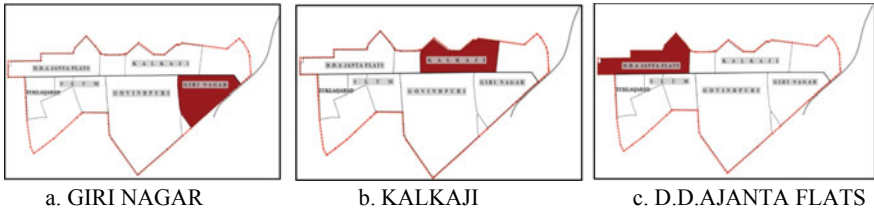


Fig. 4 Planned colonies. *Source* Author’s illustration

125 ha. The study area is bounded by three major arterial roads, i.e., the Outer Ring Road on the eastern side, Ma Anandmayee Marg on the western edge, and Mehrauli-Badarpur Road on the southern side. Mullah Issar Marg and Main Kalkaji Road are the mixed-use roads in the area that connect the Outer Ring Road and Guru Ravidas Marg. The area is well connected by roads. The markets lie close to the Govindpuri Metro Station. The residential area in the wards can be divided into the following categories—planned colonies, unauthorized colonies, and slums (Figs. 4, 5 and 6).

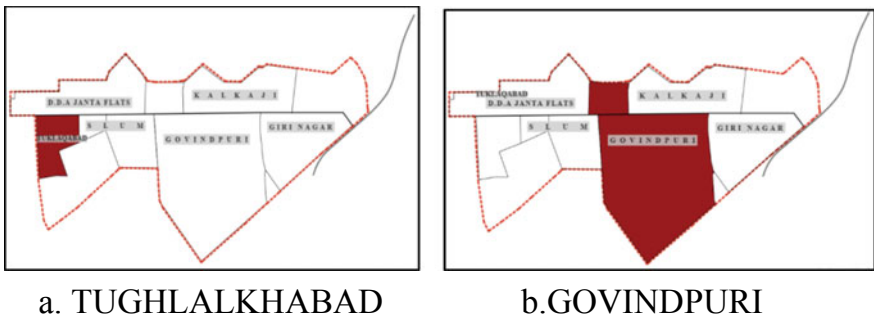


Fig. 5 Unauthorized colonies. *Source* Author’s illustration

Fig. 6 Slum. *Source* Author’s illustration

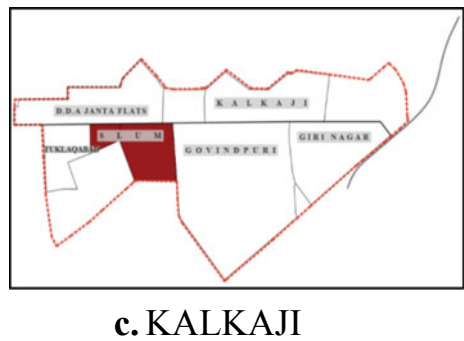




Fig. 7 Illustration of road hierarchy. *Source* Author's illustration

Giri Nagar, Kalkaji, and D. D. A Janta flats are planned residential areas. However, over the last few decades, Kalkaji has transformed into a heavy mixed-use zone area, and D. D. A Janta flats are witnessing gradual change into mixed use as ground floors are converting into commercial establishments. Unauthorized colonies are characterized by narrow lanes and heavy encroachments. Figure 7 illustrates the road hierarchy in the study area. The local roads provide access to the residential societies and are very narrow, less than 6 m, and directly open into the arterial road.

4.2 Congestion Analysis

The first step to address the congestion issue in any area is to define the level of the problem before assessing and measuring its impact. Hence, it is imperative to identify the level of congestion and to understand the issues and challenges related to congestion in any of the urban stretches. However, before identifying the congestion level, it is important here to define congestion. Congestion is defined as the state of being overcrowded especially with traffic or people [10]. There are multitudes of indicators and measurements available to analyze congestion levels. The authors adopted the common techniques of the traffic volume and level of service to establish the congestion level.

Traffic Volume

A traffic volume survey was conducted at four different timings (8 am, 2, 6, and 9 pm) to estimate the number of vehicles (PCU) on the stretch. The survey findings were alarming, and it depicted that on Ravidas Marg stretch the PCU count has already reached the maximum capacity of the road; according to the guidelines of the Indian Road Congress, the PCU on an arterial road (2-lane) should be around 2400/h. However, the average PCU count was 3838/hr, with a maximum of 4456/h and a minimum of 2532/h. Figure 8 provides the detail of PCU count at four different times. The traffic volume, i.e., the PCU count is approximately 4000/h (at 8 am, 2 pm,

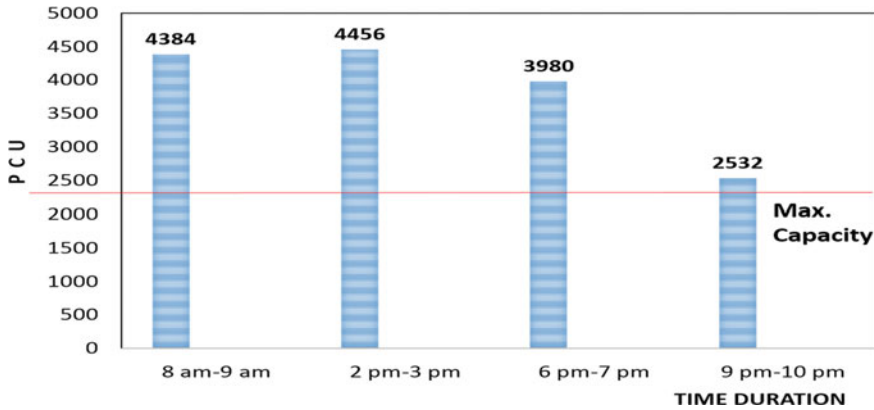


Fig. 8 Traffic volume survey. *Source* Author’s data based on primary survey

and 6 pm) for the majority of the observation period, while as per the standards it should not be more than 2400/h.

Level of Service (L.O.S.)

Level of service is used to assess the level of congestion on road. According to Indian Road Congress guidelines, six levels of service are recognized commonly and are designated from A to F, with level of service A representing the best condition (free flow—vehicle speed at 45 km/h) and level of service F representing the worst condition (major breakdown—vehicle speed at 12.5 km/h). Speed survey was conducted at four different timings (8 am, 2 pm, 6 pm, and 9 pm) from Govindpuri metro station to Okhla Estate Marg which is about 2 km, to estimate the time taken to complete the distance and the speed. The findings of the speed survey were very dismal with the average speed for four wheeler at around 4.5 km/h which is even below the walking speed of 5 km/h. Table 3 provides the detail at four different timings, and analysis of the table reveals that the stretch falls under LOS F.

The analysis of both traffic volume and level of service is suggestive of the criticality of the congestion level on the stretch. Eventually, these results in delays, wastage of precious hours, deteriorating health of the city inhabitants, and fatalities due to road accidents.

Table 3 Description of level of service—four-wheeler speed survey

S. No.	Time (in 00:00 h)	Speed (in km/h)
1	8:00–9:00	6
2	14:00–15:00	3
3	18:00–19:00	3.5
4	21:00–22:00	12

Source Author’s data based on primary survey

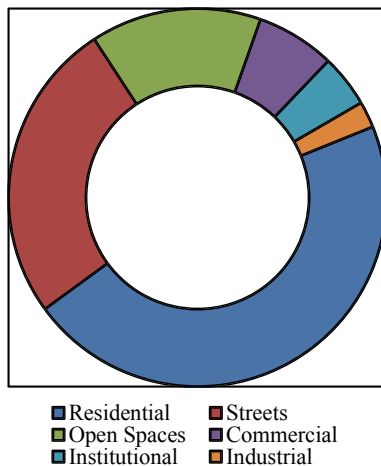
4.3 Land-Use Analysis

Residential and mixed use are the predominant land-use character of the study area which accounts for 41% and 23%, respectively (Fig. 9). Over the period, mixed-use land use has increased, people tend to convert the ground floor to commercial as a result emerging need for the parking, and people tend to park their vehicle on the road which reduces the capacity of the road and hence result in traffic congestion along with the stretch. 11% of the land use is slum, i.e., juggis, G + 1 structures with pucca structures on the ground and temporary arrangements over them. The distribution of green pockets is unbalanced between localities. The existing green parks double up as multipurpose grounds in many cases. Divided into two—one generally for children’s play areas and the other for social activities. 6% of the area is commercial, the area consists of both wholesale and retail markets, and around five different markets are there in the study area.

Street Characteristics and Parking Trend Analysis

Figure 10 explains a typical cross section of the Ravidas Marg in the Tughlakhabad area, and the width of the road varies from point to point. An analysis of the figure reveals that the minimum R.O.W of the study area is 28 M, i.e., around the Tuklaqabad area. 10 m carriageway is available for the vehicular movement, but on both sides, the carriageway is encroached by parking of vehicle from the nearby residents which reduces the road capacity and hence results in traffic congestion. Figure 11 depicts the typical road cross section (B-B’) along the Govindpuri stretch, and the width of the road varies from point to point. According to the analysis, maximum R.O.W of the study area is 36.3 M around the Govindpuri area. 8.5 m carriageway is available for the vehicular movement, but on both the sides carriageway and footpaths are encroached by parking of vehicles from the nearby residents. Further, the open area between the access road and the footpath is encroached by the residents for their

Fig. 9 Distribution of land use. *Source* Author’s data based on primary survey



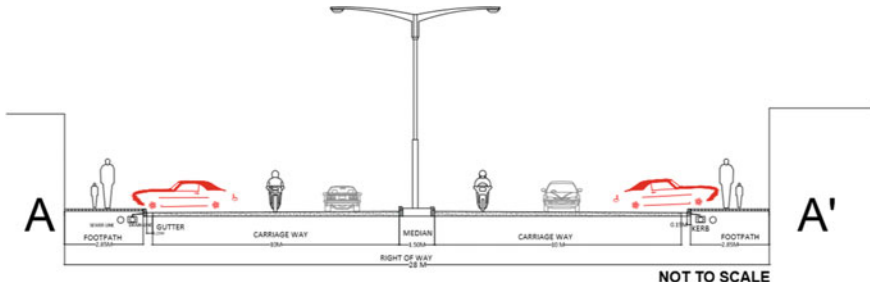


Fig. 10 Typical road cross section along Tughlakhabad. *Source* Author’s illustration based on visual survey

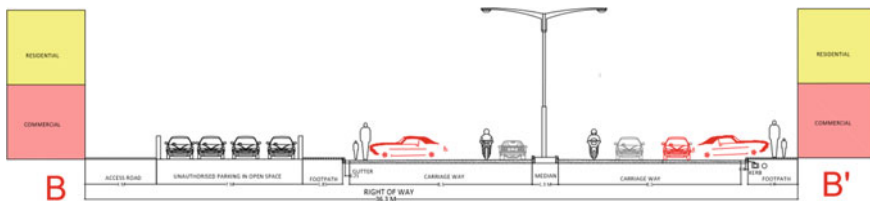


Fig. 11 Typical road cross section along Govindpuri. *Source* Author’s illustration based on visual survey

parking facilities. This encroachment and unauthorized parking reduce the traffic volume capacity of the road and contribute to traffic congestion. Footpaths have been encroached by vegetable vendors, and pedestrians are forced to walk on the carriageway which results in conflict between vehicular and pedestrian.

Analysis of the survey data reveals that the majority of the 2.1 km stretch has a footpath except for the stretch along the Kalkaji slum area. About 85% of the road stretch has footpaths and 15% have no footpaths, as stated earlier and 82% of the footpaths have shade. However, 73% of the footpaths are encroached by street vendors and parking of vehicles which forces pedestrians to walk on the carriageway and results in traffic congestion along the stretch. A further analysis discloses that only 8% of the footpath stretch has no obstruction in terms of encroachment and free movement and almost 73% of the footpath completely obstruct the pedestrian movement due to encroachment by the commercial establishments and shopkeepers.

Analysis of the parking status highlights that the study area has only one authorized parking location, i.e., Govindpuri metro parking lot except this there are no other parking lots available and hence people tend to park their vehicles on the road which is a major reason for traffic congestion along the stretch. Only 7% accounts for authorized parking and the remaining 93% is unauthorized parking. Two wheelers shared the majority of the total vehicles parked on Govindpuri metro parking lot which accounts for 58% and the remaining 42% is car parking. Parking demand for both two wheelers and car is high throughout the day, but demand for car parking is

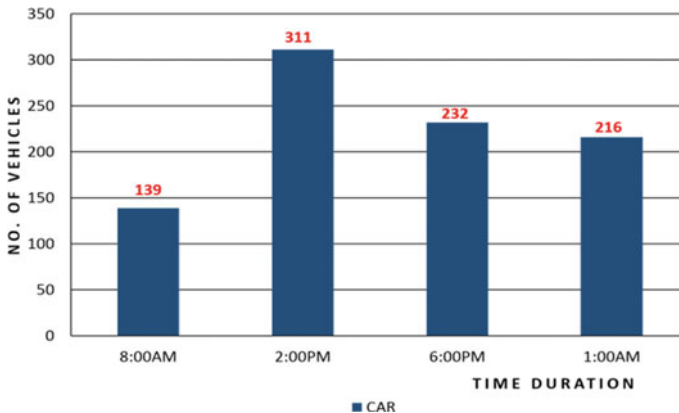


Fig. 12 On-street parking pattern on a typical day. *Source* Author's data based on primary survey

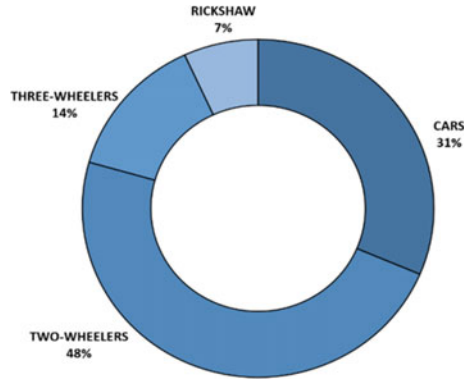
higher at night as residents of Govindpuri and Giri Nagar park their car in the parking lot due to lack of authorized parking in the area. The study area has two types of unauthorized parking, i.e., off-street parking and n-street parking. The majority of the vehicles are parked on-street which accounts for 87% of the total vehicle and the remaining 13% are off-street parking locations, which is one of the significant reasons for congestion along the stretch.

Study area has four unauthorized off-street parking locations, where residents of Govindpuri park their car. Buffer area, i.e., an open, present between the main road and the access road is being used as off-street parking locations. The total area of this parking is 2450 m², and around 105 cars are parked there. The situation pertaining to on-street parking is further worse. A random survey at four different hours of the day suggested that around 73% of the street area is occupied by illegally parked vehicles. Figure 12 provides a complete statistic at four different times of a typical day. Parking demand for cars is high throughout the day which is further higher around 2:00 pm due to the D.D.A and Tuklaqabad market which attracts visitors from the nearby area. Furthermore, analysis of the vehicular composition reveals that two wheelers shared the majority of the total vehicles parked on the street which accounts for 48, 31% is car parking and 14% is three wheelers. Figure 13 provides a detailed statistic pertaining to vehicular composition.

4.4 Market Area Analysis

The study area consists of both formal markets and informal markets. There are four formal markets, i.e., Govindpuri market, Kalkaji market, D.D.A market, and Tuklaqabad market. There is no parking available for both shopkeeper and visitor, and hence, people used to park their vehicle in front of the shop which makes difficult

Fig. 13 Vehicular composition. *Source* Author’s data based on primary survey



for pedestrian and vehicles to move smoothly on the road. There are four informal markets, i.e., two vegetable market, fish market, and a weekly market. There is no separate location for the hawkers, so vendors sit on the footpath which creates a haphazard situation on the road. On every Wednesday, weekly market sits on both sides of the road which results in a chaotic situation on the road causing traffic congestion. Analysis of the informal market area discloses that the vegetable market is located in front of the slum area, 55 shops are there in the vegetable market, and their opening and closing timings are 4:30–10:30 pm every day. The fish market is located opposite to the slum area, 12 shops are there in the fish market, and opening and closing timings are 5:00–11:00 pm every day. Figure 14 shows the typical cross section of the vegetable and fish market, footpath is fully encroached by the market and pedestrian walk on the carriageway, and vehicles are also parked on the carriageway which creates a haphazard situation.

Analysis of the above illustrations is suggestive that footpaths are fully encroached by the vegetable and fish market, during an appreciable part of the day, and pedestrians walk on the carriageway and only 3.5 m space is available for the movement of vehicles, hence result in traffic congestion along the stretch.

A further probe into the formal market area discloses that these exist along Govindpuri and Kalkaji stretch and consists of both wholesale and retail shops, 323 shops, and 110 shops, respectively. The edge acts as a shopping center (with grocery stores and hawkers) for the residents and traders of Govindpuri. The market has, thus, got a multi-use character attached to it. As stated in the earlier section that originally these wards were residential and have changed their use gradually over some time into mixed use. Owing to this, there have been many adverse impacts on the mobility pattern as well as on the surroundings. Over a spread of mixed-use market on Guru Ravidas Marg has the following impact—heavy encroachments, increase in traffic congestion, and increased parking demand. It is already established earlier that the stretch falls under the F category of L.O.S which is an alarming state. It is also important to understand the traffic composition to have clarity on the mobility pattern. Figure 15 provides detail about the predominant modes of travel on the stretch.

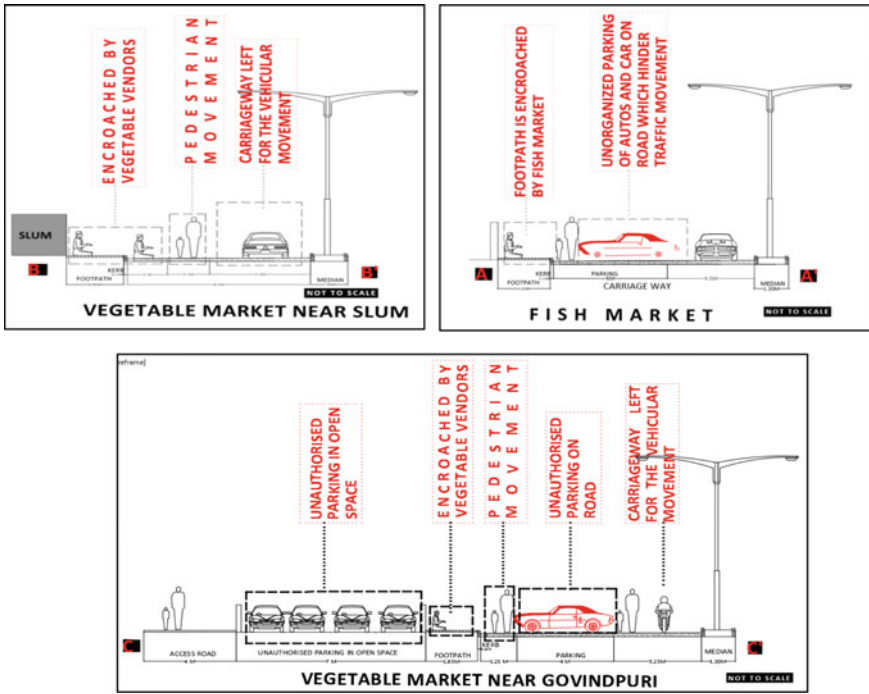


Fig. 14 Different road cross sections on a typical activity day. Source Author’s illustration based on visual survey

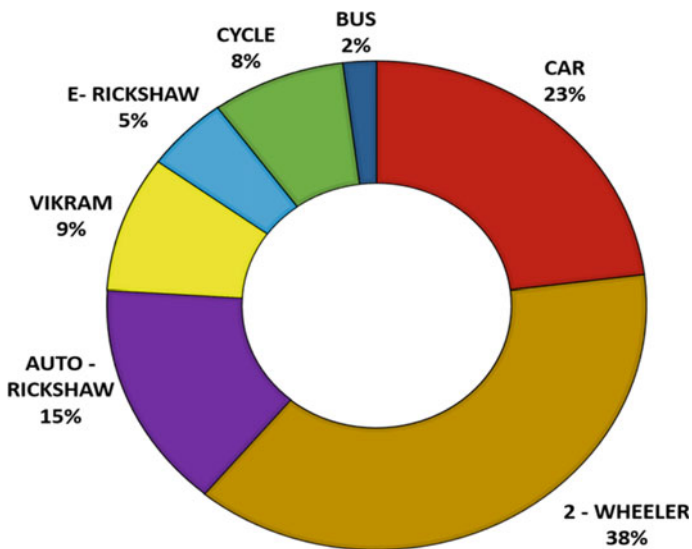


Fig. 15 Vehicular composition on road. Source Author’s data based on primary survey

Two wheeler and car are the predominant mode of travel and account for 61% of all the travel; public transport and intermediate public transport account for 2% and 29%, respectively; public transport facilities are scarce in the study area, therefore various intermediate public transport facilities, i.e., auto-rickshaw, electric rickshaw, etc., are emerging which also create chaos and haphazard movement along the stretch. Cycle trips account for 8% of all the travel. Apart from the site reconnaissance, the authors captured the information about the purpose of the visit of various users on the stretch through a qualitative survey. The analysis of the captured data suggested that the majority of trips are made for work and shopping purposes, together accounting for nearly 71% of the total trips performed. It further highlighted that 68% of the visitors are from within a radius of 2 km of the Govindpuri market. An analysis of the residential status of the shopkeepers suggested that 28% of the shopkeepers are from within the Govindpuri area. 31% of the shopkeepers of the Govindpuri market are from 2 to 4 km of the distance. 41% of the shopkeepers of the Govindpuri market are from more than 4 km, i.e., areas like Greater Kailash, Saket, East of Kailash, which increase demand for organized parking in the market area. While critically analyzing the mobility challenges along the stretch, it is realized that it is imperative to review the existing status of one of the important intersections on the road. There are five major intersections along the stretch, and the authors selected an intersection between the Govindpuri and Kalkaji market stretch (Fig. 16).

The intersection is a T-TYPE intersection, and there are no traffic signals installed in this intersection which result in the haphazard movement of vehicles and pedestrian. The footpath is fully encroached by the shopkeepers of Govindpuri market and Kalkaji market which forces pedestrians to walk on the carriageway. An analysis of the vehicular capacity ratio (V/C) conducted for three different days highlighted that V/C for the intersection has already reached the maximum capacity, and the vehicle capacity ratio in the intersection is 1.4, i.e., greater than 1. Figure 17 provides data about the 14-h traffic count conducted by the authors at the intersection. It suggests that the PCU has already reached the maximum capacity of the road. Throughout the day, PCU is beyond the capacity of the road except between 9 and 10 pm. The peak hour of the study area is (8 am, 2 pm, and 6 pm) as during this timing PCU count is maximum, i.e., 4384, 4456, and 3980, respectively.

A further visual assessment of the site suggests that the auto-rickshaw stand is very close to the intersection which causes hindrance in the traffic circulation. Footpaths are encroached by the street vendors which forces pedestrians to walk on the carriageway and hence causes traffic congestion at the intersection. Carriageways are further encroached by the parking of vehicles which reduces the traffic capacity of the intersection and impedes the smooth flow of traffic. To summarize, it is understood that the arterial road is facing a lot of challenges in terms of unauthorized parking, encroachment on streets and open areas, and rapid conversion of land use.

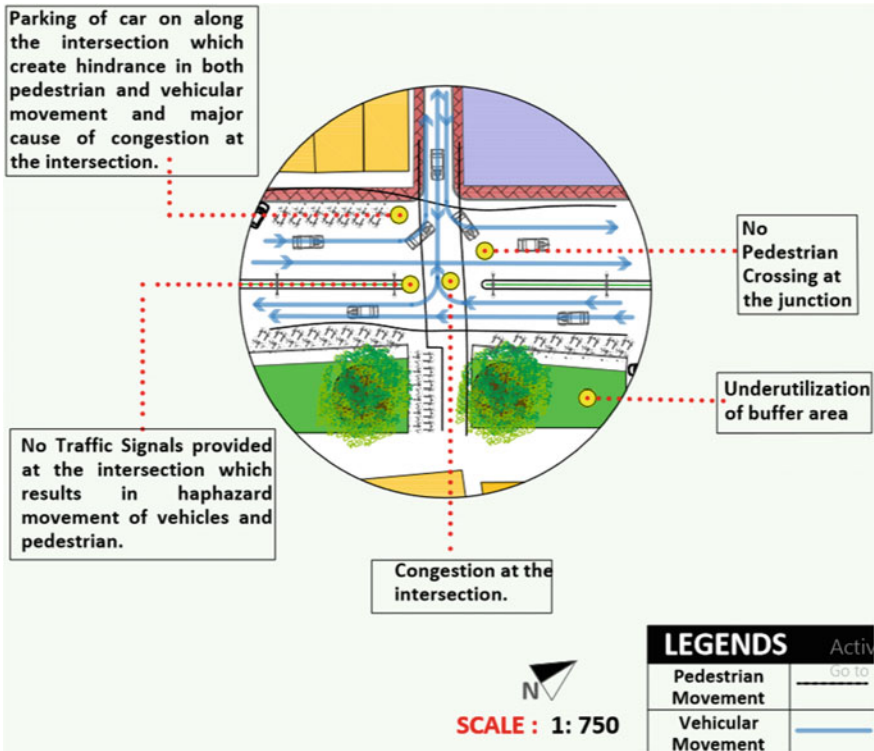


Fig. 16 Analysis of the intersection between Govindpuri and Kalkaji Stretch. *Source* Author’s analysis based on the primary survey

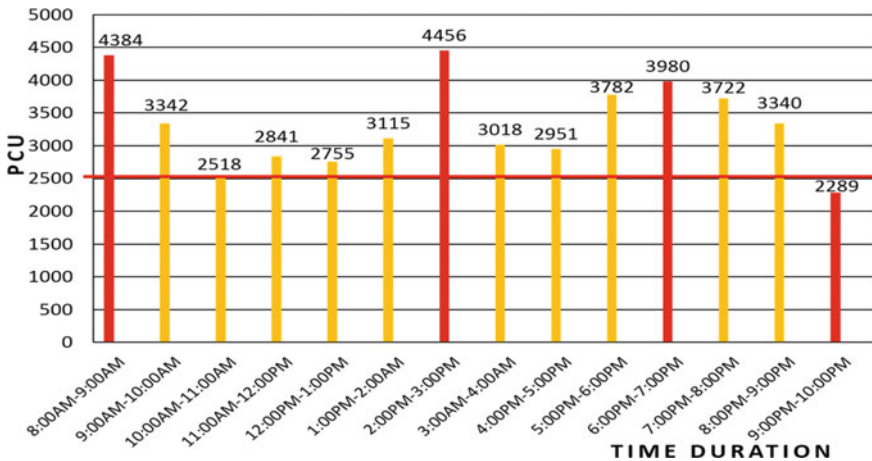


Fig. 17 Traffic volume count. *Source* Author’s data based on primary survey

5 Conclusion

The above analysis provided an exclusive assessment of the location and scope of congestion activity in different scenarios. One common highlight in the different settings was excessive traffic volume. However, apart from the excessive number and types of vehicles commuting on roads, the hindrance to smooth traffic flow also originates from different other activities competing for the use of both road and street space. These activities are loading and unloading of goods, illegal encroachments on streets, unauthorized parking, informal market activities, picking and setting down activities of public buses, private taxis and cars, and also a huge nuisance arises due to vehicles circulating on roads in search of on-street and off-street parking spaces. All these affect the traffic flow and also the operation of critical intersections. The consequences of poor traffic flow are manifold, and it incurs both tangible and intangible costs. It leads not only to increased travel time but also adversely impacts the business when goods and services are not able to reach on time. It impacts the quality of life, and the long traffic queue worsens the air quality and acts as a threat to public health. The traffic situation at Ravidas Marg is not exclusive to this stretch but is a common phenomenon on many of the urban roads across the big cities of India. There is a dire need to improve mobility across the urban roads before they assume the humongous shape and become irreversible. It is understood that government has implemented a host of traffic management measures, ranging from construction of metro lines, overpasses, ring roads, pedestrian and bicycle paths, and framing of stringent encroachment penalties, etc., to enhance the efficiency of available roads resources. Nonetheless, due to physical, environmental, and social constraints, the effectiveness of these ongoing measures is constrained. However, the effectiveness of these measures depends upon the cooperation and compliance by the communities and cohesion and interventions at different fronts. Therefore, it is imperative to identify additional measures that can work in conjunction with these ongoing measures. It is suggested that to achieve the objective of improved mobility, the policy-making institutions and responsible implementing agencies require working on four broad components, these are as follows:

Policy Interventions: To improve the regulatory framework regarding traffic and pedestrian mobility within the local municipality. To create a regulatory tool to discourage on-road parking, encroachment on streets, and prevent violation of traffic rules.

Physical Planning Parameters/Indicators: To identify potential design measures and their viability and costs and to have a policy tool that allows redesigning of the major intersections along the stretch and redesigning of the road section for easy movement and separation of traffic.

Stakeholders/Community Interventions: To have an in-depth assessment of beneficiaries and their participation in discussion and decision-making processes in the implementation of traffic improvement measures. There is a need for a communication and training plan for the stakeholder mainly—residents, local traders, and

visitors to—increase the grassroots participation and ensure adequate information flow, explain the benefit of regenerating the road, and to improve their behavioral patterns toward public amenities.

Communication/Knowledge Management/Gender streamlining: This is one of the most important and often neglected tools of governance which otherwise is very effective in increasing the benefits arising from the other policy measures and is also effective in containing ills of urbanization at the territorial level.

To conclude, the vision of all the urban communities is to have environmentally friendly, safer, and affordable mobility for the city habitants to access opportunities that promote social and economic interaction.

References

1. Alam MA, Ahmed F (2013) Urban transport systems and congestion: a case study of Indian Cities. *Transp Commun Bullet Asia Pacific* 82:33–43
2. Centre for science and environment, *move free: unlocking the traffic gridlock in our neighbourhoods* (2015)
3. Crane R (1996) On form versus function: will the New Urbanism reduce traffic, or increase it? *J Plann Educ Res* 15:117–126
4. Delhi Traffic Police (2016). Data retrieved from <https://delhitrafficpolice.nic.in/about-us/statistics/>. Accessed on 28 Oct 2016
5. Downs A (2006, June 30) Can traffic congestion be cured? Retrieved from www.brookings.edu, <https://www.brookings.edu/opinions/can-traffic-congestion-be-cured/>
6. Dunphy RT, Fisher K (1996) Transportation, congestion, and density: new insights. *Transp Res Rec J Transp Res Board* 1552(1):89–86. Retrieved from <https://doi.org/10.1177/0361198196155200112>
7. Ministry of urban development, report of the high powered committee on de-congesting traffic in Delhi, June 2016
8. Oluwoye JO (2000) Action in transport for the new millennium. In: Paper presented at South African transport conference CSIR International Convention Centre, Pretoria, South Africa 17–20 July 2000
9. Rao AM, Rao KR (2012) Measuring urban traffic congestion—a review. *Int J Traffic Transp Eng* 2(4):286–305
10. Reynolds DJ (1963) Congestion. *J Ind Econ* 11(2):132–140
11. Rosenbloom S (1978) Peak-period traffic congestion: a state-of-art analysis and evaluation of effective solution. *Transportation* 167–191. <https://doi.org/10.1007/BF00184638>
12. Sausanis J (2011, Aug 15) World's vehicle population tops 1 billion units. Retrieved from www.wardsauto.com, https://wardsauto.com/ar/world_vehicle_population_110815%E2%80%99t-controlgrowth-private-vehicle-official.html
13. TRB (2000) Highway capacity manual. National Research Council, Washington D.C.
14. Van der Loop H, Perdok J, Willigers J (2014) Economic evaluation of trends in travel time reliability in road transport. Analysis of traffic data in the Netherlands from 2001 to 2011. *Transp Res Rec J Transp Res Board* 2450:163–171
15. Yanli W, Xiaoyu Z, Linbo L, Bing W (2013) Reasons and countermeasures of traffic congestion under land redevelopment. *Proc Soc Behav Sci* 96:2164–2172

Assessing Contributions of Intensity-based Rainfall Classes to Annual Rainfall and Wet Days over Tehri Catchment, India



Sabyasachi Swain, Surendra Kumar Mishra, and Ashish Pandey

Abstract Rainfall variability has gained significant attention from the global research community, especially after the rising issues of climate change. In the present study, an assessment of the contributions of intensity-based rainfall classes (very low, low, medium, rather heavy, and heavy) to average annual rainfall as well as to the number of wet days over Tehri catchment, Uttarakhand, India, is presented. It is pertinent to mention that the very low rainfall class is not considered among wet days and hence is analyzed only for contributions to annual rainfall and not for contributions to the number of wet days. The daily rainfall data is collected for 119 years (1901–2019) from the IMD $0.25^\circ \times 0.25^\circ$ grids, whose at least 25% fell within the boundary of the catchment. Fifteen grids are selected based on the above-mentioned criteria, and the period of 1901–2019 is divided into two parts, i.e., pre-1960 and post-1960 periods for a comparative assessment. The results reveal that the medium rainfall class contributes a majority of annual rainfall followed by light rainfall, rather heavy, heavy, and very low rainfall classes. Similarly, for wet days, medium (50%) and light (45%) classes are the major contributors followed by rather heavy (4%) and heavy (1%) classes. Regarding these contributions, no significant difference is observed between pre-1960 and post-1960 periods.

Keywords Tehri catchment · Rainfall classes · Annual rainfall · Wet days

1 Introduction

Climate change has become one of the most alarming issues for the present generation [1–4]. The general impacts of climate change on hydrological cycle are well sought in hydrometeorology literature [1, 5–9]. Rainfall is a key meteorological variable, and variability under the influence of climate change has gained significant attention from the global research community [10–14]. In general, climate change

S. Swain (✉) · S. K. Mishra · A. Pandey

Department of Water Resources Development and Management, Indian Institute of Technology Roorkee, Roorkee 247667, India

e-mail: sabyasachiswain16@gmail.com

and rising temperatures leads to intensification of rainfall extremes, which causes serious consequences [15–20]. In last few years, several incidences of damaging precipitation extremes have been reported [14, 19–23]. However, most of the studies focus either on trend of rainfall patterns or analysis of particular events [16, 21, 24]. More importantly, due to issues of data availability, very few studies focus on mountainous regions, in general [25–28]. There have been some recent studies on Himalayan regions focusing on its climatic conditions [13, 28–32]. Nevertheless, no study has assessed the contribution of different intensity-based classes to total amount of rainfall or number of wet days. Therefore, the objective of this study is to carry out a detailed assessment of the contributions of these intensity-based rainfall classes toward rainfall amount as well as wet days over a mountainous catchment in India. According to the India Meteorological Department (IMD) classification system, nonzero rainfall days with rainfall amounts of below 2.49, 2.49–7.49, 7.49–37.49, 37.49–64.49, and 64.49 or above are classified as very light, light, medium, rather heavy, and heavy rainfall days, respectively [14]. As climate change often leads to intensification of rainfall extremes, assessing contributions of intensity-based rainfall classes to annual rainfall and wet days may be helpful to capture the impacts of climate change.

2 Materials and Methods

In this study, Tehri catchment located in the state of Uttarakhand, India, is considered as the study area. This is a mountainous catchment and thus has very steep slopes. The spatial extent of the study area is shown in Fig. 1. The catchment covers an area of approximately 7500 km² [33].

Since this is a mountainous catchment, the availability of ground-based rainfall records at the desired quality/resolution for a long duration may not be feasible. Therefore, daily rainfall data is collected for 119 years (1901–2019) from the IMD 0.25° × 0.25° grids, whose at least 25% fell within the boundary of the catchment. Fifteen grids are selected based on the above-mentioned criteria. The central location details of these grids are presented in Table 1.

Based on IMD classification, days with rainfall amounts 0–2.49, 2.49–7.49, 7.49–37.49, 37.49–64.49, and 64.49 or above are classified as very light, light, medium, rather heavy, and heavy rainfall days, respectively. Further, days with rainfall intensity over 2.49 mm/day are considered as wet days. Therefore, very light rainfall class is not considered as a wet day. The objective of this study is to determine the percentage contributions intensity-based rainfall classes to annual rainfall as well as to the number of wet days over Tehri catchment. The period of 1901–2019 is divided into two almost equal parts, i.e., pre-1960 and post-1960 periods, for a comparative assessment.

The daily rainfall for pre-1960 period (1901–1960) is categorized into five classes as mentioned previously. Then, the contribution of each class to total rainfall amount can be calculated as,

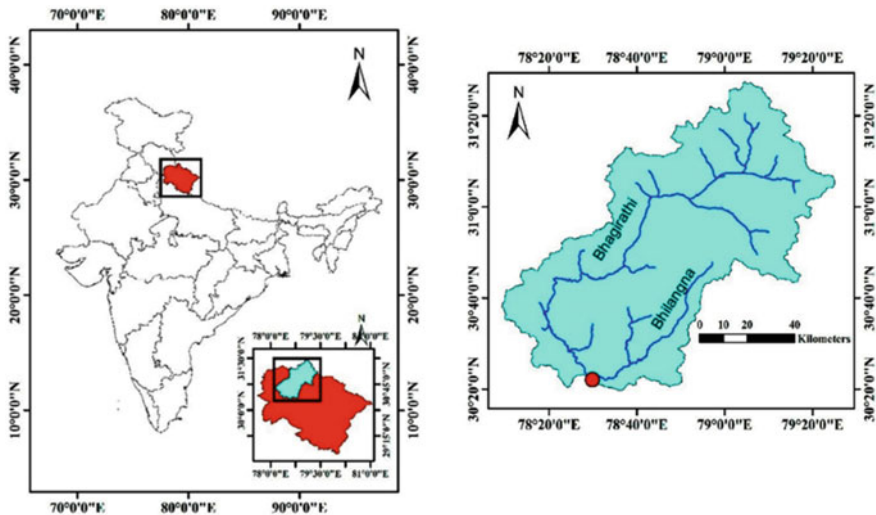


Fig. 1 Spatial extent of the Tehri catchment

Table 1 Location of IMD grids over the catchment

Grid	Latitude	Longitude	Grid	Latitude	Longitude	Grid	Latitude	Longitude
R1	30.5	78.25	R6	30.75	78.75	R11	31	79
R2	30.5	78.5	R7	30.75	79	R12	31	79.25
R3	30.5	78.75	R8	30.75	79.25	R13	31.25	78.75
R4	30.75	78.25	R9	31	78.5	R14	31.25	79
R5	30.75	78.5	R10	31	78.75	R15	31.25	79.25

$$\text{Percent Contribution to Annual Rainfall, } PCAR_j = \frac{\sum_{i=1901}^{1960} \sum P_{ij}}{\sum_{i=1901}^{1960} P_i^{\text{ann}}} \times 100 \quad (1)$$

where i represents the year, j is 1, 2, 3, 4, and 5 corresponding to $0 < P < 2.49$, $2.49 < P < 7.49$, $7.49 < P < 37.49$, $37.49 < P < 64.49$, and $P > 64.49$, respectively, P^{ann} represents the annual rainfall, and P is the rainfall on a particular day.

Now, if the total number of light, medium, rather heavy, heavy rainfall days during 1901–1960 are found to be N_1 , N_2 , N_3 , and N_4 , respectively, then their contribution toward number of wet days can be calculated as,

$$\text{Percent Contribution to Total Number of Wet Days, } PCWD_k = \frac{N_k}{\sum_{k=1}^4 N_k} \quad (2)$$

where k is 1, 2, 3, and 4 for light, medium, rather heavy, heavy rainfall, respectively. The contributions of each relevant class to total rainfall amount as well as to total number of wet days for the post-1960 period (i.e., 1961–2019) can be computed following the above-mentioned procedure.

3 Results and Discussions

The grid-wise results for percent contributions to total amount of rainfall by different rainfall classes are presented in Table 2 for both pre-1960 and post-1960 periods. For all the grids, the medium rainfall contributes majority of the annual rainfall, i.e., 43.1–64.3% over different grids for pre-1960 phase and 52.1–65.8% for post-1960 phase. However, there is no definite order of contributions from other classes.

Results of a similar analysis carried out for contributions to total number of wet days are presented in Table 3. The grid-wise results reveal that the contribution of medium and light rainfall classes is maximum to total number of wet days. On the other hand, heavy rainfall class forms a little percentage with respect to total wet days. It can also be noticed from Tables 2 and 3 that light rainfall class contributes remarkably to the number of wet days but a little to amount of rainfall. In contrast, heavy events have very little (< 1%) contribution to number of wet days over most of the grids, but noticeable contributions to total amount of rainfall.

Table 2 Percent contributions of rainfall classes to total amount of rainfall

Phase	Pre-1960					Post-1960				
	Grids	Non-wet	Light	Medium	Rather heavy	Heavy	Non-wet	Light	Medium	Rather heavy
R1	1.4	5.3	43.1	23.7	26.4	4.1	12.1	55.7	17.7	10.4
R2	3.2	11.9	60.9	16.3	7.7	4.6	13.8	59.6	14.3	7.7
R3	4.6	14.4	61.9	13.7	5.4	4.6	14.9	64.0	11.9	4.5
R4	1.4	5.4	43.9	26.0	23.3	2.9	9.1	52.1	20.6	15.3
R5	2.5	9.8	60.0	18.7	9.0	4.2	12.8	59.2	15.4	8.5
R6	5.1	16.3	62.7	11.2	4.8	4.4	14.8	63.1	12.7	5.0
R7	5.9	21.7	62.4	7.5	2.7	4.9	16.9	64.5	10.7	2.9
R8	6.1	19.7	61.1	8.6	4.6	4.9	17.5	64.8	9.4	3.4
R9	4.4	16.4	64.3	11.3	3.5	4.8	16.0	62.9	11.4	4.9
R10	5.6	20.6	63.3	7.5	3.0	4.6	15.4	64.2	11.6	4.3
R11	5.8	21.8	61.4	8.2	2.8	5.1	18.0	65.8	8.4	2.6
R12	5.8	20.5	61.4	7.9	4.4	4.8	17.5	65.2	9.2	3.2
R13	10.2	26.6	53.6	6.0	3.6	6.8	20.6	59.7	7.8	5.2
R14	7.1	22.4	60.4	6.8	3.4	5.5	19.2	65.7	7.2	2.5
R15	5.8	19.3	61.2	8.8	4.8	5.0	18.6	65.7	7.8	2.9

Table 3 Percent contributions of rainfall classes to total number of wet days

Phase	Pre-1960				Post-1960			
	Light	Medium	Rather heavy	Heavy	Light	Medium	Rather heavy	Heavy
R1	26.8	54.9	11.7	6.6	41.1	51.4	5.9	1.6
R2	38.5	54.9	5.3	1.4	43.0	51.5	4.4	1.1
R3	43.0	52.2	4.0	0.8	43.2	52.7	3.4	0.6
R4	26.7	55.0	12.6	5.8	35.4	53.9	7.7	3.0
R5	34.2	57.4	6.6	1.8	41.1	52.7	4.9	1.3
R6	45.3	50.9	3.1	0.7	43.6	52.0	3.8	0.7
R7	51.0	46.9	1.8	0.3	45.9	50.7	2.9	0.5
R8	49.4	47.9	2.1	0.6	46.1	50.9	2.5	0.5
R9	44.5	52.0	3.1	0.5	45.4	50.7	3.2	0.7
R10	49.9	47.9	1.9	0.3	44.0	52.0	3.3	0.6
R11	51.2	46.5	1.9	0.3	46.7	50.7	2.2	0.4
R12	50.2	47.3	1.9	0.6	46.0	51.0	2.5	0.5
R13	59.8	38.5	1.3	0.3	52.1	45.3	2.0	0.6
R14	52.5	45.5	1.6	0.4	48.0	49.8	1.8	0.3
R15	48.9	48.3	2.2	0.6	47.3	50.3	2.0	0.5

It is difficult to draw any robust inference from the grid-wise results as there exists substantial inter-grid variation. Therefore, the average of all the grids over the catchment is taken for adjudging the contributions of the rainfall classes. The result of the analysis for contributions to average annual rainfall is presented in Fig. 2

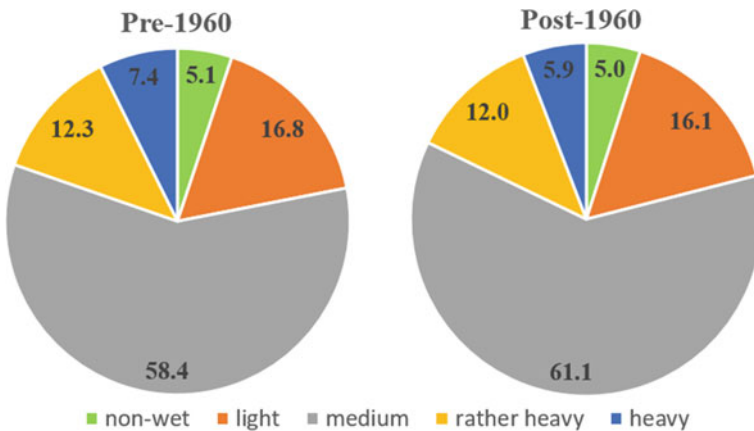


Fig. 2 Average contributions of rainfall classes to annual rainfall for pre-1960 and post-1960 periods

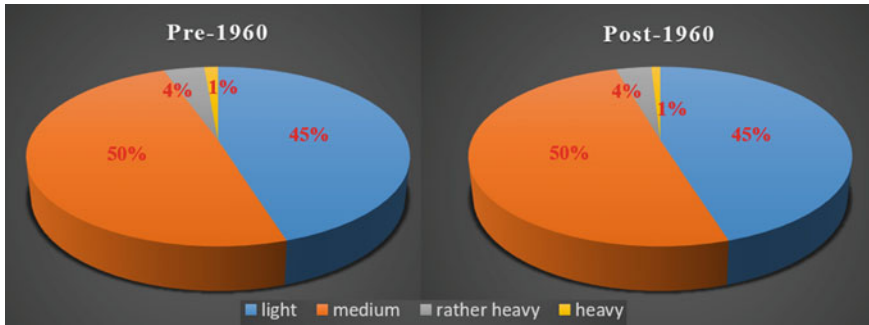


Fig. 3 Average contributions of rainfall classes to number of wet days per year for pre-1960 and post-1960 periods

and for total number of wet days is presented in Fig. 3. It can be clearly seen from Fig. 2 that the order of contributions to average annual rainfall by medium, light, rather heavy, heavy, and very low rainfall classes are 58.4% (61.1%), 16.8% (16.1%), 12.3% (12%), 7.4% (5.9%), and 5.1% (5%), respectively, for pre-1960 (post-1960) periods. Therefore, there is hardly any difference between the two periods. Regarding contributions to total number of wet days, medium (50%) and light (45%) classes are the major contributors followed by rather heavy (4%) and heavy (1%) classes, as apparent from Fig. 3, and there is no difference in the statistics for both pre- and post-1960 periods.

The result of medium rainfall class being the major contributor to annual rainfall is consistent with a recent study by Barde et al. [14] over eastern Indian region. The Tehri catchment receives a rainfall of 1500–2000 mm across different years, and a vast majority of this is confined to only monsoon season. Hence, most of the wet days belong to the monsoon season. It can be seen from Fig. 3 that about 50% of the wet days belong to the medium rainfall class, and thus, it ends up in being the major contributor to the average annual rainfall over the catchment. Similarly, 45% of wet days belong to light rainfall class, and thus, it has second-highest contribution (> 16%) to average annual rainfall. On the other hand, only 4% of the wet days belong to rather heavy rainfall class and still it contributes over 12% of annual rainfall, which is close to that of the light rainfall class. For heavy rainfall class, 7.4% and 5.9% contribution to annual rainfall in pre- and post-1960 periods, respectively, comes from only about 1% of wet days. This is also in agreement with the grid-wise analysis presented in Tables 2 and 3. This is due the fact that a rather heavy or a heavy wet day is equivalent to a number of light wet days in terms of rainfall amount.

4 Conclusions

In this study, different intensity-based rainfall classes (very low, low, medium, rather heavy and heavy) are assessed for their contribution toward the average annual rainfall. Further, percentage contribution of all the wet-day classes (excluding very low rainfall) toward total number of wet days over the catchment is also evaluated. The medium rainfall class is found to contribute a majority (nearly 60%) of annual rainfall followed by light rainfall, rather heavy, heavy, and very low rainfall classes. Similarly, for wet days, medium (50%) and light (45%) classes are the major contributors followed by rather heavy (4%) and heavy (1%) classes. Although there are some changes in the statistics of individual grids for pre- and post-1960 periods, no noticeable difference between the two periods is observed when rainfall over the entire catchment is considered.

References

1. Pattnaik DR, Dimri AP (2020) Climate change over the Indian sub-continent. In: Gupta N, Tandon S (eds) *Geodynamics of the Indian plate*. Springer geology. Springer, Cham
2. Maharana P, Dimri AP (2016) Study of intraseasonal variability of Indian summer monsoon using a regional climate model. *Clim Dyn* 46(3–4):1043–1064
3. Jamshidi S, Zand-parsa S, Pakparvar M, Niyogi D (2019) Evaluation of evapotranspiration over a semiarid region using multiresolution data sources. *J Hydrometeorol* 20(5):947–964
4. Jamshidi S, Zand-Parsa S, Kamgar-Haghighi AA, Shahsavari AR, Niyogi D (2020) Evapotranspiration, crop coefficients, and physiological responses of citrus trees in semi-arid climatic conditions. *Agric Water Manag* 227:105838
5. Swain S, Verma MK, Verma MK (2018) Streamflow estimation using SWAT model over Seonath river basin, Chhattisgarh, India. In: Singh V, Yadav S, Yadava R (eds) *Hydrologic modeling*. Water science technology library, vol 81, pp 659–665
6. Swain S, Sharma I, Mishra SK, Pandey A, Amrit K, Nikam V (2020) A framework for managing irrigation water requirements under climatic uncertainties over Beed district, Maharashtra, India. In: *World environmental and water resources congress 2020: water resources planning and management and irrigation and drainage*. American Society of Civil Engineers, Reston, VA, pp 1–8
7. Aadhar S, Swain S, Rath DR (2019) Application and performance assessment of SWAT hydrological model over Kharun river basin, Chhattisgarh, India. In: *World environmental and water resources congress 2019: watershed management, irrigation and drainage, and water resources planning and management*. American Society of Civil Engineers, Reston, VA, pp 272–280
8. Nageswararao MM, Mohanty UC, Dimri AP, Osuri KK (2018) Probability of occurrence of monthly and seasonal winter precipitation over Northwest India based on antecedent-monthly precipitation. *Theoret Appl Climatol* 132(3–4):1247–1259
9. Swain S (2017) Hydrological modeling through soil and water assessment tool in a climate change perspective a brief review. In: *2017 2nd international conference for convergence in technology (I2CT)*. IEEE, pp 358–361
10. Rai P, Dimri AP (2020) Changes in rainfall seasonality pattern over India. *Meteorol Appl* 27(1):e1823
11. Swain S, Patel P, Nandi S (2017). Application of SPI, EDI and PNPI using MSWEP precipitation data over Marathwada, India. In: *2017 IEEE international geoscience and remote sensing symposium (IGARSS)*. IEEE, pp 5505–5507

12. Swain S, Nandi S, Patel P (2018) Development of an ARIMA model for monthly rainfall forecasting over Khordha district, Odisha, India. In: Sa P, Bakshi S, Hatzilygeroudis I, Sahoo M (eds) Recent findings in intelligent computing techniques. *Advances international system computing*, vol 708, pp 325–331
13. Dimri AP, Immerzeel WW, Salzmann N, Thayyen RJ (2018) Comparison of climatic trends and variability among glacierized environments in the Western Himalayas. *Theoret Appl Climatol* 134(1–2):155–163
14. Barde V, Nageswararao MM, Mohanty UC, Panda RK, Ramadas M (2020) Characteristics of southwest summer monsoon rainfall events over East India. *Theor Appl Climatol* 141:1511–1528
15. Dimri AP, Yasunari T, Kotlia BS, Mohanty UC, Sikka DR (2016) Indian winter monsoon: present and past. *Earth Sci Rev* 163:297–322
16. Dayal D, Swain S, Gautam AK, Palmate SS, Pandey A, Mishra SK (2019) Development of ARIMA model for monthly rainfall forecasting over an Indian river Basin. In: World environmental and water resources congress 2019: watershed management, irrigation and drainage, and water resources planning and management. American Society of Civil Engineers, Reston, VA, pp 264–271
17. Swain S, Mishra SK, Pandey A (2020) Assessment of meteorological droughts over Hoshangabad district, India. *IOP Conf Ser Earth Environ Sci* 491(1):012012
18. Maharana P, Dimri AP (2019) The Indian monsoon: past, present and future. *Proc Indian Nat Sci Acad* 85(2):403–420
19. Nageswararao MM, Mohanty UC, Ramakrishna SSVS, Dimri AP (2018) An intercomparison of observational precipitation data sets over Northwest India during winter. *Theoret Appl Climatol* 132(1–2):181–207
20. Swain S, Mishra SK, Pandey A, Dayal D (2021) Identification of meteorological extreme years over central division of Odisha using an index-based approach. In: Pandey A, Mishra S, Kansal M, Singh R, Singh VP (eds) *Hydrological extremes*. Water science technology library, vol 97. Springer Cham, pp 161–174
21. Agnihotri R, Dimri AP, Joshi HM, Verma NK, Sharma C, Singh J, Sundriyal YP (2017) Assessing operative natural and anthropogenic forcing factors from long-term climate time series of Uttarakhand (India) in the backdrop of recurring extreme rainfall events over northwest Himalaya. *Geomorphology* 284:31–40
22. Swain S, Patel P, Nandi S (2017) A multiple linear regression model for precipitation forecasting over Cuttack district, Odisha, India. In: 2017 2nd international conference for convergence in technology (I2CT). IEEE, pp 355–357
23. Chevuturi A, Dimri AP (2016) Investigation of Uttarakhand (India) disaster-2013 using weather research and forecasting model. *Nat Hazards* 82(3):1703–1726
24. Swain S, Dayal D, Pandey A, Mishra SK (2019) Trend analysis of precipitation and temperature for Bilaspur District, Chhattisgarh, India. In: World environmental and water resources congress 2019: groundwater, sustainability, hydro-climate/climate change, and environmental engineering. American Society of Civil Engineers, Reston, VA, pp 193–204
25. Kumari M, Singh CK, Bakimchandra O, Basistha A (2017) Geographically weighted regression based quantification of rainfall–topography relationship and rainfall gradient in Central Himalayas. *Int J Climatol* 37(3):1299–1309
26. Kumari M, Singh CK, Bakimchandra O, Basistha A (2017) DEM-based delineation for improving geostatistical interpolation of rainfall in mountainous region of Central Himalayas, India. *Theor Appl Climatol* 130(1–2):51–58
27. Kumari M, Singh CK, Basistha A (2017) Clustering data and incorporating topographical variables for improving spatial interpolation of rainfall in mountainous region. *Water Resour Manage* 31(1):425–442
28. Kumar D, Choudhary A, Dimri AP (2018) Regional climate changes over Hindukush-Karakoram-Himalaya region. In: Goel P, Ravindra R, Chattopadhyay S (eds) *Science and geopolitics of the white world*. Springer, Cham

29. Dimri AP, Bookhagen B, Stoffel M, Yasunari T (eds) (2019) Himalayan weather and climate and their impact on the environment. Springer Nature
30. Chakraborty R, Daloz AS, Kumar M, Dimri AP (2019) Does awareness of climate change lead to worry? Exploring community perceptions through parallel analysis in rural Himalaya. *Mountain Res Dev* 39(2):R35–R54
31. Dimri AP, Chevuturi A, Niyogi D, Thayyen RJ, Ray K, Tripathi SN, Pandey AK, Mohanty UC (2017) Cloudbursts in Indian Himalayas: a review. *Earth Sci Rev* 168:1–23
32. Banerjee A, Dimri AP, Kumar K (2020) Rainfall over the Himalayan foot-hill region: present and future. *J Earth Syst Sci* 129(1):1–16
33. Agrawal NK, Lohani AK, Goel NK (2018) Physiographic analysis of Tehri Dam catchment and development of GIUH based Nash model for ungauged rivers. *Current World Environ* 14(2):215

Development of PCU Value of E-rickshaw on Urban Roads



Amir Ali Khan and Gyanendra Singh

Abstract Traffic in countries like India is heterogeneous in nature. Different types of vehicles share the same space of roadway width. These vehicles have different power, weight, and dimensions. To convert heterogeneous traffic into homogeneous traffic for capacity designing, traffic light, and intersection design, a common parameter passenger car equivalency (also called as passenger car unit) is used. Indian Roads Congress codes, IRC: 106:1990 and IRC: 64:1990, deal with the passenger car unit (PCU) of vehicle types on urban and rural roads, respectively. Although a large number of e-rickshaw are plying on urban roads, the PCU value of e-rickshaw is not provided yet. In this study, an attempt has been made to find out the PCU value of e-rickshaw and variation in PCU of e-rickshaw with different traffic volume and composition. Data were collected from different sites having different traffic conditions. Out of various methods, Chandra's method was used because of the suitability of this method in mixed traffic conditions, and the speed–volume relationship was used to assess variation in PCU of e-rickshaw with traffic volume and traffic composition. According to this study, the suggested PCU value of e-rickshaw is 0.795 and it varies with the different traffic conditions.

Keywords PCU · E-rickshaw · Chandra's method · Speed–volume relationship

1 Introduction

Heterogeneity of the traffic is the main issue that poses great difficulty while designing intersections, traffic lights, and roads in developing countries like India. To overcome this problem, a common measure passenger car equivalency is used. IRC has standardized PCU values for vehicle types for rural as well as urban roads. PCU factor depends on various factors such as rectangular area, physical dimensions of vehicles, road characteristics, and vehicular characteristics. Various methods are available for the determination of PCU of vehicle types. It is subjected to change according to the

A. A. Khan (✉) · G. Singh
Deenbandhu Chhotu Ram University of Science and Technology, Murthal, Sonipat, India
e-mail: amirm640@gmail.com

© The Author(s), under exclusive license to Springer Nature Singapore Pte Ltd. 2021
Y. A. Mehta et al. (eds.), *Advances in Water Resources and Transportation Engineering*,
Lecture Notes in Civil Engineering 149,
https://doi.org/10.1007/978-981-16-1303-6_10

123

site situation. PCU value of E-rickshaw is yet to be specified by IRC. E-rickshaw is a battery-operated vehicle nowadays used in many cities of India. E-rickshaws are used as an alternative to the auto-rickshaw and pulled rickshaws because of their low fuel cost, and less human effort compared to pulled rickshaws. So it is necessary to consider these e-rickshaws to assess the impact on traffic variables. An attempt has been made in this study to calculate the PCU value of e-rickshaw on urban roads and to check variation in PCU value with different traffic composition and traffic volume. This study will be helpful for traffic engineers and urban transport planners dealing with traffic composition in urban areas for capacity estimations, designing traffic lights, intersection designs, and other improvement measures.

2 Literature Review

Chandra et al. [2] conducted a study to examine the dynamic nature of passenger car units with traffic and geometric parameters. For this purpose, a computer program which can be executed on any computer was developed to calculate passenger car unit under prevailing traffic and geometric conditions. Chandra [3] carried out a study to assess variation in passenger car unit values with varying carriageway width. As per this study, passenger car unit values of a vehicle type increases linearly with the lane width of the section of the road. Mallikarjuna et al. [5] estimated passenger car unit values for two 2-wheelers, bus, and truck under mixed traffic conditions on Indian roads using a modified cellular automata simulation model. It was found from this study that passenger car unit factors decrease with increase in the proportion of vehicles in the stream. Werner and Morrall [10] developed PCU values for heavy vehicles like trucks, busses, and recreational vehicles for rolling and mountainous terrains. Walker's method [HCM, 1965] was used for the determination of PCU values. Srinivasa et al. [9] developed PCU value of vehicle types on the urban road and assess the variation in PCU of vehicle types with traffic volume and traffic composition. Effect of carriageway width on PCU of different vehicles was also studied, and a comparison was made between developed PCU values and PCU values given by IRC. It was found that PCU value increases with increased carriageway width. Bains et al. [6] studied the variation in passenger car unit values of vehicles with different traffic compositions of heavy vehicles and light commercial vehicles at different volumes on expressways of India. From this study, it was depicted that passenger car unit decreases with increase in volume–capacity ratio and proportion of subject vehicles irrespective of vehicle category. Arasan and Arkatkar [1] assessed the variation in passenger car unit values with traffic volume. This study was performed on intercity roads under heterogeneous traffic using microscopic simulation to check variation in PCU values with traffic volume and different roadway conditions. Metkari et al. [7] studied the available methods used for the measurement of passenger car units of vehicles. An attempt was also made to check the applicability of these methods for heterogeneous traffic conditions. Mahidadiya et al. [4] discussed an estimate to find the passenger car unit value of

vehicles. An assessment was made on the Global Scenario on the development of PCU. In countries like India, the traffic situation is heterogeneous. Parvathy et al. [8] calculated new PCU values and studied variation in the passenger car unit of the vehicle with varying lengths of the vehicle. It was found that developed values differ from the predetermined values, and these values are inversely proportional to the length of the vehicle types.

3 Methodology and Data Collection

3.1 Methodology

There are various methods available for the calculation of the PCU value of vehicle types. But Chandra's method suites Indian traffic conditions. This method uses only two parameters projected rectangular area and speed of vehicle types.

$$(\text{PCU})_i = \frac{(V_c/V_i)}{(A_c/A_i)} \quad (1)$$

where V_c and V_i are speeds of car and vehicle type (i), respectively and A_c and A_i are the projected areas of car and vehicle type (i), respectively.

When different vehicles share the same space of roadway width, the speed of a particular vehicle type is influenced by the presence of other vehicle types. If a stream has many vehicles like car (c), bike (b), auto-rickshaw (ar), e-rickshaw (er), bus (bs), truck (tr), cycle (cy), LCV (l), the general forms of the equations are as follows:

$$\begin{aligned} V_c = & a_{0-c} + a_{1-c}(n_c/v_c) + a_{2-c}(n_b/v_b) \\ & + a_{3-c}(n_{ar}/v_{ar}) + a_{4-c}(n_{er}/v_{er}) \\ & + a_{5-c}(n_l/v_l) + a_{6-c}(n_{cy}/v_{cy}) \\ & + a_{7-c}(n_{bs}/v_{bs}) + a_{8-c}(n_{tr}/v_{tr}) \end{aligned} \quad (2)$$

$$\begin{aligned} V_{er} = & a_{0-er} + a_{1-er}(n_c/v_c) + a_{2-er}(n_b/v_b) \\ & + a_{3-er}(n_{ar}/v_{ar}) + a_{4-er}(n_{er}/v_{er}) \\ & + a_{5-er}(n_l/v_l) + a_{6-er}(n_{cy}/v_{cy}) \\ & + a_{7-er}(n_{bs}/v_{bs}) + a_{8-er}(n_{tr}/v_{tr}) \end{aligned} \quad (3)$$

where V represents the space mean speed of respective vehicles in m/s and n is the vehicle count per 15 min, and $a_0, a_1, a_2 \dots a_8$ are the coefficients. These equations were solved using regression analysis with the help of SPSS software.

Table 1 Selected roads with carriageway width

S. No.	Site	Carriageway width in meter
1	Bahalgarh road	7.2
2	Tiranga Chowk	6.75
3	Chhotu Ram Chowk	6.71
4	Old DC road	4.7
5	Sonipat to Murthal road	4.1

3.2 Data Collection

For this study, data collection was done during weekdays and in sunny weather.

Data Collection for Calculation of PCU Value of E-Rickshaw

For calculating the PCU value of e-rickshaw, five different urban roads were selected. A stretch of 30 m on each road was selected, and times to cross this section by 100 cars and 100 e-rickshaws were noted. Data collection for this purpose was made manually with the help of stopwatches having the least count of 0.01 s.

1. Bulandshahr Road, Hapur
2. ITI Chowk to Narela Road, Sonipat
3. Railway Road, Sonipat
4. Sector 14, Sonipat
5. Sector 15, Sonipat.

Data Collection for Assessing Variation in PCU Value of E-Rickshaw

For this purpose, five different roads of Sonipat City having different carriageway width were taken. On each road, videos were made to know traffic volume and traffic composition. Camera was mounted at a height of 4.5 m from the carriageway, and in such a position that traffic was coming toward the camera. By frame by frame analysis, the speeds of vehicles on these roads were calculated. Table 1 shows the selected roads along with carriageway widths for the study.

4 Analysis of Data

4.1 Analysis for Calculating PCU Value of E-Rickshaw

Chandra's method was used to calculate the PCU value of e-rickshaw. It uses two factors namely space mean speed and projected rectangular area of the vehicle. Time mean speed was calculated by measuring the time taken to cross a section of 30 m by cars and e-rickshaws. Later speed was converted into space mean speed. Table 2 shows the average rectangular area of car and e-rickshaw on the ground.

Table 2 Average projected rectangular area

Vehicle type	Length in (m)	Width in (m)	Projected rectangular area in (m * m)
Car	3.72	1.44	5.36
E-rickshaw	2.79	0.98	2.72

Table 3 Space mean speed of car and vehicle and calculated PCUs

S. No.	Site	Space mean speed in KMPH		PCU of E-rickshaw
		Car	E-Rickshaw	
1	Bulandshahr road Hapur	27.169	16.998	0.811
2	ITI Chowk to Narela road	33.182	21.82	0.772
3	Railway road Sonipat	31.949	21.186	0.765
4	Sector 14 Sonipat	36.26	22.399	0.821
5	Sector 15 Sonipat	39.674	25.031	0.804
			Average	0.795

Equation 1 was used to calculate PCU values. Space mean speed of car and e-rickshaw on respective roads is shown in Table 3. Calculated PCU values of e-rickshaw on different roads are listed in Table 3.

It is usual practice to take the arithmetic average of all calculated values to suggest a parameter. The same practice is employed in many traffic experiments like the traffic volume count experiment. As per this study, the suggested PCU value of an e-rickshaw is **0.795**. It is subjected to change with different traffic and roadway conditions. Other studies may found different value for PCU of e-rickshaw.

4.2 Analysis for Assessing Variation in PCU Value

For assessing variation in PCU value, the speed–volume relationship was developed as Eqs. 2 and 3. Regression analysis was done to find out all the coefficients present in Eqs. 2 and 3 using SPSS software. After putting coefficients in equations, the final speeds of the car and e-rickshaw were determined. Table 4 shows the obtained PCU values of e-rickshaw at each road. Traffic volume count of 15 min interval was captured from the videos by frame by frame analysis at each road. Table 5 shows the average traffic composition observed at each side at 15 min intervals.

The analysis was done on Guhana to Chhotu Ram Chowk road. Table 6 shows obtained coefficients present in Eqs. 2 and 3 with *R* squared value for Guhana to Chhotu Ram Chowk road. These coefficients were obtained using SPSS software. Some coefficients are negative, and some are positives. It means speed changes with

Table 4 Obtained PCU values of e-rickshaw

S. No.	Site	PCU of E-rickshaw
1	Bahalgarh road	0.761
2	Tiranga Chowk	0.824
3	Chhotu Ram Chowk	0.799
4	Old DC road	0.710
5	Sonipat to Murthal road	0.755

the change in the traffic volume. R squared value is close to 1 for both equations that mean collected data fit the model well. Table 7 shows the estimated parameters present in Eqs. 2 and 3 for Guhana to Chhotu Ram Chowk road. N_c/V_c , N_b/V_b , ..., N_{tr}/V_{tr} are the parameters present in speed–volume Eqs. 2 and 3. In this table, data for 3 h period with an interval of 15 min was organized. With the help of speed and volume data of vehicle types for every 15 min intervals, final space mean speeds of car and e-rickshaw were determined and then PCU values of e-rickshaw for every 15 min interval were obtained.

where

- V_{cf} Final space mean speed of the car,
- V_{ef} Final space mean speed of e-rickshaw,
- A_c Average projected rectangular area of the car,
- N Traffic volume of vehicle types (vehicles per 15 min),
- A_e Average projected rectangular area of e-rickshaw,
- V Space mean speed of vehicle types.

Variation in PCU Value of E-Rickshaw with Traffic Volume

The passenger car unit factors are dependent on traffic in the stream. To analyze the variation in the passenger car unit of a vehicle type with the varying traffic volume, speed in Eqs. 2 and 3 was solved for different traffic volumes keeping the traffic composition constant on Guhana to Chhotu Ram Chowk road. The traffic volume was varied from 412 vehicles per 15 min to 1012 vehicles per 15 min with an interval of 100 vehicles per 15 min. Figure 1 shows the variation in passenger car unit (PCU) of e-rickshaw with traffic volume on Guhana to Chhotu Ram Chowk. From the study, it is clear that the passenger car unit of e-rickshaw decreases with increase in the traffic volume. When traffic in the stream will increase, the speeds of vehicle type will decrease due to more interactions between the vehicles, and hence, PCU of vehicles will decrease. Similar process was employed for Sonipat to Murthal road. Figure 2 shows the variation in passenger car unit (PCU) of e-rickshaw with traffic volume on Sonipat to Murthal road.

Variation in PCU of E-Rickshaw with Traffic Composition

To analyze the variation in the passenger car unit of e-rickshaw with different traffic compositions, speed in Eqs. 2 and 3 was solved. The proportion of vehicle types

Table 5 Observed average traffic composition in percentage

Site	Observed average traffic composition in (%)										Average traffic volume per 15 min
	Car	Bike	Auto-rickshaw	E-rickshaw	Bus	Truck	LCV	Cycle			
Bahalgarh road	46.1	33.88	1.99	7.12	0.47	5.43	0.98	4.02			213
Gohanaa to Tiranga Chowk	30.47	45.16	15.07	3.2	1.69	0.83	1.08	2.49			268
Gohana to Chhotu Ram Chowk	23.57	55.66	11.53	3.64	0.76	0.43	0.95	3.46			412
Old DC road	32.79	42.34	5.85	9.57	0.26	1.1	1.32	6.77			242
Sonipat to Murthar road	21.28	52.42	11.73	5.93	0.25	1.29	1.04	6.07			275

Table 6 Obtained coefficients for Eqs. 2 and 3 and *R* squared at Guhana to Chhoturam Chowk

Coefficients for Eq. 2	Value	<i>R</i> squared	Coefficients for Eq. 3	Value	<i>R</i> squared
a_{0-c}	+ 13.024	0.911	a_{0-er}	+ 4.616	0.854
a_{1-c}	- 0.127		a_{1-er}	+ 0.007	
a_{2-c}	- 0.011		a_{2-er}	- 0.015	
a_{3-c}	- 0.277		a_{3-er}	+ 0.265	
a_{4-c}	- 0.099		a_{4-er}	- 0.237	
a_{5-c}	+ 0.150		a_{5-er}	+ 0.492	
a_{6-c}	- 0.020		a_{6-er}	+ 0.025	
a_{7-c}	+ 0.354		a_{7-er}	+ 0.258	
a_{8-c}	- 1.744		a_{8-er}	+ 0.635	

was increased to assess variation. At a time, the proportion of a vehicle type was increased while keeping the vehicle count of other vehicle types constant and total traffic volume also increases. The analysis was done for different base traffic volumes to get many curves.

Equations 2 and 3 were solved for Guhana to Chhotu Ram Chowk road. The proportion of e-rickshaw at this road was increased while keeping the volume count of other vehicles constant. At first, the proportion of e-rickshaw was increased. This analysis was done for three different base traffic volumes that is for 412, 512, and 612 vehicles per 15 min. Figure 3 shows the variation in the passenger car unit (PCU) of e-rickshaw with the increased proportion of e-rickshaw. Figure 3 clearly shows that as the proportion of e-rickshaw increases in the stream, PCU of e-rickshaw also increases.

Similarly, the proportions of cars, LCV, and trucks were increased. Figure 4 shows the variation in passenger car unit (PCU) of e-rickshaw with the increased proportion of cars on this road. From the figure, it is clear that PCU of e-rickshaw decreases as the proportion of cars increases. Figure 5 shows the effect of the proportion of LCV on PCU of e-rickshaw. From the figure, it is clear that PCU of e-rickshaw decreases with increase in the proportion of LCV in the stream. Figure 6 shows the variation in passenger car unit (PCU) of e-rickshaw with the increased proportion of trucks. From the figure, it is clear that due to the increased proportion of trucks in the stream, PCU of e-rickshaw decreases as trucks cover more space of carriageway width as compared to other vehicles.

Similar process was done on Sonipat to Murthal road. Figures 7, 8, and 9 show the variation in passenger car unit (PCU) of e-rickshaw with the increased proportion of e-rickshaw, car and LCV, respectively, on Sonipat to Murthal road.

Variation in PCU of E-Rickshaw with Carriageway Width

The obtained PCU of e-rickshaw at each road with carriageway width as per this study is shown in Table 8. India mostly consists of heterogeneous traffic, and every vehicle type occupies different space of the same carriageway width. The effect of

Table 7 Estimated parameters present in Eqs. 2 and 3, and calculated PCUs for Guhana to Chhotu Ram Chowk road

N_c/V_c	N_b/V_b	N_{ar}/V_{ar}	N_{er}/V_{er}	N_1/V_1	N_{cy}/V_{cy}	N_{bs}/V_{bs}	N_{tr}/V_{tr}	V_{cf}	V_{ef}	V_{cf}/V_{ef}	A_c/A_e	$(PCU)_e$
9.642	20.949	5.530	1.591	1.042	1.849	0.438	0.350	9.544	6.352	1.502	1.971	0.762
12.400	22.150	5.331	2.341	0.374	3.839	0.000	0.371	8.829	5.744	1.537	1.971	0.780
9.416	25.838	5.835	1.762	0.260	3.372	0.244	0.000	9.811	5.698	1.722	1.971	0.874
8.699	18.735	5.795	1.647	0.149	3.845	0.453	0.186	9.727	5.945	1.636	1.971	0.830
10.562	25.641	5.858	2.542	0.573	4.133	0.435	0.464	8.874	6.047	1.467	1.971	0.745
9.442	26.664	5.367	2.993	0.599	5.079	0.239	0.477	8.989	5.782	1.555	1.971	0.789
10.631	25.085	5.550	1.644	0.416	4.531	0.236	0.361	9.124	6.003	1.520	1.971	0.771
9.845	22.504	6.777	2.486	0.419	2.693	0.786	0.265	9.227	6.199	1.489	1.971	0.755
10.942	27.275	5.081	3.882	0.355	3.679	0.207	0.613	8.527	5.419	1.574	1.971	0.798
12.667	27.156	6.422	6.093	0.504	4.292	0.302	0.374	8.179	5.226	1.565	1.971	0.794
11.301	30.133	5.211	2.135	0.522	3.669	0.672	0.000	9.845	5.640	1.746	1.971	0.886
12.125	22.622	5.639	2.686	0.742	1.371	0.207	0.212	9.195	5.807	1.583	1.971	0.803
											AVG.	0.799

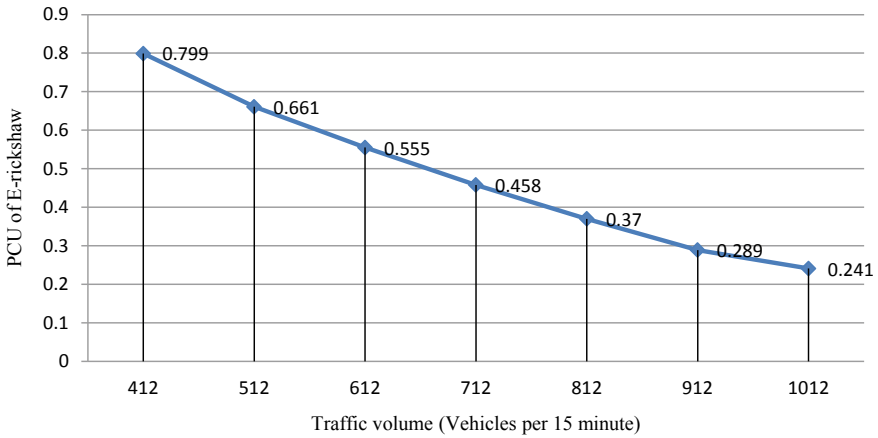


Fig. 1 Variation in PCU of e-rickshaw with traffic volume on Guhana to Chhotu Ram Chowk road

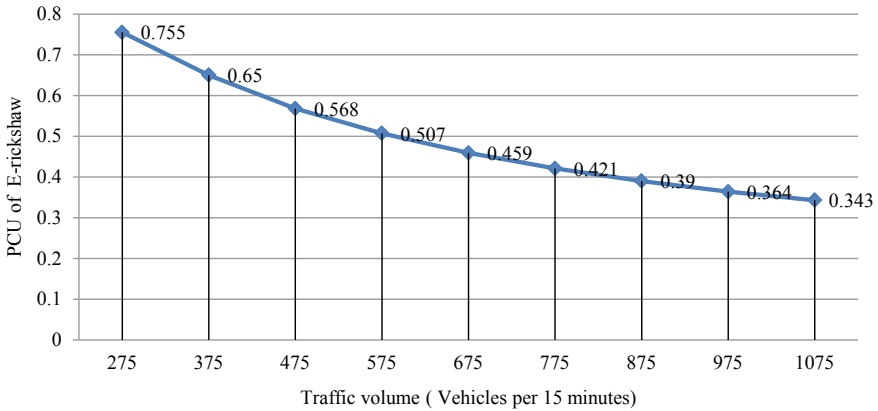


Fig. 2 Variation in PCU of e-rickshaw with traffic volume on Sonipat to Murthal road

carriageway width on passenger car unit value of e-rickshaw is shown in Fig. 10. As per this study, no comment can be made on variation in PCU of e-rickshaw with carriageway width.

5 Result and Discussion

In developing countries like India, road traffic is heterogeneous in nature. One of the methods used to convert heterogeneous traffic into equivalent homogeneous one is by using PCU factors. Out of many methods, Chandra’s method is used in mixed traffic

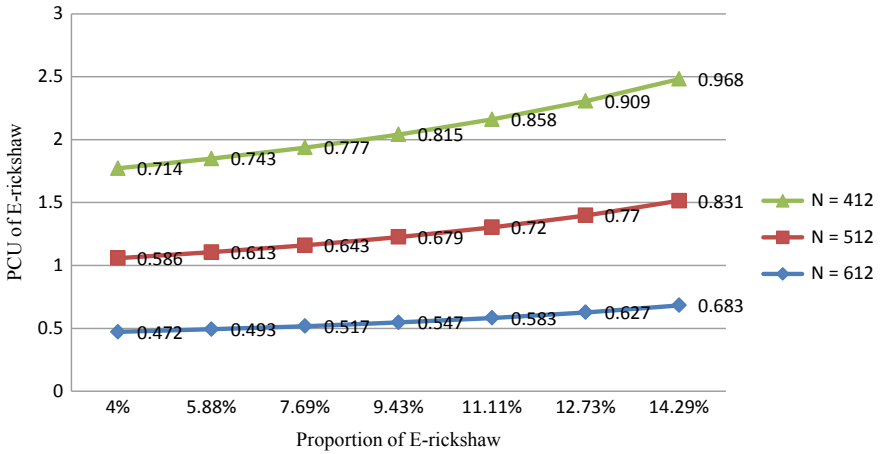


Fig. 3 Variation in PCU of e-rickshaw with increased proportion of e-rickshaw on Guhana to Chhotu Ram Chowk road

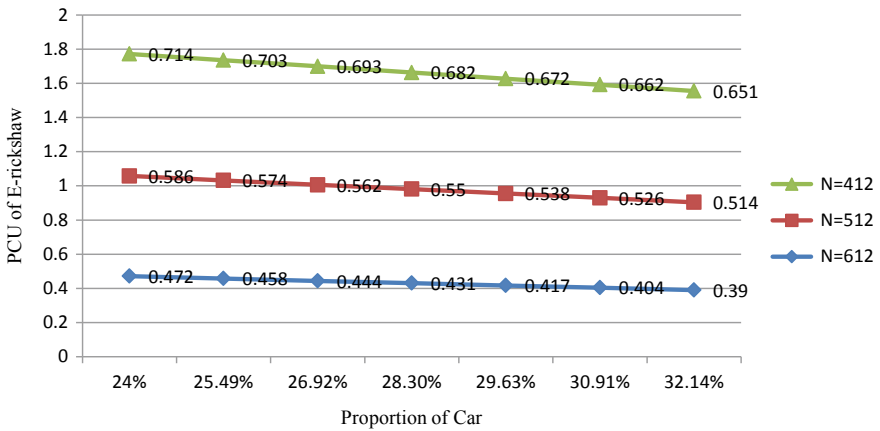


Fig. 4 Variation in PCU of e-rickshaw with increased proportion of car on Guhana to Chhotu Ram Chowk road

conditions. The main aim of this study was to develop PCU value of e-rickshaw on urban roads and to check variation in PCU value with different traffic volume and traffic compositions. This study was completed in two heads.

First, PCU of e-rickshaw was developed. For this purpose, a stretch of 30 m on five different roads was selected, and by the manual method with the help of stopwatches, time taken by cars and e-rickshaws to cross the selected stretch on each road was noted, and later, space mean speeds of these vehicles were calculated and with the help of Chandra’s method, PCU of e-rickshaw was developed on each road as listed in Table 3. As per this study, the developed PCU of e-rickshaw is 0.795.

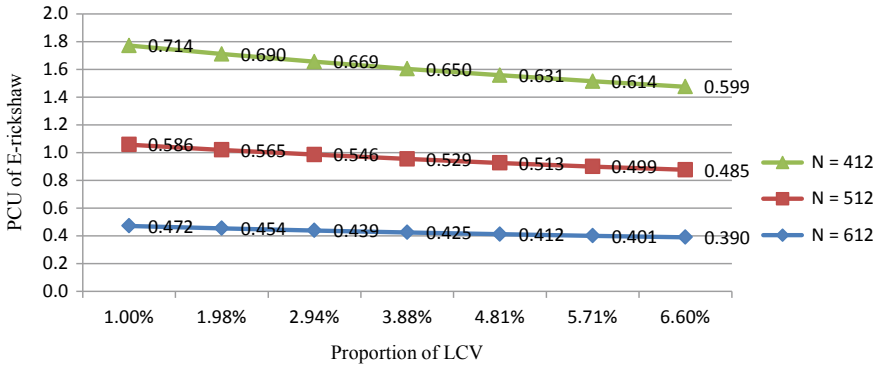


Fig. 5 Variation in PCU of e-rickshaw with increased proportion of LCV on Guhana to Chhotu Ram Chowk road

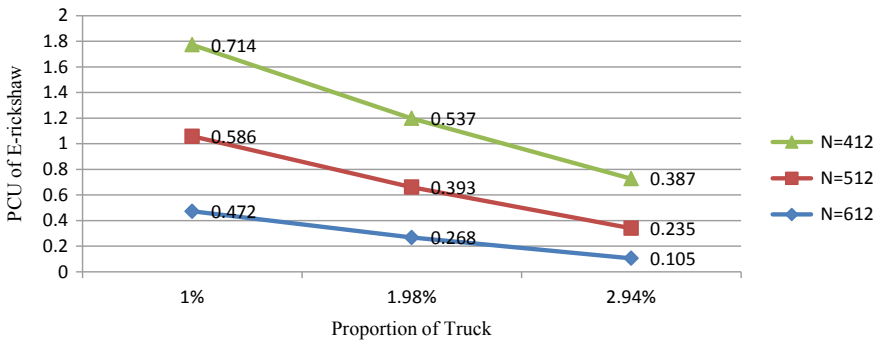


Fig. 6 Variation in PCU of e-rickshaw with increased proportion of truck on Guhana to Chhotu Ram Chowk road

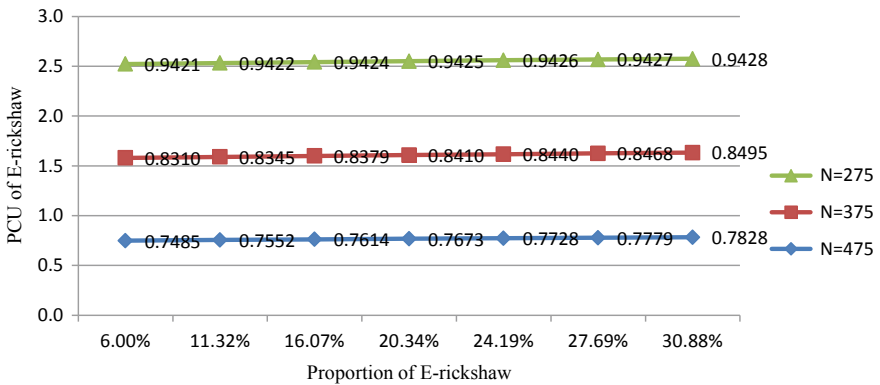


Fig. 7 Variation in PCU of e-rickshaw with increased proportion of e-rickshaw on Sonipat to Murthal road

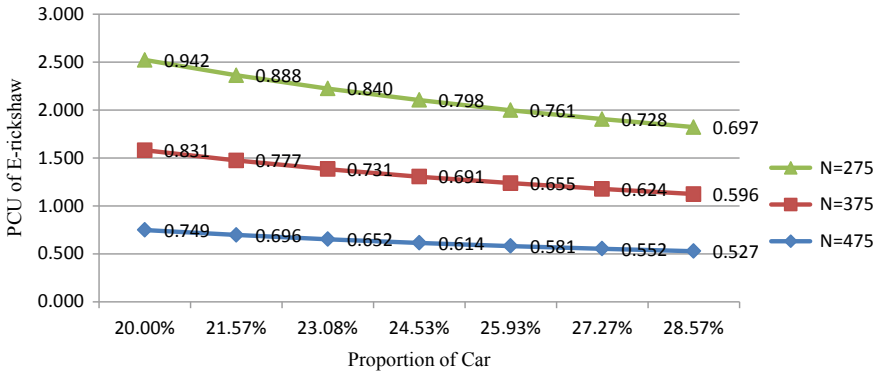


Fig. 8 Variation in PCU of e-rickshaw with increased proportion of car on Sonipat to Murthal road

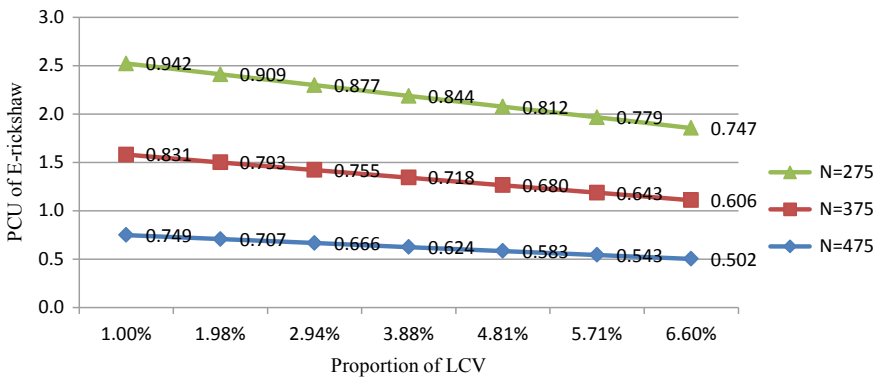


Fig. 9 Variation in PCU of e-rickshaw with increased proportion of LCV on Sonipat to Murthal road

Table 8 Carriageway width and PCU of e-rickshaw at each road

Site	Carriageway width in (m)	PCU of E-rickshaw
Bahalgarh road	7.2	0.761
Tiranga Chowk	6.75	0.824
Chhotu Ram Chowk	6.71	0.799
Old DC road	4.7	0.71
Sonipat to Murthal road	4.1	0.755

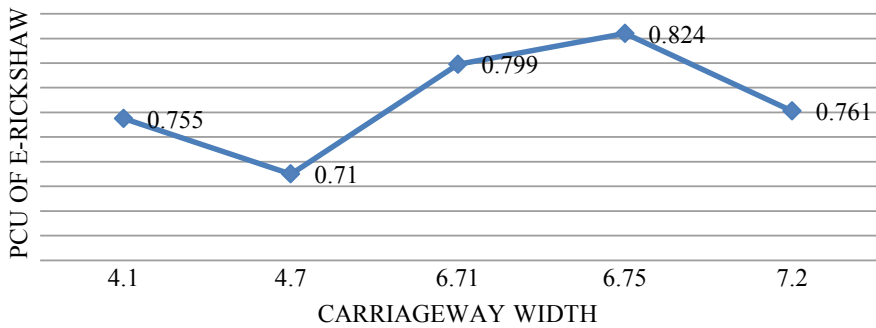


Fig. 10 Variation in PCU of e-rickshaw with carriageway width

Second, an attempt was made to check variation in PCU of e-rickshaw with varying traffic conditions. For this purpose, five different roads of Sonipat City were selected. Videos on these roads for 3-h durations from 3 to 6 PM on weekdays were captured with the help of a mobile camera mounted at a height of 4.5 m from the carriageway in such a position that traffic was coming toward the camera. Then by frame-by-frame analysis, speeds and volume data of different vehicle types of every 15 min intervals were extracted. Captured average traffic compositions on each road are listed in table 5. The speed–volume relationship was developed as in Eqs. 2 and 3. Coefficients present in Eqs. 2 and 3 were obtained with the help of SPSS software. For Guhana to Chhotu Ram Chowk road, obtained coefficients along with R squared value are listed in Table 6. Some coefficients are positive, and some are negative which mean these coefficients have some negative as well as positive effect on final speeds. Later with the help of Microsoft excel, parameters present in speed–volume equations were obtained, and finally, PCU of e-rickshaw was determined and these parameters and PCU for Guhana to Chhotu Ram Chowk road are listed in Table 7. To check variation in PCU with different traffic volumes, speed in Eqs. 2 and 3 was again solved for different traffic volume while keeping the traffic composition constant on Guhana to Chhotu Ram Chowk. Traffic volume was varied from 412 vehicles per 15 min to 1012 vehicles per 15 min with an interval of 100 vehicles per 15 min. The same analysis was employed for Sonipat to Murthal road. As per this analysis, it was found that PCU of e-rickshaw decreases with increase in the traffic volume in the stream as shown in Figs. 1 and 2. To check variation in PCU of e-rickshaw with varying traffic composition, speed in Eqs. 2 and 3 was again solved with varying composition of a single-vehicle type at a time for Guhana to Chhotu Ram Chowk road and Sonipat to Murthal road, and this analysis was done for different base traffic volume to get many curves. PCU of e-rickshaw increases with the increased composition of e-rickshaw in the stream as shown in Figs. 3 and 7. PCU of e-rickshaw decreases with the increased composition of cars, LCVs, and trucks as shown in Figs. 4, 5, 6, 8, and 9.

An attempt was also made to check the effect of carriageway width on PCU of e-rickshaw. Figure 10 depicts the effect of carriageway width on PCU of e-rickshaw. However, no comment can be made on this.

The findings of this paper are as follows:

- (1) The suggested passenger car unit (PCU) of e-rickshaw on urban roads as per this study is 0.795.
- (2) PCU value of e-rickshaw decreases when traffic volume in the stream increases.
- (3) As the proportion of e-rickshaw in the stream increases, keeping the volume of other vehicles constant, PCU of e-rickshaw increases.
- (4) As the proportion of cars in the stream increases, keeping the volume of other vehicles constant, PCU of e-rickshaw decreases.
- (5) As the proportion of LCV in the stream increases, keeping the volume of other vehicles constant, PCU of e-rickshaw decreases.
- (6) As the proportion of trucks in the stream increases, keeping the volume of other vehicles constant, PCU of e-rickshaw decreases.
- (7) No comment can be made on variation in passenger car unit of e-rickshaw with carriageway width.

PCU values of e-rickshaw are not available in any previous literature. An attempt was made to find one. But for this study, data collection was done only from one city. Interpretation of data from various cities may give different and concrete results. Limitations of the study are as follows:

1. Data collection was done only from a particular city.
2. Data collection was done only on weekdays.
3. The weather condition at the time of data collection was sunny.
4. Data collection was done only during the 3–6 PM period.

More studies are required to find conclusive PCU of e-rickshaw. Different weather conditions, roadway conditions, and traffic conditions may give different results.

References

1. Arasan VT, Arkatkar SS (2010) Micro-simulation study of the effect of volume and road width on PCU of vehicles under heterogeneous traffic. *J Transp Eng*
2. Chandra et al (2000) Factors affecting PCU in mixed traffic situations on urban roads. *Road Transp Res* 9(3):40–50
3. Chandra et al (2003) Effect of lane width on capacity under mixed traffic conditions in India. *J Transp Eng* 129(2):155–160
4. Mahidadiya et al (2016) Estimation of passenger car unit value at the signalized intersection. *IJSRSET* 2(2):1317–1324. <https://doi.org/10.32628/IJSRSET1622394>
5. Mallikarjuna C et al (2006) Modelling of passenger car equivalency under heterogeneous traffic conditions. In: Proceedings of the research into practice: 22nd Australian road research board (ARRB) conference, pp 1–13
6. Manraj Bains P, Balaji AS (2012) Modelling of traffic flow on Indian expressways using simulation technique. *Proc Soc Behav Sci* 43:475–493
7. Metkari M et al (2012) Review of passenger car equivalence studies in the Indian context. In: International conference on emerging frontiers in technology for rural area (EFITRA)

8. Parvathy R, Sreelatha T, Reebu Z Koshy (2013) Development of new PCU values and effect of length of passenger cars on PCU. In: Proceedings of international conference on energy and environment-2013 (ICEE 2013)
9. Srinivasa Rao R, Yadav N (2018) Determination and comparison of PCU on urban roads under mixed traffic conditions—a case study. *Urbanization challenges in emerging economies 2018*
10. Werner A, Morrall JF (1976) Passenger car equivalencies of trucks, buses and recreational vehicles for two-lane rural highways. *Transp Res Rec* 615:10–17

Performance Evaluation of Impact Stilling Basin Using ANSYS Fluent



Ishan Sharma, Ashish Mishra, and Rakesh Mehrotra

Abstract Impact stilling basin or USBR type VI basin is a unique energy dissipator device that is installed at downstream of culverts, detention basin, and pipe outlets to prevent erosion and scouring. Its box-type structure with hanging baffle dissipates the energy of flowing water through impact thereby creating vertical eddies and consequently reducing the velocity of flow. In this study, a 3D model of impact basin is developed using ANSYS workbench, and its performance is analyzed in different scenarios using ANSYS Fluent R15.0 software. These different scenarios are taken as per those in published experimental work. Simulations are run for these cases in ANSYS Fluent by varying the position of baffle wall from both basin inlet and basin floor. Values of parameters such as turbulent kinetic energy, velocity of flow, wall shear stress and energy losses (kinetic energy and specific energy) are computed at the basin outlet for different cases to determine the position of baffle wall for maximum energy dissipation. Results from simulations show that maximum dissipation of energy occurs when the wall is placed at a distance of $4d$ from inlet with a gap of $1d$ from the floor, where ' d ' is taken as equivalent diameter of the pipe outlet. These results are consistent with the results of previous experimental studies.

Keywords Impact stilling basin · USBR type VI impact basin · Energy dissipator · ANSYS Fluent

I. Sharma (✉)

Department of Water Resources Development and Management, Indian Institute of Technology Roorkee, Roorkee 247667, India

e-mail: isharma@wr.iitr.ac.in

A. Mishra

Department of Hydrology, Indian Institute of Technology Roorkee, Roorkee 247667, India

R. Mehrotra

Department of Civil Engineering, Delhi Technological University, New Delhi 110042, India

1 Introduction

Energy dissipation is not only required at downstream of the spillway of a dam and barrage but also an important phenomenon to prevent erosion at canal outlets and culvert outlets [1]. This is crucial for effective water resources planning and management, which is emphasized in most countries of the present world [2–4]. The failure or damage of many culverts, pipe outlets, and detention basin outlet structures is caused by unchecked erosion. Energy dissipators are structures designed to protect downstream areas as well as drainage structures from erosion and scouring by causing energy losses and reducing the velocity of flow to acceptable limits. One such structure known as the USBR type VI impact basin was developed at the US Bureau of Reclamation laboratory in 1957 [5]. The basin is contained in a box-like structure, which is relatively small and does not require any tail-water to perform successfully. Energy dissipation takes place as flow strikes the vertical portion of the hanging baffle and then deflected upstream by the horizontal portion of the baffle and finally hitting the floor, thereby creating horizontal eddies [6].

An experimental study to reduce scour at downstream and to shorten the basin length of USBR type VI impact stilling basin was carried out by Goel and Verma [7]. For this, various experiments were performed in laboratory with Froude number ranges from 1.70 to 5.50. Wedge shape splitter blocks, end sill, and baffle wall of different sizes were used at different locations from pipe outlet. It was concluded that new models developed performed better than typical USBR type VI and also the length of the basin reduced to 25% with smaller tail-water depth.

Tiwari and Goel in their experimental study carried out 57 tests in laboratory for the enhancement of energy dissipation caused by impact stilling basin [8]. These experiments were performed to find out the effect of size, shape, and position of impact wall and gap between impact wall and basin floor. The performance was evaluated in terms of the performance index. The indices are simple techniques and widely used in water resources for assessing the performance or specific characteristics [9–11]. All the dimensions of the impact stilling were calculated in terms of equivalent diameter (d). It was concluded that size, shape, and location of impact wall affect the flow condition which ultimately affects the scour downstream of the basin. Higher the perform index higher the energy dissipation, and the highest performance index was observed with impact wall of size $1.5d \times 3d$ at a distance of $4d$ from the pipe outlet with length of basin reduced up to 30% as compared to USBR type VI stilling basin and with a gap of $1d$ between wall and basin floor.

Modeling and analysis of impact stilling basin has been done in ANSYS Fluent software [12]. This software uses numerical methods like finite element analysis (FEA) for simulation purposes. The process of numerical simulation involves three basic steps, viz. preprocessing, solver, and post-processing. The R15.0 version of

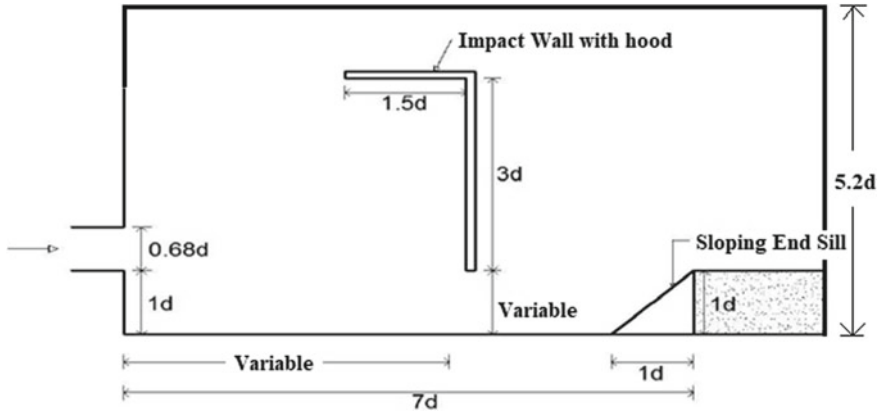


Fig. 1 Side view of the general basin model having dimensions in terms of equivalent diameter ' d '. *Note:* This figure is modified version of the original figure proposed by Tiwari and Goel [8]

ANSYS workbench is used which has its own software for drawing of geometry, i.e., design modular.

Reference Stilling Basin Model

Based on the experimental study carried out by previous studies [7, 8, 13, 14], six different models were developed and analyzed in ANSYS Fluent software in order to find the best model for energy dissipation downstream of a rectangular pipe outlet. These models were tested for three different scenarios, namely for Froude number = 1.85, 2.85, and 3.85, respectively, and the performance of stilling basin was evaluated by computing and comparing different parameters, viz. turbulent kinetic energy at outlet, kinetic energy and specific energy losses, and wall shear stress at outlet for different models in different scenarios. A general schematic diagram of stilling basin model is shown in Fig. 1 on which all the models were developed and analyzed in ANSYS.

2 Modeling in ANSYS

2.1 Calculation of Equivalent Diameter and Inlet Velocity

Equivalent diameter (d) is the most important parameter for designing an impact stilling basin as the dimensions of the basin (as well as model) is computed in terms of ' d ' (see Fig. 1). If the pipe outlet is circular in shape, the diameter of pipe outlet is taken as ' d ', but if the shape is rectangular or any other polygon, ' d ' is calculated by equating the area of that polygon to a circle. Say, for a rectangular inlet, ' d ' is calculated as the square root of $(4 * A / \pi)$, where A is the area of rectangle. In this

study, rectangular pipe of size 10.8 cm \times 6.3 cm is used for analysis, therefore for each model the value of d is fixed as 9.3 cm.

The Froude number (Fr) at the pipe outlet is defined as $Fr = V/(gd)^{1/2}$, where V = velocity in m/s; g = acceleration due to gravity in m/s^2 , and d = diameter of the pipe. Therefore, for $Fr = 1.85, 2.85,$ and 3.85 , the inlet velocity is computed as 1.767 m/s, 2.722 m/s, and 3.677 m/s, respectively.

2.2 Geometry

In this study, there are total six different models of impact stilling basin whose geometry has been drawn in design modular. All the models are drawn in shape of a rectangular box with length = $7d$ (65.1 cm), width = $6.3d$ (58.6 cm), and height = $5.2d$ (50 cm) where ' d ' is the equivalent diameter of pipe outlet ($d = 9.3$ cm). The geometry of six different models is shown in Fig. 2, and details of each model are given in Table 1.

2.3 Meshing

The meshing has been done in ICEM CFD software which is a part of ANSYS workbench. The meshing details of all the six models have been kept same. Tetrahedron method is used in assembly meshing with maximum eight inflation layers and growth rate of 1.4. Figure 3 shows the meshed model of the impact stilling basin.

2.4 Boundary Condition in Fluent Setup

The following steps are followed to set up the Fluent software for analysis: (1) In Fluent launcher 3D, *double precision* and *serial processing* option is selected and setup is started. In General tab, pressure type solver, absolute velocity formulation, transient time, and direction of gravity in $-ve$ Y -direction are selected. (2) Then in Models tab, multiphase, number of Eulerian phases 2, implicit scheme, and ' $k-\epsilon$ ' viscous model are selected. (3) In the third tab, fluid from materials is selected, as air is already present new fluid water-liquid is added from database of ANSYS. Thereafter, primary phase (i.e., Phase I) to air and secondary phase (i.e., Phase II) to water are assigned. (4) Thereafter, boundary conditions and initial conditions are entered, inlet is taken as velocity inlet and velocity of flow entering the basin is entered and 'intensity and hydraulic diameter' specification method is chosen. Also Phase II volume fraction is taken as 1 to insure only water entered from the inlet. Outlet is taken as pressure outlet. (5) The solution is initialized using hybrid initialization method and after that liquid region is patched using patch option which ensures that

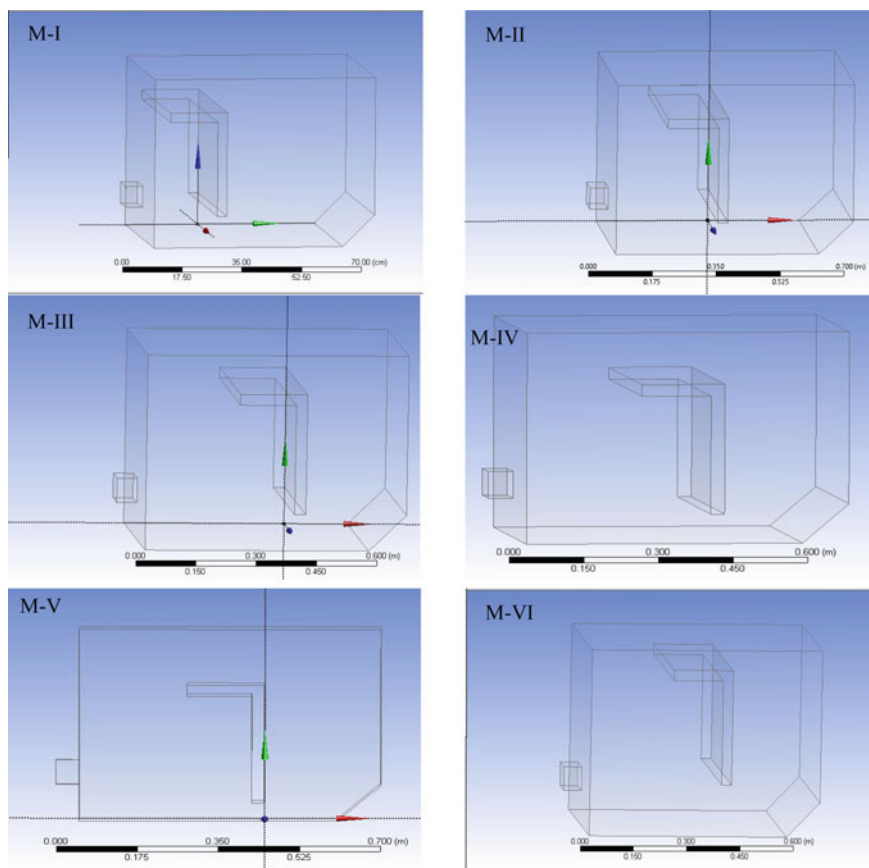


Fig. 2 Geometry of model M-I to M-VI drawn in design modular

Table 1 Various models designed in design modular by ANSYS Fluent software

S. no.	Model name	Impact wall size	Distance from inlet	Gap between wall and basin floor
1	M-I	$1.5d \times 3d$	$2d$	$1d$
2	M-II	$1.5d \times 3d$	$3d$	$1d$
3	M-III	$1.5d \times 3d$	$4d$	$1d$
4	M-IV	$1.5d \times 3d$	$4d$	$0.75d$
5	M-V	$1.5d \times 3d$	$4d$	$0.5d$
6	M-VI	$1.5d \times 3d$	$4d$	$1.5d$

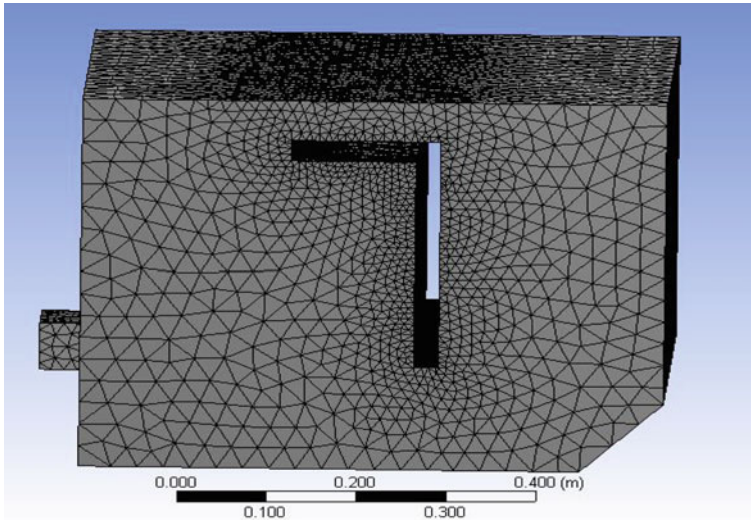


Fig. 3 Mesh diagram drawn in ICEM CFD

at the start of the simulation which portion is filled with water and which portion of basin is filled with air. (6) The last step is running simulations where time step size 1 s, number of time steps 40, and maximum iteration per time step 5 are entered and simulations are allowed to run.

3 Results and Discussion

After simulations are run for each model, the software builds stream lines plot for every model (Fig. 4) showing the simulated flow of water through the stilling basin especially after the water strikes the impact wall. As the distance between impact wall and inlet increases from $2d$ (18.6 cm) to $4d$ (37.2 cm), gap between impact wall and basin floor increases from $0.5d$ (4.65 cm) to $1.5d$ (13.95 cm).

The stream line plots from Fig. 4 give an idea of the velocity as well as the energy of the flow. The yellow and red color of stream lines denote high velocity, whereas blue and indigo colors signify low velocities; it also depicts the formation of eddies after the water strikes the impact wall as the distance between inlet and wall; the gap between basin floor and wall increases. Changes in the color of stream lines signify energy loss. Even though the stream line plots gave an idea about the energy losses and velocity vectors but the clear idea can only be known by computing the actual values of turbulent kinetic energy (TKE), kinetic energy (KE) and specific energy (SE) losses, and wall shear stress (WSS) at outlet. The results obtained from the analysis by Fluent are presented in Fig. 5 in the form of bar graphs comparing values

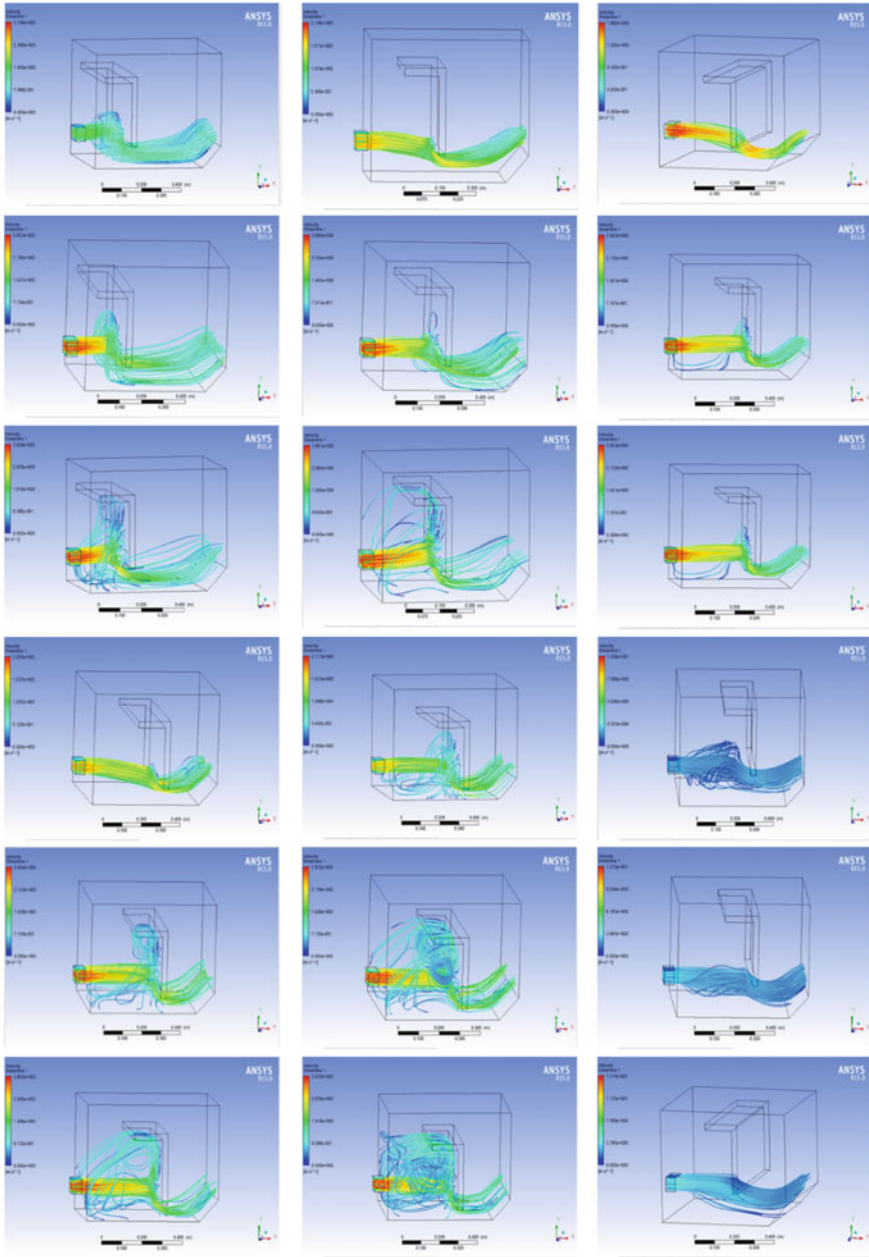


Fig. 4 Stream lines plot for each model (first row for the models M-I, M-II, and M-III corresponding to $Fr = 1.85$, second row corresponding to $Fr = 2.85$, and third row corresponding to $Fr = 3.85$; fourth row for the models M-IV, M-V, and M-VI with $Fr = 1.85$, fifth row corresponding to $Fr = 2.85$, and sixth row corresponding to $Fr = 3.85$)



Fig. 5 TKE, WSS, and the change in KE and SE between inlet and outlet for different models (M-I to M-VI) at different Fr (i.e., 1.85, 2.85, and 3.85)

of TKE, SE and KE losses, and WSS for different models with Froude numbers of 1.85, 2.85, and 3.85.

From Fig. 5, the following observations can be made:

For M-I model, the average as well as maximum value of TKE (in m^2/s^2) at the outlet of basin is highest (0.08 for $Fr = 1.85$, 0.104 for $Fr = 2.85$, and 0.126 for $Fr = 3.85$). This is because the impact wall is so close to the inlet that the jet of water strikes with more power causing more turbulence, which leads to the formation of horizontal as well as vertical eddies. This can be checked by seeing the stream lines



Fig. 5 (continued)

for M-I, M-II, and M-III model. For low Froude number (1.85), this effect is more prominent, but as the value of the Froude number increases ($Fr = 3.85$), this effect lessens.

For M-III model, the value of shear stress (in Pa) at bottom outlet is least (5.43 for $Fr = 1.85$, 5.52 for $Fr = 2.85$, and 6.26 for $Fr = 3.85$), and for M-I model, it is highest (5.61 for $Fr = 1.85$, 6.19 for $Fr = 2.85$, and 6.95 for $Fr = 3.85$). This may be because of the stream lines of the jet of water are partially hitting the wall causing more portion of jet to pass between the gaps, hence causing more shearing. This effect is more prominent for high values of Froude number.

Kinetic energy as well as specific energy loss (in m) is highest in case of M-III model (0.127 for $Fr = 1.85$, 0.331 for $Fr = 2.85$, and 0.634 for $Fr = 3.85$) and lowest in case of M-I model (0.109 for $Fr = 1.85$, 0.317 for $Fr = 2.85$, and 0.618 for $Fr = 3.85$). This may be attributed to the shearing effect and because eddies formation at the outlet is least in case of M-III model. The inferences are in agreement with the previous experimental study [8, 14].

For M-V model, the gap between the impact wall and basin floor is least (i.e., 0.5d); hence, the shearing area is least which causes value of TKE and WSS at outlet bottom to be more than other models (M-III, M-IV, and M-VI). But the value of above two parameters is least for M-III model and not M-VI model. This may be because as gap between impact wall and basin floor increases beyond 1d the jet of water that flows between this gap gets shear form one side only as the bottom portion of the wall not able to apply shear to the jet floe which can be seen from the stream lines plot.

4 Conclusion

From the different model simulations of impact stilling basin through ANSYS Fluent software, the model M-III (impact wall size $1.5d \times 3d$, the distance between inlet and impact wall = $4d$, and a gap of 1d between the basin floor and the wall) can be concluded as the best option. It produces less turbulent kinetic energy, less outlet velocity, less shear stress at the bottom outlet, and more energy losses, which lead to lesser chances of scouring in the downstream of the end sill.

References

1. Thompson PL, Corry ML, Watts FJ, Richards DL, Jones JS, Bradley JN (1983) Hydraulic design of energy dissipators for culverts and channels (No. HEC 14)
2. Swain S, Nandi S, Patel P (2018) Development of an ARIMA model for monthly rainfall forecasting over Khordha district, Odisha, India. In: Recent findings in intelligent computing techniques. Springer, Singapore, pp 325–331
3. Grafton RQ, Hussey K (eds) (2011) Water resources planning and management. Cambridge University Press, Cambridge

4. Swain S, Verma MK, Verma MK (2018) Streamflow estimation using SWAT model over Seonath river basin, Chhattisgarh, India. In: Hydrologic modeling, pp 659–665
5. Bradley JN, Peterka AJ (1957) Hydraulic design of stilling basins: hydraulic jumps on a horizontal apron (Basin I). *J Hydraul Div* 83(5):1–24
6. Vercruyse J, De Mulder T, Verelst K, Peeters P (2013) Stilling basin optimization for a combined inlet-outlet sluice in the framework of the Sigmaplan. In: IWLHS 2013-international workshop on hydraulic design of low-head structures, pp 55–66
7. Goel A, Verma DVS (2006) Development of efficient stilling basins for pipe outlets. *ASCE J Irrig Drainage Eng* 13(4):194–200
8. Tiwari HL, Goel A (2016) Effect of impact wall on energy dissipation in stilling basin. *KSCE J Civ Eng* 20(1):463–467
9. Swain S, Patel P, Nandi S (2017) Application of SPI, EDI and PNPI using MSWEP precipitation data over Marathwada, India. In: 2017 IEEE International geoscience and remote sensing symposium (IGARSS). IEEE, pp 5505–5507
10. Swain S, Mishra SK, Pandey A (2020) Assessment of meteorological droughts over Hoshangabad district, India. *IOP Conf Ser Earth Environ Sci* 491(1):012012
11. Swain S, Sharma I, Mishra SK, Pandey A, Amrit K, Nikam V (2020) A framework for managing irrigation water requirements under climatic uncertainties over Beed district, Maharashtra, India. In: World environmental and water resources congress 2020: water resources planning and management and irrigation and drainage, pp 1–8
12. Fluent, A. N. S. Y. S. (2011) Ansys fluent theory guide. ANSYS Inc., USA, 15317, pp 724–746
13. Tiwari HL (2013) Analysis of baffle wall gap in the design of stilling basin models. *Int J Civ Eng Technol* 4(4):66–71
14. Tiwari HL (2013) Design of stilling basin with impact wall and end sill. *Int Res J Recent Sci* 2(3):59–63

Shoreline Change and Rate Analysis of Gulf of Khambhat Using Satellite Images



Keval Jodhani , Pulkit Bansal , and Priyadarshna Jain 

Abstract Morphological changes are one of the most prominent concerns of coastal phenomena. The continuous alterations in sea shoreline leads to littoral transport. Hence, it is essential to identify area and rate of erosion and deposition along the coastal surface due to wave action. This can be accomplished with persistent monitoring of the coastline using satellite surveillance in regular intervals. This research is conducted to evaluate short-term shoreline modification from 2016 to 2018 in the half-yearly periodic interval in the Gulf of Khambhat (GoK). The study is carried out using remote sensing datasets from USGS and conducting imagery analysis on ArcGIS and DSAS. The proposed study and map developed in the research will contribute to shoreline protection measures. This work will be beneficial for forecasting future marine trends and planning sustainable coastline management measures.

Keywords Shoreline changes · ArcGIS · DSAS · Remote sensing

1 Introduction

Coastal zones are considered as one of the significant features on the earth's surface attributing to a rise in coastal population and marine structures over time. Therefore, study related to shoreline change is of utmost importance to safeguard coastal interest. Shoreline or coastline can be referred as an interface between land and water in the sea. Shoreline changes are alterations due to the various marine phenomena that are both natural and human induced factors. The natural factors comprise of near-shore circulation, wave characteristics, beach forms, and sediment characteristics while human-generated factors are dredging, construction of dams or reservoirs, mining, and water extraction. Shoreline changes are an outcome of a process termed as

K. Jodhani (✉) · P. Bansal · P. Jain
Department of Civil Engineering, Institute of Technology, Nirma University, Ahmedabad 382481,
Gujarat, India
e-mail: jodhanikeval@gmail.com

© The Author(s), under exclusive license to Springer Nature Singapore Pte Ltd. 2021
Y. A. Mehta et al. (eds.), *Advances in Water Resources and Transportation Engineering*,
Lecture Notes in Civil Engineering 149,
https://doi.org/10.1007/978-981-16-1303-6_12

151

Littoral transport. Littoral transport contributes mainly to moving of sediments in the coasts by means of waves and currents in the near shore zone [1].

The determination of sediment abrasion, transport, and deposition is of great importance as sensitive marine phenomena have an immediate influence on the design of ports and marine structures, and also in planning mitigation measures. Therefore, it is crucial to recognize the area and rate of abrasion and accumulation of sediments along the coastline in different intervals and to further able to compare and evaluate them for inclusion into the prognosis and decisions as to the future status and location. Along with shoreline changes another crucial outlook is the sustainable coastal development and protection of the coastal environment. Monitoring of marine areas is obliged over the different intervals of time, as shoreline modification is the most essential and dynamic natural phenomenon and alterations in one part affects the other parts. Failure to observe this fact has hampered many coastal projects development or has a negative impact on the surrounding areas. Today regional analysis is an important priority for coastal management engineering projects [2].

In this study, visual interpretation of compared satellite images over the period of two years gives preliminary information of shoreline change and from that three major sensitive regions Part A, B, C (refer Fig. 1 study area) are identified and further analysis is carried on those regions by finding area of erosion and deposition using polygon feature in ArcGIS. While DSAS is used for calculating shoreline change envelope (SCE), net shoreline movement (NSM), end point rate (EPR), least regression rate (LRR), and least median squares (LMS).

2 Study Area

The Gulf of Khambhat is also named as the Gulf of Cambay. Gulf in Arabian Sea is a trumpet shaped, located amidst the mainland Gujarat and Saurashtra peninsula as mentioned. It is located approximately between latitude $20^{\circ} 30'$ to $22^{\circ} 20'$ N and $71^{\circ} 45'$ to $72^{\circ} 53'$ E. It surrounds an area of about 3120 km^2 . It is about 70 km wide and 130 km long with a mid-depth of 30 m. Strong tidal currents in the gulf dominates which are also reliable for maximum accumulation and abrasion features of the GoK. Gulf of Khambhat is encircled by the three districts Navsari, Valsad, and Surat [3].

3 Methodology

The Flowchart 1—methodology of work—describes about the process followed in this research. Firstly the source of data is the USGS earth explorer and Satellite Landsat 7, 8 Level 1 data then the data taken was compiled and processed in ArcGIS with composite tool then we get the satellite image that is raster data and then with ArcGIS polyline function by visual interpretation that is converted to vector data for

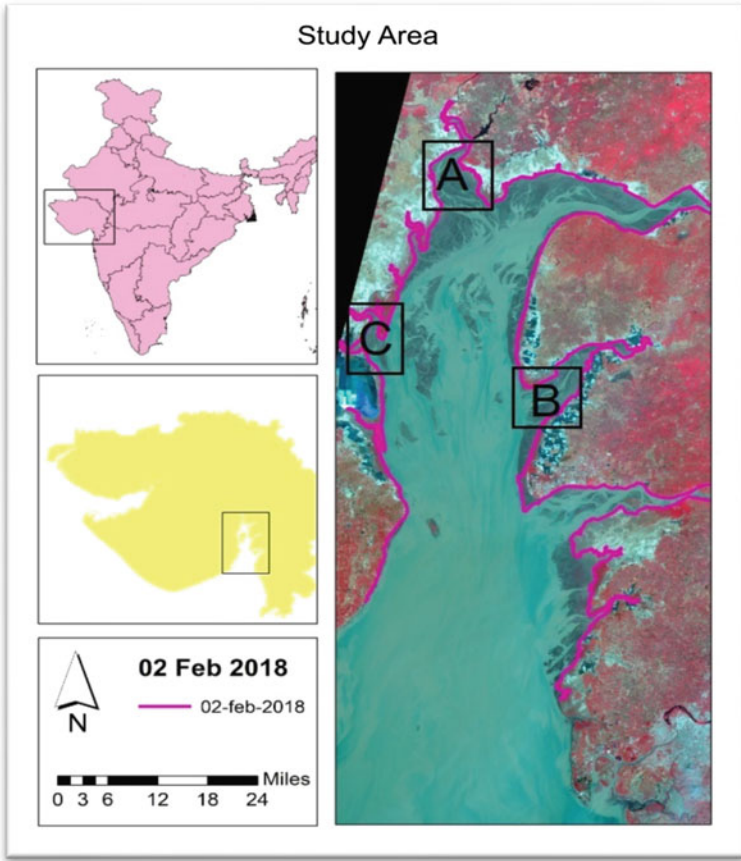
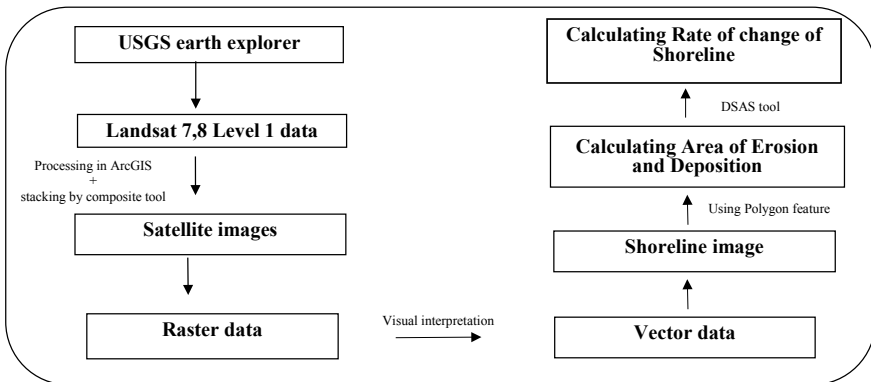


Fig. 1 Study area—Gulf of Khambhat



Flowchart 1 Methodology of work

Table 1 Datasets of the satellite images used in the research

Sr. no.	Date	Dataset	Spatial resolution
1.	February 29, 2016	Landsat 8 OLI/TIRS C1 Level 1	30
2.	October 26, 2016	Landsat 8 OLI/TIRS C1 Level 1	30
3.	February 15, 2017	Landsat 8 OLI/TIRS C1 Level 1	30
4.	October 29, 2018	Landsat 8 OLI/TIRS C1 Level 1	30
5.	February 02, 2018	Landsat 8 OLI/TIRS C1 Level 1	30

shoreline then comparing those shoreline over period of time, using polygon function and DSAS tool calculation for area of erosion and deposition and rate of change of shoreline was analyzed [4].

4 Data

The Landsat data for the various years was downloaded from the USGS Web sites [5]. After collection of the data, some basic criteria like similar tidal conditions, similar season data, uniform projection factors, etc., identify the images for further processing (Table 1) [6].

5 Results and Discussion

The three major sensitive regions Part A, B, C (refer Fig. 1 study area) are analyzed on the basis of area of erosion and deposition using polygon feature in ArcGIS. DSAS is used for calculating shoreline change envelope (SCE), net shoreline movement (NSM), end point rate (EPR), least regression rate (LRR), and least median squares (LMS).

5.1 Area Calculation

5.1.1 Part A

Figures 2, 3, 4, and 5 show the processed satellite images of sensitive Part A of Gulf of Khambhat between two consecutive time intervals and the area of erosion and deposition which is determined using polygon function with help of ArcGIS.

In Fig. 2, it was observed that erosion has taken place on the major part of western coast and deposition on eastern coast, i.e., equal to 55.79 and 8.55 km².

In Fig. 3, it was observed that erosion has taken place on the major part eastern coast and also the path of estuaries is found to be changing and total area of erosion and deposition is equal to 18.27 and 6.87 km².

In Fig. 4, it shows erosion and deposition has taken place on both eastern and western coast of GoK and that is equal to 6.9 and 7.2 km², respectively.

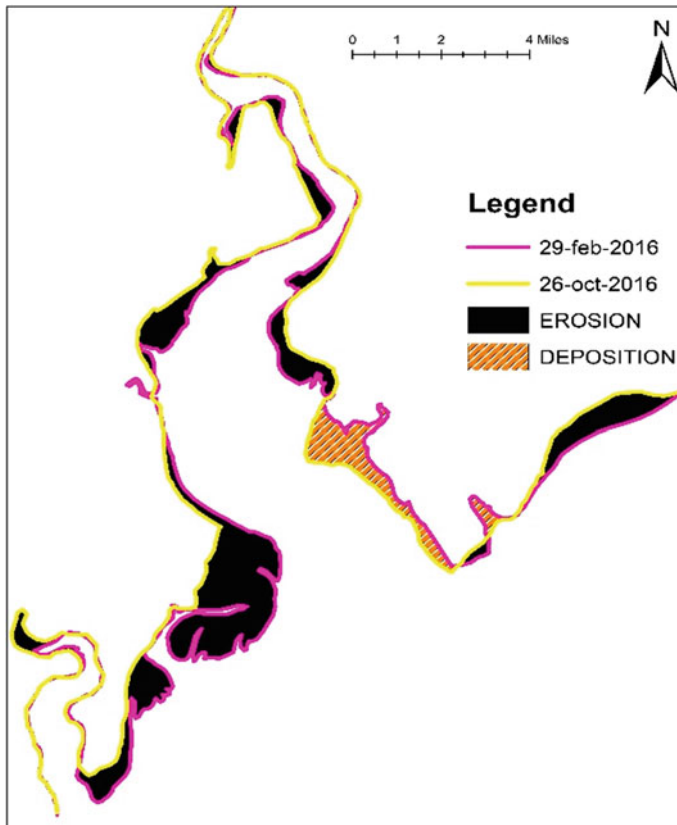


Fig. 2 Area of erosion and deposition from 29/02/2016 to 26/10/2016

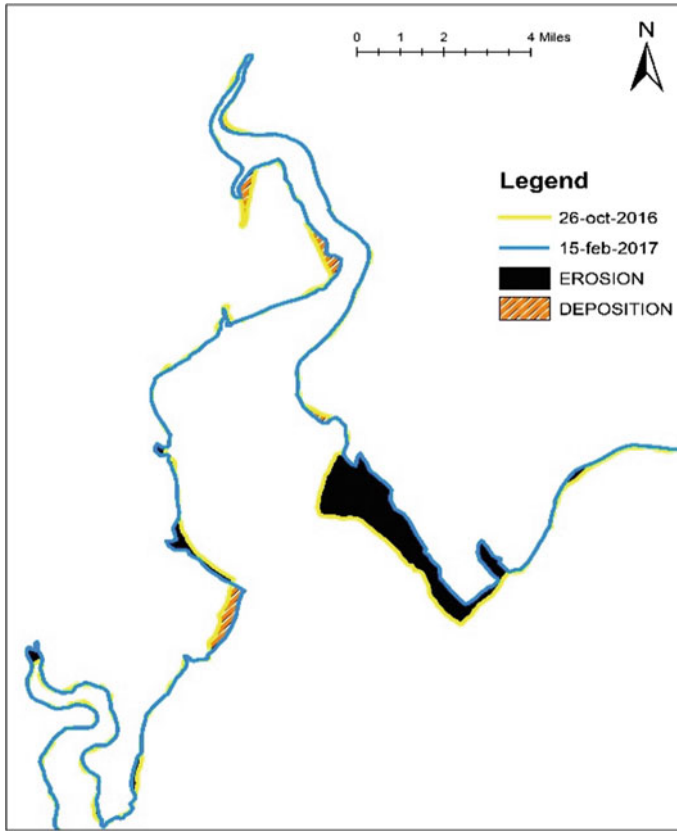


Fig. 3 Area of erosion and deposition from 26/10/2016 to 15/02/2017

In Fig. 5, it shows erosion taking place majorly on eastern coast and total area of erosion and deposition is equal to 32.96 and 8.19 km² (Table 2).

5.1.2 Part B

Figures 6, 7, 8, and 9 show the processed satellite images of sensitive Part B of Gulf of Khambhat between two consecutive time intervals and the area of erosion and deposition which is identified using polygon function with help of ArcGIS.

In Fig. 6, it was observed that erosion has taken place on the major part of eastern coast and total area of erosion and deposition is equal to 9.36 and 1.02 km².

In Fig. 7, it was observed that erosion and deposition have taken place on different part of eastern coast and total area of erosion and deposition is equal to 6.34 and 4.74 km².

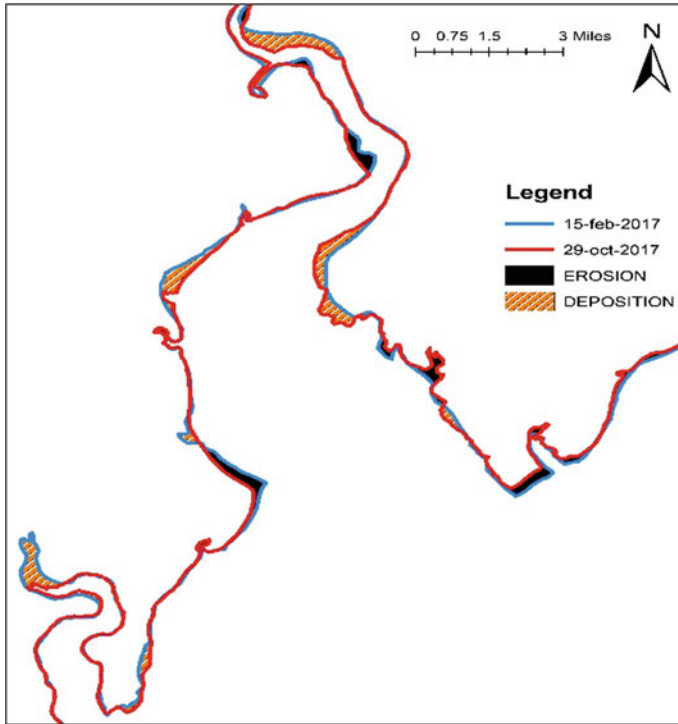


Fig. 4 Area of erosion and deposition from 15/02/2017 to 29/10/2017

In Fig. 8, it shows major deposition on eastern bank and erosion on some parts of GoK has taken place and that is equal to 11.94 and 6.49 km², respectively.

In Fig. 9, it shows erosion has taken place majorly on lower side of eastern coast and deposition on upper side of eastern coast and total area of erosion and deposition is equal to 13.46 and 13.41 km² (Table 3).

5.1.3 Part C

Figures 10, 11, 12, and 13 show the processed satellite images of sensitive Part C of Gulf of Khambhat between two consecutive time intervals and the area of erosion and deposition which is identified using polygon function with help of ArcGIS.

In Fig. 10, it was observed that erosion has taken place on the western coast and total area of erosion and deposition is equal to 2.59 and 0.59 km².

In Fig. 11, it was observed that majorly deposition has taken place on western coast and total area of erosion and deposition is equal to 4.54 and 1.93 km².

In Fig. 12, it shows major erosion on lower part and deposition on upper part of western coast of GoK has taken place and that is equal to 3.78 and 2.89 km², respectively.

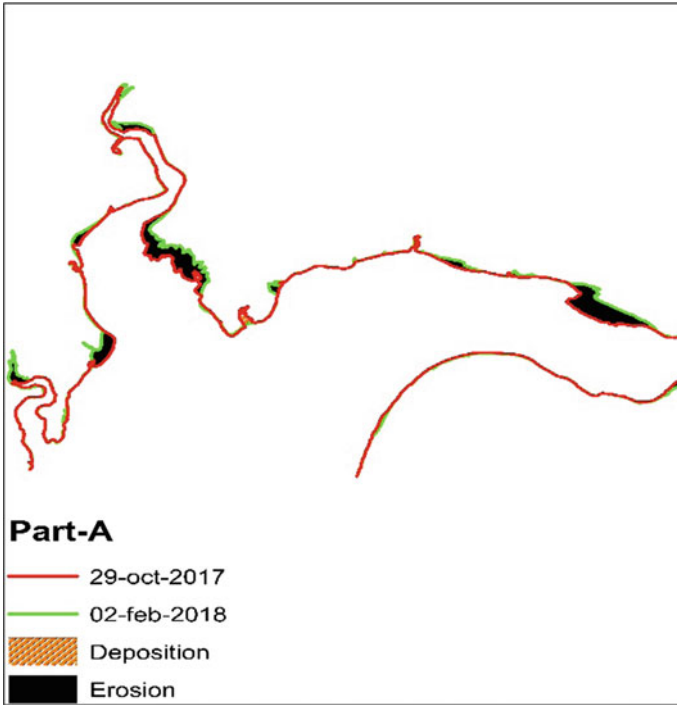


Fig. 5 Area of erosion and deposition from 29/10/2017 to 02/02/2018

Table 2 Data for area of erosion and deposition for consecutive years interval for Part A

Date	Area of erosion (km ²)	Area of deposition (km ²)
29/02/16–26/10/16	55.794	8.55
26/10/16–15/02/17	18.27	1.8711
15/02/17–29/10/17	6.9	2.1958
29/10/17–02/02/18	32.96	3.195

In Fig. 13, it shows erosion has taken place on lower part and linear deposition on upper side of western coast and total area of erosion and deposition is equal to 1.29 and 1.51 km² (Table 4).

5.2 Rate Analysis

Using DSAS transects are created to calculate statics of shoreline, such as end point rate (EPR), shoreline change envelope (SCE), net shoreline movement (NSM), and least regression rate (LRR).

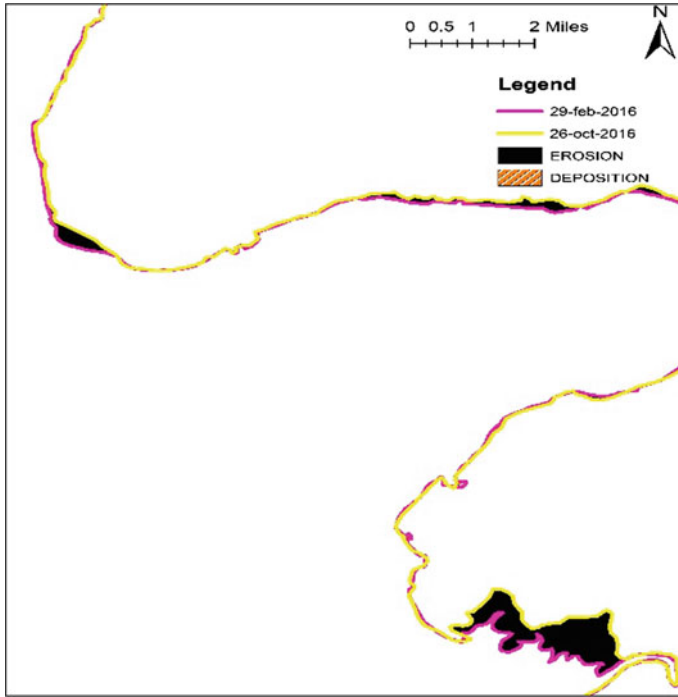


Fig. 6 Area of erosion and deposition

5.2.1 Part A

The shoreline change envelope and different rates of erosion and deposition are calculated for these parts to get the results and for further study which are given in Table 5 (Fig. 14).

5.2.2 Part B

The shoreline change envelope and different rates of erosion and deposition are calculated for these parts to get the results and for further study which are given in Table 6 (Fig. 15).

5.2.3 Part C

The shoreline change envelope and different rates of erosion and deposition are calculated for these parts to get the results and for further study which are given in Table 7 (Fig. 16).

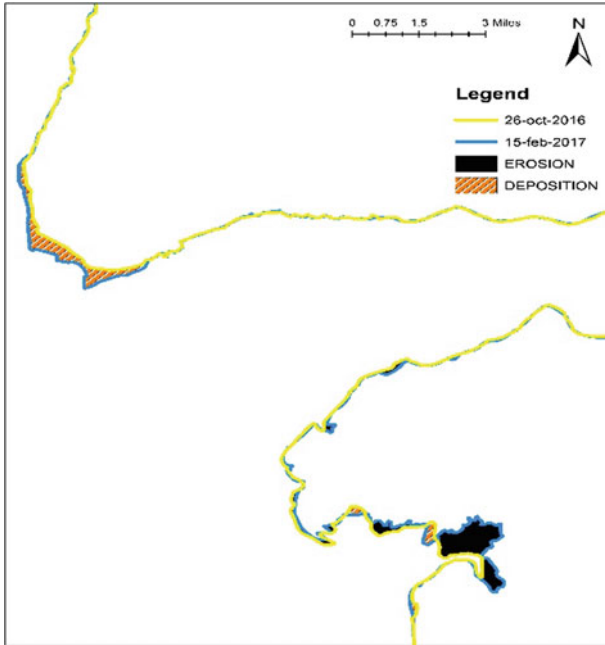


Fig. 7 Area of erosion and deposition

6 Conclusion

In GoK, the shoreline is changing very rapidly, and in this study over the period of two years major changes were observed in the sensitive regions. Visual interpretation of satellite images gives preliminary information of shoreline change which is useful to study morphology in GoK and provides the foundation for detailed study. The reason behind these regions being susceptible to these changes, more robust algorithm for geophysical parameter retrieval from satellite images will lead to proper understanding of geomorphology of the region. This study will be beneficial to researchers, government bodies, Kalpsar project, Gujarat maritime board, port authorities, various local bodies, etc., as it has identified the most sensitive region which is most vulnerable to changes.

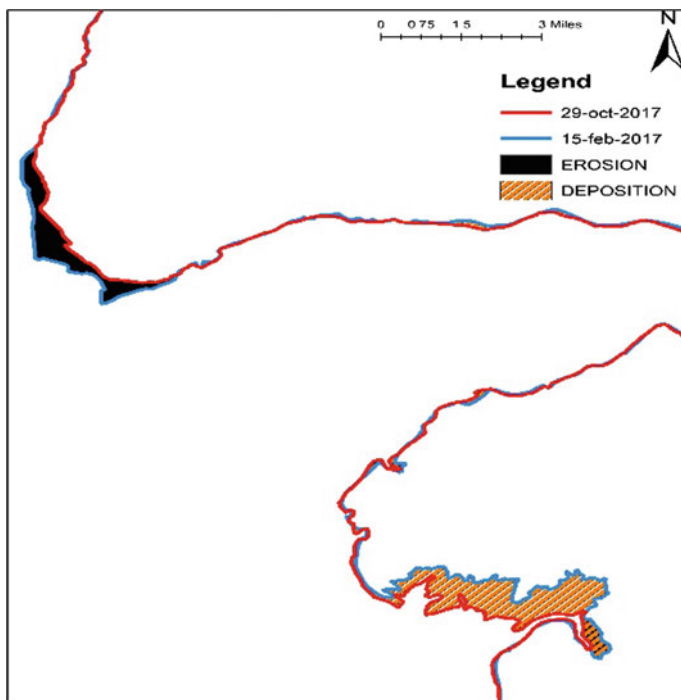


Fig. 8 Area of erosion and deposition

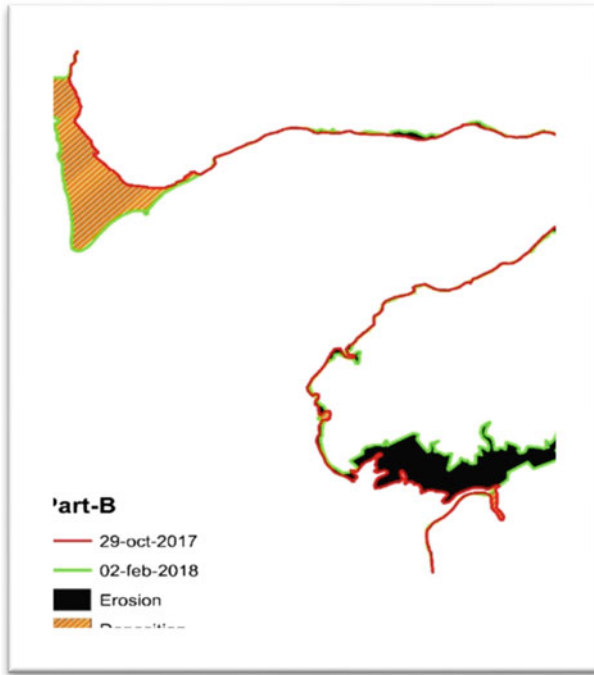


Fig. 9 Area of erosion and deposition

Table 3 Data for area of erosion and deposition for consecutive years interval for Part B

Date	Area of erosion (km ²)	Area of deposition (km ²)
29/02/16–26/10/16	9.36	1.02
6/10/16–15/02/17	6.344	4.74
15/02/17–29/10/17	6.49	11.94
29/10/17–02/02/18	13.46	13.41

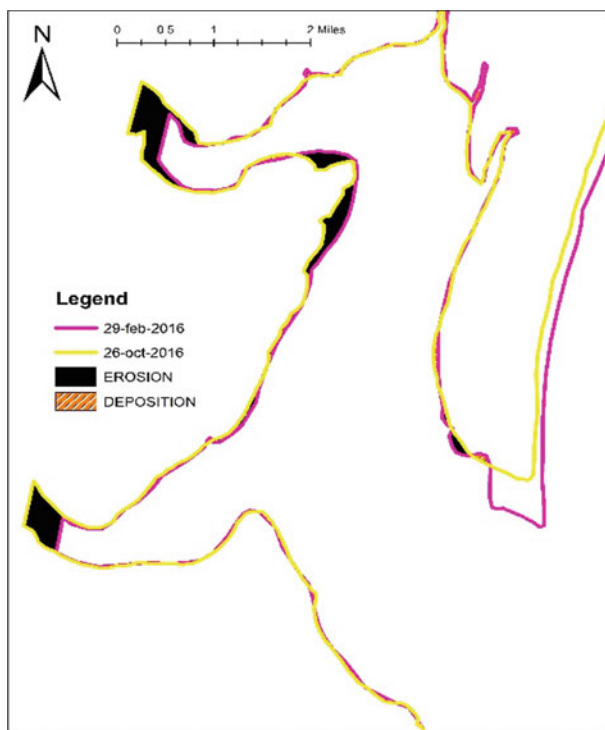


Fig. 10 Area of erosion and deposition

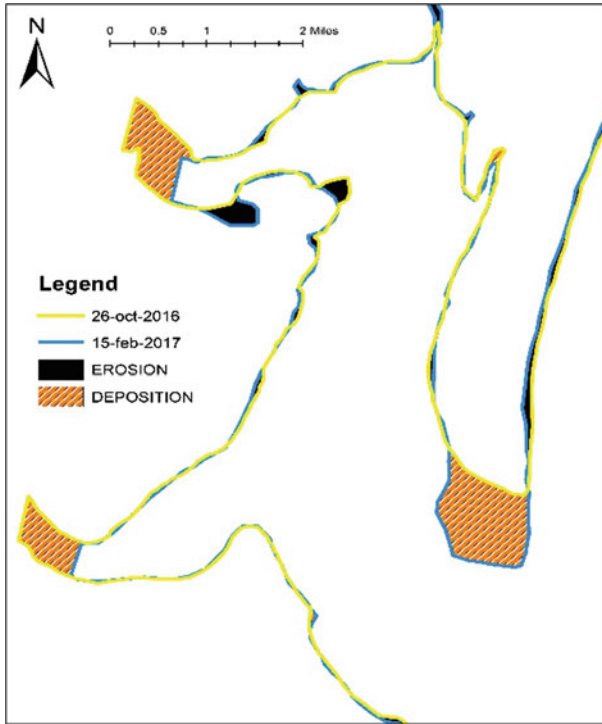


Fig. 11 Area of erosion and deposition

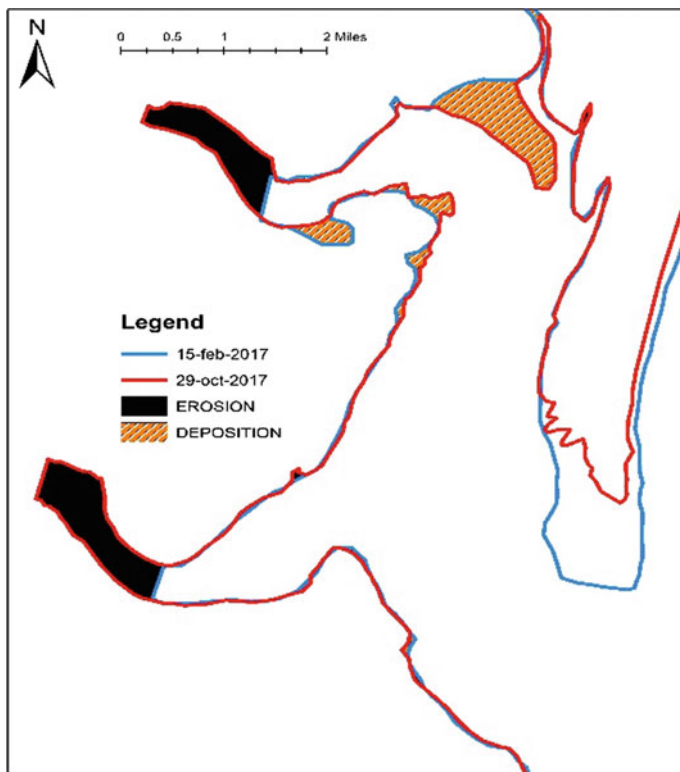


Fig. 12 Area of erosion and deposition

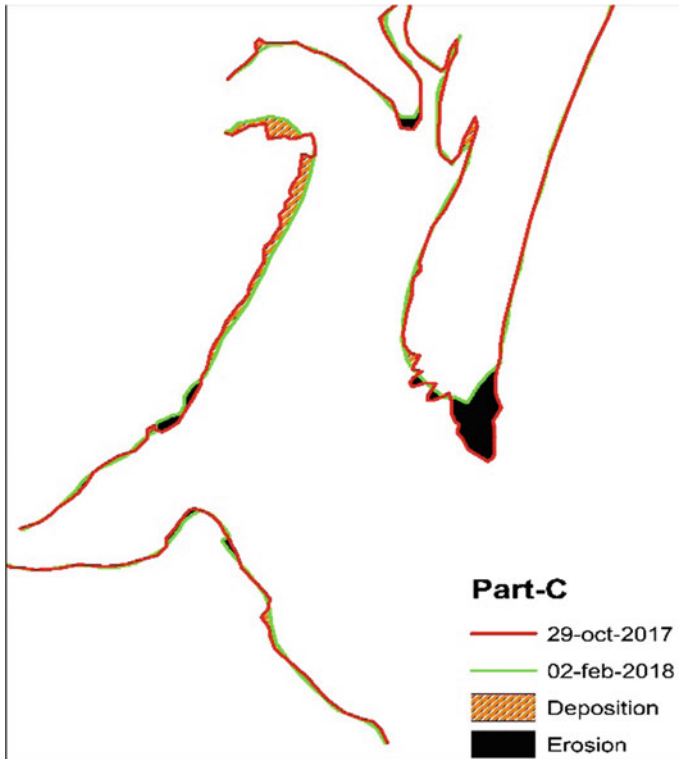


Fig. 13 Area of erosion and deposition

Table 4 Data for area of erosion and deposition for consecutive years interval for Part C

Date	Area of erosion (km ²)	Area of deposition (km ²)
29/02/16–26/10/16	2.59	0.59
26/10/16–15/02/17	4.54	1.93
15/02/17–29/10/17	3.78	2.89
29/10/17–02/02/18	1.29	1.51

Table 5 Rate of erosion and deposition and distance of shoreline movement for Part A

Date	N or P	EPR	SCE	NSM	LMS	LRR
29-02-16	N	-248.94		-452.86	-42.28	-203.48
29-02-16	P	139.41	513.02	226.34	35.29	111.90
26-10-16	N	-308.32		-470.12	-44.39	-213.16
26-10-16	P	154.94	553.28	247.62	36.04	109.17
15-02-17	N	-303.18		-470.96	-42.83	-194.91
15-02-17	P	199.52	540.25	231.95	38.60	112.24
29-10-17	N	-298.41		-473.78	-45.94	-209.56
29-10-17	P	152.52	538.02	248.12	34.87	138.55
02-02-18	N	-258.19		-431.36	-42.23	-189.36
02-02-18	P	132.94	552.31	206.55	39.74	128.93

Fig. 14 Part A transects on baseline intersecting shorelines

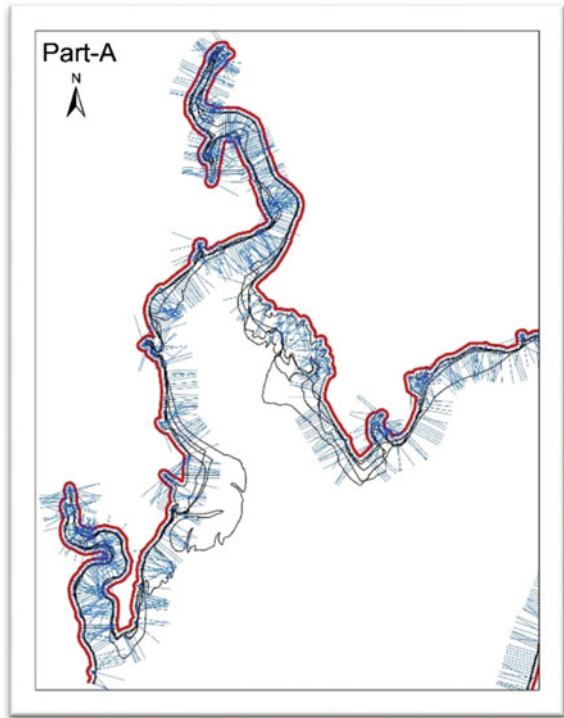


Table 6 Rate of erosion and deposition and distance of shoreline movement for Part B

Date	N or P	EPR	SCE	NSM	LMS	LRR
29-02-16	N	-201.58		-326.37	-46.92	-143.67
29-02-16	P	244.34	450.57	431.97	41.23	131.68
26-10-16	N	-183.02		-306.45	-45.15	-139.22
26-10-16	P	268.37	466.65	446.37	41.85	140.08
15-02-17	N	-192.56		-332.99	-44.30	-125.30
15-02-17	P	253.62	471.46	426.49	39.51	124.93
29-10-17	N	-199.23		-353.57	-47.58	-132.00
29-10-17	P	268.04	505.95	453.23	35.459	136.73
02-02-18	N	-235.01		-382.39	-48.66	-141.81
02-02-18	P	224.33	484.69	422.70	34.72	129.52

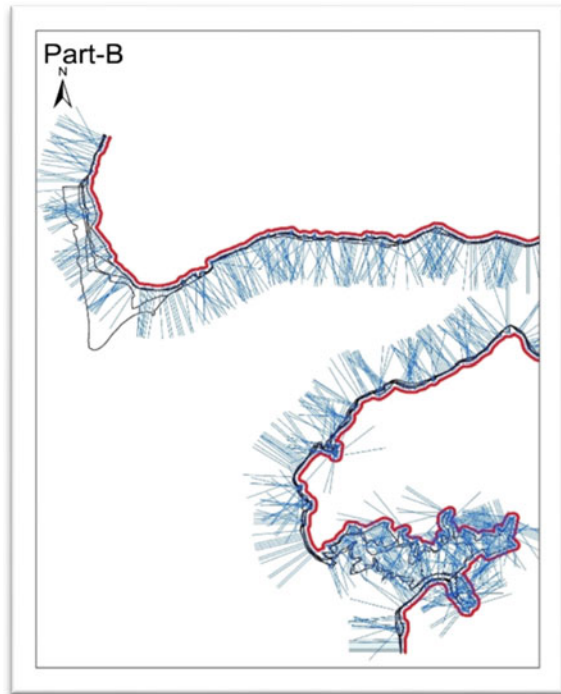
Fig. 15 Part B transects on baseline intersecting shorelines

Table 7 Rate of erosion and deposition and distance of shoreline movement for Part C

Date	N or P	EPR	SCE	NSM	LMS	LRR
29-02-16	N	-113.08		-217.55	-41.28	-120.44
29-02-16	P	132.01	364.63	253.45	28.80	189.30
26-10-16	N	-132.72		-255.63	-44.73	-136.15
26-10-16	P	159.04	434.30	306.33	29.73	206.19
15-02-17	N	-152.96		-289.96	-45.21	-152.93
15-02-17	P	186.84	461.30	359.87	29.77	214.99
29-10-17	N	-136.35		-261.08	-43.14	-142.70
29-10-17	P	193.15	432.85	372.02	33.37	240.63
02-02-18	N	-130.76		-250.82	-41.43	-130.75
02-02-18	P	178.43	462.64	343.36	31.43	246.15

Fig. 16 Part C transects on baseline intersecting shorelines

References

1. Mishra A, Balaji R (2015) A study on the shoreline changes and land use/ land cover along the South Gujarat coastline. *Procedia Eng* 116:381–389
2. Natesan U, Parthasarathy A, Vishnu Nath R, Edwin Jeba Kumar G, Ferrer VA (2015) Monitoring long-term shoreline changes along Tamil Nadu, India using geospatial techniques. *Aquat Procedia* 4:325–332

3. Bhatti H, Ramakrishnan R, Sharma AK, Rajawat AS (2018) Incessant erosion of high tidal mudflats in the northern Gulf of Khambhat. *Curr Sci* 114(12):2554–2558
4. Kankaraa RS, Chenthamil Selvana S, Markosea VJ, Rajana B, Arockiaraja S (2015) Estimation of long and short term shoreline changes along Andhra Pradesh coast using remote sensing and GIS techniques. In: ISPRS WG VIII, vol Commission VIII
5. USGS Earth Explorer
6. Bhuvan.nrsc.gov.in

Investigating Resiliency of Infrastructure Against Hurricane Events: A Review



Uriel R. D. Clark, Jeong Eun Ahn, and Sarah K. Bauer

Abstract The resilience of infrastructure, communities, and the environment in the face of hurricane events has increasingly become of public interest in the wake of recent natural disasters and environmental activism. Communities affected by natural or human-induced disasters require resources in order to recover from and withstand such disasters. Previous literature has quantified resilience for various infrastructure and disaster scenarios through the development of resilience functions and frameworks. This comprehensive review summarizes previous literature evaluating the recovery, loss, and resilience of infrastructure against hurricane events.

Keywords Infrastructure resilience · Hurricane · Loss · Recovery · Resiliency function

1 Introduction

The concept of resilience has been a popular focal point of research among the fields of engineering and urban planning for many years [1–4]. Climate change is causing more intense, destructive storms and hurricanes as recorded during the past four decades. Data collected over the last four decades show that global warming has increased the chances of storms reaching Category 3 or higher [5]. Coastal areas face the challenge of an increased potential for flooding induced by storm surges and the destruction of infrastructure. For example, Hurricane Sandy, which was the most destructive and strongest hurricane of the 2012 Atlantic hurricane season, caused \$74 billion in damage [6]. The National Oceanic and Atmospheric Administration (NOAA) estimated the economic loss based on damages to infrastructure (e.g., public infrastructure, buildings), business interruption, and offshore energy platforms [6]. When a community is impacted by a hurricane event, those affected require additional resources to survive and recover from the hazardous events. This situation not only negatively affects the surrounding community, but also creates a ripple effect

U. R. D. Clark · J. E. Ahn (✉) · S. K. Bauer

Department of Civil and Environmental Engineering, Rowan University, Glassboro, NJ, USA
e-mail: ahn@rowan.edu

© The Author(s), under exclusive license to Springer Nature Singapore Pte Ltd. 2021
Y. A. Mehta et al. (eds.), *Advances in Water Resources and Transportation Engineering*,
Lecture Notes in Civil Engineering 149,
https://doi.org/10.1007/978-981-16-1303-6_13

171

through the societal operational chains, including the disruption of transportation networks, delay of supply chains, decrease in economic activity, and decrease in productivity from the workforce [1]. Thus, it is vital to society that communities are equipped with the resources needed to quickly recover from and withstand disasters of all magnitudes. Thus, resilience functions and frameworks have been developed by researchers to follow core principles for quantifying resilience and accurately accounting for various infrastructure and disaster scenarios [2–4, 7, 8]. In order to determine the resilience of a system, loss and recovery phases must be incorporated into the resilience function. Therefore, this comprehensive review consists of previous research in recovery as well as loss and resilience. This review presents an overview of resilience functions and frameworks developed for several disaster scenarios.

2 Research in Recovery

A hazardous event is often divided into two phases: (1) the damage and loss phase and (2) the recovery phase. Simplistically, the recovery phase begins once the disaster concludes for the relative system. It is not always assumed that the system will continuously recover in the recovery phase, and periods of idle time and changes in the pace of recovery are expected. A deliberate and reliable recovery plan is necessary for any community or operation. In order to properly develop this plan, a vast array of contingencies and variables need to be accounted for and considered.

Bolin and Bolton [2] and Bolin and Stanford [3] investigated relationships between socioeconomic groups and disaster recovery. These studies considered copious amounts of data across various disasters, including: earthquakes, tornados, hurricanes, and floods, along with varying disaster victim characteristics for comparisons of recovery among different groups. Additional data categorizations were made, such as: whether the disaster occurred in an urban, suburban, small town, or rural area; and the locations of communities with respect to topographical and geographical locations, such as homes located at the mouths of canyons, near runoff channels, or closer to beachfront. While there were several correlations present throughout these studies, a main consensus is the relationship between socioeconomic status and recovery. It was shown that communities with greater socioeconomic statuses experienced expedited recoveries compared to impoverished communities, which often heavily relied upon government aid for support. Homes with faster recovery rates often had more resources to fund repairs and were able to start their own repairs without waiting for government assistance.

Gidaris et al. [4] described the versatility of the restoration model that quantifies the percentage of a structure's functionality conditional on the damage state and the time after a hazard occurs. Miles and Chang [9] presented a conceptual model of recovery that established the relationships among a community's household business, lifeline networks, and neighborhoods. Barabadi and Ayele [10] attempted to address

the complexity of restoration post-disaster. This approach is dependent on the availability, nature, and categorization of historical data. This study showed that a dataset that includes “no or missing” data will require a Bayesian approach; a heterogeneous dataset will require covariate-based models; and a homogeneous dataset will require regression models [10].

Cimellaro et al. [11] presented simplified earthquake recovery functions with a function selection process based on the response of the system and respective organizations and/or individuals that aid in the recovery and that are time-dependent. Cimellaro et al. [11] developed linear, exponential, and trigonometric recovery functions (Eqs. 1–3).

$$\text{Linear: } f_{\text{rec}}(t) = a \left(\frac{t - t_{\text{OE}}}{T_{\text{RE}}} \right) + b \tag{1}$$

$$\text{Exponential: } f_{\text{rec}}(t) = a e^{\left[-b \left(\frac{t - t_{\text{OE}}}{T_{\text{RE}}} \right) \right]} \tag{2}$$

$$\text{Trigonometric: } f_{\text{rec}}(t) = \frac{a}{2} \left[1 + \cos \left\{ \frac{\pi b (t - t_{\text{OE}})}{T_{\text{RE}}} \right\} \right] \tag{3}$$

where a and b are constant values that are calculated using curve fitting to available data sources, while t_{OE} is the instant of time when the extreme event strikes, and T_{RE} is the recovery time necessary to go back to pre-disaster condition evaluated starting from t_{OE} .

The function can be selected based on the available information and the level of preparedness and response. This selection process accounts for the shape and slope of the functionality curve throughout the recovery process, but does not account for variables that may alter the overall recovery time necessary to achieve full recovery [11].

Even though earthquakes and hurricanes have different definable strength levels that cause different measurable levels of loss and damage, the recovery function developed for earthquakes can be adapted for hurricanes since recovery from both events depends on similar parameters (e.g., preparedness, mitigation, response, recovery efforts). Tokgoz and Gheorghe [8] adapted the approach by Cimellaro et al. [11] for residential hurricane recovery and presented linear, exponential, normal, and sinusoidal recovery functions for residential homes (Eqs. 4–7).

$$\text{Linear: } f_{\text{rec}}[t, T_a(w)] = 1 - \frac{\lambda t}{100 T_a(w)} \tag{4}$$

$$\text{Exponential: } f_{\text{rec}}[t, T_a(w)] = \exp \left[\log \left(1 - \frac{\lambda}{100} \right) \frac{t}{T_a(w)} \right] \tag{5}$$

$$\text{Normal: } f_{\text{rec}}[t, T_a(w)] = \exp \left[\log \left(1 - \frac{\lambda}{100} \right) \frac{t^2}{T_a^2(w)} \right] \tag{6}$$

$$\text{Sinusoidal: } f_{\text{rec}}[t, T_a(w)] = \cos \left[a \cos \left(1 - \frac{\lambda}{100} \right) \frac{t}{T_a(w)} \right] \quad (7)$$

where $T_a(w)$ is actual recovery time with respect to the probability to be in damage state, t is time (days), and λ is denoted percent of the initial loss that is recovered at time, $T_a(w)$, where recovery is assumed to be complete (%) at a given wind speed, w .

Modeling the recovery of infrastructure following a hazardous event is imperative to the sustainability of the affected community; however, in order to fully account for infrastructure resiliency, one must also quantify damage and loss due to a hazardous event.

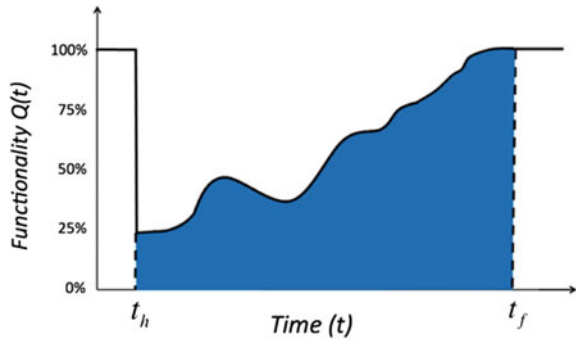
3 Research in Loss and Resilience

The damage and loss phase is more well-known compared to the recovery phase of a hazardous event. Research initiatives into determining and reducing the probability of future damages following a hazardous event are often implemented by public and private entities. This is due to the fact that damages caused by a disaster are often sudden, which lead to a lasting effect on the minds of the individuals affected, even among those that experience relatively minor damage [12]. However, the calculation of future losses and damages, along with the complexities involved, is an accomplishable task to complete. Research has often shown that the strengthening of systems is more economic than the damage repairs and recovery after a hazardous event.

Cimellaro et al. [13] defined four properties of resilience, which consists of the following: rapidity, robustness, redundancy, and resourcefulness. Mathematically, rapidity represents the slope of the functionality curve during recovery, whereas robustness is the residual functionality immediately following the hazardous event. Redundancy is the extent of which alternative elements or systems exist that are capable of satisfying operational requirements in the event of a disruption or loss of functionality. Resourcefulness is the capacity to identify problems, establish priorities, and mobilize alternative external resources when necessary. For the purposes of quantification, redundancy, and resourcefulness can be mathematically expressed as parameters that influence the rapidity and robustness of a system [13]. For example, redundancy designed into a structure may increase its robustness as additional measures are in place to maintain its stability in the event that other elements fail. The resourcefulness of a community may increase the rapidity, and therefore, shorten the time necessary for the recovery of a system following a hazardous event.

Bruneau et al. [14] introduced the concept of the functionality curve, which is necessary to quantify the loss of resilience, R , with respect to the specific earthquake (Eq. 8).

Fig. 1 Graphical expression of the functionality curve following a hazardous event [15]



$$R = \int_{t_h}^{t_f} [100 - Q(t)] dt \tag{8}$$

where functionality, $Q(t)$, is expressed as a percentage ranging from 0 to 100%, where 100% represents no degradation in the service of a system, and 0% represents no service being available, and t_h is time when hazard occurs and t_f is when it is completely repaired (i.e., functionality is 100%) [14]. Figure 1 presents that the functionality may be reduced from 100 to 25% when a hazardous event occurs [15]. Recovery, or restoration, of the system occurs after the hazardous event, where it is expected that functionality will rise over time to return to 100%. Ideally, the recovery process would be a steady increase, but as is the nature of construction, especially in times of uncertainty and crisis, the process may experience several delays and setbacks.

Xian and Jeong [16] developed a framework to model the damage and recovery of interdependent critical infrastructure when the natural disasters, such as hurricanes and earthquakes, affect communities. That is, for example, the resilience of an electrical system affects the resilience of telecommunications and water supply systems. It may be necessary to connect the influences and interactions of these systems in a comprehensive community resilience analysis.

The earthquake formulations from Cimellaro et al. [13] were modified for hurricane scenarios; however, these scenarios only accounted for wind scenarios and used simplified recovery functions (Eqs. 1–7). Tokgoz and Gheorghe [8] proposed a method for quantifying the resilience of single-family dwellings regarding a hurricane wind scenario. Dong and Li [17] adopted this framework in an attempt to disaggregate community resilience to the individual level. Ataei and Padgett [18] presented a computational methodology to assess the fragility or failure probability of bridges in a hurricane scenario. Tokgoz and Gheorghe [8] determined fragility with the failure mode being roof failure due to wind.

Analyzing the resiliency of infrastructure following a hazardous event is imperative to the sustainability of the affected community. Though the literature includes many research studies that have worked to develop such models, there are more variables to incorporate to better evaluate the resilience for varying types of hazardous

events and infrastructure. For example, when researching the resilience and loss function for a hurricane hazard, incorporating flood parameters (e.g., storm surge, surge probability) to modified residential loss and resilience functions could allow for a better understanding and evaluation of the resilience of the study area.

4 Conclusion

This review summarizes that recovery and resilience functions that have been developed from previous studies. Resilience and recovery functions for critical infrastructure were first developed for earthquake hazards and were adapted for hurricane hazards. Based on previous literature, different functions need to be selected for the scenario depending on different characteristics (i.e., types of infrastructure, communities, system, society preparedness response, and hazards).

Based on the comprehensive literature review, future studies are required to better prepare communities and systems for the effects of a hurricane event.

1. The resilience functions that need to be developed by incorporating additional variables, such as storm surge and surge probability, could increase the applicability and effectiveness of the evaluations of resilience in different hazardous events.
2. The resilience of residential housing should be studied, and the direct impact and well-being of the residents of a community should be a priority. Future studies are required for the resilience of individual residential homes in a hurricane disaster scenario.

References

1. De Mel S, McKenzie D, Woodruff C (2011) Enterprise recovery following natural disasters. *Econ J* 122:64–91. <https://doi.org/10.1111/j.1468-0297.2011.02475.x>
2. Bolin RC, Bolton PA (1986) Race, religion, and ethnicity in disaster recovery. FMHI Publications, p 88
3. Bolin RC, Stanford L (1991) Shelter, housing and recovery: a comparison of U.S. disasters. *Disasters* 15:24–34. <https://doi.org/10.1111/j.1467-7717.1991.tb00424.x>
4. Gidaris I, Padgett JE, Barbosa AR, Chen S, Cox D, Webb B, Cerato A (2016) Multiple-hazard fragility and restoration models of highway bridges for regional risk and resilience assessment in the United States: state-of-the-art review. *J Struct Eng* 143(3). [https://doi.org/10.1061/\(ASCE\)ST.1943-541X.0001672](https://doi.org/10.1061/(ASCE)ST.1943-541X.0001672)
5. Kossin JP, Knapp KR, Olander TL, Velden CS (2020) Global increase in major tropical cyclone exceedance probability over the past four decades. *Proc Natl Acad Sci* 117(22):11975–11980. <https://doi.org/10.1073/pnas.1920849117>
6. NOAA (2020) National Centers for Environmental Information (NCEI) U.S. Billion-Dollar Weather and Climate Disasters. www.ncdc.noaa.gov/billions/. <https://doi.org/10.25921/stkw-7w73>

7. Bocchini P, Frangopol DM (2012) Restoration of bridge networks after an earthquake: multi-criteria intervention optimization. *Earthq Spectra* 28:427–455. <https://doi.org/10.1193/1.4000019>
8. Tokgoz BE, Gheorghe AV (2013) Resilience quantification and its application to a residential building subject to hurricane winds. *Int J Disaster Risk Sci* 4(3):105–114. <https://doi.org/10.1007/s13753-013-0012-z>
9. Miles SB, Chang SE (2006) Modeling community recovery from earthquakes. *Earthq Spectra* 22(2):439–458. <https://doi.org/10.1193/1.2192847>
10. Barabadi A, Ayele YZ (2017) Post-disaster infrastructure recovery: prediction of recovery rate using historical data. *Reliab Eng Syst Saf* 169:209–223. <https://doi.org/10.1016/j.res.2017.08.018>
11. Cimellaro GP, Reinhorn AM, Bruneau M (2010) Framework for analytical quantification of disaster resilience. *Eng Struct* 32:3639–3649. <https://doi.org/10.1016/j.engstruct.2010.08.008>
12. Graham H, White P, Cotton J, McManus S (2019) Flood- and weather-damaged homes and mental health: an analysis using England's Mental Health Survey. *Int J Environ Res Public Health* 16. <https://doi.org/10.3390/ijerph16183256>
13. Cimellaro GP, Reinhorn AM, Bruneau M (2008) Seismic resilience of a hospital system. *Struct Infrastruct Eng* 6(1–2):127–144. <https://doi.org/10.1080/15732470802663847>
14. Bruneau M, Chang SE, Eguchi RT, Lee GC, O'Rourke TD, Reinhorn AM, Shinozuka M, Tierney K, Wallace WA, von Winterfeldt D (2003) A framework to quantitatively assess and enhance the seismic resilience of communities. *Earthq Spectra* 19(4):733–752. <https://doi.org/10.1193/1.1623497>
15. Clark U (2020) Development of a hurricane recovery function and resilience model for single-family residential homes. Master's thesis, Rowan University, New Jersey
16. Xian H, Jeong CE (2018) Modeling the damage and recovery of interdependent critical infrastructure systems from natural hazards. *Reliab Eng Syst Saf* 177:162–175. <https://doi.org/10.1016/j.res.2018.04.029>
17. Dong Y, Li Y (2017) Risk assessment in quantification of hurricane resilience of residential communities. *J Risk Uncertain Eng Syst A Civ Eng* 3(4). <https://doi.org/10.1061/AJRU6.0000932>
18. Ataei N, Padgett JE (2013) Probabilistic modeling of bridge deck unseating during hurricane events. *J Bridge Eng* 18(4):275–286. [https://doi.org/10.1061/\(ASCE\)BE.1943-5592.0000371](https://doi.org/10.1061/(ASCE)BE.1943-5592.0000371)

Extraction of Surface Imperviousness from Land Use Land Cover Analysis for Part of Hyderabad City



Vinay Ashok Rangari , N. V. Umamahesh, and Ajey Kumar Patel

Abstract Surface imperviousness is vital basin parameter and plays a major role in watershed hydrology especially in an urban environment. Estimation of surface imperviousness is crucial but tedious task in urban watershed modelling as urban land use changes very frequently. The challenge encountered in calculating surface imperviousness is the need for a simple and effective approach to the characterize impervious surfaces in the watershed without much error. Detailed land use land cover maps form a great source of information for hydrologic analysis. Recent advancements in technology have brought us the benefits of aerial photography and access to high-resolution satellite imagery. The present study highlights a methodology to extract surface imperviousness of an area by processing high-resolution satellite imagery and developing land use land cover map. Densely urbanized of part of Hyderabad city (Zone-XIII) being one of the critical flood-prone zone is picked in this study to extract surface roughness from land use land cover map. LISS-III and ETM+ satellite imagery is used to develop land use land cover maps of study. The result shows the rise in overall surface imperviousness of Zone-XIII by 20% from the period of 2001 to 2016.

Keywords Watershed · Urbanization · Impervious surface · Satellite imagery

1 Introduction

The surface imperviousness is often expressed as a percentage of the total impervious land surface of the watershed. Increased urbanization exerts a lot of pressure on land use which is responsible for the rise in total impervious surface areas [4, 9].

V. A. Rangari (✉)

Civil Engineering Department, Sree Vidyanikethan Engineering College, Tirupati 517102, India
e-mail: vinayrangari@gmail.com

N. V. Umamahesh · A. K. Patel

Water and Environment Division, National Institute of Technology Warangal, Warangal 506004, India

e-mail: mahesh@nitw.ac.in

Soil compaction for urban development, manmade structures such as roofs, roads, pavements, driveways, parking lots, industrial areas, airports, logistics, etc., are the examples of impervious surfaces. The surface imperviousness varies from (2–10)% in rural areas to (70–90)% in densely populated urban areas [16]. The rise in surface imperviousness of a watershed initiates a chain of events affecting urban water and air resources, and thus, it is a prime concern to hydrologist and environmental engineers. The direct effects of a rise in impermeability of watershed are foreseen on local streams, rivers and downstream water receiving ponds, and tanks are affected indirectly [1, 3]. Impervious surface restricts the entry of rainfall water into natural soil thereby increasing the runoff volumes. The runoff volume of fully developed urban watershed may rise up to six times and runoff peaks up to 1.8–8 times leading to flooding situations [11].

Surface imperviousness of watershed is a vital parameter in performing all hydrologic simulations, and it works like a needle to track environmental and physical changes on urban watersheds [6]. Several research studies in past show the consequence of increased surface impermeability on various resources in urban watersheds [12, 15, 17]. The importance of satellite data in estimating surface imperviousness and the need for acquiring the recent spatial information in performing analysis is explained by [10, 19, 20]. However, getting precise information regarding land cover and surface imperviousness is very difficult and remains a challenge for urban planners and modellers [5, 8]. Such studies are a common task to the hydrologists in developed countries, while only a few studies are reported on an estimation of surface imperviousness of watershed in developing countries due to lack of basic data, procedure manuals and guidelines.

Developing detailed land use land cover maps forms a great source of information for hydrologic analysis, but such studies are a lot expensive to carry out and quickly become outdated due to continuous developments in urban areas [17]. Recent advancements in technology have brought us the benefits of aerial photography and access to high-resolution satellite imagery [21]. Thus, a potential is built-up to develop land use and land cover for different periods and with more accuracy in outputs. However, the process is time consuming, and it requires proficient knowledge [13]. Here, a methodology is presented to extract surface imperviousness of an urban watershed by processing high-resolution satellite imagery and developing land use land cover map. Zone-XIII of Hyderabad is one of the critical flood-prone zone and is picked in this study to extract percentage permeability from land use land cover map.

2 Study Area and Data Collection

Hyderabad is known as one of the vivacious metro city in India and is a capital of Telangana state. But in the past few years, the city addressing the challenge of frequent urban floods. The Greater Hyderabad Municipal Corporation (GHMC) has recognized the boundary of Hyderabad Urban in reliance on sixteen storm-water



Fig. 1 Location map of the study area (Zone-XIII, Hyderabad)

zones (Zone-I to Zone-XIV). The focus of the present study is on Zone-XIII which is the low lying area and most recurrent flood affected area in the city with areal coverage of 47.08 km². Figure 1 shows the location map of the study area.

The catchment details of Zone-XIII, Hyderabad are collected from GHMC. Spatial data for the study area is obtained by processing high-resolution 10 m Cartosat digital elevation model (DEM) obtained from National Remote Sensing Centre, Hyderabad (NRSC). The Landsat TM+ and LISS-III satellite images of the study area for the year 2001 and 2016 are downloaded from USGS earth explorer to develop land use land cover maps. The Google-Earth imagery with greater accuracy for a period of 2001–2016 is used as base maps to define training classes for land use classification.

3 Materials and Method

Figure 2 shows the flow chart explaining the methodology to compute surface imperviousness of a watershed. The surface imperviousness of watershed is determined by estimating the pervious and impervious parts of the watershed surface. Manmade buildings, pavements, roads and parking lots form impervious surfaces, while pervious surfaces include vegetation, bare soil and water bodies. Thus, it is necessary to identify the different land use classes to compute the surface roughness. The technological advancement allows us to acquire high-resolution spatial data at free of cost with online open data portals. Here, we used LISS-III (23 m) and Landsat TM+ (30 m) resolution satellite images to develop LULC for Zone-XIII of Hyderabad. High-resolution LISS-III (June 2016) and Landsat TM+ (January 2001) are downloaded from USGS earth explorer. The images dataset is pre-processed in ArcGIS 10.3 for geometric corrections and extracted to study area boundary. Further, both the satellite datasets are resampled using the nearest neighbourhood data resampling algorithm to remove the discrepancy in spatial resolution. The band combination of images is adjusted to distinguish the feature classes clearly, and

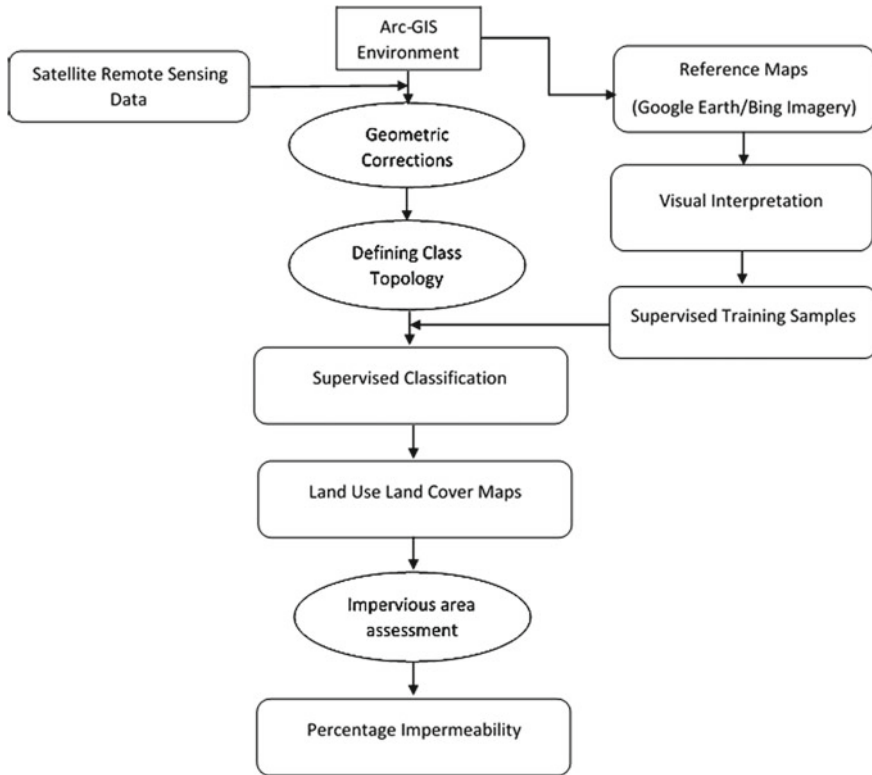


Fig. 2 Flow chart of the methodology

Google-Earth imagery is used as a reference to perform the land use classification. The maximum likelihood supervised classification method is used to prepare land use land cover maps. The maximum likelihood method of supervised classification uses user-defined training samples signifying the pixels of identical spectral characteristics to the same land use type. The maximum likelihood supervised clustering method is adopted to achieve the accuracy in classification based on knowledge of training sites. Furthermore, supervised classification is a more useful and quick method for small catchment areas [7]. Here, four training classes of land use (built-up area, barren land, water bodies and shrubs) are defined to develop land use and land cover of the study area. Google-Earth images with greater accuracy for the year 2001 and 2016 available with historical data archive are used as a background reference maps to cross-check and justify the accuracy of the land use classification. Figure 3a, b shows the Landsat (2001) and LISS-III (2016) satellite imagery for Zone-XIII, Hyderabad, respectively, and Fig. 3c, d represents the Google-Earth imagery for the corresponding period that used as reference maps to help in attaining the LULC classification accuracy.

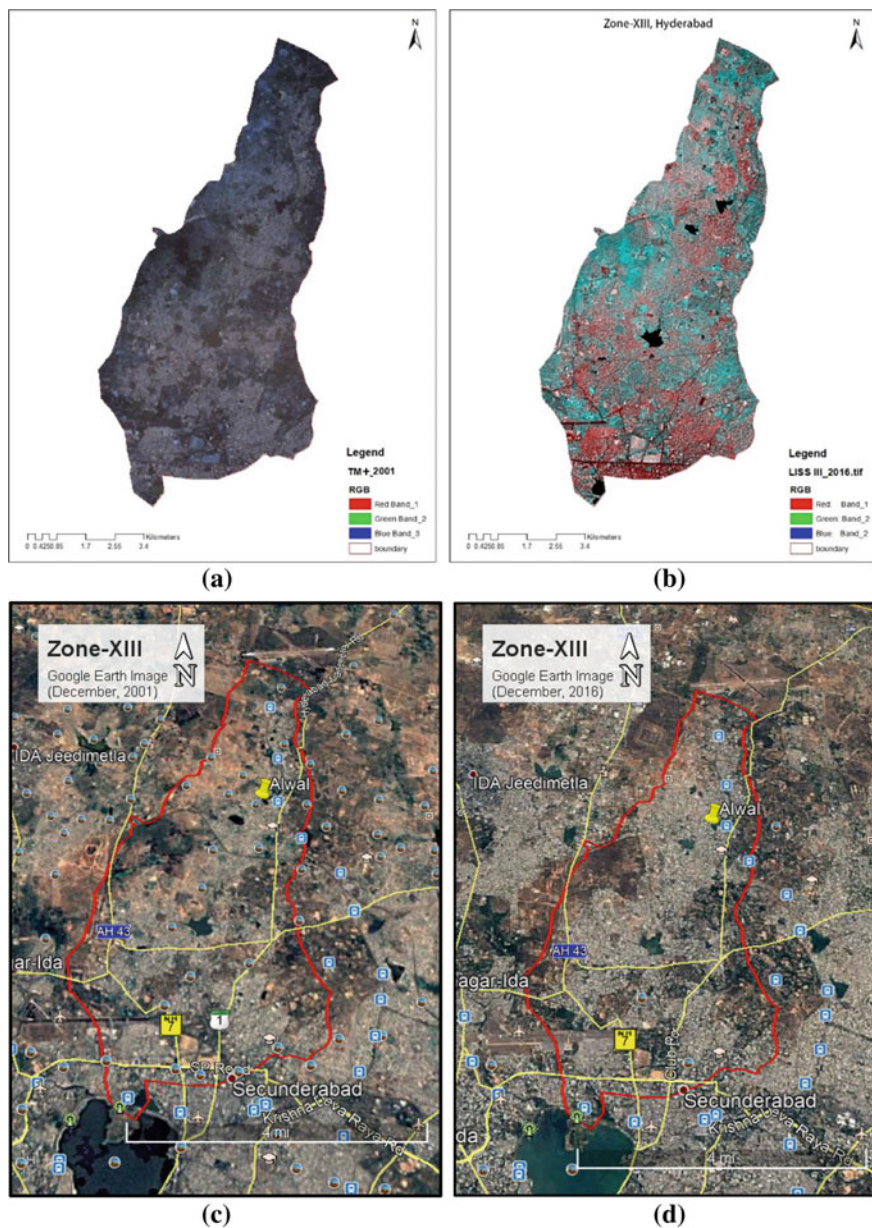


Fig. 3 a Landsat satellite image (2001). b Landsat satellite image LISS-III (2016). c Google-Earth image (2001). d Google-Earth image (2016)

4 Results and Discussion

4.1 Land Use Land Cover Analysis

Figure 4a, b shows the land use land cover maps of the study area for 2001 and 2016, respectively. Four classes of land use (built-up area, barren land, water bodies and

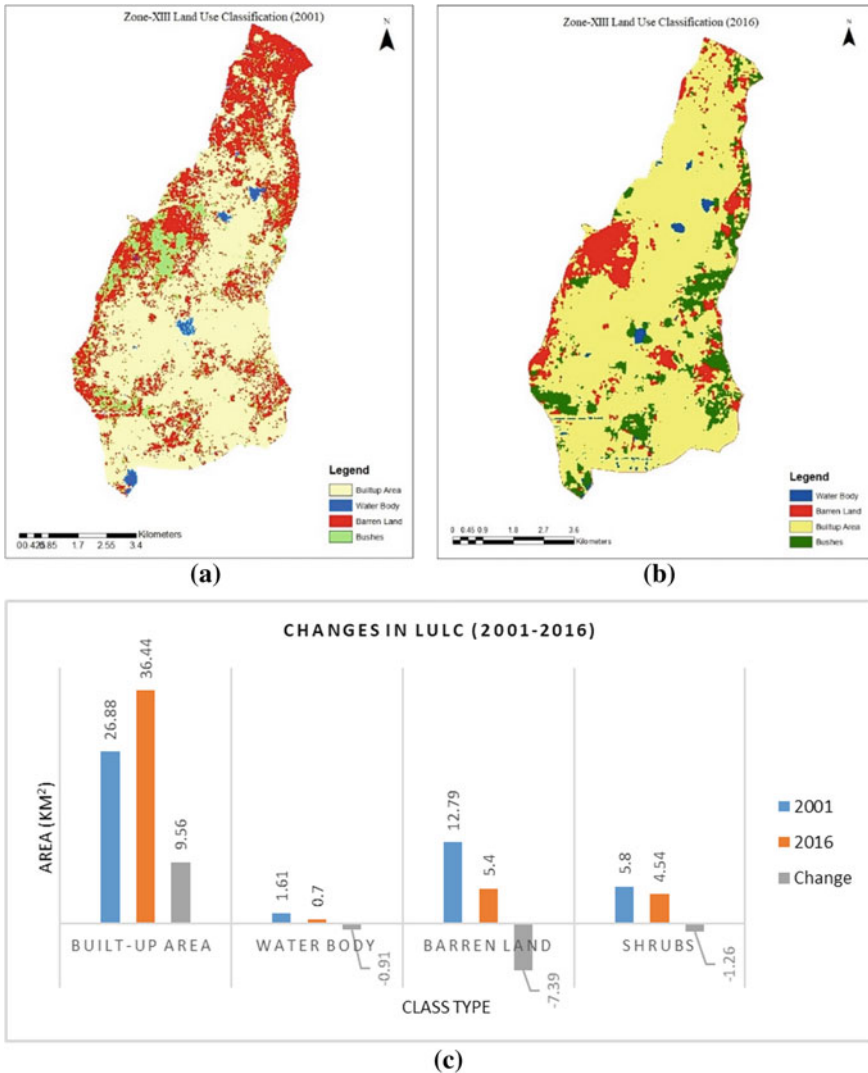


Fig. 4 a Zone-XIII LULC for 2001. b Zone-XIII LULC for 2016. c LULC changes for Zone-XIII, Hyderabad (2001–2016)

Table 1 Area falling under each class type for Zone-XIII, Hyderabad

Land use	Area in 2001 (km ²)	
	2001	2016
Built-up area	26.88	36.44
Barren land	12.79	5.40
Water body	1.61	0.70
Shrubs	5.8	4.54
Total area	47.08	47.08

shrubs) are defined to develop the land use land cover maps of the study area. The pixels belonging to each class type are calculated, and area falling under each class type is estimated. Figure 4c presents the changes in LULC over the period (2001–2016) for Zone-XIII, Hyderabad. The land use is further classified into pervious and impervious areas. The land use class type built-up area imparts the imperviousness to the land surface, whereas barren (open) land, water bodies and shrubs are the pervious areas. Thus, the total built-up area is calculated and matched with the total watershed area to compute the overall surface imperviousness of Zone-XIII, Hyderabad. Table 1 presents the land use class type and area falling under each class type for the year 2001 and 2016 for Zone-XIII, Hyderabad. The land use land cover maps are further processed and clipped to each sub-watershed, and area falling under each class of land use is computed for each sub-watershed. The built-up area of sub-watershed is matched with the total area of respective sub-watershed to compute surface roughness of that sub-watershed. Table 2 shows the surface roughness of sub-watershed for the year 2001 and 2016. The results of land use classifications show an increase in the impervious surface in all sub-watersheds of Zone-XIII which is responsible for the rise in overall surface imperviousness from 46.73% in the year 2001 to 66.81% in the year 2016 (i.e., 20.08% rise in last 16 years).

Table 2 Surface imperviousness sub-watershed of Zone-XIII, Hyderabad

Zone-XIII Sub-watershed	% Imperviousness	
	2001	2016
1	37.51	75.81
2	23.30	30.13
3	11.56	17.77
4	6.08	11.04
5	29.15	36.58
6	22.53	25.23
7	34.23	42.21
8	16.06	19.69
9	19.94	20.87
10	49.73	51.92
11	22.63	27.65

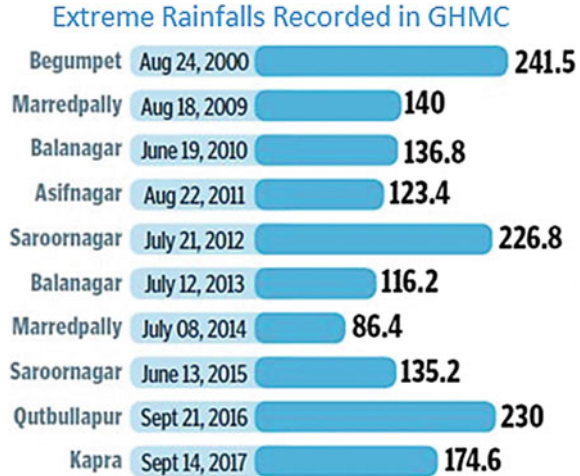
4.2 Discussion

Urbanization is an unenviable change that bound to happen with raised lifestyle and increase in population in the cities. The population of Hyderabad city is increased by 3,303,000 from 2001–2016 with an average growth rate of 3.46 [18]. This massive population growth in recent years has put forth huge stress over the land use and land cover as unbound settlements and is clearly seen through LULC analysis. The land use changes for Zone-XIII of Hyderabad city are analysed by processing remotely sensed high-resolution satellite images alongside Google-Earth images. The result analysis shows that Zone-XIII urbanization has significantly altered the natural landscape as dried waterbodies, missing drainage paths, fertile and open land have taken up by city migrations as only space available to settle. Hyderabad is once known for its lakes, connected by cascade system of a prominent natural stream network that ensured mitigate of floodwater from one lake to another. A research conducted by the [14] reported overall 404 water bodies in Hyderabad city between 1982–2012. The LULC analysis points out the substantial encroachment within the dried lake beds and its adjoining areas that are clearly visible on the Google-Earth imagery. The many lakes visible on Dec 2001 image (Fig. 3c) show no presence on Dec 2016 image (Fig. 3d). Further, the natural streams are covered with concrete roads leaving no space for water to flow. The result analysis of LULC changes for Zone-XIII, Hyderabad (Fig. 4c) shows a reduction in the water body by 2%, vegetation by 2.6%, and open land by 15.7% (20.30% in total) which is transformed to a built-up area by 2016. As a result, the percentage of imperviousness is increased by 20% in the last 16 years, and this change is having a direct impact on watershed hydrology of urban Hyderabad. The developed urban catchment reduces the flow time with an increase in peak flows (1.8–8 times) and flood volumes (6 times) [11]. Further, speedy uncontrolled urban growth is accountable for a greater risk of intensive climate change unless planned for proper adaptive measures. The effect of intense urbanization is not only limited to local weather pattern, but also heat island effect, rainfall intensity and runoff generation [2], and the impacts have started showing up ground with recurrent Hyderabad flooding's (Fig. 5).

5 Summary and Conclusions

Surface imperviousness is vital basin parameter and plays a major role in watershed hydrology especially in an urban environment. Estimation of surface imperviousness is a crucial but tedious task in urban watershed modelling as urban land use changes very frequently due to an increase in urbanisation and developments. Thus, surface imperviousness values needed to be updated on regular basis hydrological studies. Another challenge encountered in calculating surface imperviousness is the need for a simple and effective approach to the characterize impervious surfaces in the watershed without much error. A simple approach in investigating the surface

Fig. 5 Extreme rainfalls recorded in GHMC (2000–2016). *Source* IMD, GHMC



imperviousness of an urban area by using satellite imagery is presented. The method can be applied to most of the urban watersheds, and satellite imagery can effectively be used to develop land use type and thus impervious surfaces in the present time. The surface imperviousness values for Zone-XIII of Hyderabad city are calculated for years 2001 and 2016, respectively. The result shows due to unplanned urban development; the overall surface imperviousness of Zone-XIII has been increased by 20% from 2001 to 2016 with a 2.67% growth rate in impervious cover over the past 16 years. If this growth rate continues, no space will be available to water and vegetation in the city at the end of 2030, and people have to suffer water scarcity and intense hot weather throughout the year. The urbanization is bound to happen and cannot be checked. However, we can reduce sealing by adopting suitable measures such providing disconnected impervious surfaces and draining roof water to proper pervious areas, use of pervious pavement materials at feasible locations, implementing green roofs on large connected buildings and reducing driveways dimensions, parking lots and other pavements. It is our moral responsibility to emphasize the use of pervious materials to minimize the imperviousness at our homes, business places that help in reducing the impact of urbanization on the environment and society.

Acknowledgements We thank the Information Technology Research Academy, Government of India for financially supporting this work under ITRA-water grant ITRA/15(68)/water/IUFM/01. We thank GHMC for providing technical data. We thank NRSC for sharing high-resolution DEM with us and technical support. We also thank USGS and Google-Earth for the open data archive making available for research.

References

1. Arnold CL, Gibbons CJ (1996) Impervious surface coverage: the emergence of a key environmental indicator. *J Am Plan Assoc* 62(2), 243–258
2. Bazrkar MH, Zamani N, Eslamian S, Eslamian A, Dehghan Z (2015) Urbanization and climate change. In: Leal Filho W (ed) *Handbook of climate change adaptation*. Springer, Berlin. https://doi.org/10.1007/978-3-642-38670-1_90
3. Brown DG, Johnson KM, Loveland TR, Theobald DM (2005) Rural land-use trends in the conterminous United States, 1950–2000. *Ecol Appl* 15:1851–1863. <https://doi.org/10.1890/03-5220>
4. Chithra SV, Harindranathan MV, Nair A, Anjana NS (2015) Impacts of impervious surfaces on the environment. *Int J Eng Sci Invention* 4(5):27–31. ISSN (Online): 2319-6734. [https://www.ijesi.org/papers/Vol\(4\)5/E045027031.pdf](https://www.ijesi.org/papers/Vol(4)5/E045027031.pdf)
5. Dams J, Dujardin J, Reggers R, Bashir I, Canters F, Batelaan O (2012) Mapping impervious surface change from remote sensing for hydrological modeling. *J Hydrol* 485:84–95. <https://doi.org/10.1016/j.jhydrol.2012.09.045>
6. Deng Y, Fan F, Chen R (2012) Extraction and analysis of impervious surfaces based on a spectral un-mixing method using pearl river delta of china Landsat TM/ETM+ imagery from 1998 to 2008. *Sensors* 12:1846–1862. <https://doi.org/10.3390/s120201846>
7. Hoffman AB, Rehder B (2010) The costs of supervised classification: the effect of learning task on conceptual flexibility. *J Exp Psychol Gen* 139(2):319–340. <https://doi.org/10.1037/a0019042>
8. Lu D, Moran E, Hetrick S (2011) Detection of impervious surface change with multitemporal Landsat images in an urban–rural frontier. *ISPRS J Photogrammetry Remote Sens* 66:298–306. <https://doi.org/10.1016/j.isprsjprs.2010.10.010>
9. Majid M, Jamaludin J, Ibrahim W (2013) Estimation of residential impervious surface using gis technique. *Geospatial Anal Urban Plan II*:23–38. <https://doi.org/10.21837/pmjournal.v11.i2.114>
10. Mohapatra R, Wu C (2010) High resolution impervious surface estimation: an integration of Ikonos and Landsat-7 ETM+ imagery. *Photogrammetric Eng Remote Sens* 76:1329–1341. <https://doi.org/10.14358/PERS.76.12.1329>
11. NDMA (National Disaster Management Authority) (2010) *GOI: guidelines on urban flooding in India*
12. Ogden FL, Pradhan NR, Downer CW, Zahner JA (2011) Relative importance of impervious area, drainage density, width function, and subsurface storm drainage on flood runoff from an urbanized catchment. *Water Resour Res* 47:W12503. <https://doi.org/10.1029/2011WR010550>
13. Paul MJ, Meyer JL (2001) Streams in the urban landscape. *Annu Rev Ecol Syst* 32:333–365. https://doi.org/10.1007/978-0-387-73412-5_12
14. Ramachandraiah C, Prasad S (2004) *Impact of urban growth on water bodies: the case of Hyderabad*. Centre for Economic and Social Studies, Hyderabad
15. Roy AH, Shuster WD (2009) Assessing impervious surface connectivity and applications for watershed management. *J Am Water Resour Assoc (JAWRA)* JAWRA-07-0165-P. <https://doi.org/10.1111/j.1752-1688.2008.00271.x>
16. Schueler TR, Claytor R (1997) Impervious cover as an urban stream indicator and a watershed management tool. In: Roesner LA (ed) *Effects of watershed development and management in aquatic ecosystems*. Proceedings of an engineering workshop. ASCE, New York, pp 513–529. 978-0-7844-0232-0 (ISBN-13) | 0-7844-0232-9 (ISBN-10)
17. Shuster WD, Bonta J, Thurston H, Warnemuende E, Smith DR (2005) Impacts of impervious surface on watershed hydrology: a review. *Urban Water J* 2(4):263–275. <https://doi.org/10.1080/15730620500386529>
18. Wikipedia: Hyderabad (2017). Accessed Oct 2017)
19. Weng X, Hu X (2008) Medium spatial resolution satellite imagery for estimating and mapping urban impervious surfaces using LSMA and ANN. *IEEE Trans Geosci Remote Sens* 46(8):2397–2406. <https://doi.org/10.1109/TGRS.2008.917601>

20. Yuan F, Wu C, Bauer ME (2008) Comparison of spectral analysis techniques for impervious surface estimation using Landsat imagery. *Photogrammetric Eng Remote Sens* 74(8):1045–1055. <https://doi.org/10.14358/PERS.74.8.1045>
21. Zhihong G, Lu Z, Mingsheng L (2009) Estimating urban impervious surface percentage with multi-source remote sensing data. In: 2009 Urban remote sensing joint event. IEEE. 978-1-4244-3461-9/09©2009. <https://doi.org/10.1109/URS.2009.5137621>

Temporal Variation of Groundwater Levels by Time Series Analysis for NCT of Delhi, India



Riki Sarma and S. K. Singh 

Abstract Trend detection in time-series data has received a tremendous amount of attention in the last decade. This study was undertaken to analyse the trends in groundwater levels for nine districts of Delhi, India. Time series of groundwater levels (pre-monsoon and post-monsoon) for the period 1996–2019 for nine districts of Delhi were analysed using three tests, namely the Mann-Kendall test (MK), Sen's slope estimator and the Innovative Trend Analysis (ITA) method. For the pre-monsoon and post-monsoon groundwater levels, the nine districts had increasing trend as per the MK test and Sen's slope estimator, indicating that groundwater levels have declined in the study region. The Z statistic as well as the Sen's slope, Q obtained from these tests have been tabulated, and the trends have been depicted in graphical form. The ITA method also revealed increasing trends for all the districts except Central, West, South and New Delhi. For these four districts, the ITA method revealed a multiple trend structure in the time series. Analysis of the temporal variation in groundwater levels is very helpful, as it provides information about the rise or fall in the water table depths over the years which in turn can help in making the appropriate groundwater management decisions.

Keywords Trend analysis · ITA · MK test · Sen's slope

1 Introduction

Temporal variations in hydrological parameters have been studied all over the world using non-parametric statistical methods. Since non-parametric methods do not need normally distributed time-series data and can also accommodate outliers [1], they have been applied extensively with ease. The non-parametric Mann-Kendall test is most commonly used for trend detection in a time series [2, 3]. References for the usage of the Mann-Kendall test (MK) can be found throughout the world. Gocic and

R. Sarma · S. K. Singh (✉)

Department of Environmental Engineering, Delhi Technological University, New Delhi 110042, India

e-mail: sksinghdce@gmail.com

Trajkovic [4] analysed the trends of various meteorological variables such as temperature, precipitation, relative humidity and vapour pressure in Serbia from 1980 to 2010 by means of the MK test and Sen's slope estimator and reported that annual and seasonal maximum and minimum temperature showed increasing trend. This study also reported that summer and winter precipitation series did not show any significant trends. Trends in evapotranspiration and climatic parameters were studied using the MK test and Sen's slope estimator by Patle et al. [5] for Karnal district, Haryana for 1981–2011. They reported increasing trends for five climatic parameters, namely mean, minimum and maximum temperature, wind speed and relative humidity but negative trends for sunshine hours and reference evapotranspiration. A study on the trends in rainfall for the period of 1982–2011 and trends in temperature for the period of 1972–2007 in the Gomti basin using the MK test and Sen's slope estimator showed an increasing trend for rainfall in upstream areas but decreasing trend of rainfall in downstream areas [6].

A study by Tabari et al. [7] showed that groundwater level trends can also be analysed using non-parametric methods. They studied trends in groundwater level fluctuations (annual, seasonal and monthly) in Iran by MK test and Sen's slope estimator. Another study by Kawamura et al. [8] also showed that non-parametric methods can be applied to analyse temporal variations in groundwater levels. They applied the MK test and calculated Sen's slope for the unconfined Holocene aquifer in Hanoi. Pre-monsoon and post-monsoon groundwater level trends were studied via MK test and Sen's slope estimator by Patle et al. [9] for Karnal district in Haryana. They reported that groundwater levels in Karnal saw a significant decline from 1974 to 2010. Groundwater level fluctuations studied by Singh and Kasana [10] showed an average annual decline of 32.2 cm in the rice–wheat growing region in Haryana. Groundwater level time series were studied for Ghataprabha River Basin using the Mann-Kendall test [11]. Their study reported that the number of wells in the basin that showed significant decreasing trends was more than 61%.

More recently, the Innovative Trend Analysis (ITA) method has seen widespread application in water resources [12, 13]. Sen [12] reported that due to the limitations of the widely used MK test, a newer trend test was required that was not bound by restrictions such as the normality of the distribution and the length of the data in the time series. Hence, the ITA method has been applied worldwide due to its simplicity. Kisi [14] applied the ITA to monthly pan evaporation data of six locations in Turkey and reported that the ITA detected some trends for three of the stations. However, the Mann-Kendall test had showed no trend for these three stations. More recently, the ITA has been seen widespread applications and have also been compared to older trend tests [15–19].

In view of these previous studies, this study was undertaken to investigate the time-series data of groundwater levels of pre-monsoon and post-monsoon periods from 1996 to 2019. Three tests have been used, namely Mann-Kendall (MK) test, Sen's slope estimator, and Innovative Trend Analysis (ITA) method for trend detection in groundwater level time series.

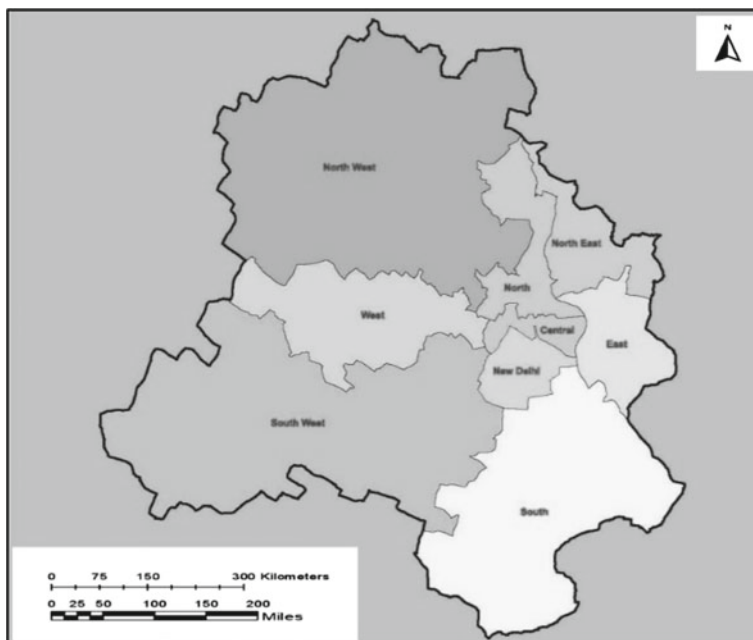


Fig. 1 Map of NCT of Delhi [22]

2 Materials and Methods

2.1 Study Area

The National Capital Territory (NCT) of Delhi is located in North India. NCT of Delhi covers 1483 km² area [20]. This region is between the latitudes—28° 24' 15" N to 28° 53' 00" N and longitudes—76° 50' 24" E to 77° 20' 30" E. Population of the NCT is 16,753,235 [21] with 75% of the area urbanised and more than 97% urban population. NCT of Delhi receives 611.8 mm rainfall, 81% of it received during the monsoon (July–September) [20]. Delhi has different geological formations—Delhi quartzite, older and younger alluvium which controls the groundwater availability [20]. A map presenting the districts of NCT of Delhi as per the Administrative Atlas of Census of India (2011) is depicted in Fig. 1 [22].

2.2 Data Used

District-wise time-series data for groundwater levels from 1996 to 2019 for the pre-monsoon (May) and post-monsoon (October/November) periods were downloaded

from the India-WRIS website [23]. The data obtained do not have any missing values. The basic statistics for this data are presented in Table 1.

2.3 Methods of Analysis

The groundwater level data obtained for nine Delhi districts were separately arranged for the pre-monsoon and post-monsoon periods. These 18 time series were each analysed by three tests for trend detection. The time series were fitted in the MAKESENS Excel template [24] for MK test and Sen's slop estimator. Due to its simplicity, this template is easily used for trend detection in groundwater data [25]. The ITA was applied on MS Excel. Descriptions of these tests are presented in the following paragraphs.

Mann-Kendall Test

Trend analysis of groundwater level time series was done by the non-parametric Mann-Kendall test [2, 3]. It tests the null hypothesis (H_0) against the alternate hypothesis (H_1). H_0 : no trend in the analysed population. H_1 : there is a trend in analysed population. Data values estimated as ordered pair of time series are compared with all subsequent data values. Equation 1 calculates the MK statistic S .

$$S = \sum_{i=1}^{n-1} \sum_{j=i+1}^n \text{sgn}(x_j - x_i) \quad (1)$$

x_i ranked from ($i = 1$ to $n - 1$); time series x_j from ($j = i + 1$ to n). Trend test is applied to both these time series. The reference points, x_i are compared to the data points, x_j (Eq. 2).

$$\text{sgn}(x_j - x_i) = \begin{cases} 1 & \text{if}(x_j - x_i) > 0 \\ 0 & \text{if}(x_j - x_i) = 0 \\ -1 & \text{if}(x_j - x_i) < 0 \end{cases} \quad (2)$$

For $n < 10$, there is a direct comparison done between the value of $|S|$ and the theoretical distribution of S . Increasing trend is shown by positive S , while negative S means decreasing trend [26, 27]. S is approximately normally distributed for $n \geq 10$. This distribution has the mean $E(s) = 0$. Equation 3 gives variance.

$$\text{Var}(S) = \frac{n(n-1)(2n+5) - \sum_{i=1}^m t_i(i)(i-1)(2i+5)}{18} \quad (3)$$

t_i number of ties upto sample i . Z determines a statistically significant trend (Eq. 4).

Table 1 Groundwater level data for 9 Delhi districts

District	Time period	Pre-monsoon groundwater level				Post-monsoon groundwater level			
		Min	Mean	Max	Std. Dev.	Min	Mean	Max	Std. Dev.
Central	1996–2019	4.43	7.14	13.51	2.04	2.76	5.89	8.60	1.56
West	1996–2019	6.01	9.94	14.54	2.46	4.22	9.60	18.59	3.13
North-West	1996–2019	4.14	6.31	9.73	1.51	2.89	5.74	8.65	1.72
South	1996–2019	15.87	30.92	42.19	8.82	13.76	29.28	37.68	8.83
New Delhi	1996–2019	8.91	13.14	16.71	1.71	7.70	12.02	14.56	1.97
North	1996–2019	3.72	5.51	9.51	1.30	2.75	4.57	6.30	0.99
East	1996–2019	5.30	8.26	12.36	1.97	4.25	7.76	12.19	2.14
South-West	1996–2019	10.02	17.24	23.02	4.29	8.73	17.04	30.01	4.99
North-East	1996–2019	3.50	6.51	22.44	3.69	2.71	5.34	7.67	1.23

$$Z_c = \begin{cases} \frac{S-1}{\sqrt{\text{Var}(S)}} & \text{if } S > 0 \\ 0 & \text{if } S = 0 \\ \frac{S+1}{\sqrt{\text{Var}(S)}} & \text{if } S < 0 \end{cases} \quad (4)$$

Time series will exhibit increasing trend if Z is positive and decreasing trend if it is negative. In the MAKESENS template, the trend test is done at four significance levels (0.1, 0.05, 0.01, 0.001).

Sen's Slope Estimator

Trend magnitude is determined by this method. In case of linear trend, the slope (change per unit time) is given by Eq. (5) [28].

$$(Q_i) = \frac{x_j - x_k}{j - k} \quad \text{for } i = 1, 2, \dots, N \quad (5)$$

x_j data values for time j , x_k data values for time k ($j > k$). N values of Q_i have a median which is Sen's slope Q . For even values of N , $Q_{\text{med}} = [Q_{N/2} + Q_{(N+2)/2}]/2$. For odd values of N , Sen's slope, $Q_{\text{med}} = Q_{(N+1)/2}$.

Innovative Trend Analysis

For a time series, the values are first separated equally into two series. Then, each is arranged in increasing order. Then, first is plotted on X -axis, second is plotted on Y -axis. Interpretations of these scatter plots are as follows.

1. No trend: Points on 1:1 line
2. Decreasing trend: Points lying beneath 1:1 line
3. Increasing trend: Points falling above 1:1 line.
4. For those that may lie both above and below the 1:1 line, interpretations have to be done accordingly where there may be both trends—increasing or decreasing, within the same series at different time scales [12, 13].

3 Results

The three methods were successfully applied to the groundwater level dataset of nine Delhi districts. The results are presented below.

3.1 Results of the Mann-Kendall Trend Test and Sen's Slope Estimator

MAKESENS template was used to analyse temporal variation in the groundwater level time series from 1996 to 2019 for nine districts of Delhi. Except for the

Table 2 Test results: MK statistic (Z) and Sen's slope (Q) for 9 districts of Delhi

District	Pre-monsoon groundwater level			Post-monsoon groundwater level		
	Z Statistic	Sen's slope Q	Trend	Z Statistic	Sen's slope Q	Trend
Central	3.99	0.199	Increasing ^a	2.95	0.146	Increasing ^b
West	5.28	0.321	Increasing ^a	4.96	0.324	Increasing ^a
North-West	5.61	0.199	Increasing ^a	5.46	0.227	Increasing ^a
New Delhi	1.22	0.075	Increasing	1.44	0.092	Increasing
South	3.45	0.956	Increasing ^a	3.35	0.989	Increasing ^a
North	4.66	0.143	Increasing ^a	3.75	0.109	Increasing ^a
East	4.29	0.235	Increasing ^a	3.84	0.238	Increasing ^a
South-West	5.78	0.603	Increasing ^a	4.62	0.560	Increasing ^a
North-East	4.44	0.186	Increasing ^a	3.03	0.131	Increasing ^b

^aTrend at 0.001 level of significance

^bTrend at 0.01 level of significance

New Delhi district, all other districts revealed significant increasing trends for pre-monsoon as well as post-monsoon time series. The datasets for New Delhi district show increasing trend as well, but the results are not statistically significant, with low values of Z statistic and Sen's slope Q . The test results for the Z statistic and Sen's slope Q for all the nine districts are presented in Table 2. The positive sign of Z and Q indicates that the trend of the series is increasing. This means that the groundwater level in all nine districts of Delhi has been declining from 1996 to 2019. The trends are depicted in Figs. 2 and 3.

3.2 Results of the Innovative Trend Analysis Method

The time series were first separated into two sub-series (one from 1996 to 2007 and one from 2008 to 2019), arranged in ascending order and plotted in a x - y coordinate system. The results from the ITA method are presented in Figs. 4 and 5. The trends obtained for the pre-monsoon time series (except the South district) are well in agreement with the results from the MK test. As per methodology for ITA given by Sen [12], as the points get closer to the 1:1 line, slope (trend magnitude) gets weaker. This observation has been made for New Delhi district which can also be corroborated by the low value of Q as per the Mann-Kendall test.

For the post-monsoon time series, all districts except Central, West, South and New Delhi show increasing trends that match well with the Mann-Kendall test. For the Central, West and New Delhi districts, data points have been observed below the 1:1 line indicating an internal trend structure, i.e. decreasing trend in this part of the series. The pre-monsoon and post-monsoon time series for South district show increasing trend for the major part of the series, but there is one data point that lies

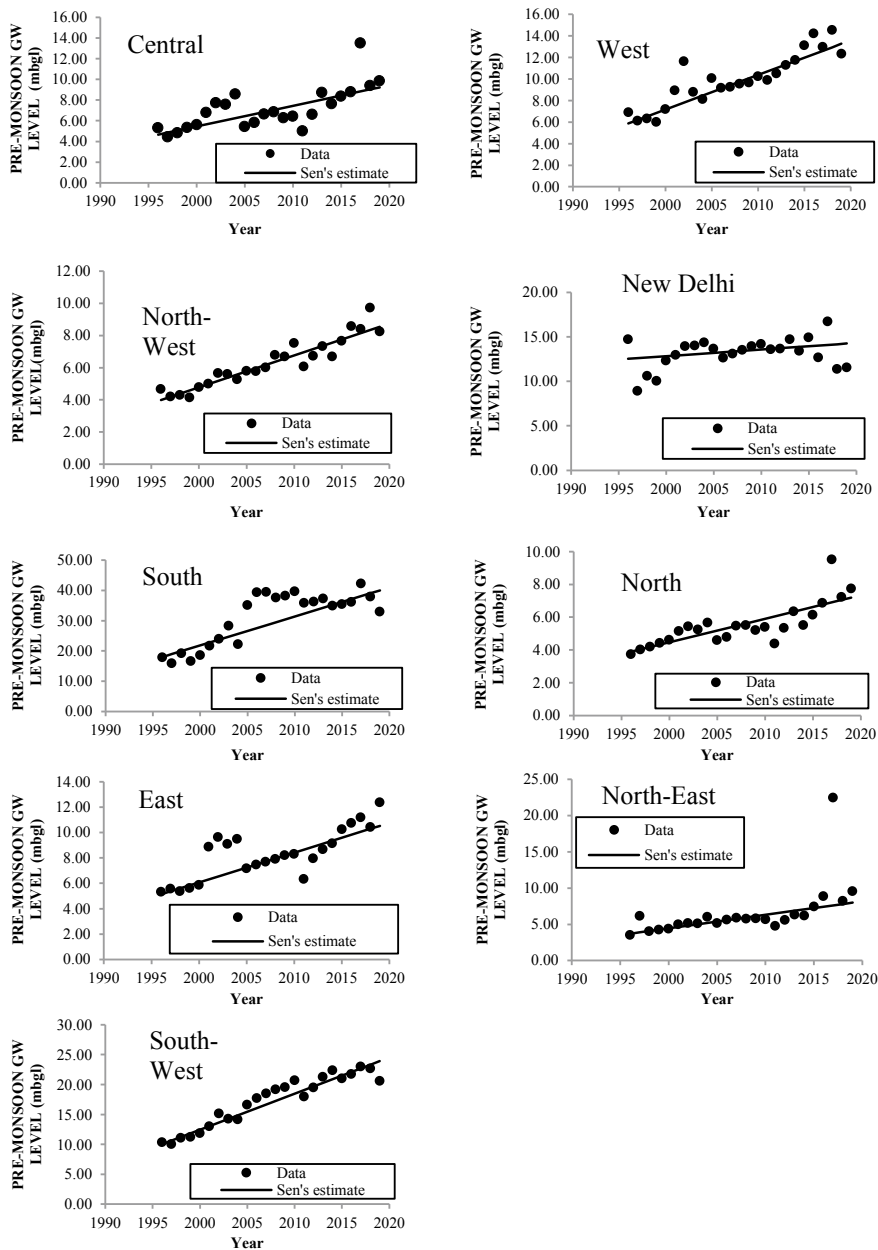


Fig. 2 Graphical representation of Mann-Kendall trend test and Sen's slope estimator results for pre-monsoon time series for nine districts of Delhi

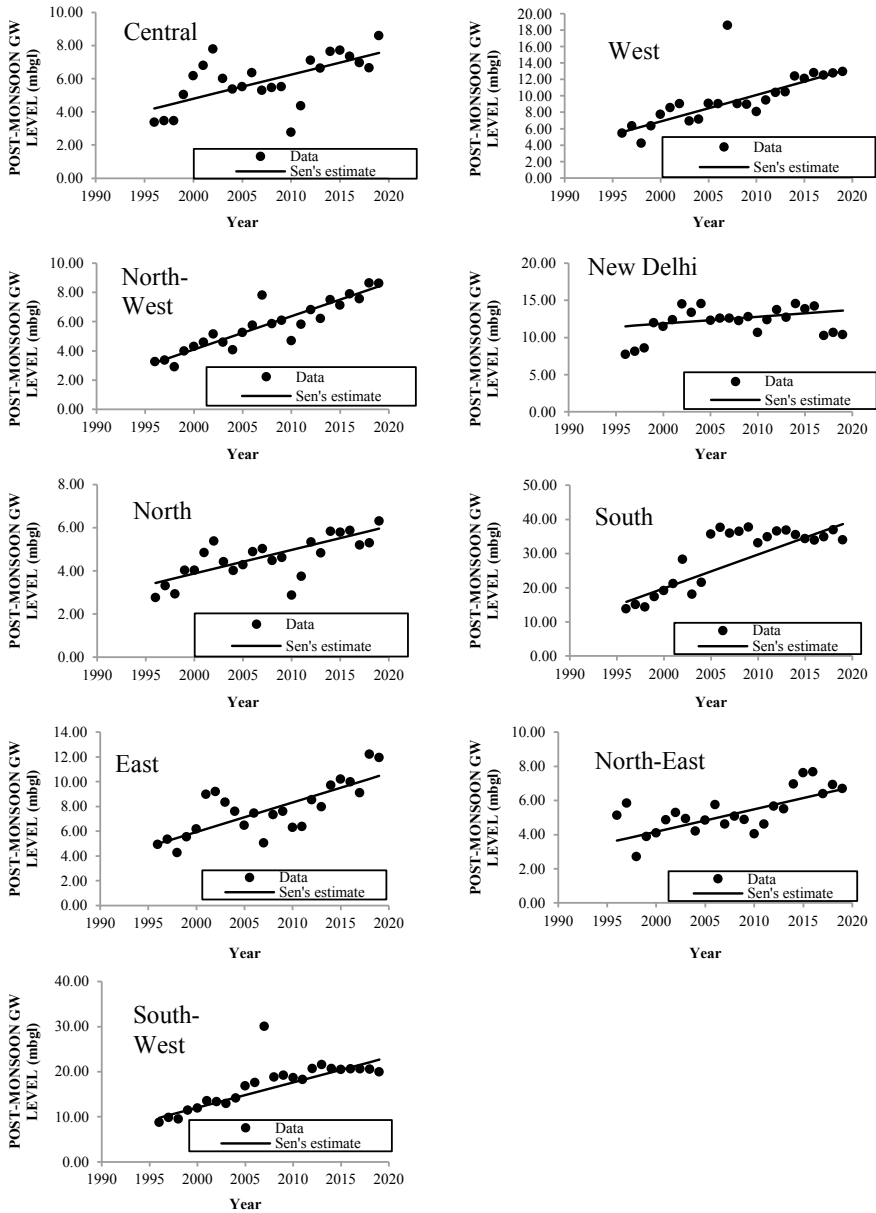


Fig. 3 Graphical representation of Mann-Kendall trend test and Sen's slope estimator results for post-monsoon time series for nine districts of Delhi

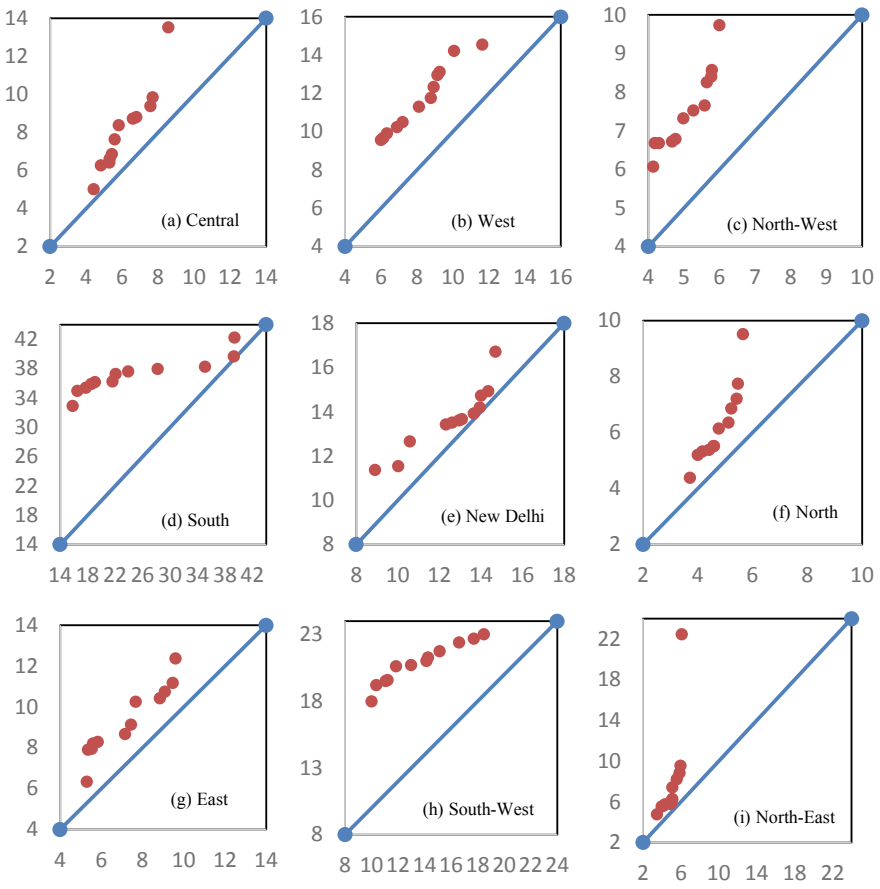


Fig. 4 Results for the Innovative Trend Analysis (ITA) method for pre-monsoon groundwater levels (in mbgl) for nine districts of Delhi. The first sub-series is plotted against the *x*-axis (1996–2007) and the second sub-series (2008–2019) against the *y*-axis

on 1:1 line indicating no trend. These internal trend structures are not observed in the Mann-Kendall test.

3.3 Discussion

Results obtained from the three tests reveal mostly increasing trends for the pre-monsoon and post-monsoon groundwater levels in Delhi from 1996 to 2019. Observing the time-series data, this increasing trend may be interpreted as declining groundwater levels over the years of study. Increased water demand due to increasing population in the NCT region may be a contributing factor to this decline. As per

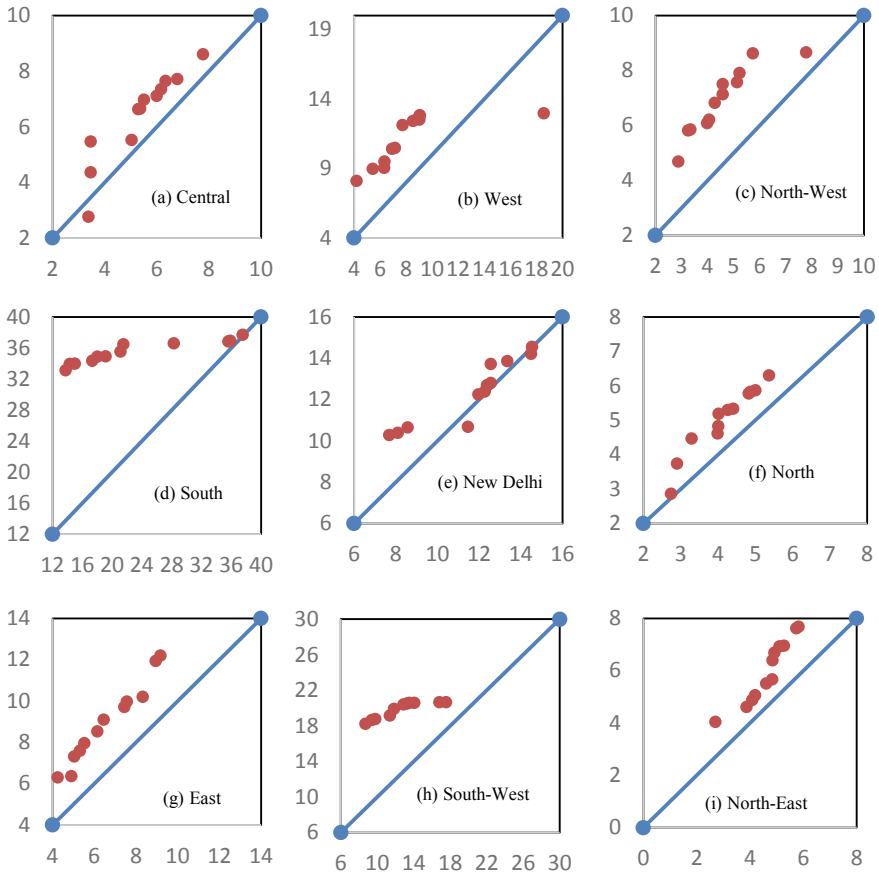


Fig. 5 Results for the Innovative Trend Analysis (ITA) method for post-monsoon groundwater levels (in mbgl) for nine districts of Delhi. The first sub-series is plotted against the *x*-axis (1996–2007) and the second sub-series (2008–2019) against the *y*-axis

Bhuvan (ISRO/NRSC) land use land cover data at 1:50,000 scale for Delhi [29], agriculture (crop land) area has decreased, and the urban built up area has increased from 2005–06 to 2015–16. This could also be related to the observed declining trends in the groundwater levels. Further investigation at the district level should be carried out to understand the exact reasons for the decline.

MK test and Sen’s slope estimator provide good understanding of the trends present in the time series; but as evidenced from this study, it is better to use them in conjunction with the newer ITA method. Comparing and corroborating the results obtained from all the three tests will give a comprehensive picture of the existing trends in the time series. Since the ITA method also reveals an internal trend structure, i.e. various trends in one time series, it is suggested that this method be further studied to understand the underlying reasons for these non-monotonic trends.

4 Conclusion

Time series of pre-monsoon and post-monsoon groundwater level for nine Delhi districts were analysed by Mann-Kendall test, Sen's slope estimator and innovative trend analysis methods. These three tests revealed increasing trends for the pre-monsoon period in eight districts implying a decline in the pre-monsoon groundwater level from 1996 to 2019. The MK test and Sen's slope estimator showed increasing trend for South district but ITA method showed one data point on 1:1 line, indicative of no trend for that phase. For the post-monsoon time series, the three tests revealed increasing trend for all districts except Central, West, South and New Delhi. The ITA method revealed data points both above, on and below the 1:1 line for Central, West, South and New Delhi time series which imply multiple trends in one time series. This requires further investigation. The reasons for this decline in the groundwater levels need further investigation as well. It is suggested that these trend analysis methods should be applied for time series of other study regions to get an understanding of the existing trends and making the best groundwater management decisions.

Acknowledgements The authors thank the Central Ground Water Board and India-WRIS for the groundwater level data. The authors are thankful to Delhi Technological University, New Delhi for providing the facilities to carry out the study.


References

1. Hamed KH, Rao AR (1998) A modified Mann-Kendall trend test for autocorrelated data. *J Hydrol* 204:182–196
2. Mann HB (1945) Non-parametric test against trend. *Econometrica* 13:245–259
3. Kendall MG (1975) Rank correlation methods, 4th edn. Charles Griffin, London, UK
4. Gocic M, Trajkovic S (2012) Analysis of changes in meteorological variables using Mann-Kendall and Sen's slope estimator statistical tests in Serbia. *Global Planet Change* 100:172–182
5. Patle GT, Singh DK, Sarangi A, Rai A, Khanna M, Sahoo RN (2013) Temporal variability of climatic parameters and potential evapotranspiration. *Indian J Agric Sci* 83(5):518–524
6. Abeysingha NB, Singh M, Sehgal VK, Khanna M, Pathak H (2014) Analysis of rainfall and temperature trends in Gomti river basin. *J Agric Phys* 14(1):56–66
7. Tabari H, Nikbakht J, Shiftesosome'e B (2012) Investigation of groundwater level fluctuations in the north of Iran. *Environ Earth Sci* 66(1):231–243
8. Kawamura A, Bui DD, Tong TN, Amaguchi H, Nakagawa N (2011) Trend detection in groundwater levels of Holocene unconfined aquifer in Hanoi, Vietnam by non-parametric approaches. In: *World Environmental and Water Resources Congress 2011: Bearing Knowledge for Sustainability*, pp 914–923
9. Patle GT, Singh DK, Sarangi A, Rai A, Khanna M, Sahoo RN (2015) Time series analysis of groundwater levels and projection of future trend. *J Geol Soc India* 85:232–242
10. Singh O, Kasana A (2017) GIS-based spatial and temporal investigation of groundwater level fluctuations under rice-wheat ecosystem over Haryana. *J Geol Soc India* 89:554–562
11. Pathak AA, Dodamani BM (2018) Trend analysis of groundwater levels and assessment of regional groundwater drought: Ghataprabha river basin, India. *Nat Res.* <https://doi.org/10.1007/s11053-018-9417-0>

12. Sen Z (2012) Innovative trend analysis methodology. *J Hydrol Eng* 17(9):1042–1046
13. Sen Z (2014) Trend identification simulation and application. *J Hydrol Eng* 19(3):635–642
14. Kisi O (2015) An innovative method for trend analysis of monthly pan evaporations. *J Hydrol* 527:1123–1129
15. Caloiero T, Coscarelli R, Ferrari E (2018) Application of the innovative trend analysis method for the trend analysis of rainfall anomalies in Southern Italy. *Water Resour Manage* 32:4971–4983
16. Wu H, Qian H (2016) Innovative trend analysis of annual and seasonal rainfall and extreme values in Shaanxi, China, since the 1950s. *Int J Climatol*. <https://doi.org/10.1002/joc.4866>
17. Wang Y, Xu Y, Tabari H, Wang J, Wang Q, Song S, Hu Z (2020) Innovative trend analysis of annual and seasonal rainfall in the Yangtze river delta, eastern China. *Atmos Res* 231
18. Li J, Wu W, Ye X, Jiang H, Gan R, Wu H, He J, Jiang Y (2018) Innovative trend analysis of main agriculture natural hazards in China during 1989–2014. *Nat Hazards*. <https://doi.org/10.1007/s11069-018-3514-6>
19. Alifujiang Y, Abuduwaili J, Maihemuti B, Emin B, Groll M (2020) Innovative trend analysis of precipitation in the lake Issyk-Kul basin, Kyrgyzstan. *Atmosphere* 11
20. Central Ground Water Board. *Groundwater yearbook 2015–16*, New Delhi
21. Census, Primary Census Abstracts, Registrar General of India, Ministry of Home Affairs, Government of India (2011). Available at: https://www.censusindia.gov.in/2011census/PCA/pca_highlights/pe_data
22. Census of India, Administrative Atlas NCT of Delhi, Director of Census Operations, NCT of Delhi (2011)
23. India-WRIS, Ministry of Jal Shakti, Government of India. <https://indiawris.gov.in/wris/#/>. Data accessed in July 2020
24. Salmi T, Maatta A, Anttila P, Airola TR, Amnell T (2002) Detecting trends of annual values of atmospheric pollutants by the Mann-Kendal test and Sen's slope estimates—the Excel template application MAKESENS. User manual, Publication on air quality, Finish Meteorological Institute, p 35
25. Rahman A, Kamruzzama M, Jahan CS, Mazumder QH (2016) Long-term trend analysis of water table using 'MAKESENS' model and sustainability of groundwater resources in drought prone Barind area, NW Bangladesh. *J Geol Soc India* 87:179–193. <https://doi.org/10.1007/s12594-016-0386-9>
26. Shahid S (2011) Trends in extreme rainfall events of Bangladesh. *Theor Appl Climatol* 104:489–499
27. Luo Y, Liu S, Fu SF, Liu J, Wang G, Zhou G (2008) Trends of precipitation in Beijing River Basin, Guangdong Province, China. *Hydrol Process* 22:2377–2386
28. Sen PK (1968) Estimates of the regression coefficient based on Kendall's tau. *J Am Stat Assoc* 39:1379–1389
29. Bhuvan, ISRO/NRSC. https://bhuvan.nrsc.gov.in/bhuvan_links.php. Accessed on 25th July 2020

Finite Element Modeling of Geogrid-Reinforced Unpaved Road



Rohan Deshmukh , S. Patel, and J. T. Shahu

Abstract In this study, finite element modeling of the geogrid-reinforced unpaved road has been done in PLAXIS 3D to investigate the benefit of geogrid reinforcement on the rutting behavior of pavement. The effect of the location of geogrid, its axial stiffness, and subgrade CBR on the performance of reinforced unpaved roads is discussed in this study. The use of geogrid reinforcement at 1/3rd from the bottom of the base layer is better than the top and middle position of geogrid in the base layer. The performance of geogrid reinforcement increases with an increase in axial stiffness of geogrid. The results also suggest that the use of geogrid reinforcement with proper tensile strength in the unpaved road is an economical and suitable solution for subgrade CBR of $\leq 4\%$.

Keywords Unpaved road · Rutting · Geogrid · FEM · PLAXIS 3D

1 Introduction

Key factors that influence the design of paved and unpaved roads are the strength and stiffness of the pavement layers. Among other factors, the strength of pavements depends on the thickness and quality of the aggregates used in the pavement base layer. There is a need for the development of sustainable construction methods that can handle aggregate requirements with the least available resources and provide good performance. Hence, it is imperative to strive for alternatives to achieve an improved quality of pavements using supplementary potential materials and methods. The solution for this is an effective use of geosynthetics. Among all the available types of geosynthetics, geogrid is mainly using for reinforcement purposes in the base and subbase layers due to its good reinforcing property. Reinforcement

R. Deshmukh (✉) · S. Patel
Civil Engineering Department, SVNIT, Surat, Gujarat 395007, India
e-mail: rohandeshmukh520@gmail.com

J. T. Shahu
Civil Engineering Department, IIT, Delhi 110016, India

of geogrid is mainly due to the interlocking of aggregate, tension membrane effect, wider distribution of loads, etc. Many researchers use different types of numerical methods such as discrete element method (DEM), finite element method (FEM), and finite difference method (FDM) for the analysis of geogrid-reinforced pavement. Tutumluer et al. [1] using an aggregate image analyzer to study the interlocking mechanism of geogrid-aggregate by considering the influence of aperture size and shape, aggregate size and shape, density, gradation, angularity as well as the shape and stiffness of rib on the interlocking mechanism. Abufarsakh et al. [2] conducted finite element analysis by using the ABAQUS software package to investigate the effect of geogrid reinforcement in the base layer in terms of reduction in lateral tensile strain and vertical compressive strain within the bituminous layer and subgrade layer, respectively. Hadi and Bodhinayake [3] also used FEM-based ABAQUS software to model geogrid-reinforced pavement subjected which subjected to cyclic loading; results show that displacements under cyclic loading when nonlinear materials are considered, then the results are closest to field measured deflections of reinforced pavement. Mousavi et al. [4] developed a finite element model in Plaxis 3D, to access the performance of geogrid reinforcement in the unpaved road. The developed FEM model was subjected to a cyclic type of loading. The typical run for 100 loading cycles was around 24 h, so this type of analysis was time-consuming, and it required huge computational efforts. Mousavi et al. [4] used a hardening soil small strain (HS small strain) constitutive model for all the layers of unpaved road. The input parameters that require for hardening soil small strain model development are based on tedious laboratory work. HS small strain model requires a value of plastic straining due to primary deviatoric loading (E_{50}), plastic straining due to primary compression (E_{oed}), elastic unloading/reloading (E_{ur}), shear stiffness modulus (G_0), stress-dependent stiffness according to a power law (m), poisons ratio (ν), and failure according to the Mohr–Coulomb model (c , ϕ , and ψ) as an input parameter for each layer of unpaved road. All the above analysis method or studies are time-consuming and tedious, so in this study, a simple FEM model is developed which predict the performance of geogrid-reinforced unpaved road in the least time.

2 Methodology

In this study, the finite element model is developed in PLAXIS 3D to found out the improvement factor for the inclusion of geogrid in the base layer of unpaved road. Improvement factor is developed by considering the effect of axial stiffness of geogrid and subgrade CBR. In the current study to explore the benefits of geogrid reinforcement in the unpaved road instead of the time-consuming cyclic type of loading, a new approach is adopted in which the FEM model is subjected to 150 mm radius circular shape predefined deformation of 5, 10, and 15 mm, and corresponding loads are measured. The analysis is completed in just 5–10 min. ‘Prescribed surface displacement’ is the in-built tool in PLAXIS 3D software which was employed for predefined deformation. Also, a simple Mohr–Coulomb (M-C) constitutive model

Table 1 Properties of different layers of pavement

Material	Model	Poisson ratio (ν)	Unsaturated unit weight (γ_{un}) kN/m ³	Saturated unit weight (γ_{sat}) kN/m ³	Friction angle (ϕ)
WMM	M-C	0.35	21.8	23	48
GSB	M-C	0.35	11	23	43
Subgrade	M-C	0.35	17.9	21.2	30

M-C Mohr–Coulomb

is used for the analysis, and the input parameter required for the model is shown in Table 1. In the current study, effect of axial stiffness (EA), location, and subgrade CBR on the rutting behavior of unpaved roads is shown in terms of loads required for predefined deformation of reinforced and unreinforced FEM model of unpaved road. The effect of geogrid location, its axial stiffness, and subgrade CBR on the performance of unpaved road was already reported in the past literature, but the main objective of current study is to validate the newly developed finite element model with those past findings.

2.1 Numerical Modeling in PLAXIS 3D

A full-scale model of the unpaved road was developed in PLAXIS 3D with Mohr–coulomb soil model for wet mix macadam (WMM) layer, granular subbase (GSB) layer, and subgrade (see Fig. 1a). All the properties of WMM, GSB, and subgrade were found out by laboratory testing (as per IS: 2720) and mention in Table 1. The thickness and modulus values of the WMM and GSB layer were chosen based on the subgrade of CBR as per IRC: 37-2012 [5].

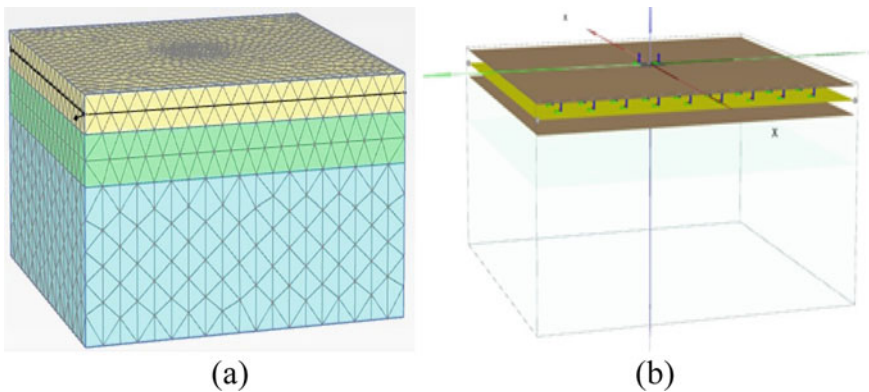


Fig. 1 Finite element model of **a** unpaved road and **b** geogrid with interface

As per IRC: 37-2012, resilient modulus (M_R) of subgrade soil, granular subbase (GSB), and wet mix macadam (WMM) is given by Eqs. (1), (2), and (3), respectively.

$$M_{R(\text{Subgrade})} = 10 \times \text{Subgrade CBR} \quad (1)$$

$$M_{R(\text{GSB})} = 0.2 \times (h)^{0.45} \times M_{R(\text{Subgrade})} \quad (2)$$

where h = thickness of subbase in mm.

$$M_{R(\text{WMM})} = 0.2 \times (h)^{0.45} \times M_{R(\text{Subgrade})} \quad (3)$$

where h = thickness of base and subbase in mm.

2.2 Prescribed Surface Displacement

To define surface displacements, ‘create surface prescribed displacement’ option is selected from the in-built menu in PLAXIS 3D. A uniformly distributed prescribed 150 mm radius circular shape displacement perpendicular to the surface is defined. A prescribed displacement perpendicular to the surface varying in the z -direction is created by defining the components and the magnitude of the displacement such as 5, 10, and 15 mm at the reference point and its increment in the z -direction.

2.3 Axial Stiffness of Geogrid

Axial stiffness (EA) of geogrid is calculated by using the following Eq. 4, where ‘ T ’ is the maximum tensile strength of geogrid, and ‘ ϵ ’ is the corresponding strain,

$$EA = (T)/(\epsilon) \quad (4)$$

Polypropylene bi-axial type of geogrid is considered in this study. Properties of geogrid in terms of EA are given in Table 2. The interface value for geogrid is 1.0

Table 2 Properties of geogrid

Type of geogrid	Maximum tensile strength (kN/m)	Tensile strength at 2% strain (kN/m)		Axial stiffness (EA) (kN/m)
GG15	15	5	250	
GG20	20	7	350	
GG40	40	14	700	

considered in this study for 100% interlocking of aggregate in the geogrid aperture (Fig. 1b).

3 Results and Discussion

In this study, the effect of location and axial stiffness of geogrid are discussed. Geogrid with different axial stiffness's 250, 350, and 700 kN/m are considered in this study. The improvements due to the inclusion of geogrid in the unpaved road are shown in terms of an increase in vertical stress requirement to achieved prescribed displacements of 5, 10, and 15 mm.

3.1 Effect of Geogrid Location

In Fig. 2, vertical stress requirements in MPa for prescribed displacements (i.e., Rut) of 5, 10, and 15 mm are shown for the unreinforced and reinforced unpaved model. In the reinforced unpaved model, three different geogrid positions are considered, at the 1/3rd from the bottom, middle, and 1/3rd from the top of the base layer. To check the effect of geogrid location on its performance, only one geogrid (GG15) is taken into consideration. Results of effect of geogrid locations are reported in Table 3.

From Fig. 2, it is observed that placement of geogrid with 15 kN/m tensile strength at 1/3rd from the bottom of base layer performing better in terms of higher vertical stress requirement than the other positions of geogrids. The highest decrease in rutting strain was observed by Saad et al. [6] in their study when the geogrid placed at 1/3rd from the bottom of the base layer of paved road. Because of this benefit for all the other parametric analysis, geogrid location was fixed at 1/3rd from the bottom of the base layer.

Fig. 2 Effect of geogrid location on a load-carrying capacity

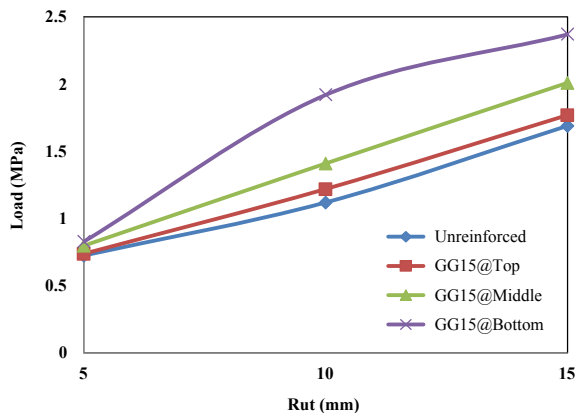


Table 3 Maximum vertical load for different location of geogrid

Rut (mm)	Maximum load (MPa)			
	UR	GG15@ 1/3rd from top	GG15@ middle	GG15@ 1/3rd from bottom
5	0.725	0.738	0.798	0.828
10	1.12	1.22	1.41	1.92
15	1.69	1.27	2.01	2.37

UR Unreinforced, GG geogrid

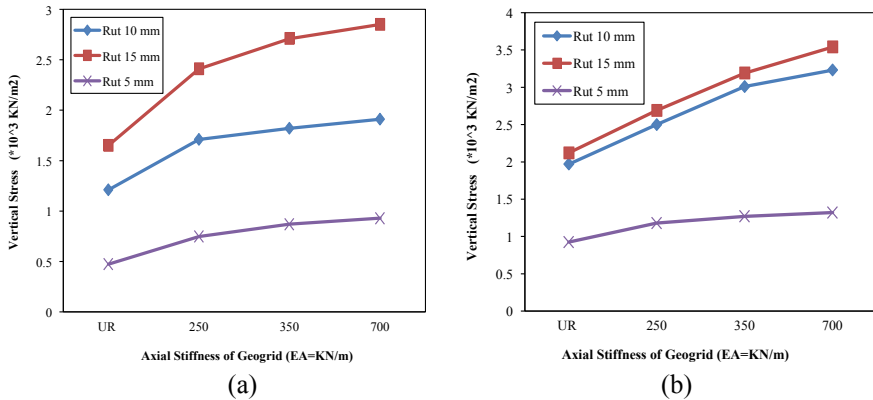


Fig. 3 Effect of axial stiffness of geogrid for subgrade CBR of **a** 1% and **b** 4%

3.2 Effect of Axial Stiffness of Geogrid

Effects of axial stiffness on vertical stress requirement are shown in Fig. 3a, b. From Fig. 3a, b, it is observed that with an increase in axial stiffness of geogrid, the requirement of vertical stress also increased with prescribed displacements. The effect of geogrid inclusion was insignificant for smaller (i.e., 5 mm Rut) prescribed displacement, but the effect of geogrid was significant for larger prescribed displacement (i.e., 10 and 15 mm Rut).

3.3 Load Improvement Percentage

Benefits of geogrid reinforcement are shown in terms of load improvement percentage required for particular rut formation. Load improvement percentage is calculated by comparing the maximum vertical load required by the geogrid-reinforced unpaved model at a particular rut (prescribed displacement) to the maximum vertical load taken by the unreinforced unpaved model at the same rut.

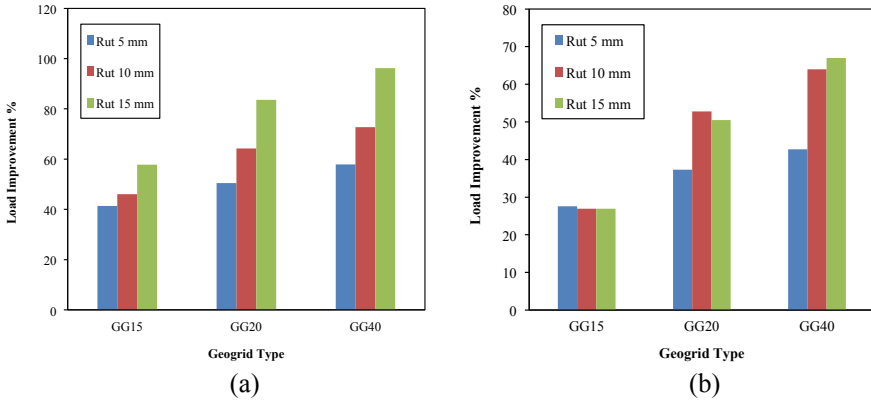


Fig. 4 Load improvement percentages for subgrade CBR of **a** 1% and **b** 4%

Load improvement percentage is given by Eq. 5. Figure 4a, b shows load improvement percentage for all three geogrid tensile strength of 15, 20, and 40 kN/m for subgrade CBR of 1 and 4%, respectively. From Fig. 4a, b, it is observed that for lower subgrade CBR, the effect of geogrid reinforcement was significant at lower rut compared to the higher subgrade CBR. Also, geogrid having lesser tensile strength (15 kN/m) is not performing well even with an increase in rut depth for higher subgrade CBR of 4%.

$$\text{Load Improvement Percentage} = \frac{[(\text{Maximum Load by Reinforced Section} - \text{Maximum Load by Unreinforced Section}) / (\text{Maximum Load by Unreinforced Section})] \times 100}{(5)}$$

3.4 Effect of Subgrade CBR

It is observed that the influence of subgrade CBR on the performance of geogrid reinforcement is substantial. From Table 4, it is observed that load improvement percentages for GG40 are reduced with an increase in subgrade CBR from 1 to

Table 4 Load improvement percentage

	GG15		GG20		GG40	
Subgrade CBR	1%	4%	1%	4%	1%	4%
Rut 5 mm	41.32	27.56	50.41	37.29	57.85	42.7
Rut 10 mm	46.06	26.9	64.24	52.79	72.72	63.95
Rut 15 mm	57.8	26.88	83.54	50.47	96.2	66.98

4%. From Table 4, it is observed that for lower subgrade CBR (1%) values, the performance of GG20 is found to be good compared to GG 15 and showing closer results to that of GG40. As discussed earlier, the use of low tensile geogrid (GG15) with higher subgrade CBR (4%) showing near about the same load improvement percentages for all three ruts. The use of geogrid reinforcement with proper tensile strength in the unpaved road is economical and suitable for subgrade CBR of $\leq 4\%$. Beyond 4% subgrade CBR, the influence of geogrid reinforcement on vertical stress requirement was found to be insignificant.

4 Conclusions

In the current study, the finite element approach is adopted to justify the benefits of geogrid reinforcement in the unpaved road. The finite element model is developed in PAXIS 3D to capture the benefits of geogrid reinforcement. The effect of geogrid location, its axial stiffness, and the influence of subgrade CBR on the performance of geogrid reinforcement is taken into account. The results of this study are summarized below,

1. The developed finite element model captures the benefits of geogrid reinforcement along with the other two benefits like lesser input parameters requirement and reduction in computational efforts.
2. The use of geogrid reinforcement at 1/3rd from the bottom of the base layer showing good performance than the top and middle position of geogrid in the base layer.
3. The performance of geogrid reinforcement increases with an increase in axial stiffness of geogrid. The performance of geogrid is not impressive at smaller ruts but as rut depth increases, the performance of geogrid also increases.
4. The influence of subgrade CBR on the performance of geogrid reinforcement is substantial. The use of geogrid reinforcement with proper tensile strength in the unpaved road is economical and suitable for subgrade CBR of $\leq 4\%$.

References

1. Tutumluer E, Huang H, Bian X (2012) Geogrid-aggregate interlock mechanism investigated through aggregate imaging-based discrete element modeling approach. *Int J Geomech* 12(4):391–398
2. Abufarsakh MY, Gu J, Voyiadjis GZ, Chen Q (2014) Mechanistic empirical analysis of the results of finite element analysis on flexible pavement with geogrid base reinforcement 15(9):786–798
3. Hadi MNS, Bodhinayake BC (2003) Non-linear finite element analysis of flexible pavements. *Adv Eng Softw* 34(11–12):657–662
4. Mousavi SH, Gabr MA, Borden RH (2017) Optimum location of geogrid reinforcement in unpaved road. *Can Geotech J* 54(7):1047–1054

5. IRC 37 (2012) Tentative guideline for the design of flexible pavements
6. Saad B, Mitri H, Poorooshab H (2006) 3D FE analysis of flexible pavement with geosynthetic reinforcement. J Transp Eng ASCE 132:402–415

Hydrological Challenges in Riverfronts: A Case Study of Dravayawati Riverfront Project in Jaipur, Rajasthan



Kedar Sharma and Priyanka Gupta

Abstract A critical review about the challenges of riverfront projects in arid or semi-arid regions is present in the present study. Dravayawati Riverfront of Jaipur city is taken as a case study. Riverfronts are the new landscapes in the urban areas to utilize the undeveloped banks of the river reaches. Recently, Dravyavati, Gomti, Patna, Sabarmati and Yamuna riverfronts are some of the landscape projects developed in the various cities. As most of the rivers are either ephemeral (water is available only during monsoon period) or tapped for canal systems, the availability of freshwater is the major challenge. A 47 km long riverfront project was planned in Jaipur city on the banks of Dravayawati River. As Jaipur is located in the semi-arid part of the Rajasthan, the water is available for limited duration during the monsoon period. In this project, treated sewage water is the prime source of water. A concrete channel is constructed in the middle of river section and parks or some developments on both the banks. This ultimately reduces the possibility of groundwater recharge in a dark zone city. There are few more hydrologic challenges in the execution of the projects and discussed in the present study. The results of the present study may be useful for the policy makers, when such projects are planned in the arid and semi-arid part of the country.

Keywords Riverfront · Urban development · Dravayawati riverfront

1 Introduction

Riverfronts projects are the new landscape projects on the banks of rivers. Riverbanks, shoreline, riparian buffer and river habitats should be considered during the planning of a riverfront [1]. Ancient Ghats on holy rivers in India is also a type of riverfront.

K. Sharma (✉)

Department of Civil Engineering, JK Lakshmipat University, Jaipur, Rajasthan, India

e-mail: kedارشarma@jklu.edu.in

P. Gupta

Department of Civil Engineering, Swami Keshvanand Institute of Technology, Management & Gramothan, Jaipur, Rajasthan, India

Spirituality is a major concern in Ghats. Fluctuations in the water level differentiate them with the present day riverfronts. A constant or predefined water level is ensured in these riverfronts. Commercial activities, gardening and walkways are the major purposes of the riverfronts. The first major riverfront project in India was developed in Ahmedabad on the banks of the Sabarmati River [2]. Simultaneously, riverfront projects were developed in Delhi, Lucknow and Patna on the banks of the Yamuna, Gomti and Ganga River [3–7]. Among these, the riverfronts of Delhi, Patna and Lucknow are located on the bank of a perennial river. Riverfront in the Lucknow is located in the upstream of Gomti Barrage. Hence, it ensures the constant water depth in the river. A rubber dam was constructed on Yamuna River in the downstream of Signature Bridge to store the water. The sewage water from Nazafgarh drain will also be treated and released in the river. This drain is in the upstream of rubber dam. Both Yamuna and Gomti are Perennial River, and hence, some freshwater is always available in the river. In Patna, Ganga River has sufficient water round the year. This riverfront is also the part of clean Ganga mission (Fig. 1).

The Sabarmati Riverfront is located on the bank of a monsoon flowing river. A weir was constructed in the river to uplift the water level (Fig. 2). To compensate the water losses due to evaporation and seepage, water is released from the Narmada canal. Some amount of treated sewage water is also released in Sabarmati River. The



Fig. 1 Riverfronts in various cities

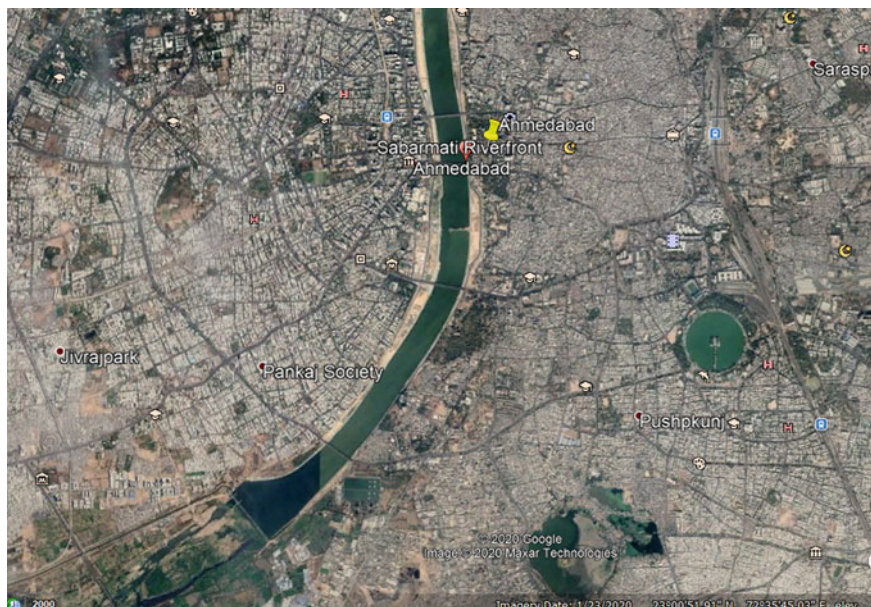


Fig. 2 Location of Sabarmati Riverfront and weir at the downstream end

excess water in the river overflows over the wall and diverted to a canal for irrigation. The length of the riverfront is approximately 10 km, and width is 300–400 m. The full width of the river is used for the project.

2 Dravayawati Riverfront

Dravayawati Riverfront project is an ambitious river rejuvenate project of Jaipur Development Authority (JDA) on Dravayawati River (also known as Amanishah Nala) flowing through the middle of Jaipur city [8–11]. This river is a monsoon river which originates from the foothills of Nahargarh and meets the Dhoondh River [10]. In the past, this river is also a perennial river due to the presence of various check dams at regular intervals. It also has a canal system from Goolar Bandh near Sanganer town. This canal system is still in operating condition. As the population of city increases, natural path of the drains, which feed the river had been disturbed, and it was converted in a dumping area of solid wastes, untreated wastewater from Sanaganeri print industries (Fig. 3). Black colour water of bed odour was observed at most of the locations. This river is severely affected by encroachment, and the present width of the river varies from 30 to 400 m at various locations. On this available land, JDA proposed a concrete channel of varying width for 47 km length (Fig. 4) [8]. Five sewage treatment plants are proposed on these stretches [8, 9]. Water depth is insured



Fig. 3 Pre-development Dravayawati River

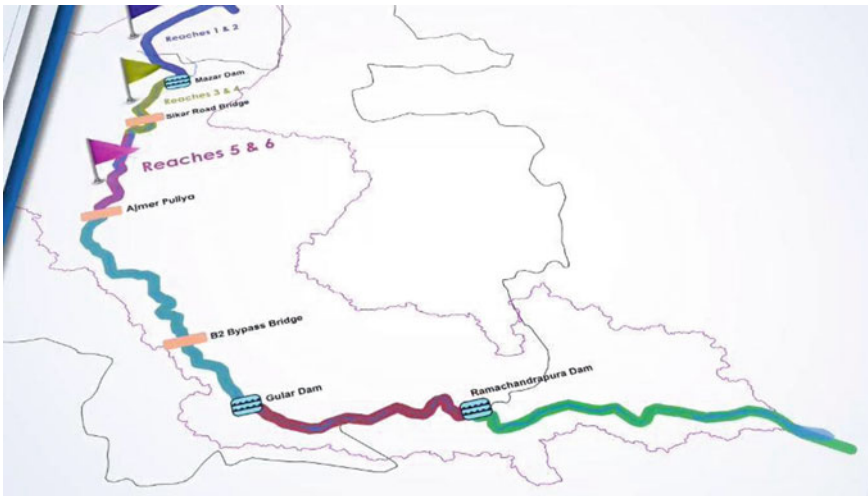


Fig. 4 Plan of development for various reaches of Dravayawati River

by providing weirs at regular intervals. As per the slope of the river, the water depths vary from 30 to 300 cm. The initial estimated cost of the project is 1100 crore. For maintenance, extra 250 crore Rs. are proposed in next five years. JDA is expecting the revenue of 2500 crore by selling land nearby to the riverfront. However, this project miss several deadlines and is not completed even till June 2020 (Fig. 5).



Fig. 5 Developed sections of Dravayawati Riverfront

3 Major Challenges in the Successful Operation of Dravywati Riverfront

Although this project is in construction phase and almost 80–85% work has been already done, still this project has some major hydraulic and hydrologic challenges, which have to be addressed. These challenges are discussed in the following sections.

3.1 Water Availability

Jaipur is located in the semi-arid part of the Rajasthan. High temperature, less rainfall, comparatively long summers, sandy soil and deep water table are general characteristic of this region [12, 13]. Particularly, in Jaipur city due to rapid urbanization, water table is very deep in comparison with another districts of the region. The worst combination is that this project is situated at the commencing point of the river in a low rainfall area (technically Jaipur is located at the beginning of the catchment area). The number of rainy days is very limited in this region, and hence, the water availability for this project is very limited [12]. Similarly, very less flow is available due to sandy soil and deep water table. Most of the water infiltrates into the soil. Whatever the water is available in the river, this is available only during the monsoon period. In this project, treated sewage water is used as the prime source. Although the concrete floor and banks have been used and seepage loss is very low, yet some water is required to balance evaporation losses. Cities like Jaipur, where the water resources are limited and water is imported from long distance, this treated sewage water can be used for another purposes. The construction of the project is not a hurdle, but the length of the project is a big challenge. If it is planned to be constructed near the Bambala Puliya in Pratap Nagar for 5–7 km, the project may have been a more

successful one. Although there is a less possibility for rainwater, still with limited length, this project can successfully run by treated sewage water.

3.2 Connections of Small drains to the Main Channel:

After the availability of water in channel, the second point is about the connection of small drains to main channel. In a river system, the main channel and small tributaries are the integrated part. In this project, both the banks of the river are made by concrete, and the level is high in comparison with original bed level. It is proposed that the treated sewer water is pumped in the channel; however, it is difficult to connect the small drains to the main channel. Connection of small drains is must for the disposal of rainwater, and it is one of the source of water during the monsoon period. In the Indian conditions, these small drains are also the source of silt and garbage in the main channel. A properly maintained mechanism for silt and garbage removal is necessary. In comparison with an open natural river system, a choked system due to plastic waste can increase the vulnerability of flood in the city. It is also estimated by various researchers that the magnitude and frequency of probable maximum flood may increase due to the impact of climate change. In the absence of properly maintained rainwater disposal network, a flood situation may arise in the city. Floods in Mumbai and Chennai cities were the example of such conditions. Water logging in Gurugram is also due to such mismanagement of rainwater drainage. This might be not the problem in riverfronts mentioned in the previous sections (Fig. 6).



Fig. 6 Accumulation of plastic waste on one of the weir near Bambala Puliya

3.3 Recharge of Ground Water

Third important issue is related to recharge of ground water. Naturally, the river is wide, and the groundwater is recharge during the high flood in monsoon. As per the design, the middle portion is a concrete channel, and garden or commercial area will be developed on both the banks of concrete channel. Although in the absence of this project also there is low probability of groundwater recharge, yet this project will minimize (or even zero) the possibility of groundwater recharge through flood plains [14]. There is minimum provision for open areas or groundwater recharge structures. On the one side, government promotes the artificial recharge and rainwater harvesting, and on the other side, this project, the rainwater, is diverted in the channel which will ultimately flow in downstream direction without recharge the groundwater table in the city (Fig. 7).

Designers proposed some structures within the channel for groundwater recharge. They have proposed the check dams at some interval in channel [8]. These check dams have both advantages and disadvantages. It is also a point of discussion that whether these check dams are within the channel or outside the channel.



Fig. 7 Newspaper information about decrease in groundwater table. Source Rajasthan Patrika, 30 Aug 2019



Fig. 8 Condition of tiles on wall in early stages of construction near Bambala Puliya, Tonk road

Case 1: If these check dams are outside the channel, the amount of water left for main channel is very less.

Case 2: When check dams are within the main concrete channel. During the monsoon period, some water will be recharged by check dams and some will flow in the channel. But after the monsoon, also some water is lost due to seepage in these check dams. The exact number of check dams and their utility is not up to the mark in this project.

3.4 Requirement of Continuous Monitoring

The amount of water coming into channel is very less, and the duration is also short. If the treated sewage water is used for this project, the success of the project is doubtful due to the poor maintenance practices in India. A continuous monitoring of water quality is required in this project. Even a slight mismanagement can spoil the whole idea of project due to bed smell. As this project cover long stretch without the closed boundaries, it is also difficult to properly maintain the various components of the project (Fig. 8).

4 Conclusion

In the present study, a critical review of Dravayawati Riverfront is discussed. Due to the less rainfall and low number of rainy days, Jaipur has minimum chances for sufficient surface water for such type of project. As an alternative treated sewage, water is the prime source of the water in this project, which requires a continuous

monitoring of the sewage treatment plants. One major negative impact of the project is the reduction of groundwater recharge. This project also increases the vulnerability of flood in case of choking of the small drains which meet the main channel. With above-mentioned limitations, a successful implementation and operation of the project will give a good landscape to the Jaipur. The points discussed in the present study can be used by policy makers for the better design of such projects in semi-arid regions of the country.

References

1. A Guide to Riverfront Development. <https://riverlifephg.org/wp-content/uploads/2016/10/A-Guide-to-Riverfront-Development.pdf>
2. Sabarmati Riverfront. <https://sabarmatiriverfront.com/UserFiles/File/INCLUSIVE%20GROWTH.pdf>
3. Gomti riverfront channelization project from harding bridge to Gomti weir, Lucknow, Uttar Pradesh. Environmental Impact Assessment Report. https://environmentclearance.nic.in/writereaddata/FormB/EC/EIA_EMP/261120188JNCO3K5EIA.pdf
4. Nagpal S, Sinha A (2009) The Gomti riverfront in Lucknow, India: revitalization of a cultural heritage landscape. *J Urban Design* 14(4):489–506
5. Yamuna Riverfront Development Indraprasth Zone. <https://e.duac.org/images/pdf/13.%20ITO%20river%20front.pdf>
6. Yamuna Riverfront Development. <https://spa.ac.in/writereaddata/Day3DDA.pdf>
7. EIA study report of proposed Riverfront Development in Patna. https://nmcg.nic.in/writereaddata/fileupload/27_FinalEnvironmentImpactAssessment%20Patna_RFD.pdf
8. Tata Projects Limited (2015) Detailed Project Report, Amanishah Nala (drain), Jaipur, Rajasthan. <https://www.tataproyects.com/dravyavati-river-project/>
9. Randhawa A, Chandra T (2017) Revitalization of Dravyawati river, Jaipur, India: a water-front development project. *J Geogr Reg Plan* 10(3):28–38
10. https://en.wikipedia.org/wiki/Dravyavati_River
11. JDA (Jaipur Development Authority) (2011) Jaipur Master Development Plan—2025
12. Rajasthan Monsoon Report 2013–2018
13. Government of India, Ministry of Water Resources: Central Ground Water Board (2013) Ground Water Information—Jaipur District, Rajasthan
14. <https://timesofindia.indiatimes.com/city/jaipur/dravyavati-river-project-fails-to-improve-citys-water-table/articleshow/76500245.cms>

Analysis of Crop Protection Techniques Involving IoT



Prakriti Bhardwaj, Ranjan Verma, Parul Kalra, and Deepti Mehrotra

Abstract The protection of crops is very important for the improved quality of agricultural production. It plays an important role in mankind and the environment. It is significant to protect the crops from pests and plant diseases that harm the crops. Proper and accurate information about the plant/crop and soil while growing can make the crop healthy and also prevent from serious harm that may occur in the future, by using pesticides and other prevention techniques. Yield and crop production can be escalated by implementing optimum methods. With the advancement of science and technology, the growing work in this domain using sensors and other IoT equipment will be a boon for the society and environment. This research paper focuses to explore different IoT-based techniques that are available or are being researched upon for protection of crops. The paper presents an IOT-based anti-noise technique that on the protection of plants by using several techniques that bring out the best possible results in crop protection.

Keywords Crop protection · Pesticides · IoT · Pest detection · Noise-based technique

1 Introduction

Crop protection has been an important concern since the emergence of agricultural practices to enhance the quality of yield by effectively diminishing the degradation. Some enhanced techniques based on AI.

IoT and image processing are limited to disease prediction and identification, smart irrigation system, and pest identification but all these methods rely on the use of pesticides for protecting crops from pests. An approach proposed by a research paper is to monitor the monkeys approaching the farmland and producing noise as a warning signal to the farmer and also, to send the monkeys away. This method, however, does not solve the problem of pesticides usage. A majority of farmers have

P. Bhardwaj (✉) · R. Verma · P. Kalra · D. Mehrotra
Amity University Uttar Pradesh, Noida, India
e-mail: bhardwaj.pakriti@gmail.com

© The Author(s), under exclusive license to Springer Nature Singapore Pte Ltd. 2021
Y. A. Mehta et al. (eds.), *Advances in Water Resources and Transportation Engineering*,
Lecture Notes in Civil Engineering 149,
https://doi.org/10.1007/978-981-16-1303-6_18

225

to suffer by the damage caused by the use of pesticides. It is important to protect crops from pests by reducing the use of pesticides, thereby improving the quality of crop yields without damaging the environment.

This research paper focuses on the protection of plants by using several techniques that bring out the best possible results on crop protection. Along with the protection of crops from pests, it is important to maintain good health of the crops. Improving moisture content of the soil can contribute greatly to producing healthy crops.

2 Crop Protection Involving IOT

The main objective of this paper was to study and analyze the recent trends and techniques in the field of crop protection associated with Internet of Things. To achieve this, we scrutinized the existing research papers and journals available online. The search started with keyword mapping containing the keywords, namely crop protection, crop protection using IoT, crop protection system from pests, technologies used to protect crops from pests. The search was advanced by using keywords such as smart irrigation system, animal detection system to protect crops, IoT techniques for pest control, pest prediction system, disease prediction system, effects of pesticides on crops, anti-noise system to protect crops from pests and insects.

Based on the selected papers, it was found that the existing IoT techniques can be into three major heads, namely disease/pest prediction based, smart irrigation based, and animal detection based. Table 1 presents the studies considered in each of these categories.

A study by Qian Jing, et al., propounds an approach for acquiring the characteristics of pests based on live data of farmland. It gives detailed description of pest activity for protection of plant [1]. Heamin Lee, et al., “Disease and pest prediction IoT system in orchard: A preliminary study” proposes an IoT-based system that identifies the decrease in crop productivity and quality due to various pests and crop diseases. It notifies when the infection rate is high which in turn reduces the need of frequent use of insecticides and fungicides [2]. A study by Dattatraya Vhatkar Shivling, et al., aims to anticipate the occurrence of risk factor in apple caused by apple scab in Himalayan region based on certain parameters. A model is developed which predicts the pest accumulation up to seven days, and based on this data,

Table 1 Crop protection involving IOT

S. no.	Focus of the studies in agriculture and crop protection	Supporting studies
1.	Studies involving prediction and identification of disease and pest damaging crops	[1, 2, 3, 4, 5, 6, 7, 8, 9, 10]
2.	Studies involving smart irrigation system	[11, 12, 13, 14, 15, 16, 17, 18, 19]
3.	Studies focused on animal detection	[20, 21, 22]

corresponding pesticides may be used [3, 8]. A research by Zhengang Yang, et al., propounds a case-based reasoning (CBR) approach for the prevention and treatment of crop disease on the basis of generated results by the forecast and prediction of crop disease and the possible extent of damage to growing crops. This CBR-based system was efficiently implemented in cucumber, taking into consideration downy mildew of cucumber [4, 16, 22].

A. K. Tripathy, et al., “Data mining and wireless sensor network for groundnut pest/disease precision protection” collects statistics and specifics of microclimate and applies multivariate regression and empirical models to improve environmental conditions and groundnut yield conditions based on the prediction of pest and disease damaging the groundnut. It does so by identifying and analyzing the correlation pattern between crop-pest and disease-weather criteria [5, 9]. A study by Kaushik Kunal Singh focuses on identification of plant disease precisely without delay by capturing images of the affected areas of the plant. This technique is 95% accurate [6]. “Application for diagnosis of diseases in crops using image processing. International Journal of life Sciences Biotechnology and Pharma Research” by Arunkumar Beyyala and Sai Priya Beyyala, research paper propounds the comprehensible techniques for diagnosis of plant maladies and disorders by a software system. It involves the capturing of images for the inspection and identification of diseases using image processing. It is used in farms to understand image patterns. The system is being modified so as to make early detection possible by the enhanced technologies [7, 10].

S. Harishankar et al., “Solar-Powered Smart Irrigation System.” The main objective of this paper is to design a model that will prove fruitful for the problem of energy crisis faced in the long run. It does so by focusing on the energy conservation and avoidance of water wastage [11]. Andre Boehman, et al., “Solar-Powered Irrigation System” present an archetype of irrigation system controlled by solar energy. Based on the requirements, water will be irrigated to the crops from the pump using solar energy. Shelek and Kazakstan are the cities chosen for the field work. It proposes a cost-effective model that is viable and eco-friendly [12, 18].

An automatically controlled irrigation system that supplies water to the plants based on the need as recorded by sensor that checks moisture content of the soil from time-to-time. PIC controller is the main component of this model. The entire system uses solar energy for its working [13]. A smart farm irrigation system based on IoT, android, and cloud computing. The data is received and handled in real time. It is a wireless communication system and reduces the human effort to a great extent. The system also allows remote controlling through android phone [14]. A study by Wali Mohammad Abdullah and Sharmin Islam proposes a smart irrigation system that uses fuzzy logic to operate the working of motor for pumping water along with the optimized use of solar energy to utilize maximum power by retaining minimal wastage of power [15, 17].

A study done by Kuei-Chung Chang and Zi-Wen Guo uses IP cameras to monitor the monkeys approaching the farmland and sends a warning signal to the farmer. When monkeys start advancing the farmland, noise is produced to send the monkeys away [20]. Bharath, H. P., “Vision-Based Animal Detection and Alerting For Crop Protection”. This paper proposes vision-based animal detection system, effective for

crop protection that constitutes a camera and a computer coupled using the technologies of computer vision and deep learning using Python. The camera is used to capture images and videos of the animals approaching the crop field. Using image processing, the captured image is matched with the database. An additional option to download the data of unregistered animals from the Web is also provided. Based on the identified creature, their details are sent as an alert message, and buzzer is played to keep the intruder at Bay [21, 19].

3 Proposed Architecture

From review of papers, we concluded that the anti-noise-based IoT technique has a better future scope as it is based on minimizing the crop destruction by removing the pest at the initial stage of crop growth.

Considering the above, we attempted to design an anti-noise device. Figure 1 shows the architecture of the proposed model with the components used to build and design the product in the paper. **ThingSpeak** is an open-source application of IoT that is used as a server to send and receive statistical data provided by the sensors for collecting and analyzing values of temperature, moisture, and humidity. **Voice Recognition kit** is used to listen and analyze voice received as input to it. Depending on the input of the voice recognition kit, anti-noise will be generated to annoy the insects that will compel them to move away from the crops.

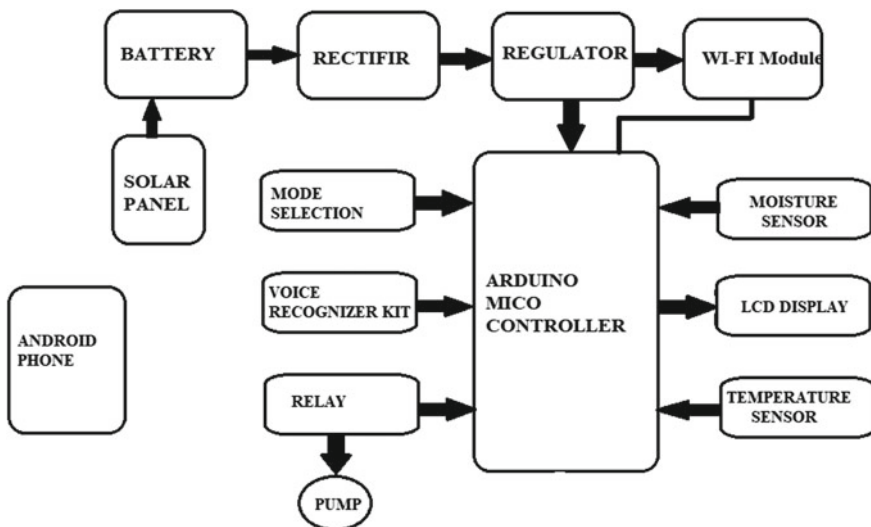


Fig. 1 Block diagram of the proposed anti-noise technique-based product

Photovoltaic solar panels get energy from sunlight which is then converted into electricity (DC current). It acts like a central control panel. It generates clean and green electricity. Moisture sensor is a sensor which senses the amount of moisture present in the soil. It has outputs in form of analog as well as digital signals. **Arduino micro-controller** is a single-board micro-controller that reads inputs and turns them into outputs. The readings from moisture sensor, temperature sensor, mode selection, relay, and voice recognition kit serve as inputs to the Arduino board. The resultant reading is shown on the screen of LCD display. All the equipments and components are inter-connected.

4 Analysis and Discussion

Crop protection has been an important concern since the emergence of agricultural practices, and its awareness has spread significantly over the past years.

This research paper analyzes the protection of plants by using the techniques mentioned in our studies and brings out the best possible results on crop protection.

Pesticides cause huge damage to the soil and environment. They kill the respective pests but also harm other living organisms and the environment, thus degrading the soil fertility. Hence, their use should be minimized.

An alternative approach should be used to protect crops from pests by reducing the use of pesticides, thereby improving the quality of crop yields without damaging the environment.

Table 2 shows a list of the pests and insects, with their respective pesticide category, whose anti-noise is available. Using the technique of anti-noise generation, use of pesticides can be reduced as the insects will be compelled to move away from the crops using anti-noise itself. In order to use anti-noise generation technique, it is important to know about the pests whose anti-noise is already known.

If a pest, whose anti-noise is not in record, approaches the crops, this method is not recommended. Although it is not recommended to use pesticide every time a pest approaches the crop, pesticides are suggested in case their anti-noise is not available or pest accumulation is in excess. If not controlled in time, pests will cause great harm to the crops.

5 Conclusion

Awareness for crop protection has spread significantly over the past years. It is important to protect crops from pests by reducing the use of pesticides, thereby improving the quality of crop yields without damaging the environment. Pesticides are used to kill and remove pests from soil and plants which decrease the nutrients of the soil and harm the environment and henceforth, damaging the crops and degeneration of their yield. To worsen the condition, impact of the pesticides remains for a long time

Table 2 List of pests/insects whose anti-noise is available

S. no.	Insects	Availability of anti-noise	Categories of pesticides used
1	Rats	Yes	Rodenticides
2	Mice	Yes	Rodenticides
3	Cockroaches	Yes	Insecticides
4	Squirrels	Yes	Rodenticides
5	Mosquitoes	Yes	Insecticides
6	Flies	Yes	Insecticides
7	Bedbugs	Yes	Insecticides
8	Reptiles	Yes	Insecticides
9	Ants	Yes	Insecticides
10	Snake	Yes	Insecticides
11	Worm	Yes	Insecticides
12	Cricket	Yes	Insecticides
13	Caterpillar	Yes	Insecticides
14	Larvae	Yes	Larvicides
15	Spider	Yes	Insecticides
16	Field Cricket	Yes	Insecticides
17	Moths	Yes	Insecticides
18	Fruit flies	Yes	Insecticides
19	Midges	Yes	Insecticides

even when pests are not present on the crops. Hence, anti-noise technique should be used to remove pests from plants as it compels the pests to move away from the plants without damaging the crops and environment. However, pesticides protect the crops by getting rid of the accumulation of pests near it. Such techniques can further be complemented with smart irrigation technique for improving the crop yield and improving the quality of produce. Thus, the advent of IoT has opened many new opportunities to improve the overall agriculture health and produce of our country.

References

1. Jing Q, Yu-man N, Yong-ping W, Ping-guo C, Jian-he L, Quan-jun S (2018, May) Dynamic features extraction system of live pests in farmland. In: 2018 33rd Youth academic annual conference of Chinese association of automation (YAC). IEEE, pp 1141–1146
2. Lee H, Moon A, Moon K, Lee Y (2017, July) Disease and pest prediction IoT system in orchard: a preliminary study. In: 2017 Ninth international conference on ubiquitous and future networks (ICUFN). IEEE, pp 525–527
3. Shivling DV, Sharma SK, Ghanshyam C, Dogra S, Mokheria P, Kaur R, Arora D (2015, October) Low cost sensor based embedded system for plant protection and pest control. In:

- 2015 International conference on soft computing techniques and implementations (ICSCTI). IEEE, pp 179–184
4. Yang Z, Luo Y, Deng F, Li L (2006) Crop disease dynamic forecast integrated with case-based reasoning methodology. In: 2006 6th World congress on intelligent control and automation, vol 1. IEEE, pp 2551–2554
 5. Tripathy AK, Adinarayana J, Merchant SN, Desai UB, Ninomiya S, Hirafuji M, Kiura T (2013) Data mining and wireless sensor network for groundnut pest/disease precision protection. In: 2013 National conference on parallel computing technologies (PARCOMPTECH). IEEE, pp 1–8
 6. Singh KK (2018) An artificial intelligence and cloud based collaborative platform for plant disease identification, tracking and forecasting for farmers. In: 2018 IEEE International conference on cloud computing in emerging markets (CCEM). IEEE, pp 49–56
 7. Beyyala A, Beyyala SP (2012) Application for diagnosis of diseases in crops using image processing. *Int J Life Sci Biotechnol Pharma Res* 1(1):172–175
 8. Sreekantha DK, Kavya AM (2017, January) Agricultural crop monitoring using IOT-a study. In: 2017 11th International conference on intelligent systems and control (ISCO). IEEE, pp 134–139
 9. Radha R, Tyagi AK, Kathiravan K, Betzy GS (2018) Precision crop protection using wireless sensor network. In: International conference on intelligent systems design and applications. Springer, Cham, pp 280–290
 10. Jha RK, Kumar S, Joshi K, Pandey R (2017) Field monitoring using IoT in agriculture. In: 2017 International conference on intelligent computing, instrumentation and control technologies (ICICICT). IEEE, pp 1417–1420
 11. Harishankar S, Kumar RS, Sudharsan KP, Vignesh U, Viveknath T (2014) Solar powered smart irrigation system. *Adv Electron Electr Eng* 4(4):341–346
 12. Abbott S, Baker I, Nakkula RJ (2015) Solar-powered irrigation for Shelek, Kazakhstan
 13. Prakash N, Balaji VR, Sudha M (2016) Solar powered automated irrigation system for agriculture. *Int J Adv Eng Technol VII(I)*:854, 858
 14. Saraf SB, Gawali DH (2017) IoT based smart irrigation monitoring and controlling system. In: 2017 2nd IEEE international conference on recent trends in electronics, information & communication technology (RTEICT). IEEE, pp 815–819
 15. Abdullah WM, Islam S (2015) A proposed smart irrigation system with enhanced solar power and logic based power generation systems. In: Proceedings of the sixth international conference on computer and communication technology 2015, pp 91–94
 16. Rau AJ, Sankar J, Mohan AR, Krishna DD, Mathew J (2017) IoT based smart irrigation system and nutrient detection with disease analysis. In: 2017 IEEE Region 10 Symposium (TENSymp). IEEE, pp 1–4
 17. Gayatri MK, Jayasakthi J, Mala GA (2015) Providing smart agricultural solutions to farmers for better yielding using IoT. In: 2015 IEEE technological innovation in ICT for agriculture and rural development (TIAR). IEEE, pp 40–43
 18. García L, Parra L, Jimenez JM, Lloret J, Lorenz P (2020) IoT-based smart irrigation systems: an overview on the recent trends on sensors and IoT systems for irrigation in precision agriculture. *Sensors* 20(4):1042
 19. Galedar MN, Jafari A, Mohtasebi SS, Tabatabaefar A, Sharifi A, O’Dogherly MJ, Richard G (2008) Effects of moisture content and level in the crop on the engineering properties of alfalfa stems. *Biosyst Eng* 101(2):199–208
 20. Chang KC, Guo ZW (2018) The Monkeys are coming—design of agricultural damage warning system by IoT-based objects detection and tracking. In: 2018 IEEE International conference on consumer electronics-Taiwan (ICCE-TW). IEEE, pp 1–2
 21. Mohanraj K, Karthikeyan BS, Vivek-Ananth RP, Chand RB, Aparna SR, Mangalapandi P, Samal A (2018) IMPPAT: a curated database of Indian medicinal plants, phytochemistry and therapeutics. *Sci Rep* 8(1):1–17
 22. Kramer PJ (1969) Plant and soil water relationships: a modern synthesis. In: Plant and soil water relationships: a modern synthesis

Microplastic Detection and Analysis in River Yamuna, Delhi



Debarshi Ghosh and Madhuri Kumari

Abstract Plastic tainting of fresh water is a mounting and unavoidable environmental concern. Litter sized less than 0.5 mm plastic pieces called microplastic can be found in high densities in water. These non-degradable microplastics are known to form carcinogenic attributes in human digestive system, alter the biochemical reaction in species, and are contaminating the fresh water and marine water. The objective of this research is to detect microplastic in River Yamuna flowing in Delhi stretch using the Synthetic Aperture Radiation (SAR) remote sensing technique and analyse the types of microplastics in the sampled water using Fourier Transform Electron Microscope. The research has enlightened the effective use of remote sensing techniques in detecting microplastics in fresh waters, and the Fourier Transform Infrared (FTIR) imaging in categorization of plastics responsible for contaminating the fresh water. The research also portrays the commonly used plastic category in the region. Such study presents the need to work on methods for extraction of the minute unwanted plastic contamination from fresh waters.

Keywords Microplastics · River pollution · SAR · FTIR

1 Introduction

Microplastic is synthetic polymers with size smaller than 5 mm. Microplastics are either the micro beads that are present in cosmetics, glues, clothes, micro beads, lost fishing nets, cosmetics products, synthetic clothes, tyres, plastic pellets, microfibers, etc. or the disintegrated form of plastic which occurs due to photolytic effect, or degradation due to mechanical or biological process. They can also be accumulated in various organisms due to bioaccumulation and affects humans as it enters the food chain. The primary microplastics are also used in air blasting technology with polyester scrubbers, acrylic and melamine. Secondary microplastics are produced

D. Ghosh (✉) · M. Kumari
Department of Civil Engineering, Amity School of Engineering and Technology, Amity
University Uttar Pradesh, Noida, India
e-mail: debarshi.ghoshjbl@gmail.com

© The Author(s), under exclusive license to Springer Nature Singapore Pte Ltd. 2021
Y. A. Mehta et al. (eds.), *Advances in Water Resources and Transportation Engineering*,
Lecture Notes in Civil Engineering 149,
https://doi.org/10.1007/978-981-16-1303-6_19

233

due to disintegration of plastics and from plastic dusts of vehicles because of tyre abrasion on roads [1]. Most of the studies are conducted on marine ecosystems and organisms rather than on freshwater ecosystems which are directly related to the terrestrial ecosystem [2]. When the analysis of plastic containments was done, the study was conducted on higher trophic level organism [2, 3], but other studies conducted showed the presence of microplastic in freshwater invertebrates such as Tubificid worms, *Hyaella azteca* [4]. The presence of microplastic have also been detected in different marine environments like beaches, water columns, surface water, benthic zones of water [5]. Over eight to twelve million tons of plastics are accumulated in the oceans, while the rivers are subject to disposal of over four million tons of plastics [6].

These secondary microplastics formed by cumulative process conjugation of physical, chemical, biological and chemo-photo-degradation of the larger plastic debris when exposed to photons of sunlight form minute structures invisible to human eye, fragmentation leads to degradation of these microplastic to its smallest range of 1.6 μm in diameter of several uneven shapes [7–9].

It is imperative to quantify the microplastic present in the water bodies for designing the strategies for mitigating such water pollution. With the help of remote sensing technology that works on the fundamentals of frequency absorbance value and radiance value of these microplastics, obtained from different satellite images, it may be possible to detect the amount of microplastic present in our rivers, lakes, ponds, canals, drains, sewage dumps, oceans and to areas which are not easily accessible.

Synthetic Aperture Radar (SAR) remote sensing, is such a technology that has enabled the study of microplastic detection with the help of microwave spectrum. The availability of technologies like Fourier Transform Infrared (FTIR) Spectroscopy have enabled the identification, extraction and sampling of microplastic but there is no standardised sampling or analytical protocols that have been established for international use [10].

The objective of this research work on Yamuna River is primarily to detect microplastics present or floating on surface water and analyse the quality of these microplastics.

2 Study Area

River Yamuna starts from the Yamunotri glacier (Saptrishi Kund) in the Greater Himalayas with its latitude and longitude as 38° 59' N and 78° 27' E, respectively, in the district of Uttarakhand with an elevation of 6387 m above mean sea level. The river flows from Himalayan foot hills to Indo-Gangetic Plain after crossing Uttarakhand and then passes along the borders of the adjacent states Uttar Pradesh and Haryana. The river then sweeps into Delhi feeding the Agra Canal and southern Delhi. The 1376 km long river meets with Ganga River near Allahabad, after traversing a path through Mathura, Etawah and Agra. Figure 1 shows the flow route of the river.

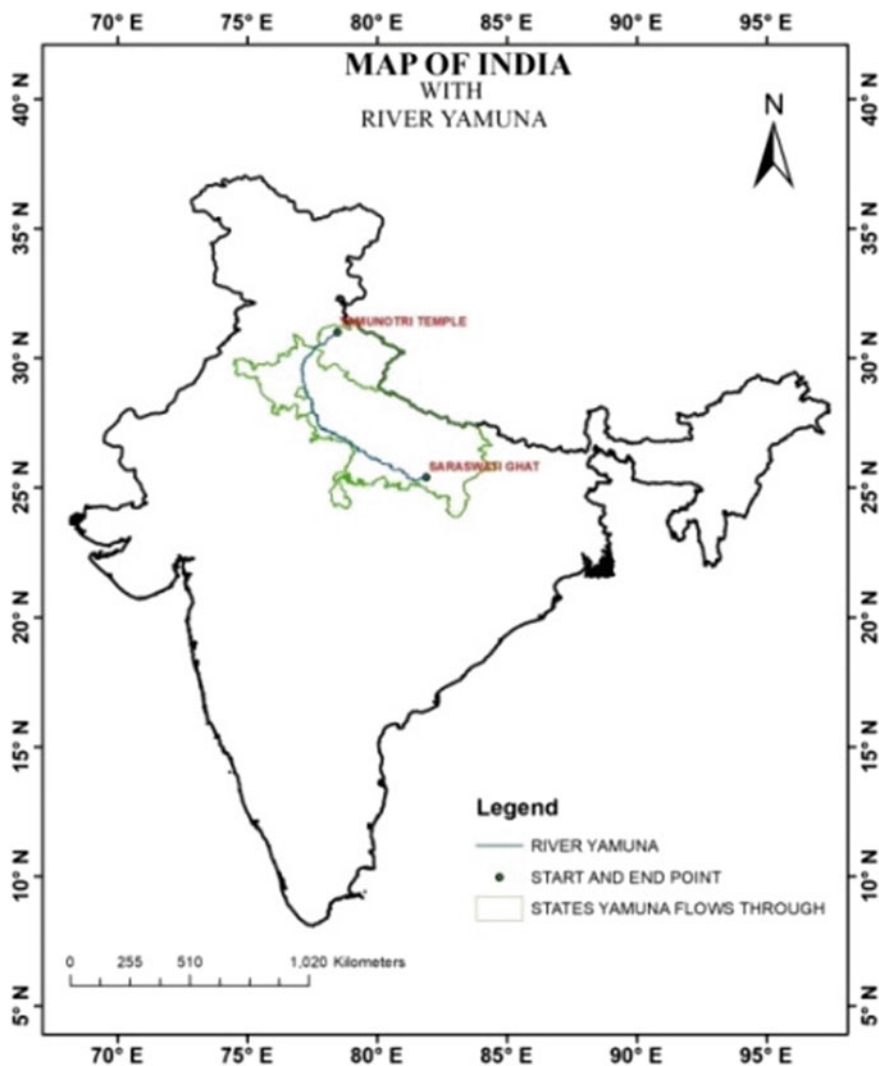


Fig. 1 River Yamuna flow route

River Yamuna is considered as one of the most polluted rivers of India. There are 5 barrages made on the course of the river Yamuna i.e. at Daakpathar, Hathnikund, Wazirabad, Okhla and Mathura. The basin area is predominantly covered by alluvial soil and contributes to 60% of cultivable land. The sample has been collected from the coordinate $28^{\circ} 32' 11.7''$ N, $77^{\circ} 19' 29.9''$ E of Yamuna River, Delhi for the study of microplastics contaminant as shown in Fig. 2.

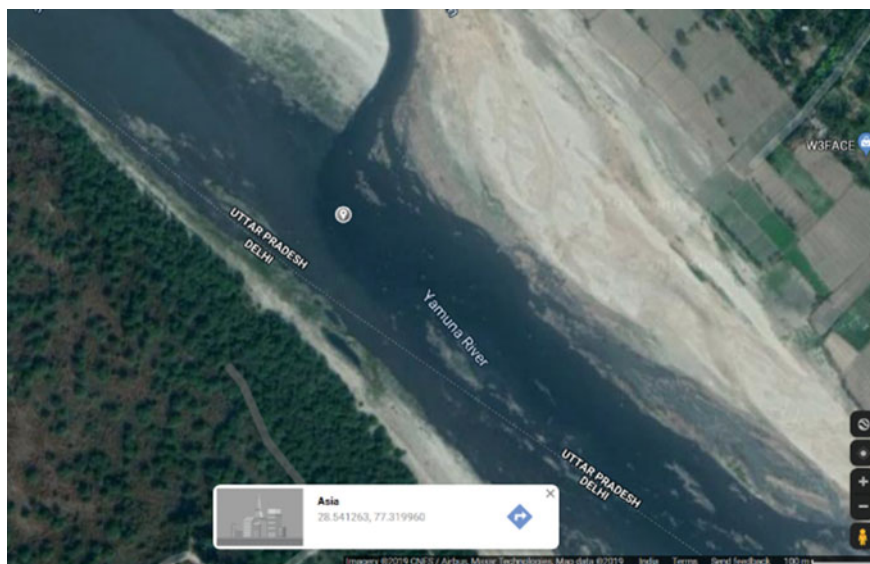


Fig. 2 Sample collection site (Google Map)

3 Methodology

3.1 Detection of Microplastic

In this study, we used Sentinel-1A SAR images of the selected site. Since the plastic concentration do not change water colour of river, microwave-based SAR image is effective in identification of floating plastics. The optical images doesn't help in detection of plastics due to formation of biofilms and surfactant on river water. In this study, we used Sentinel-1A satellite image from the European Space Agency (ESA) Copernicus program, in Level 1. The images need to be pre-processed by using SNAP software as the images are in raw state and need error correction like stripped image due to malfunctioning of the sensors. For verification of satellite image classification result, water and sediment sample was taken from sampling sites and FTIR based analysis was carried out. The remote sensing technique of detection is challenging due to limitation in availability of high-resolution images of the study area. Also, the operational process for image classification and identification is expensive as the software SNAP; an image processing software requires high-end configured central processing unit for its execution.

3.2 Sediment Extraction Method

The samples were collected in a sterilised container from the coordinates where microplastics were detected using remote sensing. A part of sample water was used for sediment extraction by allowing the water to evaporate at room temperature. The water was passed through nylon sieves of mesh size 5 and 1 mm. The sediments retained on sieve were collected and then rinsed in 250 ml of 30% hydrogen peroxide for 48 h to remove the biofilms layer. 5.3 M NaCl solution was used to rinse the collected sediments and then centrifuged at 10,000 rpm for 5 min. Organic matter that were visually identifiable were removed on being spotted. Subsequently, Whatman filter was used for vacuum filtration. On completion of filtration process, the filter paper was transferred to a petri plate for drying at room temperature for 5 days.

3.3 Selection of Sample for FTIR Analysis

The filtered sediments collected in petri plate were diluted in distilled water, packed in glass tube and sent for FTIR Spectroscopy. A part of the sample was used for microscopic imaging of the microplastic.

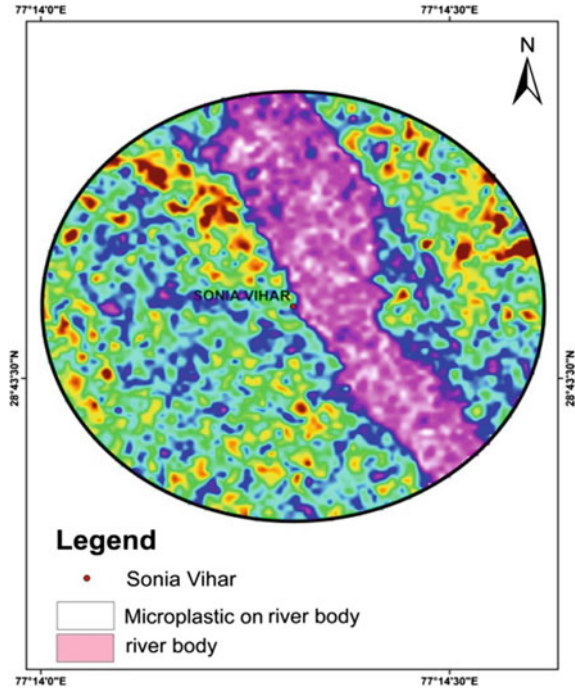
4 FTIR Analysis for Categorisation of Plastics

Microplastic collected from the selected sites was analysed for differences in post-production consumer plastics' physical and chemical properties. The polymer content of sample was assessed by FTIR. The molecular bonds attain an excited state in presence of infrared radiation. The absorption of infrared wavelengths depends on the compound of the object which absorbs the IR wavelength within the IR spectrum set in the FTIR. This absorption sequence is displayed in form of wavelength known as IR spectra. IR beam emitted from a light source splits and then recombines by the Michelson Interferometer. This beam passes through the sample absorbing and reflecting the radiation. This variance of the absorption and radiation of the IR beam is recorded using a detector. The raw data transforms into the IR spectrum for analysing the value. The microscopic analysis of the sample using the microscope was effective to take glance at the size of micro particles.

5 Result and Discussion

Figure 3 shows the classification of SAR images for detection of plastic. SNAP software was used for carrying out the image processing and further identification

Fig. 3 Detection of microplastic in sampling site using SAR imaging



of plastics using the ground truthing data collected by visual inspection of the site. The while colour patches in the satellite image mark the presence of plastics. This was further confirmed by FTIR-based analysis.

On carrying out FTIR analysis, it was found that the sediments extracted from the collected water sample contain microplastic. The FTIR graph report displayed the presence of major polymers of plastic such as Polyacetylene, polyacrylamide, polyamide, wool fibre and rayon fibre. The Automatic Infrared Microscope used for microscopic imaging of the sample shows the microplastic fibres. Figure 4 shows the FTIR graph and microscope image of the major polymers detected in sample.

Polyacrylamide is usually contained in clogs, surgery fibres, degraded carpets, and laundry wastes. Polyacetylene and polyamide is a major constituent of plastic ornaments and degraded clothes. Wool fibre and rayon fibre present in synthetic clothes were also detected in the sample.

6 Conclusion

The presence of miscellaneous plastic constituents determined by the FTIR spectroscopy proves the presence of microplastic in the river water of Yamuna. At the current rate of water pollution the quality of marine life and the ecosystem is affected

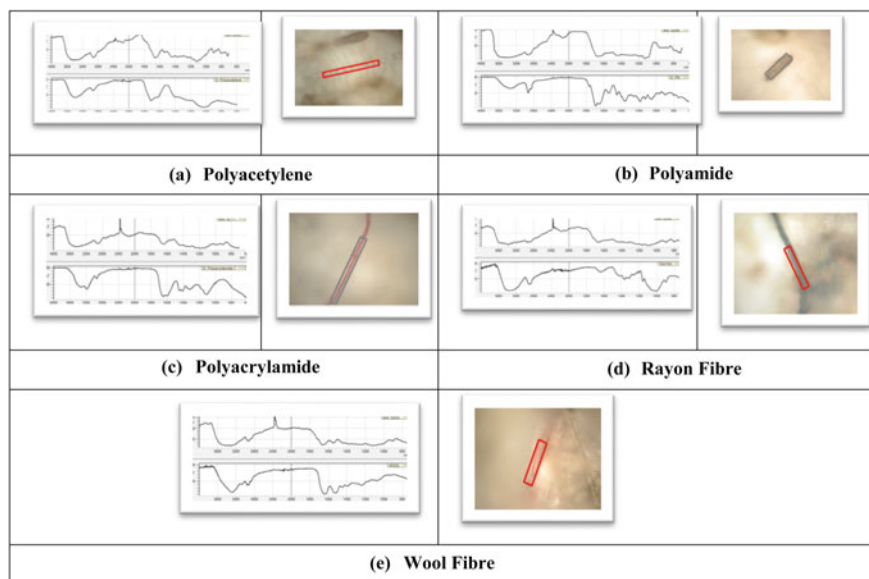


Fig. 4 FTIR graph and microscopic image of microplastic fibres detected in sample

severely. Benevolent nature perishes pollution over time; this imbibes the necessity to maintain equilibrium between the rate of degradation and plastic pollution generation by humans. Scope of research pertaining to feasible microplastic extraction persists. The need to formulate an extraction method of nano and microplastics is a necessity as the constituents are non-degradable in nature and commonly found in the fundamental elements required for life to sustain.

References

1. Boucher J, Friot D (2017) Primary microplastics in the oceans: a global evaluation of sources. IUCN, Gland, Switzerland. ISBN 978-2-8317-1827-9 IUCN. <https://doi.org/10.2305/IUCN.CH.2017.01.en>
2. Farrell P, Nelson K (2013) Trophic level transfer of microplastic: *Mytilus edulis* (L.) to *Carcinus maenas* (L.). Environ Pollut 177:1–3. <https://doi.org/10.1016/j.envpol.2013.01.046>
3. Rochman CM, Hoh E, Kurobe T, Teh SJ (2013) Ingested plastic transfers hazardous chemicals to fish and induces hepatic stress. Sci Rep 3:3263. <https://doi.org/10.1038/srep03263>
4. Lee KW, Shim WJ, Kwon OY, Kang JH (2013) Size-dependent effects of micro polystyrene particles in the marine copepod *Tigriopus japonicus*. Environ Sci Technol 47(19):11278–11283. <https://doi.org/10.1021/es401932b>
5. Tiwari M, Rathod TD, Ajmal PY, Bhangare RC, Sahu SK (2013) Distribution and characterization of microplastics in beach sand from three different Indian coastal environments. Mar Pollut Bull 140:262–273. <https://doi.org/10.1016/j.marpolbul.2019.01.055>
6. Shumilova O, Tockner K, Gurnell AM, Langhans SD, Righetti M, Lucía A, Zarfl C (2019) Floating matter: a neglected component of the ecological integrity of rivers. Aquat Sci 81:25.

<https://doi.org/10.1007/s00027-019-0619-2>

7. Klein S, Dimzon IK, Eubeler J, Knepper TP (2018) Analysis, occurrence, and degradation of microplastics in the aqueous environment. In: Wagner M, Lambert S (eds) *Freshwater microplastics: emerging environmental contaminants?*. Springer International Publishing, Cham, pp 51–67. https://doi.org/10.1007/978-3-319-61615-5_3
8. Carney Almroth BM, Åström L, Roslund S, Petersson H, Johansson M, Persson N-K (2018) Quantifying shedding of synthetic fibers from textiles; a source of microplastics released into the environment. *Environ Sci Pollut Res* 25:1191–1199. <https://doi.org/10.1007/s11356-017-0528-7>
9. Li J, Liu H, Chen JP (2018) Microplastics in freshwater systems: a review on occurrence, environmental effects, and methods for microplastics detection. *Water Res* 137:362–374. <https://doi.org/10.1016/j.watres.2017.12.056>
10. Castañeda RA, Avlijas S, Simard MA, Ricciardi A (2014) Microplastic pollution in St. Lawrence River sediments. *Can J Fish Aquat Sci* 71:1767–1771. <https://doi.org/10.1139/cjfas-2014-0281>